Faculteit Farmaceutische, Biomedische en Diergeneeskundige Wetenschappen

Faculteit Wetenschappen

Elucidation of the role of GSDME during apoptosis-driven secondary necrosis

Opheldering van de rol van GSDME tijdens secundaire necrose na apoptose

Proefschrift voorgelegd tot het behalen van de graad van Doctor in de biomedische wetenschappen aan de Universiteit Antwerpen

Proefschrift voorgelegd tot het behalen van de graad van Doctor in de wetenschappen: biochemie en biotechnologie aan de Universiteit Gent

Te verdedigen door:

Elke De Schutter

Promotoren:

Prof. Guy Van Camp
Prof. Peter Vandenabeele
Prof. Franck B. Riquet

Antwerpen, 2021

Table of contents

Summary

In 1998, the *gasdermin E* (*GSDME*) gene, also known as *DFNA5*, was identified in the lab of prof. Guy Van Camp as the genetic cause of a specific form of non-syndromic, autosomal dominant hearing loss. Next to a role in hearing loss, several studies pointed towards a contribution to different forms of cancer as well such as breast, colorectal and gastric cancer. First attempts in the lab of prof. Van Camp to elucidate the biological function of GSDME revealed that overexpression of the N-terminus of GSDME (N-GSDME) results in cell death and that the C-terminus of GSDME (C-GSDME) probably fulfills an auto-inhibitory function preventing cytotoxicity by N-GSDME. Furthermore, they showed that N-GSDME-mediated cell death was caspase-3/8 and RIPK1 independent, led to damaged mitochondria, and did not show hallmarks of ferroptotic or autophagic nature. However, it remained unclear how GSDME was activated and in which pathway(s) it was involved. In 2015, gasdermin D (GSDMD) was identified as a substrate of the inflammatory caspases-1 and -4/5 and as a mediator of pyroptosis, an inflammasome-driven cell death modality associated with the pro-IL-1β processing and IL-1β release. Similar to what was observed for GSDME, GSDMD was shown to harbor an intrinsic cell death inducing activity that is executed by its N-terminal domain while this cytotoxic activity is inhibited by its C-terminal domain, putting research on GSDME-mediated cell death back in the spotlight.

In this thesis we aimed to further investigate the biological function of GSDME both *in silico* as *in vitro*. Soon the GSDM proteins were proposed to elicit their cytotoxic function by plasma membrane pore-formation *via* a barrel-stave pore-forming mechanism. However, this hypothesis was presumably based on observations made for GSDMD and the murine GSDMA3. In the first part of this thesis, we modeled the structures of full length GSDME and N-GSDME using a homology-based strategy with the published structures of the murine GSDMA3 and N-GSDMA3 as template, to assess a similar function for GSDME *in silico*. Comparison of our modeled structures of full length GSDME with the structures of full length GSDMA3 and GSDMD showed that the overall structure of GSDM proteins is very alike and that the mechanism of auto-inhibition provided by C-GSDM is similar among GSDM proteins. In both our models of GSDME and N-GSDME, the identical position of the α1-helix compared to the α1-helix of GSDMA3 suggests a similar important function as primary recognition and binding site for negatively charged phospholipids. Nevertheless, some striking differences between N-GSDMA3 and N-GSDME were also observed. N-GSDMA3 is characterized by a 4-stranded β-sheet that is proposed to insert in the membrane. However, our model of N-GSDME showed that the outer β_{TM}4-strand in N-GSDME is disrupted by a highly conserved E197 residue. This results in a more flexible β_{TM}4-strand complicating inter-unit oligomerization. Moreover, the position of this charged residue disturbs the hydrophobic surface that is formed by the β-sheet and that is supposed to

interact with the hydrophobic lipid tails in the plasma membrane. Altogether these observations make it very unlikely that N-GSDME forms pores *via* the barrel-stave model.

In the meantime, GSDME was shown to be a substrate of capase-3. Therefore, in the second part of this thesis we investigated the contribution of GSDME to apoptosis-driven secondary necrosis in the murine fibrosarcoma cell line L929sAhFas *in vitro*, using tools specifically designed and generated for this purpose. In order to assess the contribution of GSDME to the kinetics of plasma membrane permeabilization during apoptosis-driven secondary necrosis, we measured nuclear staining by the regularly used cell impermeant nuclear dyes 7-aminoactinomycin D (7-AAD), SYTOX Blue (SB) and SYTOX Green (SG) in presence and absence of GSDME expression. Surprisingly, we showed that nuclear staining by SYTOX dyes, but not by 7-AAD, is delayed in the absence of GSDME expression during apoptosis-driven secondary necrosis. This result suggests that multiple membrane permeabilization mechanisms occur during this cell death modality that allow the selective uptake of specific nuclear dyes. At the same time, this result questions the suitability of cell impermeant dyes to study plasma membrane permeabilization processes without thorough knowledge about their membrane passing mechanism. Next, we monitored the contribution of GSDME to the influx of Texas Red-labeled dextrans relative to nuclear staining by SB during apoptosis-driven secondary necrosis. We found that GSDME allows the influx of dextrans up to 70 kDa before nuclear staining by SB. At the same time or after nuclear staining by SB, GSDME also promoted the entrance of Texas Red-labeled dextrans of 2000 kDa, indicating that GSDME-mediated plasma membrane permeabilization results in large pores. In addition, we observed a decrease in the influx of Texas Red-labeled dextrans with increasing sizes, suggesting that GSDME pores are formed with a rather variable size instead of a fixed size. Finally, in an attempt to visualize GSDME-mediated pore formation during apoptosis-driven secondary necrosis, we have put a mNeonGreen tag internally in N-GSDME before the caspase-3 cleavage site and added additionally a mScarlet tag in C-GSDME right after the caspase-3 cleavage site. After we successfully validated the functionality of the tagged GSDME molecules using differential nuclear staining by SB and 7-AAD, we were able to visualize N-GSDME and C-GSDME before and after cleavage by caspase-3 during apoptosis-driven secondary necrosis. Using live cell imaging, we confirmed plasma membrane targeting and mitochondrial targeting of N-GSDME during apoptosis-driven secondary necrosis.

Altogether, we concluded that N-GSDME probably is a pore-forming protein, but that it acts more as an amphipathic molecule and therefore probably forms pores *via* a carpet-like or toroidal pore-forming mechanism instead of a barrel-stave pore-forming mechanism as was proposed for N-GSDMA3. Future research should focus on the consequences of GSDME-mediated plasma membrane permeabilization in terms of release of pro-inflammatory molecules and clearance by phagocytic cells.

Samenvatting

In 1998 identificeerde de onderzoeksgroep van prof. Guy Van Camp het gen coderend voor gasdermin E (GSDME), ook bekend als *DFNA5*, als de genetische oorzaak van een specifieke vorm van niet-syndromaal, autosomaal dominant gehoorverlies. Naast een rol in gehoorverlies, wezen verschillende studies eveneens op een mogelijke betrokkenheid van GSDME in diverse vormen van kanker, zoals borst-, darm- en maagkanker. De eerste experimenten om de biologische functie van GSDME te achterhalen, brachten aan het licht dat overexpressie van de N-terminus van GSDME (N-GSDME) resulteert in celdood en dat de C-terminus van GSDME (C-GSDME) waarschijnlijk een auto-inhiberende functie vervult die de cytotoxiciteit door N-GSDME verhindert. Bovendien werd aangetoond dat celdood veroorzaakt door N-GSDME caspase-3/8 en RIPK1 onafhankelijk is, resulteert in beschadigde mitochondriën en geen kenmerken vertoont van ferroptose of autofagie. Het bleef echter onduidelijk hoe GSDME wordt geactiveerd en in welke celdoodpathway(s) het betrokken is. In 2015 werd gasdermin D (GSDMD) geïdentificeerd als een substraat van de inflammatoire caspases-1 en -4/5 en als een mediator van pyroptose. Dit is een door inflammasomen aangestuurde celdoodvorm geassocieerd met de activatie van pro-IL-1β en vrijzetting van IL- 1β. Vergelijkbaar met wat werd waargenomen voor GSDME, vertoonde GSDMD een intrinsieke celdood-inducerende activiteit die wordt uitgevoerd door zijn N-terminaal domein en die wordt verhinderd door zijn C-terminaal domein. Vervolgens kwam het onderzoek naar GSDME-gemedieerde celdood terug onder de aandacht.

In dit doctoraatsproject wilden we de biologische functie van GSDME verder onderzoeken, zowel *in silico* als *in vitro*. Al snel werd geopperd dat de GSDM-eiwitten hun cytotoxische functie ontlokken door middel van porievorming in de plasmamembraan, meer bepaald via een tonvormig mechanisme. Deze hypothese was echter voornamelijk gebaseerd op waarnemingen van GSDMD en muis GSDMA3. In het eerste deel van dit proefschrift hebben we de structuren van GSDME en N-GSDME gemodelleerd met behulp van de reeds gepubliceerde structuren van muis GSDMA3 en N-GSDMA3 om *in silico* te kunnen inschatten of GSDME een vergelijkbare functie vervult. De vergelijking van onze gemodelleerde structuren van GSDME met de structuren van GSDMA3 en GSDMD toonde aan dat de algemene structuur van GSDM-eiwitten erg op elkaar lijkt en dat het mechanisme van auto-inhibitie door C-GSDM behouden blijft. Daarnaast observeerden we dat de positie van de α1-helix in onze modellen van GSDME en N-GSDME identiek is aan die van GSDMA3. Dit doet vermoeden dat de α1-helix van GSDME een vergelijkbare belangrijke functie vervult als primaire herkennings- en bindingsplaats voor negatief geladen fosfolipiden. Desalniettemin werden ook enkele opvallende verschillen tussen N-GSDMA3 en N-GSDME waargenomen. N-GSDMA3 wordt gekenmerkt door een 4-strengige β-plaat die vermoedelijk in de membraan insereert. Ons model van N-GSDME

toonde echter aan dat de buitenste β_{TM}4-streng in N-GSDME wordt verstoord door een sterk geconserveerd E197-residu. Dit resulteert in een meer flexibele β_{TM}4-streng die oligomerisatie tussen N-GSDME moleculen bemoeilijkt. Bovendien verstoort de positie van dit geladen residu het hydrofobe oppervlak dat wordt gevormd door de β-plaat en dat zou moeten interageren met de hydrofobe lipidestaarten in de plasmamembraan. Al deze waarnemingen maken het zeer onwaarschijnlijk dat N-GSDME poriën vormt via het tonvormig model.

In het tweede deel van dit proefschrift hebben we de betrokkenheid van GSDME in secundaire necrose na apoptose in de muizen fibrosarcoma cellijn L929sAhFas *in vitro* onderzocht, met behulp van tools die we specifiek voor dit doel hebben ontworpen. Om de invloed van GSDME op de kinetiek van plasmamembraan permeabilisatie tijdens secundaire necrose na apoptose te beoordelen, hebben we gebruik gemaakt van de kleurstoffen 7-aminoactinomycine D (7-AAD), SYTOX Blue (SB) en SYTOX Green (SG) in aanwezigheid en afwezigheid van GSDME-expressie. Deze kleurstoffen kunnen de plasmamembraan van intacte cellen niet doordringen maar kleuren het DNA in de celkern wanneer de plasmamembraan wordt verstoord. Verrassend genoeg toonden we aan dat kleuring door SYTOX-kleurstoffen, maar niet door 7-AAD, werd vertraagd in afwezigheid van GSDME-expressie tijdens secundaire necrose na apoptose. Dit doet vermoeden dat er tijdens deze celdoodvorm meerdere mechanismen van plasmamembraan permeabilisatie optreden die de selectieve opname van specifieke kleurstoffen mogelijk maken. Tegelijkertijd stelt deze observatie de algemene bruikbaarheid van cel-ondoordringbare kleurstoffen ter discussie wanneer men permeabilisatieprocessen in de plasmamembraan wenst te bestuderen. Vervolgens hebben we de betrokkenheid van GSDME in de instroom van Texas Red-gelabelde dextranen gevolgd ten opzichte van de kleuring van de nucleus door SB tijdens secundaire necrose na apoptose. We ontdekten dat GSDME de instroom van dextranen tot 70 kDa mogelijk maakt vóór SB DNA in de nucleus kleurt. Tegelijkertijd of na de kleuring van DNA door SB bevorderde GSDME ook de instroom van Texas Red-gelabelde dextranen van 2000 kDa, wat aangeeft dat GSDME-gemedieerde plasmamembraan permeabilisatie resulteert in grote poriën in de plasmamembraan. Bovendien zagen we een afname van de instroom van Texas Red-gelabelde dextranen wanneer de grootte van de dextranen toenam. Dit doet vermoeden dat GSDME-poriën eerder met een variabele grootte worden gevormd in plaats van met een vaste grootte. Ten slotte hebben we GSDME-gemedieerde porievorming tijdens secundaire necrose na apoptose gevisualiseerd. Hiervoor hebben we een mNeonGreen-tag intern in N-GSDME geplaatst vóór de caspase-3-splitsingsplaats. Daarnaast hebben we een mScarlet-tag toegevoegd in C-GSDME meteen achter de caspase-3 splitsingsplaats. Na met succes de functionaliteit van de gelabelde GSDME-moleculen te hebben gevalideerd, waren we in staat om N-GSDME en C-GSDME voor en na de splitsing door caspase-3 te visualiseren tijdens secundaire necrose na apoptose. Met behulp van het in beeld brengen van levende

cellen hebben we de rekrutering van GSDME naar de plasmamembraan en mitochondria kunnen vaststellen tijdens secundaire necrose na apoptose.

Op basis van al deze observaties hebben we geconcludeerd dat N-GSDME waarschijnlijk een poriënvormend eiwit is, maar dat het meer als een amfipatisch molecule werkt en daarom waarschijnlijk poriën vormt via een tapijtachtig of toroïdaal porievormend mechanisme in plaats van via een tonvormig mechanisme zoals voorgesteld voor N-GSDMA3. Toekomstig onderzoek zou zich moeten richten op de gevolgen van GSDME-gemedieerde plasmamembraan permeabilisatie op de afgifte van pro-inflammatoire moleculen en het wegruimen van dode cellen door fagocytische cellen.

Introduction

Chapter 1

Punching holes in cellular membranes: biology and evolution of gasdermins

REVIEW

Published in 'Trends in Cell Biology', 2021, 31(6):500-513

Elke De Schutter[1,2,3], Ria Roelandt[1,2], Franck B. Riquet[1,2,4], Guy Van Camp[3,5], Andy Wullaert[1,2,6] and Peter Vandenabeele[1,2,7]

[1] VIB Center for Inflammation Research, 9052 Ghent, Belgium

[2] Department of Biomedical Molecular Biology, Ghent University, 9052 Ghent, Belgium

[3] Center of Medical Genetics, University of Antwerp and Antwerp University Hospital, Prins Boudewijnlaan 43/6, BE-2650 Edegem, Antwerp Belgium.

[4] Université de Lille, Lille, France

[5] Center for Oncological Research, University of Antwerp and Antwerp University Hospital, Universiteitsplein 1, BE-2610 Wilrijk, Antwerp Belgium.

[6] Department of Internal Medicine and Pediatrics, Ghent University, Ghent, Belgium.

[7] Methusalem program CEDAR-IC, Ghent University, Ghent, Belgium.

Abstract

The Gasdermin (GSDM) family has evolved as six gene clusters (*GSDMA-E* and *Pejvakin*), which are characterized by a unique N-terminal domain (N-GSDM). Except for Pejvakin, the N-GSDM domain is capable of executing plasma membrane permeabilization. Pending on the cell death modality, several protease- and kinase-dependent mechanisms directly regulate the activity of GSDME and GSDMD, two widely expressed and best-studied GSDMs. We provide a systematic overview of all GSDMs in terms of biological function, tissue expression, activation, regulation and structure. In-depth phylogenetic analysis reveals that *GSDM* genes show many gene duplications and deletions suggesting strong evolutionary forces and a unique position of the *Pejvakin* gene associated with the occurrence of complex inner ear development in Vertebrates.

1.1 Gasdermins: same same but different

The human genome contains six **gasdermin** (GSDM) genes: *GSDMA-E* and *Pejvakin* (*PJVK*), located on 4 different chromosomes (Table 1). The mouse genome lacks a *GSDMB* orthologue, but repetitive duplication events resulted in three *Gsdma* genes (*Gsdma1*, *Gsdma2* and *Gsdma3*), four *Gsdmc* genes (*Gsdmc1*, *Gsdmc2*, *Gsdmc3* and *Gsdmc4*) and single genes for *Gsdmd*, *Gsdme* and *Pjvk,* raising questions about functional differences between gasdermins and which evolutionary selective forces have driven gene losses and amplifications. The gasdermins, originally coined according to their expression pattern along gastrointestinal tract and skin (dermis) [1,2], were until recently considered as orphan genes with unknown physiological functions, though some members have been associated with skin diseases such as alopecia [3,4], with asthma [5–8], hearing loss [9,10] and cancer [1,11–16]. Since several members of the gasdermin gene family were shown to execute plasma membrane permeabilization during different forms of **regulated necrosis** [17–21], GSDMs recently gained a lot of interest regarding their role in inflammation and host defense.

All GSDMs (except PJVK) consist of N-terminal (N-GSDM) and C-terminal domain (C-GSDM) connected by a linker region. Structural insights in the activation and pore-forming mechanisms of N-GSDM domains are largely based on the structures of GSDMA3 [22,23] and GSDMD [24]. The pore-forming mechanism involves three steps: interdomain proteolytic cleavage releasing N-GSDM from the autoinhibitory C-GSDM domain (Figure 1); phospholipid-mediated recruitment of the N-GSDM domain to the plasma membrane (Table 1); and finally oligomerization and **pore formation** leading to plasma membrane permeabilization. Nevertheless, it is still unclear whether this three step model applies for all GSDMs. For example, there is no experimental evidence for proteolytic cleavage of GSDMA, implying other mechanisms of activation.

Table 1. Biological and biochemical properties of the GSDM protein family. ND: not determined.

	GSDMA	GSDMB	GSDMC	GSDMD	GSDME	PJVK	References
Chromosomal location							
Human	*GSDMA*: chr17q21.1	*GSDMB:* chr17q21.1	*GSDMC*: chr8q24.21	*GSDMD*: chr8q24.3	*GSDME*: chr7p15.3	*PJVK*: chr2q31.2	
Mouse	*Gsdma1, Gsdma2, Gsdma3*: chr11D	-	*Gsdmc1, Gsdmc2, Gsdmc3, Gsdmc4*: chr15D1	*Gsdmd*: ChrD3	*Gsdme*: chr6B2.3	*Pjvk*: chr2.3	
Domain							
Gasdermin N (N-GSDM)	+	+	+	+	+	+	[2,32]
Gasdermin_C (C-GSDM)	+	+	+	+	+	-	[32]
Zinc finger	-	-	-	-	-	+	[32]
Cytotoxicity							
Full length	-	-	-	-	-	-	[8,17,22,53,54]
N-GSDM	+	+	+	+	+	-	[8,17,22,53,54]
Activating proteolytic cleavage	ND	Caspase-1 Granzyme A	Caspase-8	Caspase-1 Caspase-4/5 Caspase-8 Cathepsin G ELANE	Caspase-3 Granzyme B	ND	[8,17,40–42, 45,48,53,80,81, 18–21,28,29,31,37]
Membrane targeting	Plasma membrane	ND	ND	Plasma membrane Nucleus Mitochondria Neutrophil granules $LC3^+$ autophagosomes	Plasma membrane Mitochondria	Peroxisomes	[22,31,32,37,44, 52–55,82]
Lipid binding							
Full length	-	Phosphoinositides Phosphatidic acid Phosphatidylglycerol sulfatide	ND	-	-	ND	[21,22,53,62]
N-GSDM	Phosphoinositides Cardiolipin Phosphatidic acid Phospatidylserine	Phosphoinositides Phosphatidic acid Phosphatidylglycerol sulfatide	ND	Phosphoinositides Cardiolipin Phosphatidic acid	Phosphoinositides Cardiolipin Phosphatidylserine	ND	[21,22,53,62]

Since the discovery that particular GSDMs are implicated in the execution of different cell death modalities, their activation has been proposed as a marker of **pyroptosis** [25]. However, by doing so, “pyroptosis” becomes a rather generic term. One can have inflammasome-mediated activation of GSDMD by caspase-1/4/5/11 [18,19], chemotherapy-induced activation of GSDME by caspase-3 [21,26–28] or natural killer cell-induced activation of GSDME by granzyme-B [29], all leading plasma membrane permeabilization without signs of apoptosis. Additionally, to narrow down all GSDM-mediated cell death modalities to “pyroptosis” may also become confusing in cases of GSDME-mediated **secondary necrosis** following **apoptosis** (apoptosis-driven secondary necrosis) [17] and GSDMD-mediated release of NETs during **NETosis** [30,31].

In this review, we outline the differential expression of GSDM proteins in various tissues, showing ubiquitous expression of GSDME. Furthermore, we report on inflammasome dependent and independent cellular conditions leading to GSDM activation as well as on checkpoints involving proteolysis, phosphorylation and exosome formation that prevent N-GSDM cytotoxicity. Finally, we performed an in-depth phylogenetic analysis of the gasdermin family in many species, in order to understand possible evolutionary forces driving *GSDM* gene loss and amplification. Altogether, the evolutionary emergence of multiple *GSDM* genes and the restricted expression pattern of some of them reflect their crucial role in particular cell types in an organism living a life full of challenges.

1.2 Gasdermins: executioners on the necrotic battle field

All gasdermins but PJVK share the feature that (over)expression of their N-GSDM domain causes plasma membrane permeabilization [22]. In case of PJVK the N-GSDM domain is directly followed by a small C-terminal domain containing a zinc finger domain with an unknown function (Figure 1A) [10,32]. In contrast, GSDMA-E comprise clear two-domain arrangements consisting of the cytotoxic N-GSDM domain separated from an autoinhibitory C-GSDM domain by a flexible hinge region with highly conserved aspartate residues, making them potential substrates for aspartate-specific proteases such as caspases and granzymes. More information on the mechanisms of autoinhibition and release of N-GSDM from C-GSDM is provided in Box 1. GSDME cleavage by caspase-3 at D270 generates an N-GSDME fragment that causes membrane permeabilization during apoptosis-driven secondary necrosis [17] occurring after apoptotic features such as membrane blebbing, PS exposure and DNA fragmentation. However, GSDME does not explain all cases of membrane permeabilization following apoptosis. In some cells apoptosis-driven secondary necrosis occurs independently of GSDME, such as in immortalised *Gsdme*$^{-/-}$ macrophages [33], human T cells and monocytes [34], suggesting redundant mechanisms. Recently, the ill-characterized nerve injury-induced protein 1 (NINJ1), a cell surface protein, was shown to be essential for plasma membrane rupture following apoptosis-driven secondary necrosis, pyroptosis and necroptosis [35].

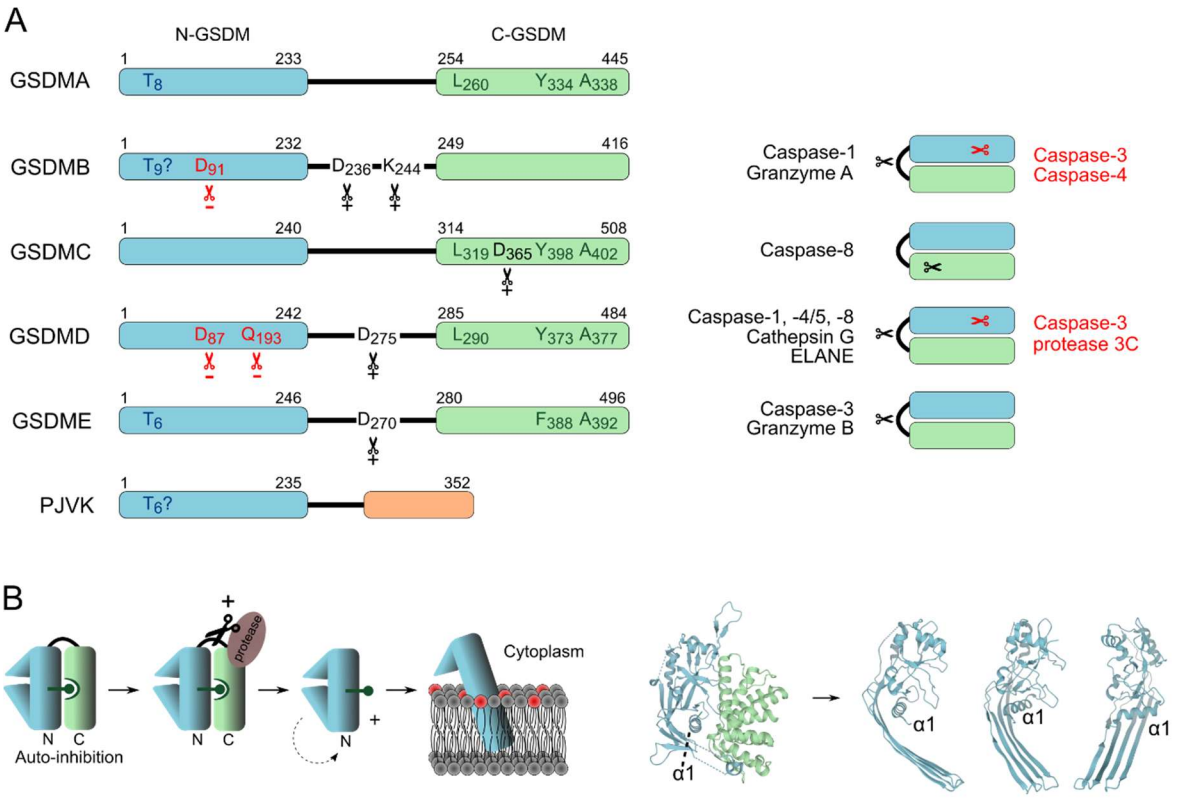

Figure 1. Schematic overview of the conserved structure and regulatory residues of the GSDM proteins. Sequences of the putative GSDMA-E and PJVK homologs were aligned using Clustal Omega (v1.2.4) and adapted in JalView (v2.10.5). The schematic overview is based on the crystal structures of GSDMA3 (PDB: 5B5R) [22] and N-GSDMA3 (PDB: 6CB8) [23]. **(A)** GSDMA-E contain a membrane permeabilizing domain (N-GSDM) (blue) and inhibitory domain (C-GSDM) (green). In case of PJVK the latter is replaced by a zinc finger domain (orange). Interaction between N-GSDM and C-GSDM is provided by conserved hydrophobic residues (dark green) forming a hydrophobic groove in C-GSDM (green). Phosphorylation of Thr6 inhibits membrane permeabilization by GSDME [54]. A conserved Threonine residue (dark blue) is found as well in GSDMA, -B and PJVK, but in case of the latter two this is a putative regulatory site based on location and indicated by '?'. Activating (black) and inactivating (red) cleavage sites are indicated by scissors with '+' and '-' symbols, respectively. Inactivating cleavage sites D91 and D87, are conserved in GSDMB (caspase-3, -4) and –D (caspase-3), respectively. Similarly, viral protease 3C cleaves GSDMD at the conserved site Q193. GSDMB, -D and –E are proteolytically activated by cleavage in the hinge region. GSDMB is cleaved by caspase-1 and granzyme A at D236 and K244, respectively. Human caspase-1/4/5/8 cleave GSDMD at D275. Nor the human ELANE cleavage site C268 nor cathepsin G cleavage site L273 in GSDMD are conserved. Both human caspase-3 and granzyme B cleave GSDME at D270. In addition, caspase-8 activates GSDMC at D365 within C-GSDMC. **(B)** N-GSDM destabilizes the plasma membrane after interaction of basic residues in the α1 helix with negatively charged phospholipids (red).

Canonical and **non-canonical** inflammasome activation of caspase-1/11 (mouse) or caspase-1/4/5 (human) leads to proteolytic activation of GSDMD [18,19,36–38] and the consecutive release of pro-inflammatory cytokines such as IL-1β [39], linking inflammasome-mediated GSDMD activation with pyroptosis. Next to caspase-1/11, recent studies in mouse macrophages revealed that in conditions of TAK1 and IKK inhibition (such as by YopJ during Yersinia infection), also caspase-8 directly activates GSDMD initiating pyroptosis [40–42] in a RIPK1 kinase activity dependent [40] or independent way [43]. This illustrates a proteolytic convergence during pyroptosis execution. However, in cancer cell lines treated with chemotherapeutic drugs, caspase-3-mediated cleavage of GSDME can directly proceed to plasma membrane permeabilization without inducting apoptotic features

such as blebbing, suggesting that also GSDME can trigger **primary necrosis** [21,26–28]. Likewise, granzyme B from killer cells can directly activate GSDME resulting in direct pyroptotic death of tumor cells rather than apoptosis-driven secondary necrosis [29].

While GSDMD-mediated pyroptosis in macrophages and neutrophils is associated with release of inflammasome substrates such as processed IL-1β [30,39,44], GSDMD activation in neutrophils *via* non-canonical inflammasome mediated cytosolic sensing of LPS or Gram-negative bacteria results in the release of neutrophil extracellular traps (NETs) [30]. Alternatively, in PMA-stimulated human neutrophils, ELANE (elastase from neutrophils) proteolytically activates GSDMD resulting in NETosis [31]. Also cathepsin G following serpin inhibition can function as backup for GSDMD activation in neutrophils and monocytes [45]. Furthermore, caspase-8–dependent GSDMD activation in macrophages provides host defense against *Yersinia* infection [46]. The fact that both GSDME (caspase-3, granzyme B) and GSDMD (caspase-1/4/5/11, caspase-8, ELANE, cathepsin G) can be activated by multiple proteases and directly cause plasma membrane permeabilization represents a redundant backup mechanism for pyroptosis to ensure necrotic death and consecutive release of cytokines, chemokines and DAMPs eliciting a strong immune response during infection, inflammation and anti-cancer responses [29].

In contrast to GSDME and –D, full size human GSDMB is capable of promoting pyroptosis by activating caspase-4 through interaction with the CARD domain, while the same caspase-4 also proteolytically inactivates GSDMB [47]. As such, GSDMB-mediated activation of caspase-4 may represent a mechanism for triggering non-canonical inflammasome activation and pyroptosis in humans, but also a dampening mechanism. Recently, GSDMB was shown to mediate pyroptosis after cleavage by granzyme A delivered by natural killer cells [48] and caspase-1 [8].

Like their relatives, overexpression of the N-terminus of GSMDA or -C is cytotoxic [8,22]. Cancer cells expressing PDL1-induced GSDMC switch from chemotherapy- and TNF/cycloheximide-induced apoptosis to pyroptosis which is due to caspase-8-mediated generation of a cytotoxic N-GSDMC [20]. In contrast to other GSDMs, GSDMC is cleaved by caspase-8 at D365 within its C-GSDM domain instead of the hinge region (Figure 1A). With regard the physiological functions and upstream activating pathways of GSDMA, we are still groping in the dark (Table 1). In that respect, next to proteolytic cleavage by caspases, granzymes, cathepsins or ELANE, GSDMs might be activated by other mechanisms including gain-of-function mutations or splicing mechanisms. Indeed, gain-of-function mutations in mGSDMA3 and hGSDME associated with alopecia and hearing loss, respectively, apparently disrupt the C-GSDM domain and its autoinhibitory function resulting in cell death following transfection in Human Embryonic Kidney (HEK)293T cells [19,32]. Similarly, different splice variants of hGSDMB are associated with asthma [6], cancer [14] and multiple sclerosis [49], suggesting that GSDMB activity next to proteases might be regulated by alternative splicing as well.

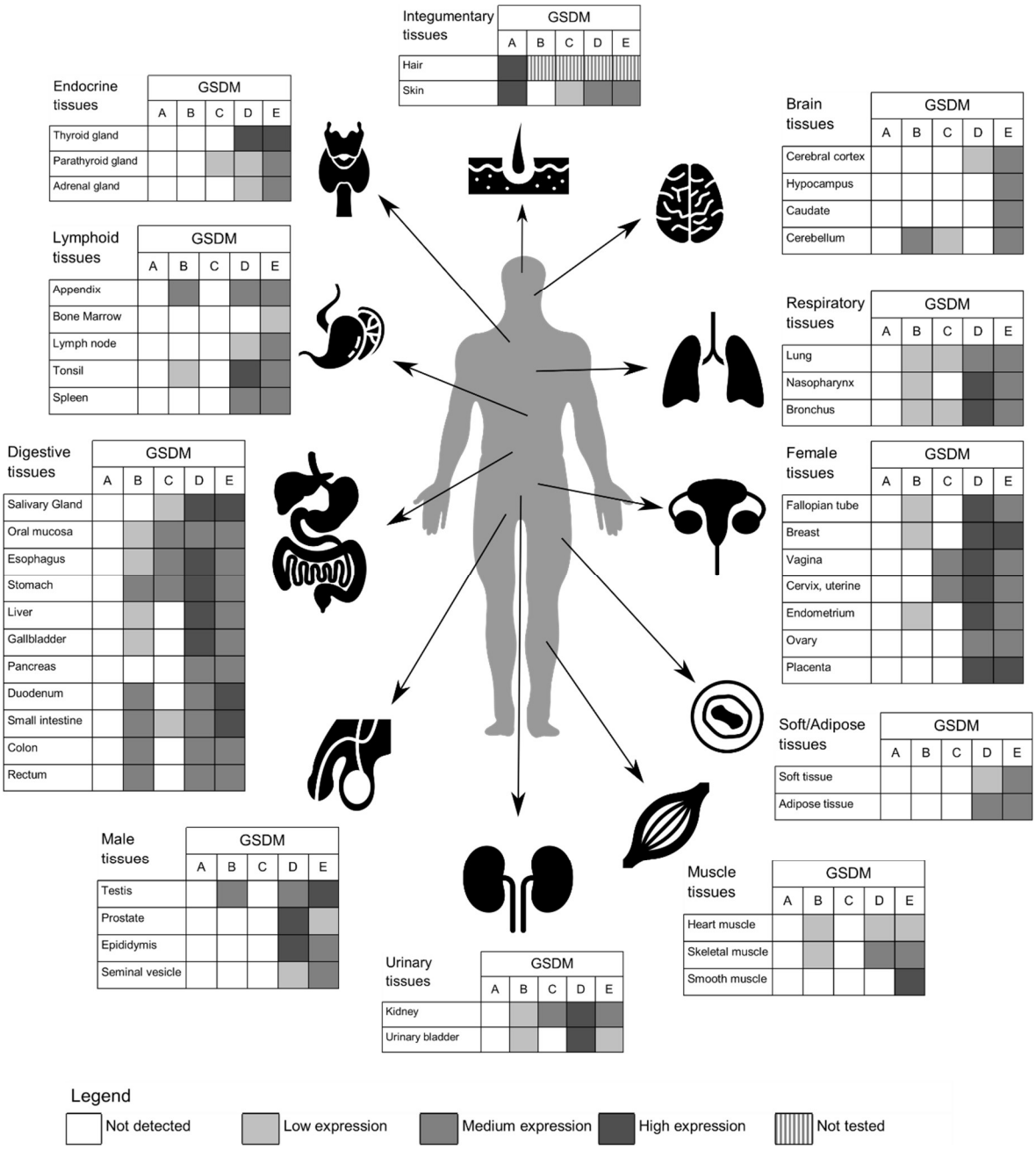

Figure 2. Protein expression overview of GSDMA-E in humans according to The Human Protein Atlas. Grayscale represents weighted and arbitrary annotation of cellular protein levels based on immunohistochemistry staining of tissues (intensity and relative fraction of positive cells) as described by the Human protein Atlas. Processing of the 3,3'-diaminobenzidine substrate by HRP linked to the secondary antibodies resulted in brown staining and the sections were furthermore counterstained with haematoxylin to enable visualization of microscopical features. All images of tissues stained by immunohistochemistry were annotated manually and can be found at v20.proteinatlas.org.

1.3 GSDMs show various expression patterns in human tissues

The various GSDMs show very different expression profiles in tissues, cell types and subcellular localizations, suggesting functions restricted to particular cells and organelles. Both GSDMD (inflammasome-mediated pyroptosis) and GSDME (apoptosis-driven secondary necrosis or pyroptosis) are widely expressed in many tissues and cell types (Figure 2, Figure S1 and Table S1). However, despite their ubiquitous expression, *Gsdmd*$^{-/-}$ and *Gsdme*$^{-/-}$ mice lack a spontaneous phenotype. This suggests a specific role during various challenges such as infection and cancer, which is supported by the high expression of GSDMD at sites of pathogen entry in humans such as the respiratory tract, the gastrointestinal tract and the urogenital system (Figure 2). In addition, GSDME expression was shown to increase macrophage-mediated phagocytosis and the number and function of tumour-infiltrating natural-killer and CD8+ T lymphocytes, thereby suppressing tumour growth [29]. The restricted expression pattern of GSDMA and -C in the skin (GSDMA) or in lung, buccal mucosa, esophagus and stomach (GSDMC) (Figure 2) may also be associated with particular challenge conditions. Moreover, some GSDMs are highly induced during conditions of cellular stress. GSDME expression is transcriptionally induced after dexamethasone treatment [50] and GSDMC expression is elevated *via* the immune checkpoint ligand PD-L1 under conditions of hypoxic stress [20]. Except from immunohistochemistry data of a limited amount of cell types (Table S1) and early studies distinguishing GSDM expression between differentiating (GSDMD, -C), differentiated (GSDMA, -C) and proliferating (GSDMB) esophagus and stomach epithelium [12], profound knowledge about GSDM expression in particular cell types is still lacking.

1.4 Mechanisms of auto-inhibition and release of N-GSDM from C-GSDM

The N- and C-terminal domains of unprocessed GSDM are kept in a closed autoinhibitory conformation. The crystal structure of GSDMA3 revealed that auto-inhibition is provided by two fitting hydrophobic interfaces and two regions of hydrogen bonds between N-GSDMA3 and C-GSDMA3 [22,78]. The hydrophobic interaction residues are highly conserved in the gasdermin family (GSDMA: L260, Y334, A338; GSDMA3: L270, Y344, A348; GSDMC: L319, Y398, A402; GSDMD: L290, Y373, A377; GSDME: F388, A392) (Figure 1A). Mutation of these residues even resulted in cytotoxicity of full-length GSDMA, -A3, -C, -D and -E after transient transfection in HEK293T cells [22], suggesting that the mechanism of auto-inhibition is shared between these members of the gasdermin family. For GSDMA, GSDMD and GSDME, the release of the auto-inhibitory C-terminal domain is required because the full-length proteins are not able to bind negatively charged phospholipids including phosphoinositides and cardiolipin [21,22,53]. However, the membrane recruitment mechanisms of GSDMB and PJVK are very different. N-GSDMB cannot bind cardiolipin but instead targets phosphoinositides and sulfatide (Table 1).

Moreover, the GSDMB C-terminal domain is not auto-inhibitory because it lacks the self-inhibitory hydrophobic residues mentioned above [62,78], allowing a more open conformation in its unprocessed form. As shown for GSDMA3, release from C-GSDM facilitates a drastic conformational change of N-GSDM, resulting in an open, elongated structure characterized by a large β-sheet composed of four intact β-strands (Figure 1B), crucial for membrane insertion [23]. Electrostatic binding to negatively charged phospholipids is conducted by a positively charged pocket between the α1 helix and inserting β-sheet of the open conformation that is shielded by C-GSDM in the closed conformation. Basic arginine and lysine residues (R9, R13 in GSDMA3) in the α1 helix are responsible for cardiolipin binding and are conserved among all GSDMs, including PJVK [22,23,78]. Nevertheless, this positively charged patch cannot explain the distinct binding of GSDMs to various lipids suggesting that other not yet defined lipid binding sites may be present or that distinct patches formed by oligomerization are required for membrane targeting.

Proteolytic cleavage in the hinge region (GSDMD and –E) or in C-GSDM (GSDMC) in order to expose N-GSDM requires docking of a protease on the unprocessed closed form of GSDM. In case of GSDMD the mechanism has been explored and involves an additional hydrophobic groove provided by a set of highly conserved residues in C-GSDMD (L304, L308, V364 and L367) (Figure S3). These hydrophobic residues are crucial for docking of activated caspases-1/4/11 through its small enzymatic domain (p10) followed by cleavage in the hinge region ($FLTD_{275}$) [79]. Sequence alignment between GSDMD and other GSDMs reveals that this hydrophobic docking station for caspase-1/4/11 in C-GSDMD apparently is a unique feature of GSDMD (Figure S3). Therefore, proteolytic activation of GSDMD by other proteases such as caspase-8, ELANE and cathepsin G (Table 1) probably involves other yet unrevealed protease docking stations in GSDMD and other GSDMs.

1.5 Gasdermins target different organelle membranes

At subcellular level, GSDM proteins during homeostasis are associated with the cytosol (GSDMA and –E; GSDMB to a lesser extent), nucleoplasm (GSDMB and –D; GSDMA to a lesser extent) and mitochondria (GSDMD and PJVK) [51] (data available from v20.proteinatlas.org). The physiological relevance of the distinct subcellular locations of the GSDM family members and whether it represents their processed form or not is currently unknown. N-GSDM domains of GSDMA3, -D, -E interact with negatively charged phosphoinositides at the inner leaflet of the plasma membrane, but also with the acidic lipid cardiolipin as revealed by binding of N-GSDM to phospholipid strips and membrane mimicking liposomes [21,22,52,53]. Cardiolipin under conditions of cellular stress is exposed at the outer membrane leaflet of bacteria and, in accordance with the endosymbiotic origin of mitochondria, also at the outer mitochondrial membrane. Indeed, it was shown that N-GSDMA, N-GSDMD and N-GSDME target mitochondria facilitating cyt c

release [54,55]. Likewise, during LPS-induced NETosis, N-GSDMD in a caspase-11 dependent manner is recruited to the nuclear envelop [30], suggesting that N-GSDMD may participate in nuclear envelop permeabilization allowing release of nuclear DNA. During PMA-induced NETosis, N-GSDMD targets ELANE-containing granules close to the plasma membrane, thereby releasing elastase in the cytosol and propagating plasma membrane permeabilization and release of NETs [31]. Similarly, N-GSDME generated by caspase-3 creates a positive feedback loop expediting apoptosis by facilitating mitochondrial cyt c release leading to apoptosome formation, further propagating caspase-3-mediated GSDME activation and plasma membrane targeting [54]. However, GSDM organelle targeting can be uncoupled from pyroptotic cell death as well. In NLRP3-activated neutrophils, N-GSDMD targets granules resulting in elastase release and inducing formation of $LC3^+$ autophagosomes, without targeting the plasma membrane nor facilitating lytic death [44]. Finally, N-GSDM activation is associated with **autophagy**, a cytoprotective adaptation mechanism to various forms of cellular stress. Expression of N-GSDMA3 and N-GSDMD in HEK293T cells resulted in an increase of the autophagic marker LC3-II next to mitochondria with decreased mitochondrial membrane potential [56], reflecting a possible role in mitophagy. These examples suggest that organelle targeting by GSDMs may precede eventual plasma membrane permeabilization or constitute an adaptive response following cellular stress. Another member of the GSDM family is PJVK that does not induce cell death but fulfils specialized functions in the homeostasis and adaptive responses following peroxisomal stress, explaining its localization at peroxisomal membranes [57,58]. Peroxisomal dynamics are indeed affected in PJVK knockout mice [57] as a result of impaired **pexophagy** [59], a peroxisome-specific form of autophagy [60].

1.6 Checkpoints of the cytotoxic function of N-GSDM by specific proteolysis, phosphorylation and exosome formation

Release of C-GSDM is not sufficient for oligomerization of N-GSDM, suggesting that additional regulatory mechanisms are implicated. Indeed, specific proteolysis and phosphorylation events within the N-terminal GSDM domain result in inactivation of their pore-forming function, providing an extra checkpoint functioning as a safeguard mechanism. Caspase-3 cleaves GSDMB and GSDMD at evolutionary conserved D91 and D87 residues, respectively [61,62], thereby generating an inactive p20 fragment instead of a membrane permeabilizing p30 N-GSDM domain (Figure 1A). The inactivating caspase-3 cleavage site is only present in the inflammasome-associated GSDMD and –B proteins, but not in GSDMA, -C and –E (Figure S2). As such, active caspase-3 generated during apoptotic conditions, may provide a conserved mechanism to prevent GSDMD-mediated pyroptosis and GSDMB's contribution to non-canonical caspase-4 activation [47], allowing apoptosis to occur instead of pyroptosis. This bias towards promoting apoptosis while preventing pyroptosis may favor a cellular fate that results in containment and phagocytic uptake of the cellular corpse, forming an additional mechanism how apoptosis contributes

to anti-inflammatory mechanisms by preventing pyroptosis. Similarly, enterovirus 71 (EV71) disrupts N-GSDMD activity by cleavage at the conserved residue Q193 by the viral protease 3C, showing that pathogens may conduct a similar strategy to repress inflammatory and antiviral responses [63]. In that respect, active N-GSDMD was shown to prevent EV71 replication in host cells [63].

Another mechanism inactivating the cytotoxicity of particular GSDMs is by phosphorylation at Thr6 in hGSDME or Thr8 in hGSDMA, preventing oligomerization of their N-terminal domains [54]. This kinase-sensitive threonine residue is only present and highly conserved in GSDMA, -B, -E and PJVK but absent in GSDMC and –D (Figure S2), suggesting that both regulatory mechanisms (inactivating proteolysis and phosphorylation) are shared by some but not all GSDM family members (Figure 1A).

Finally, ESCRT-mediated exosome formation established another protective mechanism against N-GSDM-mediated cell death [64]. Ca^{2+} influx through GSDMD pores, which is one of the first GSDMD-dependent events occurring during the pyroptotic process [65], triggers ESCRT-III proteins to repair the damaged plasma membrane by shedding the perforated plasma membrane areas as exosomes and thus removing the GSDMD pores [64]. In this scenario, only when the ESCRT-III machinery is inhibited or is overpowered by too many GSDMD pores, a cell will ultimately undergo necrotic cell death. The interaction between GSDMs and ESCRT-mediated protection mechanisms [64] may fine tune release of pro-inflammatory intracellular factors and may even represent a reversible way of GSDM activation. In conclusion, certain GSDMs share highly conserved residues that reflect similar mechanisms of autoinhibition based on hydrophobic interaction between N- and C-terminal domains (GSDMA,-C,-D,-E) (Box 1 and Figure 1) and similar mechanisms of recruitment to plasma membranes (GSDMA-E) (Table 1). Several mechanisms of negative regulation provided by phosphorylation (GSDMA,-B,-E), by alternative proteolytic cleavage within the cytotoxic N-GSDM domain (GSDMB,D) (Figure 1A) and by exosome formation *via* the ESCRT mechanism (GSDMD) serve as back up mechanism to dampen cell death. Also in case of MLKL-induced necroptosis [66,67] and bacterial toxins [68], ESCRT-III dependent detoxification mechanisms have been reported.

1.7 Phylogenetic analysis reveals a strong evolutionary variation in GSDM genes

Most gasdermins operate as final executioner molecules of different cell death modalities (apoptosis-driven secondary necrosis, pyroptosis, NETosis). This puts them in the frontline of selective pressure during infection and may explain some remarkable findings in the phylogenetic analysis such as sporadic GSDM gene ablations and numerous gene duplications (Figure 3). The global picture reveals that *GSDME* genes were found in all animals starting with the phylum of Cnidaria (hydroids, jellyfish, anemones, corals), the superphylum of Lophotrochozoa (molluscs, brachiopods, but not in annelids), and

Deuterostomata (echinoderms, hemichordates and chordates). Apparently, *GSDM*-like genes are absent in the whole superphylum of Ecdysozoa including arthropods and nematods. This almost ubiquitous presence of *GSDME* is probably related to its function as an executioner of apoptosis-driven secondary necrosis and pyroptosis. Indeed, biochemical and cellular studies revealed that coral GSDME is activated by caspase-3 cleavage and elicits pyroptosis following bacterial infection [69], representing the most ancestral function of GSDMs.

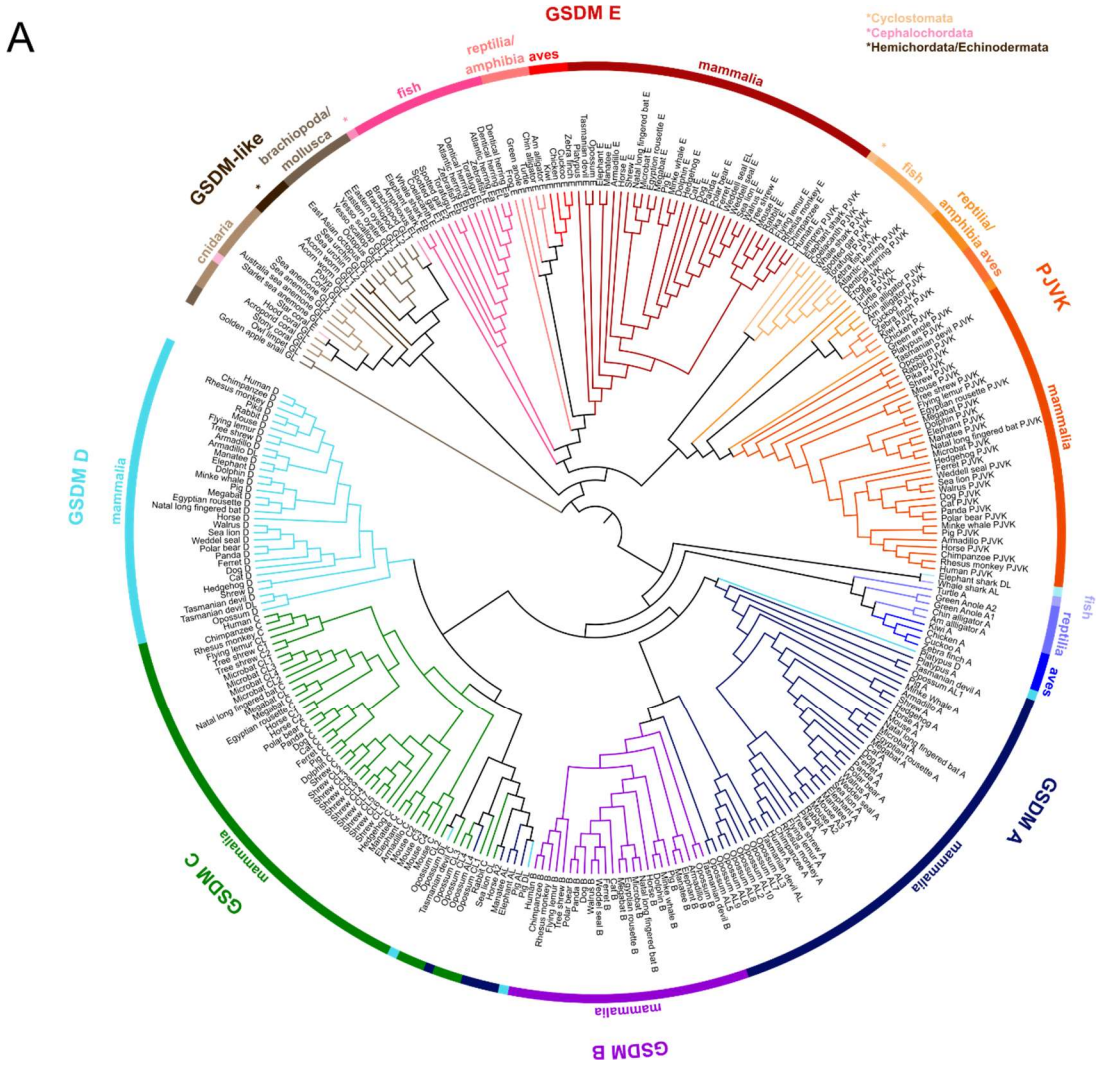

Figure 3. Phylogenetic analysis of GSDMA-E and PJVK Homologs. (A) A phylogenetic analysis was done on the publicly available genome assemblies of the indicated species for the presence or absence of GSDMA-E and PJVK proteins by utilizing the BLASTP algorithm against the predicted proteomes of these species. The presence or absence of these proteins was validated by a BLAST search of conserved sequences against the genome assemblies in combination with an evaluation of the completeness of the genomic context in the ENSEMBL, NCBI, and UCSC genome browsers. Species in each clade from which the genomes were investigated can be found in Table S2. If all of the above-mentioned analyses were negative, a gene was considered absent. The protein sequences of the putative GSDMA-E and PJVK homologs were aligned using Clustal Omega (v1.2.4) and the data are presented as unrooted circular phylogenetic tree by maximum likelihood using Mega (Molecular Evolutionary Genetics Analysis v.10.2.4). Final phylogenetic tree was edited with iTOL (Interactive Tree Of Life v5.7).

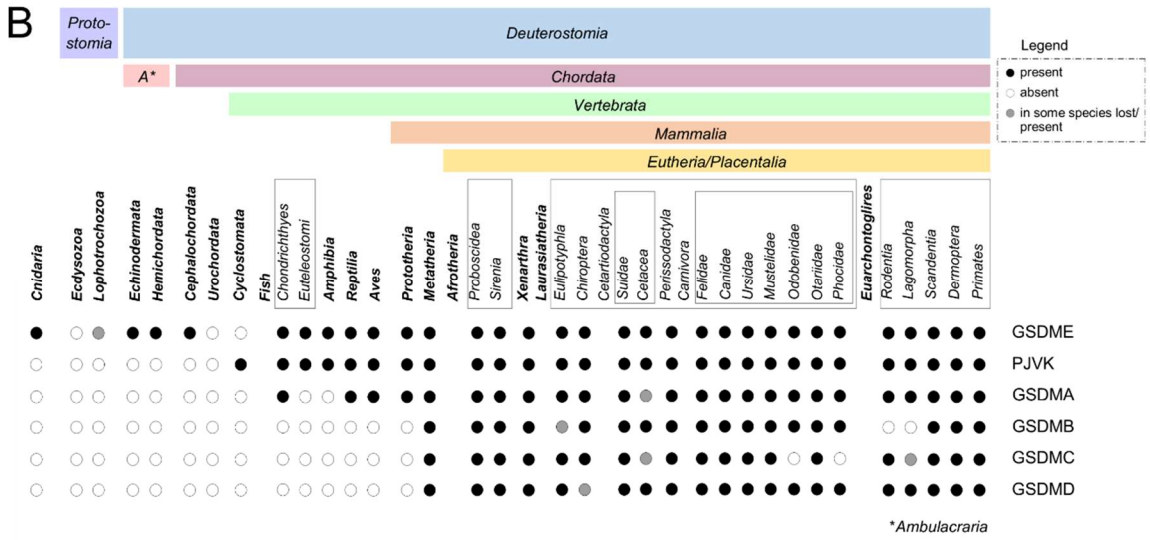

Figure 3 (continued). (B) Presence and absence of GSDMA-E and PJVK homologs in the Animal Kingdom based on the phylogenetic tree.

The PJVK gene emerged first in the subphylum of the Vertebrata, starting with the Cyclostomata (lamprey) and is found ubiquitously in fish, amphibians, reptiles, birds and mammalians. The phylogenetic tree reveals that it occurred by gene duplication from the ancestral *GSDME* gene. PJVK differs from other GSDMs in the sense that it has no pore forming capacity, while it acquired a novel unrelated function in peroxisome homeostasis [57]. *PJVK* mutants (a.o. DFNB59) in humans have been associated with noise-induced ROS-damage of hair cells and auditory neurons due to non-functional **pexophagy** [57,58]. This function of PJVK in hair cells and auditory neurons coincides with the evolution of a complex inner ear system in vertebrates, starting with the cyclostomes (lampreys) [70,71].

The next bifurcation in the evolution of the GSDM family is the occurrence of the *GSDMA* gene cluster in a few species of fish, and reptile, bird and mammalian species, while apparently lacking in amphibians. The *GSDMB* gene, located on the same chromosome as *GSDMA* gene, occurred by gene duplication of the *GSDMA* gene within marsupials (Metatheria) and placentals (Eutheria), together with two other gasdermin genes, *GSDMC* and *GSDMD*. This implies that fish, amphibians, reptiles, birds and platypus (an ancestral egg laying mammalian) lack the prototype inflammasome-activated GSDMD. In platypus a *GSDMD* gene has been annotated but appears in the phylogenetic cluster of *GSDMA* genes, suggesting it may result from a *GSDMA* gene duplication. That fish, amphibians, reptiles, birds and platypus lack GSDMD suggests that inflammasome-dependent pyroptosis in these clades may be accomplished by GSDME alone or in combination with GSDMA. Indeed, in case of fish (teleosts) it was reported that fish GSDME during infection and tissue damage can be activated both by caspase-1 representing inflammasome-mediated activation leading to pyroptosis and by caspase-3, representing an executioner role in pyroptosis and apoptosis-driven secondary necrosis [72–74]. Similar double

functions of GSDME during pyroptosis and apoptosis may occur also in other clades lacking GSDMD (cnidarians, molluscs, echinoderms, hemichordates, lampreys), as was shown experimentally in case of a coral species [69].

In marsupials (Metatheria) and placentals (Eutheria) an additional bifurcation of *GSDMA* genes led to the occurrence of the *GSDMB* gene. GSDMB is involved in regulating non-canonical pyroptosis as a direct activator of caspase-4, but is also negatively regulated by the latter [47]. In opossum, an explosion of *GSDMA* genes occurred, most of which annotate within the *GSDMB* phylogenetic cluster, and may therefore in fact belong to the latter class.

The occurrence of *GSDMB, GSDMC* and *GSDMD* genes in marsupials and placentals, and the many gene amplifications of *GSDMA* and *GSDMC* in partiular species (such as mice, but not in rats) argue for a strong evolutionary pressure favouring duplication and amplification of these genes. On the other hand, some orders and species completely lost *GSDMB, GSDMC* and *GSDMD* genes. There is an apparent loss of the *GSDMC* gene in several mammals that returned independently to the sea, representing a possible example of parallel evolution. Whales, but not dolphins, walrus and earless seals independently lost GSDMC, possibly as an adaptation to a different pathogen exposure associated with the return to sea life in which GSDMC-mediated responses may have been counter selected. However, this gene loss did not happen in the sea lions, fur seals and sea otter, questioning the general applicability of this return to the sea hypothesis.

In the monophyletic clade of rodents, lagomorphs, treeshrews, colugos and primates (Euarchontoglires) *GSDMB* is absent in the branch that includes mice, rats and rabbits, while it is present in the branch that delivered flying lemurs, tree shrew and primates, [68]. In mice, but not in rats or rabbits, *Gsdma* duplicated twice (*Gsdma1, Gsdma2, Gsdma3*) and *Gsdmc* duplicated even thrice (*Gsdmc1, Gsdmc2, Gsdmc3, Gsdmc4*). While the selective forces responsible for these gene losses and multiple gene duplications remain elusive, they feed the speculation that they may be associated with particular exposure to infectious microorganisms or viruses. In line with this hypothesis, GSDMA and –C are mainly expressed at sites of pathogen entry such as skin (GSDMA) and esophagus, stomach, cervix and vagina (GSDMC) (Figure 2). Some species (not all) of the Chiroptera (microbats) have lost the prototype pyroptotic *GSDMD*. Therefore it is tempting to speculate that absence (reptiles, birds) or loss (microbats) of *GSDMD*, although potentially compensated by other GSDMs, may explain why both birds and bats function as primary reservoirs for zoonotic viruses such as influenza A virus in birds and coronaviruses, hepaciviruses, pegiviruses and Ebola virus in bats [75,76]. Dampened Nlrp3 inflammasome responses have been hypothesized as an immunological explanation why bats can host many viruses without apparent pathological consequences for the host [77]. The absence of GSDMD may allow propagation of viruses without devastating immune responses in these reservoir species, facilitating viral transmission to other species [77].

Altogether, our phylogenetic analysis suggests that from gene duplication events in the Mammalia, except for the Prototheria, have evolved an extended set of gasdermin genes on top of the G*SDME* and *PJVK* genes: GSDMB by duplication of GSDMA in the same gene cluster, and further duplication of *GSDMC and GSDMD* in a next gene cluster. Although occurring in different phylogenetic clusters, both GSDMB and GSDMD are implicated in regulation of inflammasome-mediated pyroptosis, the former as an amplifier of caspase-4 activation [42] and the latter as the executioner of pyroptosis.

Most likely, evolution provided redundancy in the GSDM gene family to ensure pyroptotic cell death following cellular stress and infection, and the generation of an immunogenic environment to cope with associated threats. This implies that GSDM membrane targeting mechanisms may have a primary role as conduit for intra- and intercellular signalling following stress and infection preceding the cell death process. In that respect specific marking of organelles for pexophagy, **mitophagy** or **nucleophagy**, may be considered when studying the non-cell death related functions of GSDM family members. Furthermore, the high conservation of aspartate cleavage sites in the hinge region between the N-GSDM pore forming domain and the C-GSDM regulatory domain emphasizes the importance of caspase-dependent cleavage in their evolutionary selective function (Figure S2). The same applies for the highly conserved protective threonine-residue (Figure S2), reflecting the need for a tight regulation of these deadly proteins.

1.8 Concluding remarks

Functional GSDME was shown already in corals [69], suggesting that it fulfilled ancestral functions as final executioner of apoptosis-driven secondary necrosis and pyroptosis. The first gene amplification with the occurrence of the *PJVK* gene in Cyclostomes and all higher Vertebrates illustrates a second set of functions of GSDM family proteins in adaptive responses following organelle stress, marking stressed peroxisomes [57,59]. In more complex organisms in the animal kingdom starting from the Vertebrates, a combination of the need for specific execution mechanisms in particular cell types and their localization in particular organelles such as nucleus, mitochondria, granules, autophagosomes and peroxisomes (Table 1) may be reflected by the amplification of gasdermin genes. The organelle-specific functions need further research to reveal the molecular mechanisms implicated. The critical importance of GSDM activation is reflected by the fact that the two most common GSDME and GSDMD are a point of convergence for activation by different proteases (caspases, elastases, granzymes, cathepsins) as a point of integration of adaptive responses following infection or cellular stress, and explaining the high conservation of cleavage sites in the hinge region between the N-GSDM membrane permeabilizing domain and the C-GSDM regulatory domain (Figure S2). Moreover, additional checkpoints of GSDM functioning include negative regulation by phosphorylation of conserved threonine residues (GSDMA, -B, -E and PJVK) and proteolytic inactivation by

caspase-3 or viral protease 3C (GSDMB and –D), reflecting the need for fine-tuning and dampening after activation [54,61–64]. Also the functional interaction with ESCRT-III reflects the need for a dampening system following GSDM activation [64].

Bearing in mind that particular gene ablation and extensive *GSDM* duplications have occurred in particular taxa (some rodents, microbats and mammals returned to the sea) (Figure 3) may reflect a high evolutionary pressure associated with new habitats that have shaped species-specific balances of GSDMs, but also illustrates the high redundancy of some GSDM members compensating the loss. The restricted expression pattern of some GSDM family members in normal conditions might be misleading and may hide important adaptive functions of GSDMA, -B, and -C during infection and cellular stress, as was recently shown for GSDMC showing upregulated expression and execution of pyroptosis-like cell death during hypoxic stress [20].

Acknowledgements

Research in the Vandenabeele group is supported by Flemish grants (EOS MODEL-IDI, FWO Grant 30826052), FWO research grants G.0E04.16N, G.0C76.18N, G.0B71.18N, G.0B96.20N), Methusalem (BOF16/MET_V/007), Foundation against Cancer (FAF-F/2016/865), CRIG and GIGG consortia, and VIB. Research in the lab of G.V.C is supported by research grants awarded by the University of Antwerp (BOF/Methusalem grant 42/FA020000/FFB190208). Research in the A.W. lab is supported by the Fund for Scientific Research-Flanders (Odysseus grant G.0C49.13N and FWO research grants G035117N, 3G0H5517, 3G044718, 3G044818, 1.5.091.18N and S008419N), by Ghent University (BOF24Y2019003201) and by the Cure-AID Grant from the European Union ERA-Net for Research Programs on Rare Diseases.

Declaration of Interests

The authors declare no competing interests.

References

1. Saeki, N. *et al.* (2000) Gasdermin (Gsdm) localizing to mouse Chromosome 11 is predominantly expressed in upper gastrointestinal tract but significantly suppressed in human gastric cancer cells. *Mamm. Genome* 11, 718–24
2. Tamura, M. *et al.* (2007) Members of a novel gene family, Gsdm, are expressed exclusively in the epithelium of the skin and gastrointestinal tract in a highly tissue-specific manner. *Genomics* 89, 618–629
3. Runkel, F. *et al.* (2004) The dominant alopecia phenotypes Bareskin, Rex-denuded, and Reduced Coat 2 are caused by mutations in gasdermin 3. *Genomics* 84, 824–835
4. Lunny, D.P. *et al.* (2005) Mutations in Gasdermin 3 Cause Aberrant Differentiation of the Hair Follicle and Sebaceous Gland. *J. Invest. Dermatol.* 124, 615–621
5. Yu, J. *et al.* (2011) Polymorphisms in GSDMA and GSDMB are associated with asthma susceptibility, atopy and BHR. *Pediatr. Pulmonol.* 46, 701–708
6. Das, S. *et al.* (2016) GSDMB induces an asthma phenotype characterized by increased airway responsiveness and remodeling without lung inflammation. *Proc. Natl. Acad. Sci.* 113, 13132–13137
7. Zihlif, M. *et al.* (2016) Association Between Gasdermin A and Gasdermin B Polymorphisms and Susceptibility to Adult and Childhood Asthma Among Jordanians. *Genet. Test. Mol. Biomarkers* 20, 143–148
8. Panganiban, R.A. *et al.* (2018) A functional splice variant associated with decreased asthma risk abolishes the ability of gasdermin B to induce epithelial cell pyroptosis. *J. Allergy Clin. Immunol.* 142, 1469–1478
9. Van Laer, L. *et al.* (1998) Nonsyndromic hearing impairment is associated with a mutation in DFNA5. *Nat. Genet.* 20, 194–197
10. Delmaghani, S. *et al.* (2006) Mutations in the gene encoding pejvakin, a newly identified protein of the afferent auditory pathway, cause DFNB59 auditory neuropathy. *Nat. Genet.* 38, 770–8
11. Saeki, N. *et al.* (2007) GASDERMIN, suppressed frequently in gastric cancer, is a target of LMO1 in TGF-β-dependent apoptotic signalling. *Oncogene* 26, 6488–6498
12. Saeki, N. *et al.* (2009) Distinctive expression and function of four *GSDM* family genes (*GSDMA-D*) in normal and malignant upper gastrointestinal epithelium. *Genes, Chromosom. Cancer* 48, 261–271
13. Carl-McGrath, S. *et al.* (2008) Differential expression and localisation of gasdermin-like (GSDML), a novel member of the cancer-associated GSDMDC protein family, in neoplastic and non-neoplastic gastric, hepatic, and colon tissues. *Pathology* 40, 13–24
14. Hergueta-Redondo, M. *et al.* (2014) Gasdermin-B promotes invasion and metastasis in breast cancer cells. *PLoS One* 9, 1–15
15. Miguchi, M. *et al.* (2016) Gasdermin C Is Upregulated by Inactivation of Transforming Growth Factor β Receptor Type II in the Presence of Mutated Apc, Promoting Colorectal Cancer Proliferation. *PLoS One* 11, 1–18
16. Katoh, M. and Katoh, M. (2004) Identification and characterization of human DFNA5L, mouse Dfna5l, and rat Dfna5l genes in silico. *Int. J. Oncol.* 25, 765–70
17. Rogers, C. *et al.* (2017) Cleavage of DFNA5 by caspase-3 during apoptosis mediates progression to secondary necrotic/pyroptotic cell death. *Nat. Commun.* 8, 14128
18. Kayagaki, N. *et al.* (2015) Caspase-11 cleaves gasdermin D for non-canonical inflammasome signalling. *Nature* 526, 666–671

19. Shi, J. *et al.* (2015) Cleavage of GSDMD by inflammatory caspases determines pyroptotic cell death. *Nature* 526, 660–665
20. Hou, J. *et al.* (2020) PD-L1-mediated gasdermin C expression switches apoptosis to pyroptosis in cancer cells and facilitates tumour necrosis. *Nat. Cell Biol.* 22, 1264–1275
21. Wang, Y. *et al.* (2017) Chemotherapy drugs induce pyroptosis through caspase-3 cleavage of a gasdermin. *Nature* 547, 99–103
22. Ding, J. *et al.* (2016) Pore-forming activity and structural autoinhibition of the gasdermin family. *Nature* 535, 111–116
23. Ruan, J. *et al.* (2018) Cryo-EM structure of the gasdermin A3 membrane pore. *Nature* 557, 62–67
24. Kuang, S. *et al.* (2017) Structure insight of GSDMD reveals the basis of GSDMD autoinhibition in cell pyroptosis. *Proc. Natl. Acad. Sci. U. S. A.* DOI: 10.1073/pnas.1708194114
25. Galluzzi, L. *et al.* (2018) Molecular mechanisms of cell death: recommendations of the Nomenclature Committee on Cell Death 2018. *Cell Death Differ.* 25, 486–541
26. Yu, J. *et al.* (2019) Cleavage of GSDME by caspase-3 determines lobaplatin-induced pyroptosis in colon cancer cells. *Cell Death Dis.* 10, 1–20
27. Lu, H. *et al.* (2018) Molecular targeted therapies elicit concurrent apoptotic and GSDME-dependent pyroptotic tumor cell death. *Clin. Cancer Res.* 24, 6066–6077
28. Wang, Y. *et al.* (2018) GSDME mediates caspase-3-dependent pyroptosis in gastric cancer. *Biochem. Biophys. Res. Commun.* 495, 1418–1425
29. Zhang, Z. *et al.* (2020) Gasdermin E suppresses tumour growth by activating anti-tumour immunity. *Nature* 579, 1–6
30. Chen, K.W. *et al.* (2018) Noncanonical inflammasome signaling elicits gasdermin D-dependent neutrophil extracellular traps. *Sci. Immunol.* 3, eaar6676
31. Sollberger, G. *et al.* (2018) Gasdermin D plays a vital role in the generation of neutrophil extracellular traps. *Sci. Immunol.* 3, 1–12
32. Op de Beeck, K. *et al.* (2011) The DFNA5 gene, responsible for hearing loss and involved in cancer, encodes a novel apoptosis-inducing protein. *Eur. J. Hum. Genet.* 19, 965–973
33. Lee, B.L. *et al.* (2018) ASC- and caspase-8-dependent apoptotic pathway diverges from the NLRC4 inflammasome in macrophages. *Sci. Rep.* 8, 3788
34. Tixeira, R. *et al.* (2018) Gasdermin E Does Not Limit Apoptotic Cell Disassembly by Promoting Early Onset of Secondary Necrosis in Jurkat T Cells and THP-1 Monocytes. *Front. Immunol.* 9, 2842
35. Kayagaki, N. *et al.* (2021) NINJ1 mediates plasma membrane rupture during lytic cell death. *Nature* DOI: 10.1038/s41586-021-03218-7
36. Kang, R. *et al.* (2018) Lipid Peroxidation Drives Gasdermin D-Mediated Pyroptosis in Lethal Polymicrobial Sepsis. *Cell Host Microbe* 24, 97–108
37. Sborgi, L. *et al.* (2016) GSDMD membrane pore formation constitutes the mechanism of pyroptotic cell death. *EMBO J.* 35, 1766–78
38. Xia, X. *et al.* (2018) Atypical Gasdermin D and Mixed Lineage Kinase Domain-like Protein Leakage Aggravates Tetrachlorobenzoquinone-Induced Nod-like Receptor Protein 3 Inflammasome Activation. *Chem. Res. Toxicol.* 13, 1418–1425
39. He, W. *et al.* (2015) Gasdermin D is an executor of pyroptosis and required for interleukin-1β secretion. *Cell Res.* 25, 1285–1298
40. Orning, P. *et al.* (2018) Pathogen blockade of TAK1 triggers caspase-8-dependent cleavage of gasdermin D and cell death. *Science* 362, 1064–1069

41. Sarhan, J. *et al.* (2018) Caspase-8 induces cleavage of gasdermin D to elicit pyroptosis during Yersinia infection. *Proc. Natl. Acad. Sci. U. S. A.* 115, E10888–E10897
42. Chen, K.W. *et al.* (2019) Extrinsic and intrinsic apoptosis activate pannexin-1 to drive NLRP3 inflammasome assembly. *EMBO J.* 38, 1–12
43. Malireddi, R.K.S. *et al.* (2020) Innate immune priming in the absence of TAK1 drives RIPK1 kinase activity-independent pyroptosis, apoptosis, necroptosis, and inflammatory disease. *J. Exp. Med.* 217, 1–13
44. Karmakar, M. *et al.* (2020) N-GSDMD trafficking to neutrophil organelles facilitates IL-1β release independently of plasma membrane pores and pyroptosis. *Nat. Commun.* 11, 1–14
45. Burgener, S.S. *et al.* (2019) Cathepsin G Inhibition by Serpinb1 and Serpinb6 Prevents Programmed Necrosis in Neutrophils and Monocytes and Reduces GSDMD-Driven Inflammation. *Cell Rep.* 27, 3646–3656
46. Demarco, B. *et al.* (2020) Caspase-8-dependent gasdermin D cleavage promotes antimicrobial defense but confers susceptibility to TNF-induced lethality. *Sci. Adv.* 6, 3465–3483
47. Chen, Q. *et al.* (2018) GSDMB promotes non-canonical pyroptosis by enhancing caspase-4 activity. *J. Mol. Cell Biol.* 11, 496–508
48. Zhou, Z. *et al.* (2020) Granzyme A from cytotoxic lymphocytes cleaves GSDMB to trigger pyroptosis in target cells. *Science (80-.).* 368, 1–9
49. Cardamone, G. *et al.* (2017) The Characterization of GSDMB Splicing and Backsplicing Profiles Identifies Novel Isoforms and a Circular RNA That Are Dysregulated in Multiple Sclerosis. *Int. J. Mol. Sci.* 18, 576
50. Webb, M.S. *et al.* (2007) In CEM cells the autosomal deafness gene dfna5 is regulated by glucocorticoids and forskolin. *J. Steroid Biochem. Mol. Biol.* 107, 15–21
51. Thul, P.J. *et al.* (2017) A subcellular map of the human proteome. *Science (80-.).* 356, 1–12
52. Aglietti, R.A. *et al.* (2016) GsdmD p30 elicited by caspase-11 during pyroptosis forms pores in membranes. *Proc. Natl. Acad. Sci.* 113, 7858–7863
53. Liu, X. *et al.* (2016) Inflammasome-activated gasdermin D causes pyroptosis by forming membrane pores. *Nature* 535, 153–8
54. Rogers, C. *et al.* (2019) Gasdermin pores permeabilize mitochondria to augment caspase-3 activation during apoptosis and inflammasome activation. *Nat. Commun.* 10, 1689
55. Platnich, J.M. *et al.* (2018) Shiga Toxin/Lipopolysaccharide Activates Caspase-4 and Gasdermin D to Trigger Mitochondrial Reactive Oxygen Species Upstream of the NLRP3 Inflammasome. *Cell Rep.* 25, 1525-1536.e7
56. Shi, P. *et al.* (2015) Loss of conserved Gsdma3 self-regulation causes autophagy and cell death. *Biochem. J.* 468, 325–336
57. Delmaghani, S. *et al.* (2015) Hypervulnerability to Sound Exposure through Impaired Adaptive Proliferation of Peroxisomes. *Cell* 163, 894–906
58. Mardones, P. and Hetz, C. (2015) Peroxisomes Get Loud: A Redox Antidote to Hearing Loss. *Cell* 163, 790–791
59. Defourny, J. *et al.* (2019) Pejvakin-mediated pexophagy protects auditory hair cells against noise-induced damage. *Proc. Natl. Acad. Sci. U. S. A.* 116, 8010–8017
60. Dunn, Jr., W.A. *et al.* (2005) Pexophagy: The Selective Autophagy of Peroxisomes. *Autophagy* 1, 75–83

61. Taabazuing, C.Y. *et al.* (2017) Pyroptosis and Apoptosis Pathways Engage in Bidirectional Crosstalk in Monocytes and Macrophages. *Cell Chem. Biol.* 24, 507–514
62. Chao, K.L. *et al.* (2017) Gene polymorphism linked to increased asthma and IBD risk alters gasdermin-B structure, a sulfatide and phosphoinositide binding protein. *Proc. Natl. Acad. Sci.* 114, E1128–E1137
63. Lei, X. *et al.* (2017) Enterovirus 71 Inhibits Pyroptosis through Cleavage of Gasdermin D. *J. Virol.* 91,
64. Rühl, S. *et al.* (2018) ESCRT-dependent membrane repair negatively regulates pyroptosis downstream of GSDMD activation. *Science (80-.).* 362, 956–960
65. de Vasconcelos, N.M. *et al.* (2018) Single-cell analysis of pyroptosis dynamics reveals conserved GSDMD-mediated subcellular events that precede plasma membrane rupture. *Cell Death Differ.* DOI: 10.1038/s41418-018-0106-7
66. Gong, Y.-N. *et al.* (2017) ESCRT-III Acts Downstream of MLKL to Regulate Necroptotic Cell Death and Its Consequences. *Cell* 169, 286-300.e16
67. Yoon, S. *et al.* (2017) MLKL, the Protein that Mediates Necroptosis, Also Regulates Endosomal Trafficking and Extracellular Vesicle Generation. *Immunity* 47, 51-65.e7
68. Romero, M. *et al.* (2017) Intrinsic repair protects cells from pore-forming toxins by microvesicle shedding. *Cell Death Differ.* 24, 798–808
69. Jiang, S. *et al.* (2020) Coral gasdermin triggers pyroptosis. *Sci. Immunol.* 5, eabd2591
70. Fritzsch, B. and Beisel, K.W. (2003) Molecular Conservation and Novelties in Vertebrate Ear Development. *Curr. Top. Dev. Biol.* 57, 1–44
71. Higuchi, S. *et al.* (2019) Inner ear development in cyclostomes and evolution of the vertebrate semicircular canals. *Nature* 565, 347–350
72. Jiang, S. *et al.* (2019) Teleost Gasdermin E Is Cleaved by Caspase 1, 3, and 7 and Induces Pyroptosis. *J. Immunol.* 203, 1369–1382
73. Wang, Z. *et al.* (2020) Zebrafish GSDMEb Cleavage-Gated Pyroptosis Drives Septic Acute Kidney Injury In Vivo. *J. Immunol.* 204, 1929–1942
74. Li, J.Y. *et al.* (2020) The zebrafish NLRP3 inflammasome has functional roles in ASC-dependent interleukin-1β maturation and gasdermin E-mediated pyroptosis. *J. Biol. Chem.* 295, 1120–1141
75. Quan, P.L. *et al.* (2013) Bats are a major natural reservoir for hepaciviruses and pegiviruses. *Proc. Natl. Acad. Sci. U. S. A.* 110, 8194–8199
76. Van Nguyen, D. *et al.* (2018) Detection and characterization of homologues of human hepatitis viruses and pegiviruses in rodents and bats in Vietnam. *Viruses* 10, 102
77. Ahn, M. *et al.* (2019) Dampened NLRP3-mediated inflammation in bats and implications for a special viral reservoir host. *Nat. Microbiol.* 4, 789–799
78. Ruan, J. (2019) Structural Insight of Gasdermin Family Driving Pyroptotic Cell Death. In *Structural Immunology* pp. 189–205
79. Wang, K. *et al.* (2020) Structural Mechanism for GSDMD Targeting by Autoprocessed Caspases in Pyroptosis. *Cell* 180, 941–955
80. Kambara, H. *et al.* (2018) Gasdermin D Exerts Anti-inflammatory Effects by Promoting Neutrophil Death. *Cell Rep.* 22, 2924–2936
81. Zhou, B. *et al.* (2018) Tom20 senses iron-activated ROS signaling to promote melanoma cell pyroptosis. *Cell Res.* 28, 1171–1185
82. Chen, X. *et al.* (2016) Pyroptosis is driven by non-selective gasdermin-D pore and its morphology is different from MLKL channel-mediated necroptosis. *Cell Res.* 26, 1007–20

Glossary

Autophagy: A biological process that involves the enzymatic breakdown of a cell's cytoplasm or cytoplasmic components (such as damaged or unneeded organelles or proteins) within the lysosomes of the same cell.

Canonical inflammasome activation: Canonical inflammasome activation involves cytosolic detection of pathogen-associated molecular patterns (PAMPs) or damage/danger-associated molecular patterns (DAMPs), followed by the formation of inflammasome complexes leading to caspase-1 dependent processing of GSDMD as well as the pro-forms of IL-1β and IL-18, culminating in pyroptosis and cytokine secretion.

Gasdermin: Gasdermin (GSDM) is a member of the gasdermin protein family, characterized by a conserved gasdermin-domain at the N-terminal end (N-GSDM). Release of N-GSDM from the autoinhibitory C-terminal end (C-GSDM) by specific proteolysis or other yet to be determined mechanisms results in organelle membrane translocation and plasma membrane recruitment and permeabilization, contributing to necrotic cell death modalities.

Mitophagy: Type of specialized macroautophagy that selectively recognizes damaged or stressed mitochondria and targets them to lysosomes for degradation.

NETosis: Regulated necrotic cell death fate characterized in neutrophils following contact with PAMPs leading to the release of neutrophil extracellular traps (NETs) consisting of decondensed chromatin and granular contents to the extracellular space ensnaring extracellular pathogens.

Non-canonical inflammasome activation: Non-canonical inflammasome activation involves cytosolic detection of LPS derived from a Gram-negative infection leading to activation of caspase-11 in mice and caspase-4/5 in humans, after which caspase-4/5/11 directly cleaves GSDMD and initiates pyroptosis without the need for caspase-1 activity. Caspase-1 is activated secondary to GSDMD pore formation and subsequently facilitates maturation and secretion of IL-1β and IL-18.

Nucleophagy: Type of specialized macroautophagy that selectively recognizes damaged or stressed nuclear envelopes and targets them to lysosomes for degradation.

Pexophagy: Type of specialized macroautophagy that selectively recognizes damaged or stressed peroxisomes and targets them to lysosomes for degradation.

Pore formation: Membranous conformational changes resulting in membrane permeabilization due to amphipathic interaction of membrane targeting proteins or peptides with cellular (plasma) membranes.

Primary necrosis: Immediate regulated necrotic cell death fate without preliminary signs of apoptosis as opposed to apoptosis-driven secondary necrosis.

Pyroptosis: Current definition: GSDM-mediated cell death. Former definition: Regulated primary necrotic cell death fate associated with infection and induced by canonical or non-

canonical inflammasome activation resulting in caspase-1/4/5/11-mediated activation of GSDMD as well as IL-1β and IL-18 maturation and secretion.

Regulated necrosis: Necrotic cell death fate involving active mechanisms of plasma membrane permeabilization such as protease-dependent gasdermin activation (secondary necrosis, pyroptosis), kinase-dependent MLKL activation (necroptosis) or lipid peroxidation (ferroptosis). The morphology is characterized by cellular swelling (oncosis) and plasma membrane permeabilization.

Secondary necrosis: Regulated necrotic cell death fate following caspase-dependent apoptosis. Occurs *in vitro* and *in vivo* in the absence of phagocytic cell capacity. Recently, plasma membrane permeabilization during secondary necrosis has been associated with caspase-3-mediated GSDME activation.

Supplementary material

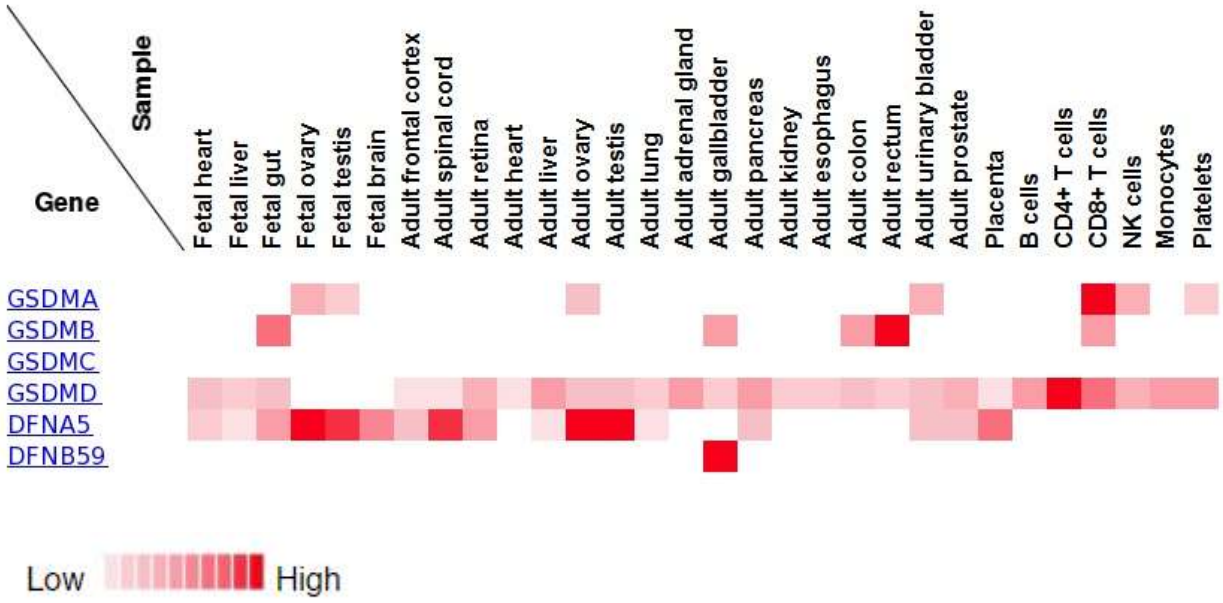

Figure S1. Protein expression overview of GSDMA, -B, -C, -D, -E (DFNA5) and PJVK (DFNB59) in humans according to The Human Proteome Map in different tissues and cell types. Expression levels are based on mass spectrometry-based proteomics data. Averaged spectral counts per gene per sample were used to plot the white-to-red gradient heat map for the gasdermin genes. Data can be found on http://www.humanproteomemap.org/ [1].

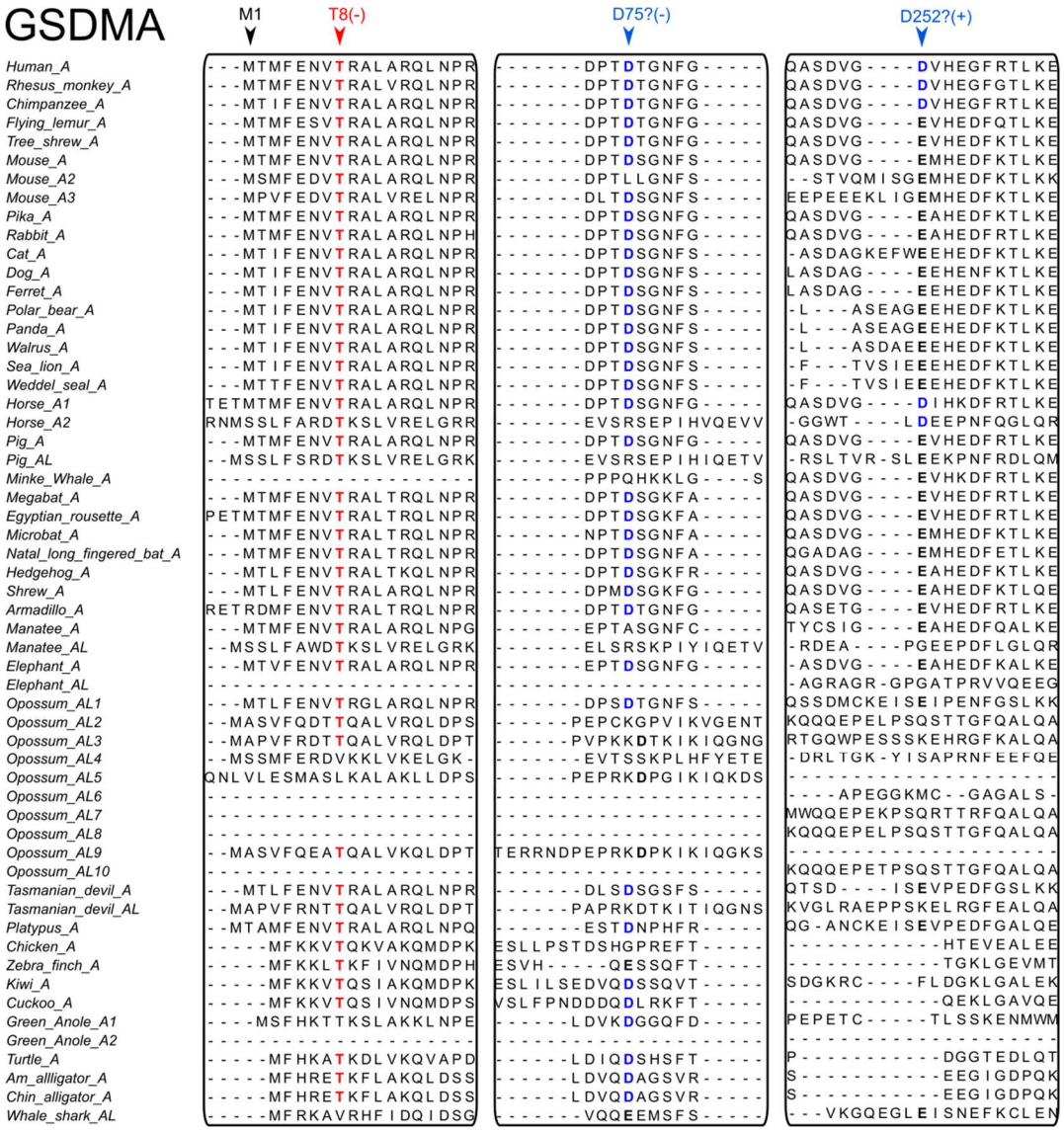
GSDMA
M1
T8(-)
D75?(-)
D252?(+)
Human_A
Rhesus_monkey_A
Chimpanzee_A
Flying_lemur_A
Tree_shrew_A
Mouse_A
Mouse_A2
Mouse_A3
Pika_A
Rabbit_A
Cat_A
Dog_A
Ferret_A
Polar_bear_A
Panda_A
Walrus_A
Sea_lion_A
Weddel_seal_A
Horse_A1
Horse_A2
Pig_A
Pig_AL
Minke_Whale_A
Megabat_A
Egyptian_rousette_A
Microbat_A
Natal_long_fingered_bat_A
Hedgehog_A
Shrew_A
Armadillo_A
Manatee_A
Manatee_AL
Elephant_A
Elephant_AL
Opossum_AL1
Opossum_AL2
Opossum_AL3
Opossum_AL4
Opossum_AL5
Opossum_AL6
Opossum_AL7
Opossum_AL8
Opossum_AL9
Opossum_AL10
Tasmanian_devil_A
Tasmanian_devil_AL
Platypus_A
Chicken_A
Zebra_finch_A
Kiwi_A
Cuckoo_A
Green_Anole_A1
Green_Anole_A2
Turtle_A
Am_alligator_A
Chin_alligator_A
Whale_shark_AL

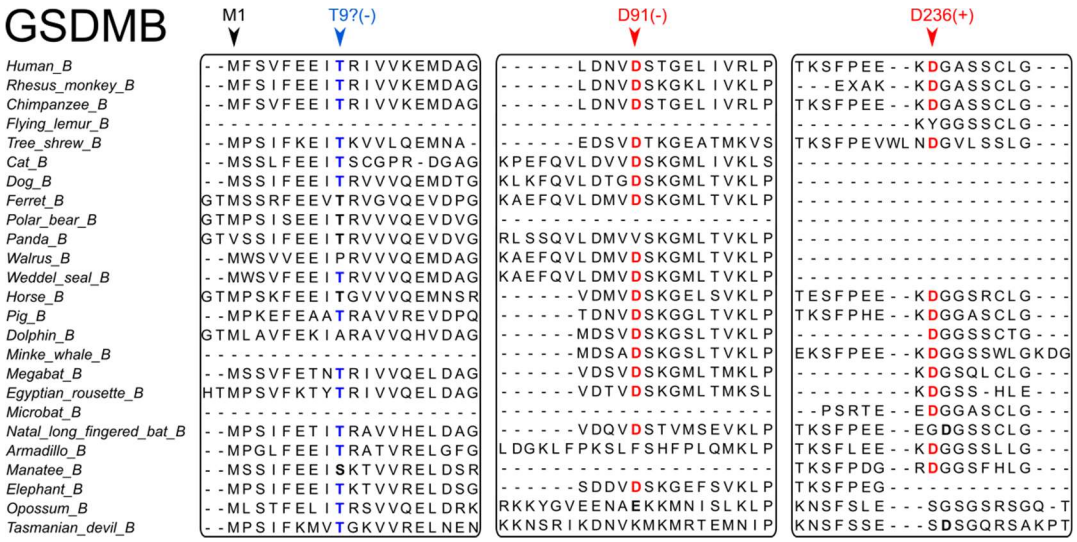
GSDMB
M1
T9?(-)
D91(-)
D236(+)
Human_B
Rhesus_monkey_B
Chimpanzee_B
Flying_lemur_B
Tree_shrew_B
Cat_B
Dog_B
Ferret_B
Polar_bear_B
Panda_B
Walrus_B
Weddel_seal_B
Horse_B
Pig_B
Dolphin_B
Minke_whale_B
Megabat_B
Egyptian_rousette_B
Microbat_B
Natal_long_fingered_bat_B
Armadillo_B
Manatee_B
Elephant_B
Opossum_B
Tasmanian_devil_B

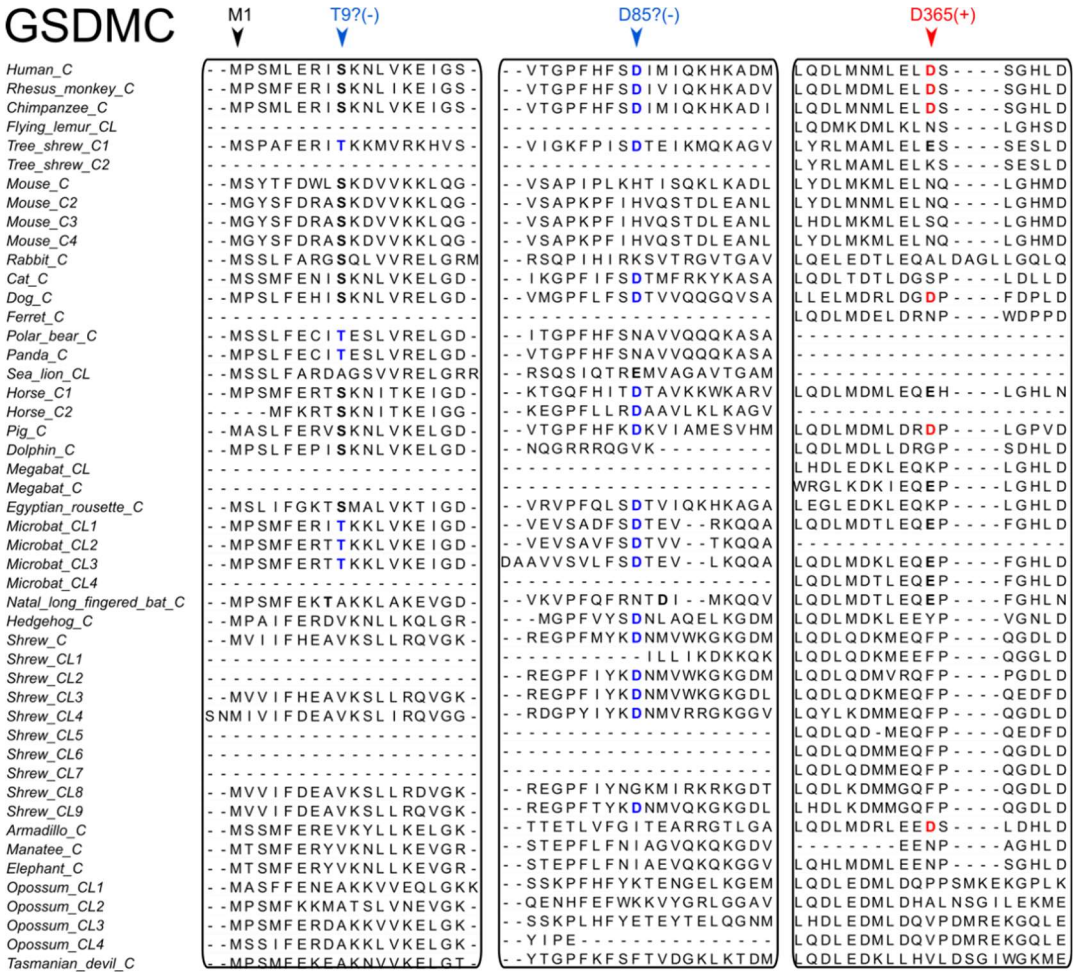
GSDMC
M1
T9?(-)
D85?(-)
D365(+)
Human_C
Rhesus_monkey_C
Chimpanzee_C
Flying_lemur_CL
Tree_shrew_C1
Tree_shrew_C2
Mouse_C
Mouse_C2
Mouse_C3
Mouse_C4
Rabbit_C
Cat_C
Dog_C
Ferret_C
Polar_bear_C
Panda_C
Sea_lion_CL
Horse_C1
Horse_C2
Pig_C
Dolphin_C
Megabat_CL
Megabat_C
Egyptian_rousette_C
Microbat_CL1
Microbat_CL2
Microbat_CL3
Microbat_CL4
Natal_long_fingered_bat_C
Hedgehog_C
Shrew_C
Shrew_CL1
Shrew_CL2
Shrew_CL3
Shrew_CL4
Shrew_CL5
Shrew_CL6
Shrew_CL7
Shrew_CL8
Shrew_CL9
Armadillo_C
Manatee_C
Elephant_C
Opossum_CL1
Opossum_CL2
Opossum_CL3
Opossum_CL4
Tasmanian_devil_C

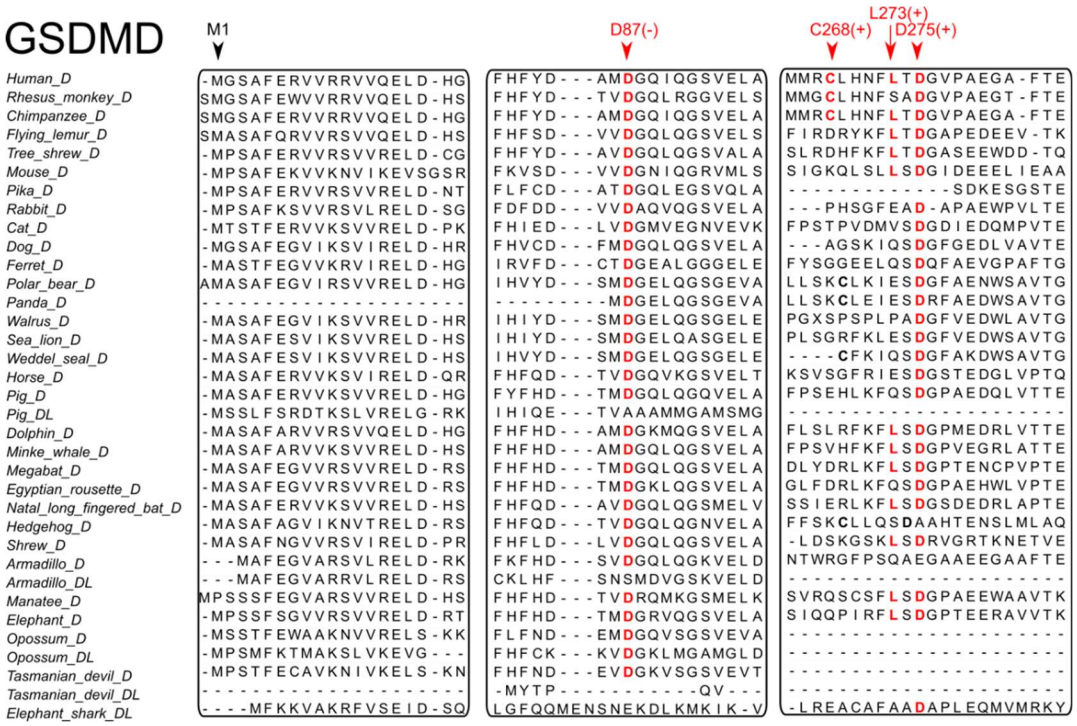
GSDMD
M1
D87(-)
C268(+)
L273(+)
D275(+)
Human_D
Rhesus_monkey_D
Chimpanzee_D
Flying_lemur_D
Tree_shrew_D
Mouse_D
Pika_D
Rabbit_D
Cat_D
Dog_D
Ferret_D
Polar_bear_D
Panda_D
Walrus_D
Sea_lion_D
Weddel_seal_D
Horse_D
Pig_D
Pig_DL
Dolphin_D
Minke_whale_D
Megabat_D
Egyptian_rousette_D
Natal_long_fingered_bat_D
Hedgehog_D
Shrew_D
Armadillo_D
Armadillo_DL
Manatee_D
Elephant_D
Opossum_D
Opossum_DL
Tasmanian_devil_D
Tasmanian_devil_DL
Elephant_shark_DL

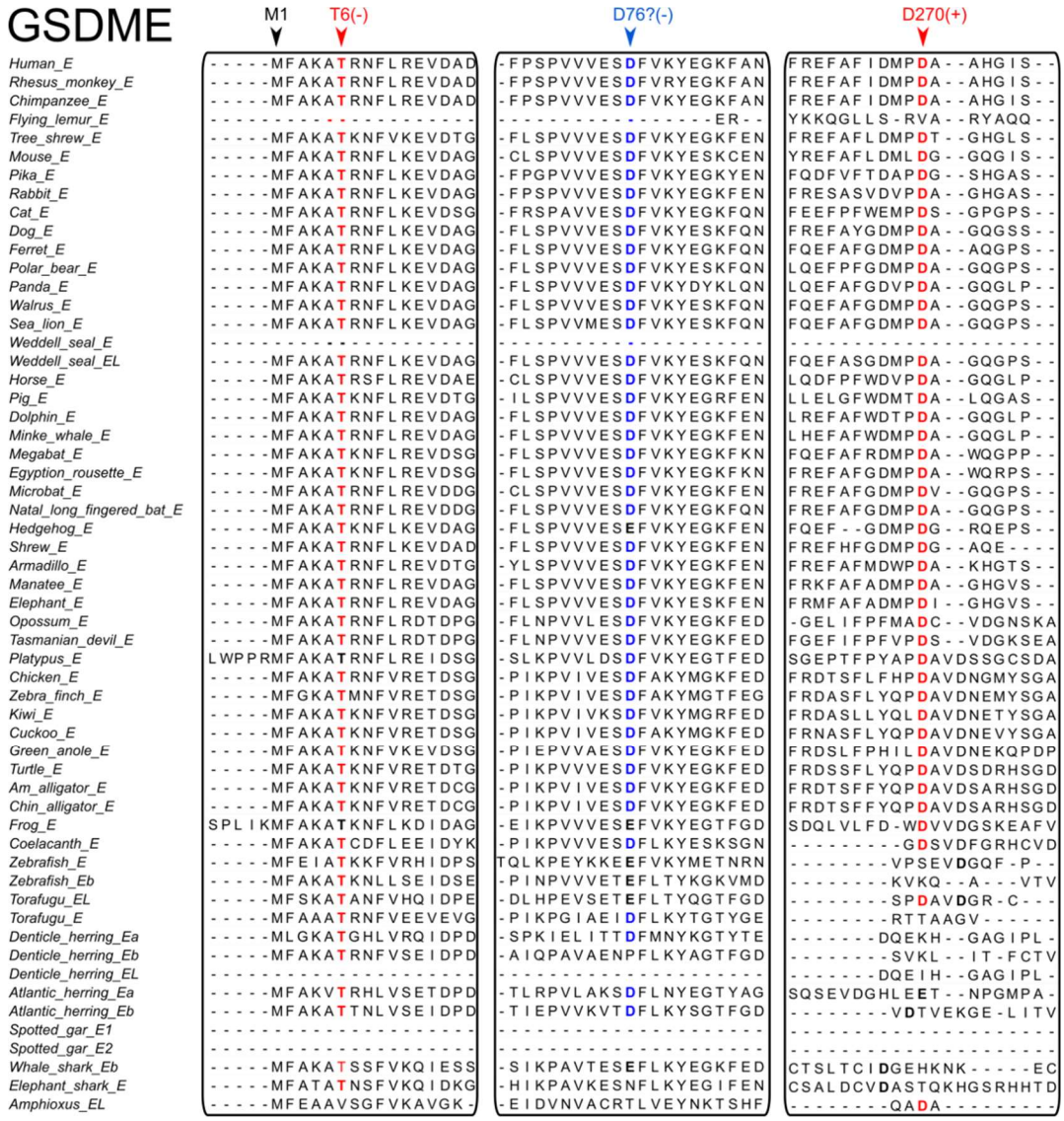
GSDME
M1
T6(-)
D76?(-)
D270(+)
Human_E
Rhesus_monkey_E
Chimpanzee_E
Flying_lemur_E
Tree_shrew_E
Mouse_E
Pika_E
Rabbit_E
Cat_E
Dog_E
Ferret_E
Polar_bear_E
Panda_E
Walrus_E
Sea_lion_E
Weddell_seal_E
Weddell_seal_EL
Horse_E
Pig_E
Dolphin_E
Minke_whale_E
Megabat_E
Egyption_rousette_E
Microbat_E
Natal_long_fingered_bat_E
Hedgehog_E
Shrew_E
Armadillo_E
Manatee_E
Elephant_E
Opossum_E
Tasmanian_devil_E
Platypus_E
Chicken_E
Zebra_finch_E
Kiwi_E
Cuckoo_E
Green_anole_E
Turtle_E
Am_alligator_E
Chin_alligator_E
Frog_E
Coelacanth_E
Zebrafish_E
Zebrafish_Eb
Torafugu_EL
Torafugu_E
Denticle_herring_Ea
Denticle_herring_Eb
Denticle_herring_EL
Atlantic_herring_Ea
Atlantic_herring_Eb
Spotted_gar_E1
Spotted_gar_E2
Whale_shark_Eb
Elephant_shark_E
Amphioxus_EL

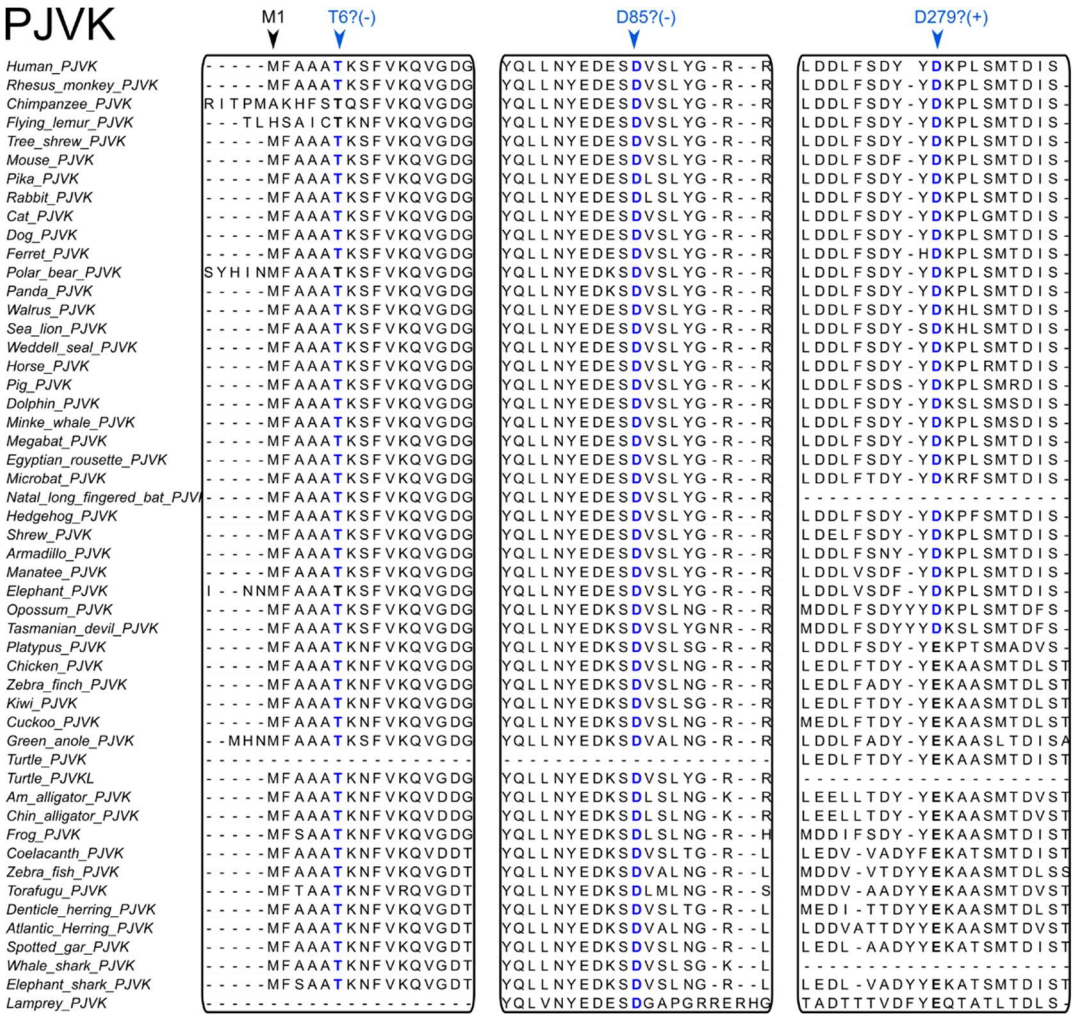

Figure S2. Conservation between species of crucial regulatory sites in the protein sequences of GSDMA-E and PJVK. The sequences of the putative GSDMA-E and PJVK homologs were aligned using Clustal Omega (v1.2.4) and adapted in JalView (v2.10.5). Regulatory sites confirmed in human and mice are shown in red. Possible regulatory sites based on location in other gasdermins are shown in blue and indicated by '?'. Activating and inactivating regulatory sites are indicated by with (+) and (-) symbols, respectively. Conservation between species of the inhibitory Threonine residues [2] was investigated within the first 10 amino-acids: T8 of human GSDMA is found in 46 out of 57 sequences (80% conserved). T9 of human GSDMB is found in 19 out of 25 sequences (76% conserved). T6 of human GSDME is found in 51 out of 57 sequences (89% conserved). T9 of human PJVK is found in 49 out of 51 sequences (96% conserved). In human GSDMC the Threonine is replaced by a conserved Serine residues at the same position which might have the same regulatory function. In GSDMD neither a Threonine nor a Serine residue is found around that position, suggesting the absence of this presumed regulatory mechanism. Next, inactivating proteolytic sites were investigated around residue 90. Caspase-3 mediated inactivating cleavage sites D91 and D87 [3,4], were conserved in GSDMB (17 out of 25 sequences) and –D (31 out of 35 sequences), respectively. In some species an Aspartic residue around position 90 is found as well, but up to now there is no evidence for inactivating cleavage at these sites. Finally, proven activating proteolytic sites within the hinge regions of the GSDMs were inspected. The human casp-1, -4/5, -8 cleavage site D275 in GSDMD [5–7] is found in 26 out of 35 sequences (74% conserved). Nor the human ELANE cleavage site C268 [8,9] nor cathepsin G cleavage site L273 [10] in GSDMD are conserved (8% and 34%, respectively). The human caspase-3 [11] and granzyme B [12] cleavage site D270 in GSDME is found in 43 out of 57 sequences (75% conserved). Some species do contain a Aspartic residue (D252) in GSDMA as well, but this is only found in 5 out of 57 sequences (9% conserved). GSDMC is not cleaved in the hinge region, but is activated by caspase-8 mediated cleavage at D365 [13] in its C-GSDM domain which is only found in 6 out of 45 sequences (13% conserved). However, the conservation of these phosphorylation and cleavage residues is only suggestive for a preserved function since caspase-cleavage sites and phosphorylation sites involve also contextual constraints involving nearby sequences and 3D structure.

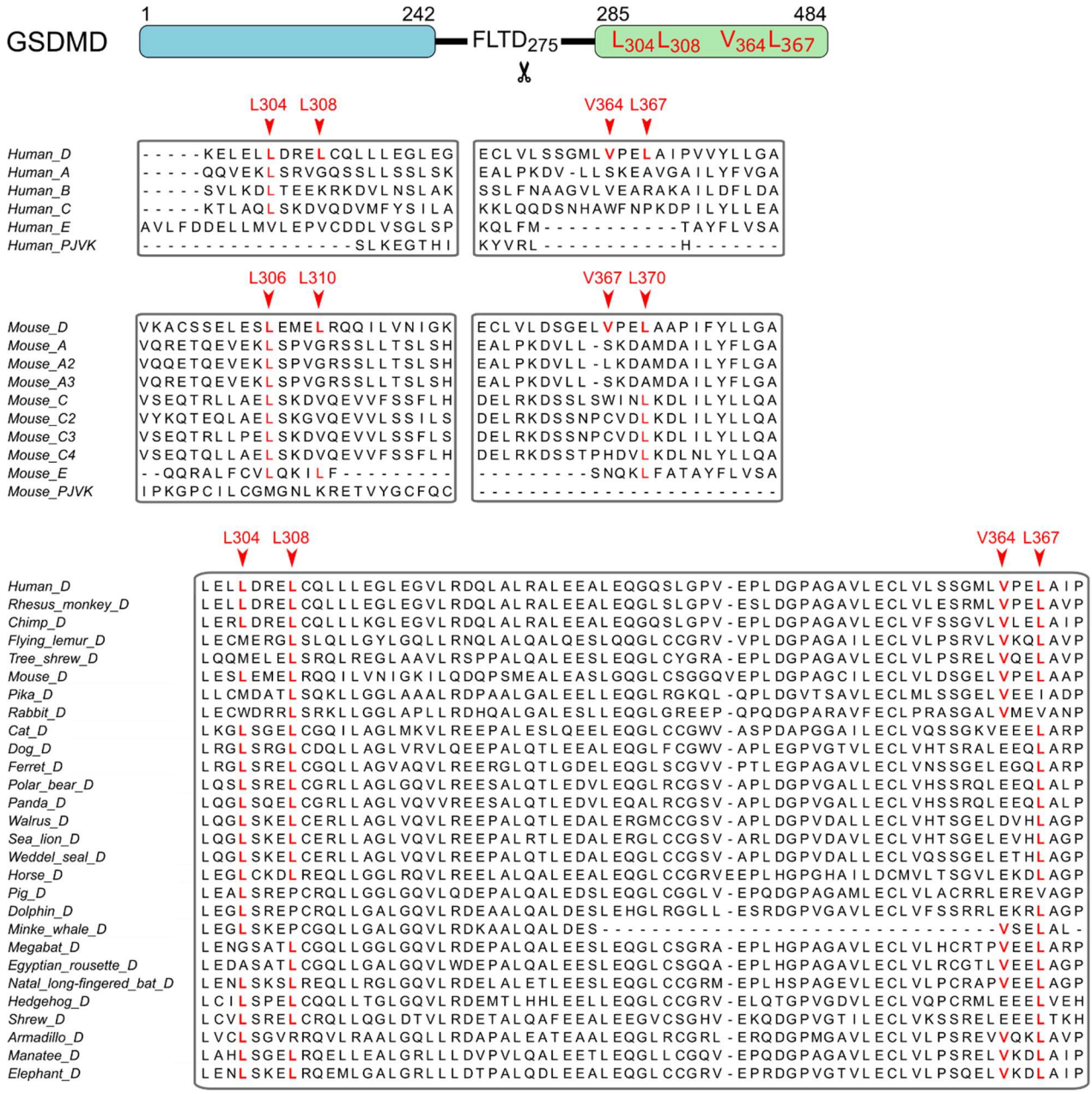

Figure S3. Conservation between species of crucial regulatory sites in the protein sequences of GSDMA-E and PJVK. GSDMD contains a hydrophobic groove formed by L304, L306, V364 and L367 (red) for interaction with the active caspase-1/4/11 p10 domain. This groove is conserved between species, but is lacking in other GSDM proteins making it a unique feature of GSDMD.

Table S1. Protein expression overview of GSDMA-E in humans according to The Human Protein Atlas in different cell types.

Integumentary tissues

Tissue	Cell type GSDM	A	B	C	D	E
Skin	*Epidermal cells*					
	Fibroblasts					
	Keratinocytes					
	Langerhans					
	Melanocytes					
	Sebaceous cells					
	Secretory cells					
	Sweat ducts					
Hair	*Cells in cortex/medulla*					
	Cells in cuticle					
	Cells in external root sheath					
	Cells in internal root sheath					

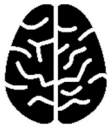

Brain tissues

Tissue	Cell type GSDM	A	B	C	D	E
Cerebral cortex	*Endothelial cells*					
	Glial cells					
	Neuronal cells					
	Neuropil					
Hypocampus	*Glial cells*					
	Neuronal cells					
Caudate	*Glial cells*					
	Neuronal cells					
Cerebellum	*Cells in granular layer*					
	Cells in molecular layer					
	Purkinje cells					
	Bergmann glia					
	GLUC cells					
	Granular cells					
	Synaptic glomeruli					
	White matter cells					
	Molecular layer					

Endocrine tissues

Tissue	Cell type	GSDM	A	B	C	D	E
Thyroid gland	*Glandular cells*						
Parathyroid gland	*Glandular cells*						
Adrenal gland	*Glandular cells*						

Respiratory tissues

Tissue	Cell type	GSDM	A	B	C	D	E
Lung	*Alveolar cells*						
	Macrophages						
Nasopharynx	*Respiratory epithelial cells*						
Bronchus	*Respiratory epithelial cells*						

Lymphoid tissues

Tissue	Cell type	GSDM	A	B	C	D	E
Appendix	*Glandular cells*						
	Lymphoid tissue						
Bone marrow	*Hematopoietic cells*						
Lymph node	*Germinal center cells*						
	Non-germinal center cells						
Tonsil	*Germinal center cells*						
	Non-germinal center cells						
	Squamous epithelial cells						
Spleen	*Cells in red pulp*						
	Cells in white pulp						

Digestive tissues

Tissue	Cell type	GSDM	A	B	C	D	E
Salivary gland	*Glandular cells*						
Oral mucosa	*Squamous epithelial cells*						
Esophagus	*Squamous epithelial cells*						
Stomach	*Glandular cells*						
Liver	*Cholangiocytes*						
	Hepatocytes						
Gallbladder	*Glandular cells*						

Pancreas	*Exocrine glandular cells*					
	Pancreatic endocrine cells					
Duodenum	*Glandular cells*					
Small intestine	*Glandular cells*					
Colon	*Endothelial cells*					
	Glandular cells					
	Peripheral nerve/ganglion					
Rectum	*Glandular cells*					

Urinary tissues

Tissue	**Cell type**	**GSDM**	**A**	**B**	**C**	**D**	**E**
Kidney	*Cells in glomeruli*						
	Cells in tubules						
Urinary bladder	*Urothelial cells*						

Soft/Adipose tissues

Tissue	**Cell type**	**GSDM**	**A**	**B**	**C**	**D**	**E**
Soft tissue	*Chondrocytes*						
	Fibroblasts						
	Peripheral nerve						
Adipose tissue	*Adipocytes*						

Muscle tissues

Tissue	**Cell type**	**GSDM**	**A**	**B**	**C**	**D**	**E**
Heart muscle	*Cardiomyocytes*						
Skeletal muscle	*Myocytes*						
Smooth muscle	*Smooth muscle cells*						

Male tissues

Tissue	**Cell type**	**GSDM**	**A**	**B**	**C**	**D**	**E**
Testis	*Cells in seminiferous ducts*						
	Leydig cells						
	Elongated or late spermatids						
	Pachytene spermatocytes						
	Peritubular cells						
	Preleptotene spermatocytes						

	Round or early spermatids					
	Sertoli cells					
	Spermatogonia cells					
Prostate	*Glandular cells*					
Epididymis	*Glandular cells*					
Seminal vesicle	*Glandular cells*					

Female tissues

Tissue	**Cell type**	**GSDM**	**A**	**B**	**C**	**D**	**E**
Fallopian tube	*Glandular cells*						
Breast	*Adipocytes*						
	Glandular cells						
	Myoepithelial cells						
Vagina	*Squamous epithelial cells*						
Cervix, Uterine	*Glandular cells*						
	Squamous epithelial cells						
Endometrium	*Cells in endometrial stroma*						
	Glandular cells						
Ovary	*Follicle cells*						
	Ovarian stroma cells						
Placenta	*Decidual cells*						
	Trophoblastic cells						

Based on immunohistochemistry data from v20.proteinatlas.org [14].

Table S2. Species searched and Gasdermins used in the phylogenetic analysis

Species	Gasdermin	Accession number
Human	GSDMA	NP_835465
	GSDMB	NP_001159430
	GSDMC	NP_113603
	GSDMD	NP_001159709
	GSDME	NP_004394
	PJVK	NP_001036167
Rhesus monkey	GSDMA	XP_014975037
	GSDMB	XP_014975035
	GSDMC	XP_028708741
	GSDMD	XP_015001615
	GSDME	XP_001096213
	PJVK	XP_014965926
Chimpanzee	GSDMA	XP_001171222
	GSDMB	XP_009430521
	GSDMC	XP_001153860
	GSDMD	XP_009454389
	GSDME	XP_003318404
	PJVK	XP_009442090
Flying lemur	GSDMA	XP_008580237
	GSDMB	XP_008591469
	GSDMC-like	XP_008584607
	GSDMD	XP_008581297
	GSDME	XP_008591692
	PVJK	XP_008565263
Chinese tree shrew	GSDMA	XP_014446163
	GSDMB	XP_027630559
	GSDMC1	XP_027630809
	GSDMC2	XP_027630808
	GSDMD	XP_006152136
	GSDME	XP_014448712
	PJVK	XP_006151718
Mouse	GSDMA	NP_067322
	GSDMA2	NP_084003
	GSDMA3	NP_001007462
	GSDMC	NP_113555
	GSDMC2	NP_001161746
	GSDMC3	NP_899017
	GSDMC4	NP_083268
	GSDMD	NP_081236
	GSDME	NP_061239
	PJVK	NP_001074180
American pika	GSDMA	XP_004591215
	GSDMD	XP_004580923
	GSDME	XP_004582613
	PJVK	XP_004577070
Rabbit	GSDMA	XP_002719393
	GSDMC	XP_017197091
	GSDMD	XP_008252155
	GSDME	XP_002713872
	PVJK	XP_002712360

Domestic cat	GSDMA	XP_019673388
	GSDMB	XP_019672505
	GSDMC	XP_019678683
	GSDMD	XP_023104116
	GSDME	XP_006929316
	PVJK	XP_023115271
Dog	GSDMA	XP_005624601
	GSDMB	XP_038474963
	GSDMC	XP_022282826
	GSDMD	XP_022282557
	GSDME	XP_853956
	PJVK	XP_535979
Domestic ferret	GSDMA	XP_012917953
	GSDMB	XP_012917958
	GSDMC	XP_012907169
	GSDMD	XP_012904826
	GSDME	XP_004743370
	PJVK	XP_004769035
Polar bear	GSDMA	XP_008687533
	GSDMB	XP_008688086
	GSDMC	XP_008687605
	GSDMD	XP_008682309
	GSDME	XP_008684626
	PJVK	XP_008685415
Giant panda	GSDMA	XP_011235679
	GSDMB	XP_034496569
	GSDMC	XP_034524413
	GSDMD	XP_034524619
	GSDME	XP_034525218
	PJVK	XP_002918869
Pacific walrus	GSDMA	XP_012416038
	GSDMB	XP_012415968
	GSDMD	XP_012417918
	GSDME	XP_004397435
	PJVK	XP_004403794
California sea lion	GSDMA	XP_027423431
	GSDMB*	XP_027423591
	GSDMC-like	XP_035582972
	GSDMD	XP_027467804
	GSDME	XP_027429302
	PJVK	XP_027447016
Weddell seal	GSDMA	XP_006749918
	GSDMB	XP_030876680
	GSDMD	XP_030875078
	GSDME	XP_006729473
	GSDME-like	XP_030877431
	PJVK	XP_006733299
Horse	GSDMA1	XP_001500838
	GSDMA2	XP_023504739
	GSDMB	XP_003362433
	GSDMC1	XP_023504738
	GSDMC2	XP_023504730

	GSDMD	XP_014583675
	GSDME	NP_001075358
	PVJK	XP_001500909
Pig	GSDMA	XP_003131545
	GSDMA-like	XP_020944580
	GSDMB	XP_005653979
	GSDMC	XP_013843492
	GSDMD	XP_020946163
	GSDMD-like1	XP_020944583
	GSDME	XP_013841242
	PVJK	XP_003133557
Bottlenose dolphin	GSDMB	XP_033703583
	GSDMC	XP_033698771
	GSDMD	XP_033698887
	GSDME	XP_033718980
	PJVK	XP_004311474
Minke whale	GSDMA	XP_007198413
	GSDMB	XP_028021127
	GSDMD	XP_007167001
	GSDME	XP_007171559
	PJVK	XP_007190463
Megabat	GSDMA	XP_011381342
	GSDMB	XP_023380639
	GSDMC-like	XP_023386757
	GSDMC	XP_023375471
	GSDMD	XP_011373217
	GSDME	XP_023387299
	PVJK	XP_011355082
Egyptian rousette	GSDMA	XP_016020091
	GSDMB	XP_036078993
	GSDMC	XP_036088920
	GSDMD	XP_036089037
	GSDME	XP_036086308
	PJVK	XP_016008059
Little brown bat (microbat)	GSDMA	XP_023620107
	GSDMB	XP_023620143
	GSDMC-like1	XP_014315172
	GSDMC-like2	XP_023613534
	GSDMC-like3	XP_023613522
	GSDMC-like4	XP_023613535
	GSDME	XP_006088855
	PJVK	XP_006083120
Natal long-fingered bat	GSDMA	XP_016057700
	GSDMB	XP_016057754
	GSDMC	XP_016071620
	GSDMD	XP_016075669
	GSDME	XP_016072537
	PJVK	XP_016065696
Hedgehog	GSDMA	XP_007531080
	GSDMB*	ENSEEUG00000006496
	GSDMC	XP_016043463
	GSDMD	XP_007516119

	GSDME	XP_007529121
	PJVK	XP_007534290
European shrew	GSDMA	XP_004608992
	GSDMC	XP_004602662
	GSDMC-like1	XP_012790627
	GSDMC-like2	XP_012791379
	GSDMC-like3	XP_012791545
	GSDMC-like4	XP_012791352
	GSDMC-like5	XP_012791368
	GSDMC-like6	XP_012791290
	GSDMC-like7	XP_012791289
	GSDMC-like8	XP_012791287
	GSDMC-like9	XP_012791286
	GSDMD	XP_004618751
	GSDME	XP_004604319
	PJVK	XP_004601427
Nine-banded armadillo	GSDMA	XP_004450182
	GSDMB	XP_023441904
	GSDMC	XP_012377894
	GSDMD	XP_004480061
	GSDMD-like	XP_004480063
	GSDME	XP_004447610
	PJVK	XP_004476912
Florida manatee	GSDMA	XP_012411464
	GSDMA-like	XP_004373092
	GSDMB	XP_012411408
	GSDMC	XP_004373091
	GSDMD	XP_023597400
	GSDME	XP_004377520
	PJVK	XP_004375524
Elephant	GSDMA	XP_023409167
	GSDMA-like	XP_023401773
	GSDMB	XP_023409166
	GSDMC	XP_023401449
	GSDMD	XP_010600014
	GSDME	XP_023400115
	PJVK	XP_003406242
Opossum	GSDMA-like1	XP_007482349
	GSDMA-like2	XP_007483072
	GSDMA-like3	XP_007482353
	GSDMA-like4	XP_007488390
	GSDMA-like5	XP_007482352
	GSDMA-like6	XP_007506689
	GSDMA-like7	XP_007506688
	GSDMA-like8	XP_007506687
	GSDMA-like9	XP_007483073
	GSDMA-like10	XP_007482351
	GSDMB	XP_007482357
	GSDMC-like1	XP_007488380
	GSDMC-like2	XP_016288126
	GSDMC-like3	XP_007488386
	GSDMC-like4	XP_007488391
	GSDMD	XP_007488897

	GSDMD-like	XP_007488392
	GSDME	XP_007505411
	PVJK	XP_001368857
Tasmanian devil	GSDMA	XP_012403790
	GSDMA-like	XP_012403763
	GSDMB	XP_023358160
	GSDMC	XP_031803207
	GSDMD	XP_012397449
	GSDMD-like	XP_031803406
	GSDME	XP_031796450
	PJVK	XP_003764058
Platypus	GSDMA	XP_028931691
	GSDMD	XP_028917767
	GSDME	XP_028926175
	PJVK	XP_028928169
Chicken	GSDMA	NP_001026532
	GSDME	NP_001006361
	PJVK	XP_426573
Zebra finch	GSDMA	XP_012426589
	GSDME	XP_004186180
	PJVK	XP_002199531
North Island brown kiwi	GSDMA	XP_013800181
	GSDME	XP_013796819
	PJVK	XP_013816192
Common cuckoo	GSDMA	XP_009568865
	GSDME	XP_009561166
	PJVK	XP_009553924
Green anole	GSDMA1	XP_008111551
	GSDMA2	XP_008111549
	GSDME	XP_003222077
	PJVK	XP_003225734
Painted turtle	GSDMA	XP_008160950
	GSDME	XP_023962559
	PJVK	XP_005300562
	PJVK-like	XP_005293660
American alligator	GSDMA	XP_014451785
	GSDME	XP_006275179
	PJVK	XP_014454831
Chinese alligator	GSDMA	XP_006022649
	GSDME	XP_025063881
	PJVK	XP_006034600
Frog	GSDME	XP_014351702
	PJVK	XP_014354128
Coelacanth	GSDME	XP_014351702
	PJVK	XP_014354128
Zebrafish	GSDME	XP_005170134
	GSDMEb	NP_001001947
	PJVK	XP_021332701
Torafugu	GSDME-like	XP_029701077
	GSDMEb	XP_011604087
	PJVK	XP_003966800
Denticle herring	GSDMEa	XP_028847771

	GSDMEb GSDME-like pjvk	XP_028835239 XP_028847120 XP_028809593
Atlantic herring	GSDMEa GSDMEb PJVK	XP_031441875 XP_031432605 XP_031414807
Spotted gar	GSDME1 GSDME2 PJVK	XP_015213331 XP_015213253 XP_006636618
Whale shark	GSDMA-like GSDMEb PJVK	XP_020385528 XP_020389028 XP_020381727
Elephant shark	GSDMD-like GSDMEb PJVK	XP_007907597 NP_001279331 XP_007888272
Lamprey	PJVK	ENSPMAG00000005499
Sea squirt	-	-
Amphioxus	GSDME-like	XP_035697721
Acorn worm	GSDM-like1 GSDM-like2	XP_006824139 XP_002740828
Sea urchin	GSDM-like1 GSDM-like2	XP_030830372 XP_030830813
Brachiopod	GSDM-like1 GSDM-like2	XP_013387687 XP_013387688
Octopus	GSDM-like	XP_014790989
East Asian octopus	GSDM-like	XP_029658425
Owl limpet	GSDM-like	XP_009046123
Sea hare	-	-
Golden apple snail	GSDM-like	XP_025094672
Eastern oyster	GSDM-like1 GSDM-like2	XP_022326085 XP_022328273
Yesso scallop	GSDM-like1 GSDM-like2	XP_021351821 XP_021351818
Polychaete worm	-	-
Leech	-	-
Fruit fly	-	-
Western honey bee	-	-
Roundworm (*Caenorhabditis elegans*)	-	-
Roundworm (*Pristionchus pacificus*)	-	-
Starlet sea anemone	GSDM-like	XP_001622420
Fresh-water polyp	GSDM-like	XP_012557585
Acroporid coral	GSDM-like	XP_015769608
Stony coral	GSDM-like	XP_029180327
Star coral	GSDME	XP_020607257
Coral	GSDM-like	XP_028402809
Hood coral	GSDM-like	XP_022788280
Sea anemone	GSDM-like1 GSDM-like2	XP_020910515 XP_020910462
Australia sea anemone	GSDM-like	XP_031556688

References Supplemental Information

1. Kim, M.S. *et al.* (2014) A draft map of the human proteome. *Nature* 509, 575–581
2. Rogers, C. *et al.* (2019) Gasdermin pores permeabilize mitochondria to augment caspase-3 activation during apoptosis and inflammasome activation. *Nat. Commun.* 10, 1689
3. Chao, K.L. *et al.* (2017) Gene polymorphism linked to increased asthma and IBD risk alters gasdermin-B structure, a sulfatide and phosphoinositide binding protein. *Proc. Natl. Acad. Sci.* 114, E1128–E1137
4. Taabazuing, C.Y. *et al.* (2017) Pyroptosis and Apoptosis Pathways Engage in Bidirectional Crosstalk in Monocytes and Macrophages. *Cell Chem. Biol.* 24, 507–514
5. Orning, P. *et al.* (2018) Pathogen blockade of TAK1 triggers caspase-8-dependent cleavage of gasdermin D and cell death. *Science* 362, 1064–1069
6. Kayagaki, N. *et al.* (2015) Caspase-11 cleaves gasdermin D for non-canonical inflammasome signalling. *Nature* 526, 666–671
7. Shi, J. *et al.* (2015) Cleavage of GSDMD by inflammatory caspases determines pyroptotic cell death. *Nature* 526, 660–665
8. Kambara, H. *et al.* (2018) Gasdermin D Exerts Anti-inflammatory Effects by Promoting Neutrophil Death. *Cell Rep.* 22, 2924–2936
9. Sollberger, G. *et al.* (2018) Gasdermin D plays a vital role in the generation of neutrophil extracellular traps. *Sci. Immunol.* 3, 1–12
10. Burgener, S.S. *et al.* (2019) Cathepsin G Inhibition by Serpinb1 and Serpinb6 Prevents Programmed Necrosis in Neutrophils and Monocytes and Reduces GSDMD-Driven Inflammation. *Cell Rep.* 27, 3646–3656
11. Rogers, C. *et al.* (2017) Cleavage of DFNA5 by caspase-3 during apoptosis mediates progression to secondary necrotic/pyroptotic cell death. *Nat. Commun.* 8, 14128
12. Zhang, Z. *et al.* (2020) Gasdermin E suppresses tumour growth by activating anti-tumour immunity. *Nature* 579, 1–6
13. Hou, J. *et al.* (2020) PD-L1-mediated gasdermin C expression switches apoptosis to pyroptosis in cancer cells and facilitates tumour necrosis. *Nat. Cell Biol.* 22, 1264–1275
14. Thul, P.J. *et al.* (2017) A subcellular map of the human proteome. *Science (80-.).* 356, 1–12

Chapter 2

GSDME and its role in cancer: from behind the scenes to the front of the stage

REVIEW

Published in 'International Journal of Cancer', 2021, 148(12):2872-2883

Elke De Schutter[1,2,3,*], Lieselot Croes[1,4,*], Joe Ibrahim[1,4], Patrick Pauwels[4], Ken Op de Beeck[1,4], Peter Vandenabeele[2,3], Guy Van Camp[1,4]

[1] Center of Medical Genetics, University of Antwerp and Antwerp University Hospital, Prins Boudewijnlaan 43/6, 2650 Edegem, Antwerp, Belgium.

[2] Molecular Signaling and Cell Death Unit, VIB Center for Inflammation Research, VIB, Technologiepark 71, 9052 Ghent, Belgium.

[3] Department Biomedical Molecular Biology, Gent University, Technologiepark 71, 9052 Ghent, Belgium.

[4] Center for Oncological Research, University of Antwerp and Antwerp University Hospital, Universiteitsplein 1, 2610 Wilrijk, Antwerp, Belgium.

* Equally contributed

Abstract

Gasdermin E (GSDME), a gene originally involved in hereditary hearing loss, has been associated with several types of cancer in the last two decades. Recently, GSDME was identified as a pore forming molecule which is activated following caspase-3-mediated cleavage resulting in so-called secondary necrosis following apoptotic cell death, or in primary necrotic cell death without an apoptotic phase, so-called pyroptosis-like. This implication in cell death execution suggests its potential role as a tumor suppressor. *GSDME* also exhibited a cancer type-specific differential methylation pattern between tumor tissues and normal cells, implying *GSDME* gene methylation both as a pan-cancer and cancer-type specific detection biomarker. A bit paradoxically, GSDME protein expression is considered to be less suited as biomarker, and although its ablation does not protect the cell against eventual cell death, its protein expression might still operate in tumor immunogenicity due to its capacity to induce (secondary) necrotic cell death which has enhanced immunogenic properties. Additionally, *GSDME* gene expression has been shown to be associated with favorable prognosis following chemotherapy, and could therefore be a potential predictive biomarker. We provide an overview of the different associations between *GSDME* gene methylation, gene expression and tumorigenesis, and explore their potential use in the clinic. Our review only focuses on *GSDME* and summarizes the current knowledge and most recent advances on *GSDME*'s role in cancer formation, its potential as a biomarker in cancer and on its promising role in immunotherapies and anti-tumor immune response.

2.1 INTRODUCTION

The *gasdermin E* (*GSDME*) gene, also known as *deafness, autosomal dominant 5* (*DFNA5*), was identified in 1998 on chromosome 7p15.3 in patients with a specific form of autosomal dominant, progressive, sensorineural and non-syndromic hearing loss [1]. Remarkably, although the identified *GSDME* mutations in families with hearing loss are distinct at DNA level, they all result in skipping of exon 8 and truncation of the protein [2–12]. *GSDME* belongs to the gasdermin (*GSDM*) family, which owes its nomenclature to its high expression pattern along the gastrointestinal tract and skin (dermis) [13,14]. In addition, expression of *GSDME* is reported in all vital organs [1,15]. Until now, six *GSDM* genes have been identified in humans: *GSDMA*, *GSDMB*, *GSDMC*, *GSDMD*, *GSDME* and *Pejvakin* (*PJVK*) [14]. Except for PJVK, all GSDM proteins consist of a conserved N- and C-terminal globular domain, separated by a flexible hinge region [16]. Recently, the N-terminal (N-GSDM) domain of GSDMA, -D and -E was shown to execute cell death by pore formation [17], and this function is apparently inhibited by the C-terminal domain (C-GSDM) in the full length protein. In case of hearing loss, it is hypothesized that truncation of C-GSDME by skipping of exon 8, represents a gain-of-function mutation that unleashes the intrinsic pore

forming activity and might result in increased death of terminally differentiated cochlear hair cells or other cells important for hearing [3,4,16,18,19] (Figure 1).

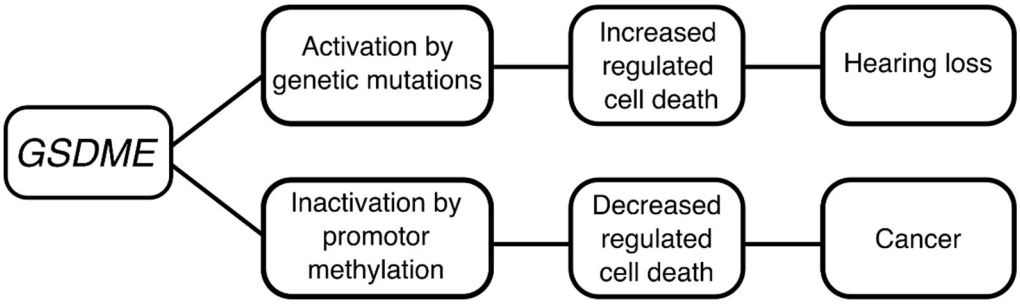

Figure 1. Original hypothesis of the function of GSDME in hearing loss and cancer.

Next to hearing loss, *GSDME* has been associated with cancer [15,16,20–40]. Genomic methylation screens unveiled *GSDME* as a possible tumor suppressor gene [35,37,38]. In general, methylation of promotor CpGs, frequently associated with transcriptional silencing, may serve as a mechanism to inactivate tumor suppressor genes in cancer [41,42]. In that respect it was hypothesized that DNA promoter methylation of *GSDME* prevents GSDME-mediated regulated cell death and in that way contributes to tumorigenesis (Figure 1). However, recent breakthroughs on the function of the *GSDM* gene family shed new light on the role of GSDME in cell death and consequently on its contribution to tumor biology. In this review we first focus on the biological function of GSDME in order to understand the current associations between GSDME and cancer. Next, we evaluate *GSDME* methylation/expression as a detection, prognostic and predictive cancer biomarker. Finally, the effect of *GSDME* protein expression on chemotherapeutic treatment will be explored. Overall we conclude that *GSDME* methylation and expression may have substantial clinical utility as diagnostic and prognostic marker, and even as a therapeutic target during chemotherapy-mediated cell death.

2.2 FUNCTION OF GSDME

2.2.1 GSDME executes necrotic cell death by pore formation

The physiological function of GSDMs was unknown for decades, despite their association with different diseases such as alopecia [43,44], asthma [45–48], hearing loss [1,49] and cancer [13,50–55]. The conserved N-terminal domain of all GSDMs but PJVK is shown to execute necrotic cell death [17]. Under physiologically normal conditions, this cytotoxic function is impeded by C-GSDM [16,56]. Depending on the cell death trigger, GSDMs are activated by proteolytic cleavage by different proteases, thereby liberating N-GSDM [33,46,56–62]. GSDME is cleaved by the crucial apoptotic executioner caspase-3 [33,59] (Figure 2). In essence, apoptosis is a containment program preparing the dead cell corpse to be removed by phagocytosis [63]. It is morphologically characterized by plasma

membrane blebbing and the release of apoptotic bodies that contain cellular material (Table 1). Usually, apoptotic cells are cleared by neighboring phagocytes before they lose membrane integrity. When phagocytes are absent, the contained apoptotic cells progress to a necrotic cell death modality associated with swelling and plasma membrane permeabilization, termed 'secondary necrosis' (Table 1) [64]. In bone marrow derived macrophages, induction of the mitochondrial apoptotic pathway by overexpressing Bax results, among others, in caspase-3-mediated cleavage of GSDME and secondary necrosis following apoptotic plasma membrane blebbing (Figure 2) [59]. When the *GSDME* gene is ablated, the necrotic morphology of late apoptotic cells remains absent and the cells remain for longer time in the apoptotic phase characterized by membrane blebbing and containment of the plasma membrane, suggesting that GSDME is responsible for the necrotic plasma membrane permeabilization and dispersion of cellular content in the environment. Moreover, N-GSDME apparently targets mitochondria and facilitates the release of cytochrome c (cyt c) [65], thereby creating a self-amplifying feed-forward loop during apoptosis by the consecutive activation of the apoptosome and caspase-3 (Figure 2). Next to secondary necrosis following apoptosis, cells can die directly by primary necrosis *via* different pathways (Table 1). For example, GSDMD is responsible for the execution of pyroptosis, an inflammasome-dependent necrotic cell death modality involving processing of pro-interleukin-1β (pro-IL-1β) by caspase-1 [56,66]. Pyroptosis is characterized by ballooning of the cell and release of processed IL-1β. Similarly, GSDME executes primary necrosis as well. Chemotherapy treatment of different cancer cell lines results in caspase-3-mediated cleavage of GSDME and pyroptotic ballooning without passing through an apoptotic morphology [25,33], suggesting that necrotic plasma membrane permeabilization by GSDME in this case precedes the apoptotic process which seems paradoxical since the same upstream apoptotic machinery is triggered in case of secondary necrosis. This is probably due to different buffering capacities to restrain GSDME activation. Moreover, the simultaneous detection of biochemical markers for apoptosis and pyroptosis after chemotherapy treatment [20] argues for concurrent occurrence of apoptosis and pyroptosis. In absence of GSDME, a prolonged apoptotic morphology and dominance of apoptotic markers is seen [20,33], indicating that GSDME activation induces the final membrane permeabilization, as an early event in case of pyroptosis and a late event in case of secondary necrosis. Whether this can be defined as real pyroptosis, is a matter of definition (Table 1). Pyroptosis s.s. is defined as inflammasome-dependent and associated with the release of IL-1β (previously called "pyrogen") and more recently with caspase-1/4-mediated proteolytic activation of GSDMD [66]. GSDME-mediated cell death mentioned above is not inflammasome-dependent and is therefore called "pyroptosis-like" (Table 1). All together these data suggest that caspase-3 mediated cleavage of GSDME results in necrotic cell death, either called secondary necrosis when following an apoptotic phase or called pyroptosis-like. However, the presence of cleaved GSDME is not always associated with cell death. Indeed, despite caspase-3-mediated cleavage and a clear apoptotic phenotype,

N-GSDME apparently does not regulate secondary necrosis in human T-cells and monocytes [67]. Interestingly, phosphorylation at threonine (Thr) 6 was recently reported to prevent GSDME pore formation even when processed, revealing an extra layer of regulation (Figure 2) [65].

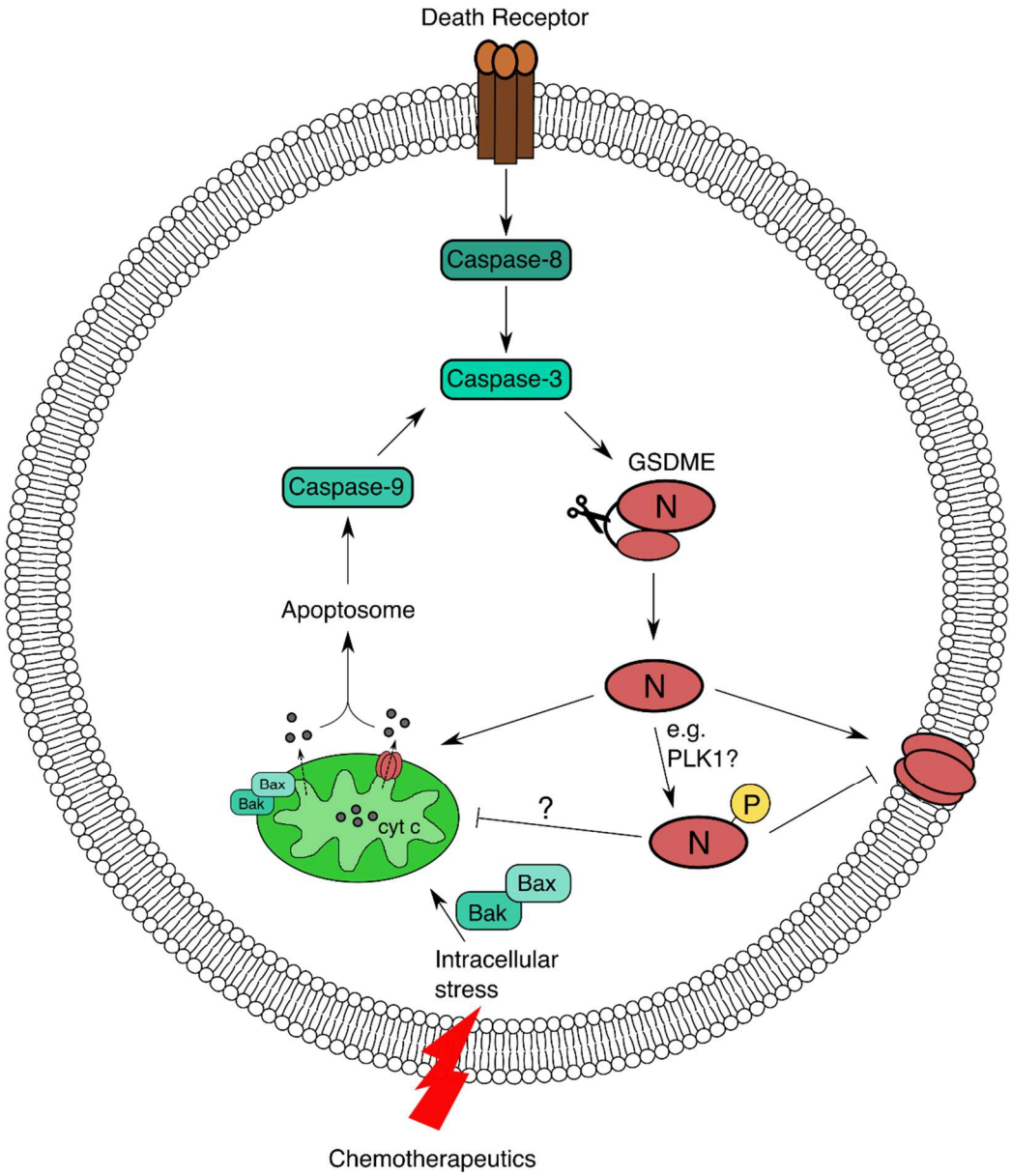

Figure 2. Cell death pathways wherein GSDME is involved. Apoptosis can be triggered by internal or external stimuli, leading to the activation of the intrinsic or extrinsic apoptotic pathway respectively. In the intrinsic apoptotic pathway, mitochondrial outer membrane permeabilization (MOMP) by Bak/Bax is triggered by internal stress such as DNA damage or oxidative stress, causing the release of cyt c into the cytoplasm. Cyt c initiates the formation of the apoptosome which facilitates the autocleavage of caspase-9, which activates caspase-3, a common executioner caspase, involved in both the intrinsic and extrinsic apoptotic pathway. In the extrinsic apoptotic pathway, activation of death receptors by ligand binding results in the consecutive activation of caspase-8 and caspase-3. Caspase-3 cleaves GSDME in its hinge-region, thereby releasing the N-terminus from the inhibitory C-terminal domain. Next, N-GSDME targets both the mitochondrial and the plasma membrane. By targeting the mitochondrial membrane, more cyt c is released from the mitochondria, resulting in a self-amplification loop by activation of caspase-3 and GSDME. On the other hand, the increasing plasma membrane permeabilization results in necrotic cell death. If GSDME becomes phosphorylated, N-GSDME oligomerization and pore formation are prevented.

Table 1. Overview of the different characteristics and corresponding morphology of GSDM-mediated cell death modalities.

Apoptosis		Primary Necrosis	
Shrinking of cytoplasm, condensation (pyknosis) and fragmentation (karyorrhexis) of nucleus		Cell swelling, permeabilization and rupture of the plasma membrane	
Formation of apoptotic bodies (membrane contained vesicles enclosing elements of cytosol, organelles and nuclear material)		Differential leakage of cellular content	
Apoptosis	**Secondary Necrosis**	**Pyroptosis - like**	**Pyroptosis**
No loss of membrane integrity; apoptotic caspases are crucial for the apoptotic containment program	Associated with cell swelling (oncosis) and plasma membrane permeabilization of cells that started the apoptotic program	Formation of large pyroptotic bodies	Formation of large pyroptotic bodies
Efficient phagocytosis of apoptotic cells and fragments	Occurs in case of inefficient clearance		
Apoptotic caspases dependent	Proteolytic activation of GSDME by caspase-3	Direct activation of GSDME by caspase-3 without apoptotic phase	Inflammasome dependent, inflammatory caspase-1/4 are crucial for proteolytic activation of *GSDMD*
	Release of DAMPs, chemokines and cytokines	Release of DAMPs, chemokines and cytokines	Proteolytic activation of pro-IL-1β. Release of DAMPs, chemokines and cytokines
Less immunogenic	Immunogenic?	Immunogenic	Immunogenic
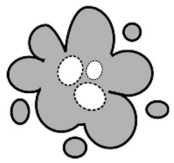	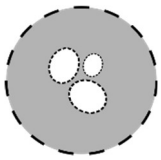	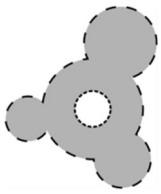	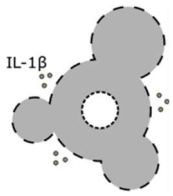

2.3 *GSDME* AND CANCER

Currently no recurrent genetic mutations in *GSDME* were found in tumors [21,23]. Instead, *GSDME* expression seems to be epigenetically regulated. *GSDME* promoter methylation, *GSDME* mRNA and protein expression were analyzed in different cancer types in different studies [15,21–27,29–33,35–40,59]. For detailed information on *GSDME* methylation/expression per tumor type for patient samples and cell lines see Table 2 and Supplementary Table 1, respectively.

Table 2. GSDME and cancer – patient studies

Reference	Analysis	Technique	Number of samples	Result
BREAST CANCER				
Croes *et al*, 2018 [21]	Methylation	TCGA - Infinium HumanMethylation450k array (22 CpGs in *GSDME*)	668 cancer samples 85 paired normal breast samples	Higher *GSDME* promoter methylation (14/14 CpGs) in cancer compared to normal samples (*p value* range: $9.8*10^{-14}$ – $2.2*10^{-4}$) Lower *GSDME* gene body methylation (6/6 CpGs) in cancer compared to normal samples (*p value* range: $1*10^{-12}$ – $4.5*10^{-3}$)
	Gene expression	TCGA - Agilent 244K Custom Gene Expression array	476 cancer samples 56 normal breast samples	Lower *GSDME* expression in cancer compared to normal samples (*p value*: $1.8*10^{-9}$ (array); *p value*: $2.2*10^{-16}$ (RNA-seq))
		RNA-sequencing	666 cancer samples 71 normal breast samples	Mean *GSDME* expression: cancer samples: -1.8 (array); 7.2 (RNA-seq) normal samples: -0.99 (array), 8.2 (RNA-seq)
Stoll *et al*, 2017 [23]	Methylation	TCGA – *not specified* (16 CpGs in *GSDME* promoter)	743 breast cancer samples 98 normal breast samples	*GSDME* promoter hypermethylation not explaining *GSDME* expression
	Gene expression	TCGA – not specified	*not specified*	Lower *GSDME* expression in cancer compared to normal samples (*p value*: $2.1*10^{-9}$) Lower *GSDME* expression for all groups of breast cancers (ER+, HER2+/ER-, triple negative) (*p value* range: $2.4*10^{-7}$ – $9.3*10^{-5}$)
		METABRIC – not specified	*not specified*	Lower *GSDME* expression in cancer compared to normal samples (*p value:* $1.1*10^{-12}$) Lower *GSDME* expression for all groups of breast cancers (luminal A, luminal B, HER2, basal) (*p value* range: $1.1*10^{-22}$ – 0.0083)

Reference	Analysis	Technique	Number of samples	Result
Croes *et al*, 2017 [22]	Methylation	Pyrosequencing (cut-off for positive methylation: 7%)	123 cancer samples 24 normal breast samples* 16 paired normal breast samples	Higher *GSDME* promoter methylation in cancer compared to normal samples (*p value*: $6.1*10^{-4}$) Median *GSDME* methylation: cancer samples: 12% [range: 0%–96%] normal samples: 4% [range: 1%–7%] No significant differences between paired cancer and normal breast tissues median *GSDME* methylation difference: 3.5% [range: -29%–73%]
Fujikane *et al*, 2010 [38]	Methylation	Pyrosequencing (cut-off for positive methylation: 10%)	73 cancer samples 17 normal breast samples* 15 paired normal breast samples	Higher *GSDME* promoter methylation in cancer compared to normal samples ($p < 0.001$) Mean *GSDME* methylation: cancer samples: 8.5; 95% CI [6.2-10.8] normal samples: 3.4; 95% CI [2.5-4.3] No significant differences between the paired cancer and normal breast tissues Mean *GSDME* methylation: cancer samples: 7.3; 95% CI [2.3-12.3] normal samples: 3.5; 95% CI [2.5-4.5]
Kim *et al*, 2008 [36]	Methylation	TaqMan-MSP (cut-off for positive methylation: 0.81)	34 cancer samples 13 paired normal breast samples 7 normal breast samples*	*GSDME* promoter: more often methylated in cancer compared to normal samples (*p value*: 0.006) *GSDME* methylated in: 18/34 (53%) cancer samples 2/13 (15.3%) paired normal breast samples 0/7 (0%) healthy normal breast samples
	Gene expression	Real-time RT-PCR	1 cancer sample 1 paired normal breast sample 1 normal breast sample*	Lower *GSDME* expression in cancer compared to normal samples (paired: *p value* = 0.003; unpaired: *p value* = 0.002)
		Cancer Profiling Array	10 paired cancer – normal breast samples	Lower *GSDME* expression in 6/10 (60%) of cancer compared to normal samples
Thompson and Weigel, 1998 [15]	Gene expression	Semi-quantitative RT-PCR	29 cancer samples: 15 ER+ 14 ER- 2 normal breast samples (ER-)	Lower *GSDME* expression in ER+ compared to ER- breast samples ($p < 0.001$)

Reference	Analysis	Technique	Number of samples	Result
COLORECTAL CANCER				
Ibrahim *et al*, 2019 [28]	Methylation	TCGA - Infinium HumanMethylation450k array (22 CpGs in *GSDME*)	389 cancer samples 43 paired normal colon samples	Higher *GSDME* promoter (12/14 CpGs) methylation in cancer compared to normal samples (*p value* range: $1.7*10^{-16}$ – 0.025) Lower *GSDME* gene body methylation (5/6 CpGs) in cancer compared to normal samples (*p value range*: $8.3*10^{-9}$ – $4.5*10^{-3}$)
	Gene expression	TCGA - Agilent 244K Custom Gene Expression array	221 cancer samples 20 normal colon samples	No significant differences in *GSDME* expression between cancer samples and normal samples
		RNA-sequencing	437 cancer samples 39 normal colon samples	Mean *GSDME* expression: cancer samples: -0.46 (array); 5.45 (RNA-seq) normal samples: -3.18 (array), 5.8 (RNA-seq)
Yokomizo *et al*, 2012 [39]	Methylation	qMSP	85 cancer samples 85 paired normal colorectal samples	*GSDME* methylated in: 29/85 (34%) cancer samples *No results for normal samples*
Kim *et al*, 2008 [37]	Methylation	COBRA	10 cancer samples 9 paired normal colorectal samples	*GSDME* methylated in: 4/10 (40%) cancer samples 0/9 (0%) paired normal colorectal samples
		Bisulfite sequencing	5 cancer samples 10 paired normal colorectal samples	*GSDME* methylated in: 5/5 (100%) cancer samples 0/10 (0%) paired normal colorectal samples
		TaqMan-MSP (cut-off: 0.65)	100 cancer samples 100 paired normal colorectal samples 11 normal colorectal samples*	*GSDME* promoter: more often methylated in cancer compared to normal samples ($p < 0.001$) *GSDME* methylated in: 65/100 (65%) cancer samples 3/100 (3%) paired normal colorectal samples 1/11 (9%) normal colorectal samples*
	Gene expression	Real Time RT-PCR	5 cancer sample 5 paired normal breast sample 1 normal colon sample*	4/5 cancer samples reduced *GSDME* expression compared to pared normal samples *GSDME* expression in cancer 5x lower than in normal colon sample* (*p value*: 0.007)
GASTRIC CANCER				
Akino *et al*, 2006 [35]	Methylation	COBRA	89 cancer samples 89 paired normal gastric samples	46/89 (52%) cancer samples: increased *GSDME* methylation 0/89 paired normal gastric samples: *GSDME* barely detectable (~ 0%)
		Bisulfite sequencing (of region around TSS)		46 samples shown to be methylated by COBRA: all analyzed CpG sites densely methylated

Reference	Analysis	Technique	Number of samples	Result
	Gene expression	qRT-PCR	10 cancer samples	Methylated *GSDME*: Almost no *GSDME* expression (N = 5) Unmethylated *GSDME*: varying levels of *GSDME* expression (N = 5)
Kim *et al*, 2008 [36]	Methylation	TaqMan-MSP (cut-off: 1)	31 cancer samples 11 paired normal gastric samples	*GSDME* methylated in: 17/31 (54%) cancer samples 1/11 (9%) paired normal gastric samples
ESOPHAGEAL CANCER				
Wu *et al*, 2019 [26]	Protein expression	IHC (tissue microarray)	105 cancer samples 75 normal esophageal samples	Higher GSDME expression in cancer compared to normal esophageal samples
Kim *et al*, 2008 [36] (Supplementary Material)	Methylation	TaqMan-MSP (cut-off: 0.001)	18 cancer samples 20 paired normal esophageal samples	*GSDME* methylated in: 2/18 (11.1%) cancer samples 0/20 (0%) paired normal esophageal samples
BLADDER CANCER				
Kim *et al*, 2008 [36]	Methylation	TaqMan-MSP (cut-off: 0.001)	55 cancer samples 30 paired normal bladder samples	*GSDME* methylated in: 12/55 (21.8%) cancer samples 0/30 (0%) paired normal bladder samples
LUNG CANCER				
Lu *et al*, 2018 [20]	Protein expression	Western blot	20 cancer samples (10 EGFR+ and 10 EGFR-) 20 paired normal samples	Ubiquitous *GSDME* expression in all samples, both normal and cancer samples
		TMA	208 lung cancer samples of varying histotypes	*GSDME* pervasive expressed in 58.9% of TMA cases
		IHC	155 lung cancer samples: 15 *KRAS*-mutant 103 *EGFR*-mutant 37 *ALK*-rearranged	*GSDME* pervasive expressed in: 60.0% *KRAS*-mutant cases 67.0% *EGFR*-mutant cases 56.8% *ALK*-mutant cases

*: Normal samples from people without cancer; TCGA, The cancer genome atlas; METABRIC, Molecular taxonomy of breast cancer international consortium; COBRA, Combined bisulfite restriction analysis; MSP, Methylation specific PCR; TMA, Tissue microarray, IHC, Immunohistochemistry.

2.3.1 *GSDME* methylation is both a pan-cancer and cancer type specific biomarker

The potential of *GSDME* methylation as a marker for cancer detection, was initially explored in two studies involving data from *The Cancer Genome Atlas* (*TCGA*) for breast and colorectal cancer [21,28]. All of the 22 *GSDME* CpGs (Figure 3) interrogated by the Illumina 450K methylation array showed differential methylation between primary tumor and paired normal tissues. Increased methylation of promoter CpGs was observed in cancer compared to normal samples, concordant with *GSDME*'s suggested role as tumor suppressor gene. Furthermore, *GSDME* gene body methylation exhibited an opposite pattern to that in the promoter, namely a higher methylation in normal samples compared to cancer samples. Methylation levels of CpGs in the promoter region were highly correlated

with each other, as was the case with CpGs in the gene body region, but not between these two distinct regions. Interestingly, methylation levels of a combination of two *GSDME* CpGs, one in the gene body and one in the promoter, performed exceptionally well as detection biomarker. In breast cancer, the final model reached a cross validated area under the curve (AUC) of 0.93, with a sensitivity of 85.3% without false positives and overall accuracy of 87% [21]. Moreover, colorectal adenocarcinomas are reliably predicted *in silico* with a cross validated AUC of 0.95, sensitivity of 93.3%, specificity of 93.7% and overall accuracy of 97.6% in the TCGA dataset [28]. These predictions were unaffected by age and disease stage, making *GSDME* an excellent candidate for early detection irrespective of tumor stage.

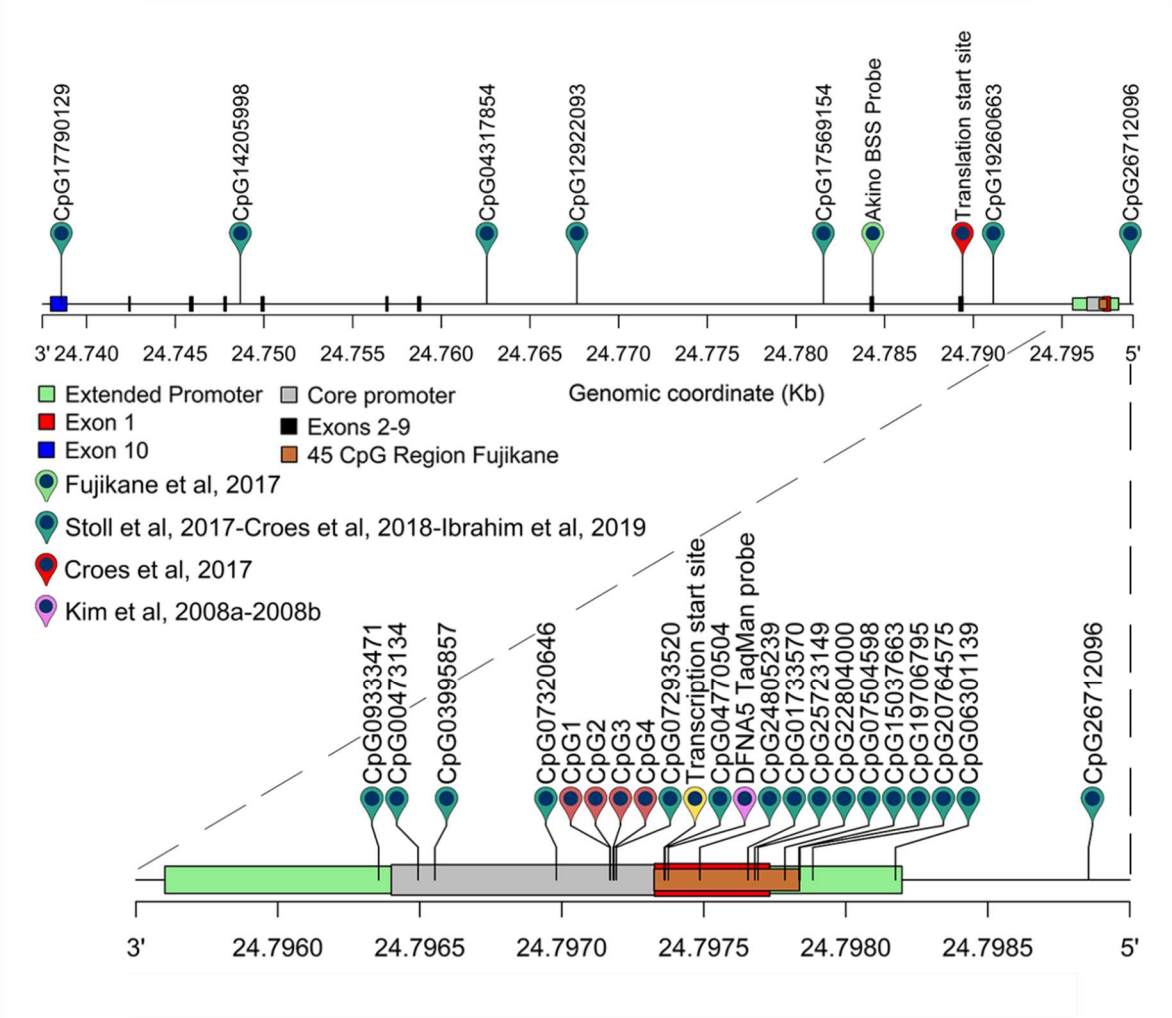

Figure 3. The *GSDME* gene with annotation of the CpGs analyzed in the different studies. The *GSDME* gene layout shows the CpGs interrogated by the different studies. The upper track outlines the full scope of the *GSDME* gene which extends from 24 737 972 to 24 809 244 on chromosome 7. The lower track is a zoomed-in section of the promoter region where several of the interrogated CpGs are located. Translation and transcription start sites are indicated by the red and yellow pins respectively. The 22 CpGs analyzed in the TCGA study are depicted in dark green [21,23,28], while CpGs 1-4 were analyzed by pyrosequencing in the study of Croes et *al* [22]. CpGs 5-8 were the ones studied by Fujikane *et al* [38]. The pink taqman probe was used in the studies of Kim *et al* [36,37]. The brown bar delimits the 514 bp region where Akino *et al* interrogated CpGs [35]. All annotations are based on the "Regulatory build of the *GSDME* gene" in Ensembl, using the Human Genome Feb. 2009 (GRCh37/hg19) assembly.

The analysis of *GSDME* methylation as a cancer detection biomarker has been expanded using TCGA methylation datasets for 14 different types of cancer [29]. A widespread hypermethylation of gene promoter CpGs and hypomethylation of gene body CpGs in different cancer tissues was reported. Combinations of six *GSDME* CpGS were able to predict cancer versus normal tissue accurately across different tumor types with an AUC of 0.87. Predictions in individual datasets using only three CpGs still resulted in AUCs ranging between 0.80 and 0.95, further highlighting *GSDME*'s potential as a pan-cancer detection biomarker. Interestingly, six of 22 CpGs were distinctly recurring in all high scoring CpG combinations. Moreover, around 75 000 combinations of six *GSDME* CpGs were tested for their ability to distinguish between different tissue types based on methylation in a combined dataset of more than 5000 tumor and 700 control tissues, exhibiting maximal AUC values ranging between 0.79 and 0.98 for predicting individual cancer types against all others, with esophageal cancer scoring the lowest and prostate, thyroid and colorectal cancer scoring the highest [29]. Altogether, these data strongly suggest that *GSDME* methylation can be reliably used as both a pan-cancer and cancer type specific biomarker, highlighting the potential of *GSDME* methylation as a universal cancer detection biomarker.

2.3.2 *GSDME* methylation has potential as prognostic biomarker in breast cancer

Next to methylation differences between normal and cancer tissues, associations of *GSDME* methylation and different clinicopathological parameters were studied. In breast cancer, lobular adenocarcinomas have significantly higher *GSDME* promoter methylation values compared to ductal adenocarcinomas [21]. In addition, a significant association of *GSDME* promoter methylation and tumor stage was observed, with stage III showing the highest methylation while stage I and II performed identical [21]. Furthermore, a significant association with progesterone receptor (PR) and estrogen receptor (ER) status was found. *GSDME* promoter methylation was higher in PR+ breast adenocarcinomas compared to PR- ones, while for *GSDME* gene body methylation the opposite was true. A similar pattern as with PR was found for ER status [21]. This association was not found in previous studies in patient samples [22,36], analyzing different CpGs in less samples with a different technique (Table 2). Instead, they reported a positive association with lymph node metastasis [36] and with *HER2* amplification [22]. Surprisingly, *GSDME* gene body (not promotor) methylation, showed a (negative) association with 5-year overall survival time in ductal breast adenocarcinomas [21], revealing *GSDME* methylation as potential prognostic biomarker in breast cancer. In colorectal cancer this association was not found [28]. Instead, a significant increase of *GSDME* promoter methylation was reported in tumors with lymphatic vessel invasion and high tumor-node-metastasis (TNM) stage [39] as well as differential methylation between left sided and right sided colorectal cancer, with a higher methylation observed in right sided tissue [28]. For gastric cancer, correlations of *GSDME* methylation with positivity for Epstein Barr virus, absence of metastasis and presence of the

CpG island methylator phenotype (CIMP) were found [35]. For most of these associations, the clinical importance is still unknown, but they may provide valuable information for further studies. Especially the association of *GSDME* gene body methylation with 5-year overall survival might have impact on clinical practice.

2.3.3 No clear difference in *GSDME* expression between normal and cancer cells

In addition to methylation, *GSDME* mRNA or protein expression were compared between cancer and normal tissue [20,21,23,26,28,36,37] (Table 2). Mostly, *GSDME* expression is downregulated in cancer compared to normal samples [21,23,36,37]. However, some studies reported no differences in *GSDME* mRNA [28] nor protein [20] expression between cancer and paired normal samples. In one study, *GSDME* protein expression was even higher in cancer compared to normal samples [26]. These divergent results prevent uniform conclusions about the difference in *GSDME* expression between normal and cancer samples. Therefore, in contrast to methylation, *GSDME* expression does not provide a solid basis for a universal cancer detection marker [21,28]. Despite the clear differences in *GSDME* methylation between cancer and normal tissue, no clear correlation between *GSDME* methylation and *GSDME* expression was found in patients [21,23,28,36].

2.3.4 *GSDME* expression may have potential as prognostic marker in esophageal cancer

For *GSDME* mRNA and protein expression, several associations with clinicopathological parameters were reported. Several studies found an inverse correlation between ER status and *GSDME* expression [15,21,36] (Table 2), forming the basis for another name for *GSDME*, namely *ICERE* (*inversely correlated with estrogen receptor expression*) [15]. Moreover, a significantly higher *GSDME* expression in lobular adenocarcinomas as compared to ductal adenocarcinomas was reported in breast cancer [21]. In lung adenocarcinoma, associations with *EGFR*, *STK11* and *KEAP1/NFEL2* mutation status were found [20]. *GSDME* mRNA was modestly upregulated in *EGFR*-mutant neoplasms, but downregulated in *STK11*- or *KEAP1/NFEL2*-mutant tumors, as compared with the respective wild-type counterparts. In squamous esophageal cancer, *GSDME* protein expression level was positively correlated with a better prognosis [26]. The 5-year survival rate of the GSDME high expression group was significantly higher compared to the GSDME low expression group, suggesting GSDME's potential as prognostic biomarker in squamous esophageal cancer. The better outcome is explained by the potential of *GSDME* expressing esophageal cancer cells to die by pyroptosis following cisplatin and BI2536 co-treatment, which is a strongly immunogenic type of cell death [26]. Remarkably, also other *GSDME* expressing cancer types such as melanoma have been reported to generate strong immune infiltration (see later) [68].

2.3.5 Introduction of GSDME in cancer cell lines decreases cell growth

In contrast to patient samples, a clear correlation between GSDME methylation and expression was found in several individual cell line experiments. After treatment with the demethylating agent 5-aza-2'-deoxycytidine or decitabine, cell lines that first did not express methylated *GSDME* alleles, now expressed *GSDME* after demethylation [33,35–38]. Moreover, introduction of GSDME in cancer cell lines markedly decreased cell growth and colony forming ability [24,35–37]. In contrast, knock down of GSDME increased cellular invasiveness and growth *in vitro* [36,37,65]. Furthermore, different studies suggested the involvement of GSDME in p53-dependent pathways [34,35,37,38]. *GSDME* is a target of the p53 family and especially p63γ [38] as its expression can be upregulated by p63γ through direct interaction with the p53 response element of *GSDME* [34].

2.3.6 The role of GSDME expression on tumor growth in mice is still ambiguous

Despite promising in vitro studies, in vivo experiments in mice are inconclusive about the role of GSDME in tumor biology. Two independent intestinal cancer mouse models exhibited no major differences in tumor development between GSDME KO and WT mice, neither for the number of affected mice, nor for the multiplicity of proliferative lesions per mouse [69]. Similarly, the size and weight of GSDME depleted xenograft tumors were comparable to WT xenograft tumors in colorectal cancer [70], lung cancer [20] and melanoma [30] models. However, in another melanoma study GSDME KO tumors formed and grew significantly faster than those expressing GSDME. This tumor suppressive activity of GSDME might be related to its ability to execute necrosis and potentiate caspase-3 activation through the release of cyt c from the mitochondria [65] (Figure 2). In line with the enhanced and accelerated cell death in presence of GSDME, more severe inflammation was found in intestinal tumors in GSDME WT compared to GSDME KO mice [69]. As GSDME expressing tumors also increase macrophage-mediated phagocytosis and attract more tumor-infiltrating natural-killer and CD8+ T lymphocytes [71], GSDME might be involved in creating a more inflammatory tumor microenvironment by induction of necrotic cell death [69].

2.3.7 GSDME as potential predictive biomarker in cancer: an important ally in chemotherapy treatment

As GSDME protein expression does not always affect tumor volume and weight [20,70], GSDME is probably not directly involved in tumor development. Nevertheless, its presence seems an important determinant for the type of cell death induced by chemotherapy, thereby influencing the efficiency of the chemotherapy treatment. Several cancer cell lines that do express GSDME show caspase-3-dependent GSDME activation following chemotherapy treatment [20,25,27,30,32,33,70,72,73], e.g. SH-SY5Y (neuroblastoma) following doxorubicin [33] or dasatinib [72], etoposide treated MeWo (skin melanoma) [30,33] cell lines and cisplatin + BIX-01294 treated SGC-7901 (shown to be a HeLa derivative (endocervical adenocarcinoma)) [73]. These cells exhibit a necrotic morphology,

characterized by swelling and direct lysis of the plasma membrane, thereby releasing their content into the tumor microenvironment (Table 1). Remarkably, in absence of GSDME expression (e.g. as is the case in Jurkat cells), the same treatment induces apoptotis characterized by cell shrinkage, plasma membrane blebbing and the release of apoptotic bodies (Table 1) [33,70]. In addition, GSDME expression affects chemotherapy efficiency as *GSDME* knockdown in A-549 cells attenuated cisplatin-induced cell death compared to WT cells [32]. Similarly, combined administration of sulfasalazine with iron dextran no longer inhibited A-375 xenograft tumor growth after *GSDME* knock down [31]. Furthermore, Ceritinib performs partially impaired treatment efficacy upon *GSDME* KO in NCI-H3122 cells [20]. An improvement of therapeutic index was observed as well in case of exogenous *GSDME* expression in HCC827 cells [20]. Moreover, combined treatment of decitabine, a DNA methyltransferase inhibitor elevating *GSDME* expression, with chemotherapy or phototherapy improved anti-tumor treatment efficiencies [33,74,75]. Nevertheless, in some cases *GSDME* expression had no effect on cell survival after chemotherapy treatment [25,70], complicating the role of *GSDME* in chemotherapy-induced cell death. An interesting finding in that respect is that the pore-forming activity of GSDME is prevented by phosphorylation at Thr6 [65]. As GSDMA, a close relative of GSDME, is phosphorylated by Polo like kinase 1 (Plk1) at Thr8 [76], the same kinase might inactivate *GSDME* [65]. Plk1 is a known oncogene that is often activated in cancer cells, suggesting a second way of inactivation of *GSDME* in cancer cells, next to methylation. Remarkably, co-treatment of the Plk1 inhibitor BI2536 with cisplatin sensitizes esophageal cancer cells, which show a high intrinsic *GSDME* expression and GSDME cleavage after cisplatin treatment [26]. This might indicate that despite high *GSDME* expression in these cells, GSDME cannot execute its cell death function due to phosphorylation by Plk1, and that inhibition of GSDME phosphorylation can intensify the response to chemotherapy treatment. Moreover, in those cases where *GSDME* depletion didn't affect tumor formation in treated cancer cells, it did reduce the release of pro-inflammatory factors, including IL-1β and lactate dehydrogenase (LDH) [25,70], changing the inflammatory status of the tumor microenvironment. Furthermore, *GSDME* depletion reduces tissue injury and inflammation in the lungs, spleen and gastrointestinal tract after chemotherapy in healthy mice [33], again suggesting that GSDME-meditated cell death influences the extent of inflammation. Moreover, implanted GSDME-deficient melanoma tumors show impaired HMGB1 release and reduced tumor-associated T cell and activated dendritic cell infiltrates in response to BRAFi + MEKi treatment compared to the control counterparts [68]. As *GSDME* KO tumors also showed more frequent tumor regrowth after BRAFi + MEKi removal, *GSDME* dependent inflammation around the tumor can be considered anti-tumorigenic.

Next to chemotherapeutics, the efficiency of other therapeutics is influenced by *GSDME* expression. For example, treatment of CCRF-CEM cells with glucocorticoids induces *GSDME* expression followed by cell death and enhancement of caspase-3 activation [40,65]. As glucocorticoids are used, in combination with other therapeutics, for the

treatment of lymphoid malignancies, the expression of *GSDME* in these malignancies might be an important factor in their response to this kind of therapy. In conclusion, *GSDME* expression sometimes correlates with tumor growth, but often contributes to therapeutic efficiency and is therefore an important ally in (chemotherapy) treatment.

2.4 CONCLUSION

Overall, *GSDME* shows a broad applicability in cancer diagnosis, monitoring and therapy. Especially *GSDME* methylation shows strong potential as detection biomarker in different cancer types. The methylation of different CpG combinations proved diagnostically useful in predicting cancer versus normal tissue accurately across 14 different tumor types, irrespective of tissue type, highlighting the potential of *GSDME* methylation as a pan-cancer biomarker. Furthermore, other combinations were able to differentiate between different types of cancer. Therefore, *GSDME* methylation patterns and their generalizability over different tumor types could form the basis of a minimally invasive biomarker assay for early cancer detection. In addition to detection, *GSDME* methylation and protein expression may show promise as prognostic markers. To evaluate this, current studies should be expanded to more tumor types, as until now the potential of *GSDME* as prognostic marker is only investigated in breast, colorectal and esophageal cancer. Moreover, large prospective studies, with homogenous cancer populations are needed.

A next step to develop *GSDME* methylation as a minimally invasive pan-cancer biomarker could be the analysis of *GSDME* methylation in liquid biopsies. A liquid biopsy is defined as the analysis of tumor material (e.g. cells or nucleic acids) obtained through sampling of blood or other body fluids. One approach to identify tumor specific (epi)genetic aberrations is the analysis of tumor DNA present in plasma, called circulating tumor DNA (ctDNA). ctDNA is released primarily *via* dying tumor cells, which may occur throughout a tumor, giving a more representative picture of the tumor genome compared to single biopsies. Moreover, it is believed that ctDNA is readily detected in plasma of even early stage cancer patients. Several studies have provided proof of principle for the detection of tumor specific methylation changes on ctDNA [77–79].

For the association of *GSDME* mRNA and protein expression with cancer, the conclusions are less clear, hampering the use of GSDME expression as detection marker. Given a higher promoter methylation, most studies report a downregulation of *GSDME* expression in cancer as compared to normal tissues. Nevertheless, identical or even higher *GSDME* expression in cancer compared to normal samples has been found as well, which seems contrary to GSDME's potential tumor suppressive function. However, recent insights argue for a second possibility, viz. that despite its processing by caspase-3, mechanisms exist that keep GSDME inactive. While methylation of specific CpGs in the *GSDME* gene inhibits its expression, post-translational phosphorylation of Thr6 in the GSDME protein prevents its pore forming capacity in plasma membranes and mitochondria. The kinases

responsible for direct phosphorylation of this residue have not yet been characterized, but PLK1 seems to be a likely candidate, as it induces phosphorylation of many cellular proteins including GSDMA. Importantly, PLK1 is an oncogene, which counteracts the potential tumor suppressor activity of *GSDME*.

Finally, recent breakthroughs on the function of the GSDMs have shed new light on the importance of GSDME expression in cancer and cancer treatment. Growing evidence suggests that *GSDME* indirectly acts as a tumor suppressor by promoting a more inflammatory and immunogenic microenvironment *via* the release of cellular content such as danger- or damage-associated molecular patterns (DAMPs), chemokines and cytokines. Nevertheless, pending on the stage of tumorigenesis, inflammation can have pro- or anti-tumorigenic effects. On the one hand, inflammation attracts e.g. natural killer and CD8+ T cells to the tumor site, which are able to eliminate cancer cells. On the other hand, tumor-associated macrophages and regulatory T cells can be attracted and dampen the effect of innate and adaptive effector immune cells at various levels through different mechanisms. As GSDME expressing tumors are shown to attract more natural killer and CD8+ cells, which act anti-tumorigenic, it makes sense that cancer cells are selected that silence *GSDME*, resulting in a more hidden niche for the immune system. Moreover, several studies pointed GSDME expression levels as an important determinant in response to chemotherapy, thereby influencing therapeutic efficacy. Therefore, the potential of *GSDME* as new therapeutic target to boost the immunogenicity of cancer death should be studied in more detail. For instance, therapeutic induction and activation of *GSDME* can be of clinical value to turn ‘cold’ tumors, which contain few infiltrating T cells, into ‘hot’ ones, containing high levels of infiltrating T cells and more antigen processing, all contributing to an improved response to immunotherapy. As proof of concept, the controlled release of N-GSDMA3 from an antibody-drug conjugate selectively into tumor cells in mice using a bioorthogonal chemical system, was shown to enhance anti-tumor responses such as increased $CD3^+$ T cell infiltration [80]. Moreover, induction of pyroptosis in only 15% of the cells proved sufficient to clear the entire tumor graft [80], emphasizing the need for selective delivery methods, specific small-molecule GSDME activators or gene therapy methods for direct induction of pyroptotic cell death. However, caution is advised as GSDME mediated pyroptosis is not always beneficial. Activation of GSDME mediated pyroptosis by chimeric antigen receptor (CAR) T cells was recently shown to activate caspase-1 and subsequent GSDMD in macrophages during CAR T cell therapy, leading to extensive cytokine release and cytokine release syndrome eliciting undesirable side effects in patients [81]. Altogether, more fundamental research on the biology of GSDME is required to unravel its full clinical potential.

Acknowledgements

Research in the lab of GVC is supported by research grants awarded by the University of Antwerp (BOF/Methusalem grant 42/FA020000/FFB190208). LC is supported by a Ph.D. fellowship of the Research Foundation – Flanders (FWO; 11Y9817N). JI is supported by a Ph.D. fellowship of the Research Foundation – Flanders (FWO; 11B5220N). PV is senior full professor at the UGent and senior PI at the VIB. Research in the Vandenabeele group is supported by Flemish grants (EOS MODEL-IDI, FWO Grant 30826052), FWO research grants G.0E04.16N, G.0C76.18N, G.0B71.18N, G.0B96.20N), Methusalem (BOF16/MET_V/007), Foundation against Cancer (FAF-F/2016/865), CRIG and GIGG consortia, and VIB. EDS's PhD is supported by the Foundation against Cancer project.

Conflict of Interest

The authors declare no conflict of interest.

References

1. Van Laer, L. *et al.* (1998) Nonsyndromic hearing impairment is associated with a mutation in DFNA5. *Nat. Genet.* 20, 194–197
2. Bischoff, A.M.L.C. *et al.* (2004) A novel mutation identified in the DFNA5 gene in a Dutch family: a clinical and genetic evaluation. *Audiol. Neurootol.* 9, 34–46
3. Op De Beeck, K. *et al.* DFNA5, a gene involved in hearing loss and cancer: A review. , *Annals of Otology, Rhinology and Laryngology*, 121. (2012) , 197–207
4. Wang, H. *et al.* (2018) Further evidence for “gain-of-function” mechanism of DFNA5 related hearing loss. *Sci. Rep.* 8, 1–7
5. Yu, C. *et al.* (2003) A 3-nucleotide deletion in the polypyrimidine tract of intron 7 of the DFNA5 gene causes nonsyndromic hearing impairment in a Chinese family. *Genomics* 82, 575–9
6. Cheng, J. *et al.* (2007) A novel DFNA5 mutation, IVS8+4 A>G, in the splice donor site of intron 8 causes late-onset non-syndromic hearing loss in a Chinese family. *Clin. Genet.* 72, 471–477
7. Park, H.-J. *et al.* (2010) Evidence for a founder mutation causing DFNA5 hearing loss in East Asians. *J. Hum. Genet.* 55, 59–62
8. Nishio, A. *et al.* (2014) A DFNA5 mutation identified in Japanese families with autosomal dominant hereditary hearing loss. *Ann. Hum. Genet.* 78, 83–91
9. Chai, Y. *et al.* (2014) A novel splice site mutation in DFNA5 causes late-onset progressive non-syndromic hearing loss in a Chinese family. *Int. J. Pediatr. Otorhinolaryngol.* 78, 1265–8
10. Li-Yang, M.-N. *et al.* (2015) IVS8+1 DelG, a Novel Splice Site Mutation Causing DFNA5 Deafness in a Chinese Family. *Chin. Med. J. (Engl).* 128, 2510–5
11. Nadol, J.B. *et al.* (2015) Histopathology of the Human Inner Ear in a Patient With Sensorineural Hearing Loss Caused by a Variant in DFNA5. *Otol. Neurotol.* 36, 1616–1621
12. Booth, K.T. *et al.* (2018) Exonic mutations and exon skipping: Lessons learned from DFNA5. *Hum. Mutat.* 39, 433–440
13. Saeki, N. *et al.* (2000) Gasdermin (Gsdm) localizing to mouse Chromosome 11 is predominantly expressed in upper gastrointestinal tract but significantly suppressed in human gastric cancer cells. *Mamm. Genome* 11, 718–24
14. Tamura, M. *et al.* (2007) Members of a novel gene family, Gsdm, are expressed exclusively in the epithelium of the skin and gastrointestinal tract in a highly tissue-specific manner. *Genomics* 89, 618–629
15. Thompson, D.A. and Weigel, R.J. (1998) Characterization of a gene that is inversely correlated with estrogen receptor expression (ICERE-1) in breast carcinomas. *Eur. J. Biochem.* 252, 169–177
16. Op de Beeck, K. *et al.* (2011) The DFNA5 gene, responsible for hearing loss and involved in cancer, encodes a novel apoptosis-inducing protein. *Eur. J. Hum. Genet.* 19, 965–973
17. Ding, J. *et al.* (2016) Pore-forming activity and structural autoinhibition of the gasdermin family. *Nature* 535, 111–116
18. Van Rossom, S. *et al.* (2012) The splicing mutant of the human tumor suppressor protein DFNA5 induces programmed cell death when expressed in the yeast Saccharomyces cerevisiae. *Front. Oncol.* 2, 1–14
19. Van Rossom, S. *et al.* (2015) The deafness gene DFNA5 induces programmed cell death through mitochondria and MAPK-related pathways. *Front. Cell. Neurosci.* 9, 1–15

20. Lu, H. *et al.* (2018) Molecular targeted therapies elicit concurrent apoptotic and GSDME-dependent pyroptotic tumor cell death. *Clin. Cancer Res.* 24, 6066–6077
21. Croes, L. *et al.* (2018) Large-scale analysis of DFNA5 methylation reveals its potential as biomarker for breast cancer. *Clin. Epigenetics* 10, 1–13
22. Croes, L. *et al.* (2017) DFNA5 promoter methylation a marker for breast tumorigenesis. *Oncotarget* 8, 31948–31958
23. Stoll, G. *et al.* (2017) Pro-necrotic molecules impact local immunosurveillance in human breast cancer. *Oncoimmunology* 6, 1–8
24. Wang, C.J. *et al.* (2013) The expression and regulation of DFNA5 in human hepatocellular carcinoma DFNA5 in hepatocellular carcinoma. *Mol. Biol. Rep.* 40, 6525–6531
25. Wang, Y. *et al.* (2018) GSDME mediates caspase-3-dependent pyroptosis in gastric cancer. *Biochem. Biophys. Res. Commun.* 495, 1418–1425
26. Wu, M. *et al.* (2019) A PLK1 kinase inhibitor enhances the chemosensitivity of cisplatin by inducing pyroptosis in oesophageal squamous cell carcinoma. *EBioMedicine* 41, 244–255
27. Yu, P. *et al.* (2019) Eukaryotic elongation factor-2 kinase regulates the cross-talk between autophagy and pyroptosis in doxorubicin-treated human melanoma cells in vitro. *Acta Pharmacol. Sin.* 40, 1237–1244
28. Ibrahim, J. *et al.* (2019) Methylation analysis of Gasdermin E shows great promise as a biomarker for colorectal cancer. *Cancer Med.* 8, 2133–2145
29. Ibrahim, J. *et al.* (2019) The Gasdermin E gene Potential as a Pan-Cancer Biomarker, While Discriminating between Different Tumor Types. *Cancers (Basel).* 11, 1810
30. Lage, H. *et al.* (2001) DFNA5 (ICERE-1) contributes to acquired etoposide resistance in melanoma cells. *FEBS Lett.* 494, 54–59
31. Zhou, B. *et al.* (2018) Tom20 senses iron-activated ROS signaling to promote melanoma cell pyroptosis. *Cell Res.* 28, 1171–1185
32. Zhang, C. *et al.* (2019) Chemotherapeutic paclitaxel and cisplatin differentially induce pyroptosis in A549 lung cancer cells via caspase-3/GSDME activation. *Apoptosis* 24, 312–325
33. Wang, Y. *et al.* (2017) Chemotherapy drugs induce pyroptosis through caspase-3 cleavage of a gasdermin. *Nature* 547, 99–103
34. Masuda, Y. *et al.* (2006) The potential role of DFNA5, a hearing impairment gene, in p53-mediated cellular response to DNA damage. *J. Hum. Genet.* 51, 652–664
35. Akino, K. *et al.* (2007) Identification of DFNA5 as a target of epigenetic inactivation in gastric cancer. *Cancer Sci.* 98, 88–95
36. Kim, M.S. *et al.* (2008) Methylation of the DFNA5 increases risk of lymph node metastasis in human breast cancer. *Biochem. Biophys. Res. Commun.* 370, 38–43
37. Kim, M.S. *et al.* (2008) Aberrant promoter methylation and tumor suppressive activity of the DFNA5 gene in colorectal carcinoma. *Oncogene* 27, 3624–3634
38. Fujikane, T. *et al.* (2010) Genomic screening for genes upregulated by demethylation revealed novel targets of epigenetic silencing in breast cancer. *Breast Cancer Res. Treat.* 122, 699–710
39. Yokomizo, K. *et al.* (2012) Methylation of the DFNA5 gene is frequently detected in colorectal cancer. *Anticancer Res.* 32, 1319–22
40. Webb, M.S. *et al.* (2007) In CEM cells the autosomal deafness gene dfna5 is regulated by glucocorticoids and forskolin. *J. Steroid Biochem. Mol. Biol.* 107, 15–21
41. Esteller, M. (2007) Epigenetic gene silencing in cancer: the DNA hypermethylome. *Hum. Mol. Genet.* 16, R50–R59

42. Herman, J.G. (1999) Hypermethylation of tumor suppressor genes in cancer. *Semin. Cancer Biol.* 9, 359–367
43. Runkel, F. *et al.* (2004) The dominant alopecia phenotypes Bareskin, Rex-denuded, and Reduced Coat 2 are caused by mutations in gasdermin 3. *Genomics* 84, 824–835
44. Lunny, D.P. *et al.* (2005) Mutations in Gasdermin 3 Cause Aberrant Differentiation of the Hair Follicle and Sebaceous Gland. *J. Invest. Dermatol.* 124, 615–621
45. Das, S. *et al.* (2016) GSDMB induces an asthma phenotype characterized by increased airway responsiveness and remodeling without lung inflammation. *Proc. Natl. Acad. Sci.* 113, 13132–13137
46. Panganiban, R.A. *et al.* (2018) A functional splice variant associated with decreased asthma risk abolishes the ability of gasdermin B to induce epithelial cell pyroptosis. *J. Allergy Clin. Immunol.* 142, 1469–1478
47. Zihlif, M. *et al.* (2016) Association Between Gasdermin A and Gasdermin B Polymorphisms and Susceptibility to Adult and Childhood Asthma Among Jordanians. *Genet. Test. Mol. Biomarkers* 20, 143–148
48. Yu, J. *et al.* (2011) Polymorphisms in GSDMA and GSDMB are associated with asthma susceptibility, atopy and BHR. *Pediatr. Pulmonol.* 46, 701–708
49. Delmaghani, S. *et al.* (2006) Mutations in the gene encoding pejvakin, a newly identified protein of the afferent auditory pathway, cause DFNB59 auditory neuropathy. *Nat. Genet.* 38, 770–8
50. Carl-McGrath, S. *et al.* (2008) Differential expression and localisation of gasdermin-like (GSDML), a novel member of the cancer-associated GSDMDC protein family, in neoplastic and non-neoplastic gastric, hepatic, and colon tissues. *Pathology* 40, 13–24
51. Hergueta-Redondo, M. *et al.* (2014) Gasdermin-B promotes invasion and metastasis in breast cancer cells. *PLoS One* 9, 1–15
52. Katoh, M. and Katoh, M. (2004) Identification and characterization of human DFNA5L, mouse Dfna5l, and rat Dfna5l genes in silico. *Int. J. Oncol.* 25, 765–70
53. Miguchi, M. *et al.* (2016) Gasdermin C Is Upregulated by Inactivation of Transforming Growth Factor β Receptor Type II in the Presence of Mutated Apc, Promoting Colorectal Cancer Proliferation. *PLoS One* 11, 1–18
54. Saeki, N. *et al.* (2009) Distinctive expression and function of four *GSDM* family genes (*GSDMA-D*) in normal and malignant upper gastrointestinal epithelium. *Genes, Chromosom. Cancer* 48, 261–271
55. Saeki, N. *et al.* (2007) GASDERMIN, suppressed frequently in gastric cancer, is a target of LMO1 in TGF-β-dependent apoptotic signalling. *Oncogene* 26, 6488–6498
56. Shi, J. *et al.* (2015) Cleavage of GSDMD by inflammatory caspases determines pyroptotic cell death. *Nature* 526, 660–665
57. Kayagaki, N. *et al.* (2015) Caspase-11 cleaves gasdermin D for non-canonical inflammasome signalling. *Nature* 526, 666–671
58. Orning, P. *et al.* (2018) Pathogen blockade of TAK1 triggers caspase-8-dependent cleavage of gasdermin D and cell death. *Science* 362, 1064–1069
59. Rogers, C. *et al.* (2017) Cleavage of DFNA5 by caspase-3 during apoptosis mediates progression to secondary necrotic/pyroptotic cell death. *Nat. Commun.* 8, 14128
60. Sarhan, J. *et al.* (2018) Caspase-8 induces cleavage of gasdermin D to elicit pyroptosis during Yersinia infection. *Proc. Natl. Acad. Sci. U. S. A.* 115, E10888–E10897

61. Kambara, H. *et al.* (2018) Gasdermin D Exerts Anti-inflammatory Effects by Promoting Neutrophil Death. *Cell Rep.* 22, 2924–2936
62. Sollberger, G. *et al.* (2018) Gasdermin D plays a vital role in the generation of neutrophil extracellular traps. *Sci. Immunol.* 3, 1–12
63. Green, D.R. *et al.* (2016) The clearance of dying cells: table for two. *Cell Death Differ.* 23, 915–926
64. Vanden Berghe, T. Vanden *et al.* (2010) Necroptosis, necrosis and secondary necrosis converge on similar cellular disintegration features. *Cell Death Differ.* 17, 922–930
65. Rogers, C. *et al.* (2019) Gasdermin pores permeabilize mitochondria to augment caspase-3 activation during apoptosis and inflammasome activation. *Nat. Commun.* 10, 1689
66. Galluzzi, L. *et al.* (2012) Molecular definitions of cell death subroutines: recommendations of the Nomenclature Committee on Cell Death 2012. *Cell Death Differ.* 19, 107–120
67. Tixeira, R. *et al.* (2018) Gasdermin E Does Not Limit Apoptotic Cell Disassembly by Promoting Early Onset of Secondary Necrosis in Jurkat T Cells and THP-1 Monocytes. *Front. Immunol.* 9, 2842
68. Erkes, D.A. *et al.* (2020) Mutant BRAF and MEK inhibitors regulate the tumor immune microenvironment via pyroptosis. *Cancer Discov.* 10, 255–269
69. Croes, L. *et al.* (2019) Determination of the potential tumor-suppressive effects of Gsdme in a chemically induced and in a genetically modified intestinal cancer mouse model. *Cancers (Basel).* 11,
70. Yu, J. *et al.* (2019) Cleavage of GSDME by caspase-3 determines lobaplatin-induced pyroptosis in colon cancer cells. *Cell Death Dis.* 10, 1–20
71. Zhang, Z. *et al.* (2020) Gasdermin E suppresses tumour growth by activating anti-tumour immunity. *Nature* 579, 1–6
72. Zhang, J. *et al.* (2020) Distinct characteristics of dasatinib-induced pyroptosis in gasdermin E-expressing human lung cancer A549 cells and neuroblastoma SH-SY5Y cells. *Oncol. Lett.* 20, 145–154
73. Deng, B.B. *et al.* (2020) BIX-01294 enhanced chemotherapy effect in gastric cancer by inducing GSDME-mediated pyroptosis. *Cell Biol. Int.* DOI: 10.1002/cbin.11395
74. Fan, J.-X. *et al.* (2019) Epigenetics-Based Tumor Cells Pyroptosis for Enhancing the Immunological Effect of Chemotherapeutic Nanocarriers. *Nano Lett.* 19, 8049–8058
75. Zhao, P. *et al.* (2020) Programming cell pyroptosis with biomimetic nanoparticles for solid tumor immunotherapy. *Biomaterials* 254,
76. Santamaria, A. *et al.* (2011) The Plk1-dependent phosphoproteome of the early mitotic spindle. *Mol. Cell. Proteomics* 10, 1–18
77. Gai, W. and Sun, K. (2019) Epigenetic Biomarkers in Cell-Free DNA and Applications in Liquid Biopsy. *Genes (Basel).* 10, 32
78. Larsen, L.K. *et al.* (2019) DNA-Methylation-Based Detection of Urological Cancer in Urine: Overview of Biomarkers and Considerations on Biomarker Design, Source of DNA, and Detection Technologies. *Int. J. Mol. Sci.* 20, 2657
79. Locke, W.J. *et al.* DNA Methylation Cancer Biomarkers: Translation to the Clinic. , *Frontiers in Genetics*, 10. 14-Nov-(2019) , Frontiers Media S.A., 1150
80. Wang, Q. *et al.* (2020) A bioorthogonal system reveals antitumour immune function of pyroptosis. *Nature* 579, 421–426
81. Liu, Y. *et al.* (2020) Gasdermin E-mediated target cell pyroptosis by CAR T cells triggers cytokine release syndrome. *Sci. Immunol.* 5, 1–13.

Supplementary material

Supplementary table 1. GSDME and cancer – cell line studies

Reference	Analysis	Technique	Cell line	Result
BREAST CANCER				
Fujikane *et al*, 2010 [38]	Methylation	Pyrosequencing (cut-off for positive methylation: 10%)	MCF-7	Densely methylated *GSDME* (86.8%)
		Bisulfite sequencing	MCF-7, MDA-MB-436, MDA-MB-468, SK-BR-3	Densely methylated *GSDME*: MCF-7 Little or no *GSDME* methylation: MDA-MB-436, MDA-MB-468, SK-BR-3
		Real-Time PCR	MCF-7, MDA-MB-436, MDA-MB-468, SK-BR-3	*GSDME* expression: MDA-MB-436, MDA-MB-468, SK-BR-3 *GSDME* silenced: MCF-7
Kim *et al*, 2008 [36]	Methylation	TaqMan-MSP (cut-off: 0.81)	MCF-7, BT-20, MDA-MB-231, Hs 578T	Methylated *GSDME*: MCF-7, BT-20 No *GSDME* methylation: MDA-MB-231, Hs 578T
	Gene expression	Real-time RT-PCR	MCF-7, BT-20, MDA-MB-231	*GSDME* expression: MDA-MB-231 *GSDME* silenced: MCF-7, BT-20
Thompson and Weigel, 1998 [15]	Gene expression	Differential display	ER+: MCF-7, T-47D ER-: MDA-MB-231	Overexpression of *GSDME* in ER- cell lines
		Northern blot	ER+: MCF-7, T-47D, MDA-MB-361, ZR-75-1, BT-474, BT-20 ER-: MDA-MB-231	Abundant *GSDME* expression: ER- No or low *GSDME* expression: ER+
Yu *et al*, 2019 [27]	Protein expression	Western blot	MCF-7	No *GSDME* expression
Zhou *et al*, 2018 [31]	Protein expression	Western blot	MDA-MB-231	High *GSDME* expression
Wang *et al*, 2017 [33]	Protein expression	Western blot	MCF-7, MDA-MB-231, MDA-MB-468, Hs 578T, BT-549, T-47D	High *GSDME* expression: MCF-7 Low *GSDME* expression: MDA-MB-231 No *GSDME* expression: MDA-MB-468, Hs 578T, BT-549, T-47D

Reference	Analysis	Technique	Cell line	Result
COLORECTAL CANCER				
Yu *et al*, 2019 [70]	Protein expression	Western blot	HT-29, HCT 116, Caco-2	High *GSDME* expression: HT-29, HCT 116 No *GSDME* expression: Caco-2
Kim *et al*, 2008 [37]	Methylation	COBRA	HCT 116, HT-29, DLD-1	*GSDME* methylated in all cell lines tested
		Bisulfite sequencing	HCT 116, HT-29, DLD-1, RKO, SW48, LoVo, SW480	*GSDME* methylated in all cell lines tested
		TaqMan-MSP (cut-off: 0.65)	HCT 116, HT-29, DLD-1	*GSDME* methylated in all cell lines tested
	Gene expression	Microarray (Affymetrix GeneChip Human Genome U133A Array)	HCT 116, HT-29, DLD-1	*GSDME* upregulated after treatment with 5-aza-2'-deoxycytidine in all cell lines tested
		RT-PCR	HCT 116, HT-29, DLD-1, RKO, SW48, LoVo, SW480	Weak *GSDME* expression: HCT 116 No *GSDME* expression: HT-29, DLD-1, RKO, SW48, LoVo, SW480
Wang *et al*, 2017 [33]	Protein expression	Western blot	COLO 205, HCC2998, HCT 116, HCT 15, HT-29, KM12, SW620	No *GSDME* expression in all cell lines tested
GASTRIC CANCER				
Wang *et al*, 2018 [25]	Protein expression	Western blot	MKN45	*GSDME* expression
Akino *et al*, 2006 [35]	Methylation	MCA coupled with RDA	MKN7, MKN45, MKN74	Methylated *GSDME* alleles: MKN7: 0%, MKN45: 19%, MKN74: 92%
		COBRA	MKN7, MKN45, MKN74, JR-St, NUGC-3, NUGC-4, SNU-1, SNU-638, SH101, KATO III	*Figure 2B in [35]*
		Bisulfite sequencing	NUGC-3, NUGC-4, SNU-638	Methylation of almost all CpG sites analyzed in *GSDME*: NUGC-3, SNU-638 No *GSDME* methylation: NUGC-4

Reference	Analysis	Technique	Cell line	Result
	Gene expression	RT-PCR	MKN7, MKN45, MKN74, JR-St, NUGC-3, NUGC-4, SNU-1, SNU-638, SH101, KATO III	High *GSDME* expression: MKN7, NUGC-4, SNU-1, SH101 Low *GSDME* expression: MKN45, MKN74, JR-St, SNU-638 No *GSDME* expression: NUGC-3, KATO III
ESOPHAGEAL CANCER				
Wu *et al*, 2019 [26]	Protein expression	Western blot	YES-2, KYSE-30, KYSE-70, KYSE-140, KYSE-150, KYSE-180, KYSE-410, KYSE-450, KYSE-510	High *GSDME* expression: KYSE-30, KYSE-70, KYSE-140, KYSE-150, KYSE-510 Low *GSDME* expression: YES-2, KYSE-180, KYSE-410, KYSE-450
DUODENAL CANCER				
Akino *et al*, 2006 [35]	Methylation	COBRA	AZ-521	Methylated *GSDME*, *Figure 2B in [35]*
	Gene expression	RT-PCR	AZ-521	No *GSDME* expression
LIVER CANCER				
Wang *et al*, 2013 [24]	Protein expression	Western blot	Hep-G2	Low *GSDME* expression compared to MRC-5 cells (normal human fetal lung cells)
Rogers *et al*, 2017 [59]	Protein expression	Western blot	Hep-G2	High *GSDME* expression
Zhou *et al*, 2018 [31]	Protein expression	Western blot	Huh-7	No *GSDME* expression
MELANOMA				
Yu *et al*, 2019 [27]	Protein expression	Western blot	SK-MEL-5, SK-MEL-28, A-375	High *GSDME* expression in all tested cell lines
Zhou *et al*, 2018 [31]	Protein expression	Western blot	A-375, SK-MEL-1, M14, INT-MEL-17, UISO-MEL-11, IgR3, Mel-RM	High *GSDME* expression: A-375, Mel-RM, M14 Intermediate *GSDME* expression: SK-MEL-1, IgR3 No *GSDME* expression: INT-MEL-17, UISO-MEL-11

Reference	Analysis	Technique	Cell line	Result
Lage *et al*, 2001 [30]	Gene expression	Differential display (Northern blot analysis)	MeWo ETO 1 (33-fold increased resistance level against etoposide)	*GSDME* expression distinctly decreased in MeWo ETO 1 compared to MeWo
Fujikane *et al*, 2010 [38]	Methylation	Pyrosequencing (cut-off for positive methylation: 10%)	MDA-MB-435S	No *GSDME* methylation (6.8%)
		Bisulfite sequencing	MDA-MB-435S	Little or no *GSDME* methylation
		Real-Time PCR	MDA-MB-435S	*GSDME* expression
Wang *et al*, 2017 [33]	Protein expression	Western blot	MeWo, LOX-IMVI, M14, SK-MEL-2, SK-MEL-5, MDA-MB-435, SK-MEL-28, UACC-257, UACC-62	High *GSDME* expression: MeWo Low *GSDME* expression: LOX-IMVI, M14, SK-MEL-2, SK-MEL-5 No *GSDME* expression: MDA-MB-435, SK-MEL-28, UACC-257, UACC-62
LUNG CANCER				
Zhang *et al*, 2019 [32]	Protein expression	Western blot	A-549	High *GSDME* expression
Lu *et al*, 2018 [20]	Protein expression	Western blot	*EGFR*-mutant: PC-9, HCC827, HCC4006, NCI-H1975 *ALK*-mutant: NCI-H3122, NCI-H2228 *KRAS*-mutant: A-549, NCI-H23, NCI-H460, SW1573, NCI-H358, NCI-H2009, HCC44, NCI-H441 *MET*-mutant: NCI-H1437, NCI-H596, NCI-H1838, NCI-H1993, NCI-H1648 *HER2*-mutant: Calu-3, NCI-H1793 *BRAF*-mutant: NCI-H1651, NCI-H1666, NCI-H1395 Other: LXF 289, HCC366, NCI-H2073, NCI-H2170, NCI-H920, NCI-H522, NCI-H1581, HCC2270,	*GSDME* readily detected in most lung cancer cell lines disregarding oncogenic drivers No *GSDME* expression: NCI-H1838, NCI-H1395, NCI-H1581, NCI-H2030, NCI-H2172 → *Figure 2A in [20]*

Reference	Analysis	Technique	Cell line	Result
			NCI-H1915, NCI-H2030, BEN, NCI-H1568, NCI-H1435, NCI-H2172	
Wang *et al*, 2017 [33]	Protein expression	Western blot	HOP-92, NCI-H226, NCI-H522, A-549, HOP-62, NCI-H460, NCI-H522, EKVX, NCI-H23, NCI-H322M	High *GSDME* expression: HOP-92, NCI-H226, NCI-H522 Low *GSDME* expression: A-549, HOP-62, NCI-H460, NCI-H522 No *GSDME* expression: EKVX, NCI-H23, NCI-H322M
Zhou *et al*, 2018 [31]	Protein expression	Western blot	A-549	High *GSDME* expression
LEUKEMIA				
Webb *et al*, 2007 [40]	Gene expression	Microarray (Affymetrix HG_U95 Av2)	CCRF-CEM	*GSDME* expression repressed in basal state
Wang *et al*, 2017 [33] Wang *et al*, 2018 [25]	Protein expression	Western blot	HL-60	No *GSDME* expression
Wang *et al*, 2017 [33]	Protein expression	Western blot	Jurkat, CCRF-CEM, K-562, MOLT-4, RPMI-8226	No *GSDME* expression in all cell lines tested
BRAIN CANCER				
Wang *et al*, 2017 [33]	Protein expression	Western blot	SH-SY5Y, SF268, SF295, SNB-75, U-251MG, SF539	High *GSDME* expression: SH-SY5Y Low *GSDME* expression: SF268, SF295, SNB-75, U-251MG No *GSDME* expression: SF539
KIDNEY CANCER				
Wang *et al*, 2017 [33]	Protein expression	Western blot	ACHN, TK-10, 786-O, A-498, Caki-1, RXF 393L, UO-31, SN12C	High *GSDME* expression: ACHN, TK-10 Low *GSDME* expression: 786-O, A-498, Caki-1, RXF 393L, UO-31 No *GSDME* expression: SN12C

Reference	Analysis	Technique	Cell line	Result
OVARIAN CANCER				
Wang *et al*, 2017 [33]	Protein expression	Western blot	OVCAR-3, OVCAR-8, IGROV-1, OVCAR-4, SK-OV-3	Low *GSDME* expression: OVCAR-3, OVCAR-8 No *GSDME* expression: IGROV-1, OVCAR-4, SK-OV-3
PROSTATE CANCER				
Wang *et al*, 2017 [33]	Protein expression	Western blot	PC-3	Low *GSDME* expression
CERVICAL CANCER				
Thompson and Weigel, 1998 [15]	Gene expression	Northern blot	HeLa	High *GSDME* expression
Wang *et al*, 2018 [25]	Protein expression	Western blot	SGC-7901	High *GSDME* expression
ENDOMETRIAL CANCER				
Thompson and Weigel, 1998 [15]	Gene expression	Northern blot	HEC-1-B	Low *GSDME* expression

COBRA, combined bisulfite restriction analysis; MSP, methylation specific PCR; MCA, methylated CGI amplification; RDA, representational difference analysis.

Chapter 3

State of the art and research objectives

3.1 Historical perspective

The *gasdermin E* (*GSDME)* gene was originally identified in the lab of prof. Guy Van Camp at the University of Antwerp as the genetic cause of an autosomal dominant, non-syndromic form of hearing loss (originally called *DFNA5 – deafness autosomal dominant 5)* and has been intensively studied since. Remarkably, every *GSDME* mutation that was found in families affected with hearing loss, resulted in skipping of exon 8 at the messenger RNA level. Next to a role in hearing loss, several tumor suppressor genomic screens revealed *GSDME* as a possible tumor suppressor gene. Subsequent experiments demonstrated epigenetic silencing through methylation of *GSDME* and downregulation of GSDME expression in many different cancer types, pointing towards a role in cancer as well. Although clear evidence existed for the contribution of GSDME to both disorders, the physiological function of GSDME and how it could explain a role in both hearing loss and tumor biology remained unclear. In the meantime, GSDME was shown to share a strong sequence homology with other genes with unknown function of which some were associated with skin diseases and asthma, leading to the identification of the gene family of the gasdermin genes. First experiments in the lab of prof. Guy Van Camp to allocate a biological function to GSDME led to the observation that expression of exon 8 skipped GSDME resulted in cell death. Furthermore they showed that wild type (WT) GSDME consists of two domains, separated by a hinge region and that this structure is shared by other gasdermin proteins. The observation that the N-terminal domain of GSDME (N-GSDME) induced cell death to the same extent as the exon 8 skipped form, led to the hypothesis that N-GSDME induces cell death while the C-terminus probably has a regulatory role that is lost due to exon 8 skipping. Further attempts to characterize N-GSDME-mediated cell death in yeast showed a role for mitochondria and the ADP/ATP translocator genes. Moreover, preliminary analyses in eukaryotic cell lines showed that cell death induced by N-GSDME was caspase-3/8 and RIPK1 independent, resulted in damaged mitochondria, and did not show hallmarks of ferroptotic or autophagic nature. However, it remained unknown in which cell death modality GSDME is involved as did the function of other GSDM proteins. In 2015, gasdermin D (GSDMD), another member of the GSDM protein family, was identified as a substrate of the inflammatory caspases-1 and -4/5 and refocused the attention back on the GSDM proteins. Especially the resemblance of GSDME with GSDMD was striking, as both proteins were shown to have intrinsic cell death inducing activity that is executed by a homologous N-terminal domain while this activity is intramolecularly inhibited by its C-terminal domain. Hence, in this PhD project we aimed to contribute to the further investigation of GSDME-mediated cell death. Therefore, we started a collaboration with prof. Peter Vandenabeele and prof. Franck Riquet at the University of Ghent. Peter Vandenabeele established an assay portfolio and experimental tools to evaluate cell death processes at the morphological, initiator, mediator and executioner level.

Franck Riquet is specialized in biosensing and quantitative visualization of dynamic processes during cell death.

3.2 Research objectives

The first objective of this PhD project intends to investigate in which cell death modality GSDME is involved. Therefore, we chose to investigate the function of GSDME in the murine fibrosarcoma cell line L929sAhFas. This cell line is frequently used in the lab of prof. Peter Vandenabeele and hence well characterized. Moreover, it allows to study several cell death modalities such as apoptosis, TNF-mediated necroptosis and both canonical and non-canonical pyroptosis in the same cellular context. To assess the contribution of GSDME to cell death, we generated L929sAhFas cell lines with inducible GSDME expression upon doxycycline treatment. As GSDME was soon reported to be a substrate of the apoptotic caspase-3, we refined this objective and chose to focus specifically on the contribution of GSDME to apoptosis-driven secondary necrosis, which is a caspase-3 dependent cell death modality. In a first step, we measured the kinetics of plasma membrane permeabilization during apoptosis-driven secondary necrosis in the presence and absence of GSDME expression using the cell impermeant nuclear dyes, SYTOX Blue and 7-AAD, which are frequently used in the lab of prof. Vandenabeele.

Soon other members of the GSDM protein family such as N-GSDMD and N-GSDMA3 were suggested to form pores in plasma membranes *via* a barrel-stave pore mechanism. Therefore, our second objective aims to evaluate whether GSDME executes cell death *via* pore-formation as well and to elucidate its pore-forming mechanism. An *in silico* analysis of the GSDME structure and comparison with other GSDM structures might give clues about whether GSDME contributes to plasma membrane permeabilization *via* similar mechanisms. To further investigate GSDME's pore-forming characteristics and its contribution to apoptosis-driven secondary necrosis, we measured the in- and efflux of dextrans of different sizes from L929sAhFas cells with and without GSDME expression. Finally, we determined the cellular localization of N-GSDME and C-GSDME to assess plasma membrane recruitment during apoptosis-driven secondary necrosis using fluorescent tags and live cell imaging.

Part 1:
In silico analysis of GSDME

Chapter 4

In silico homology-based modeling suggests different permeabilization mechanisms for gasdermins

RESEARCH ARTICLE

Manuscript in preparation

Elke De Schutter[1,2,3], Emma Ruysseveldt[4], Paco Hulpiau[5], Savvas Savvides[1,6] and Peter Vandenabeele[1,2]

[1] VIB Center for Inflammation Research, 9052 Ghent, Belgium

[2] Department of Biomedical Molecular Biology, Ghent University, 9052 Ghent, Belgium

[3] Center of Medical Genetics, University of Antwerp and Antwerp University Hospital, Prins Boudewijnlaan 43/6, BE-2650 Edegem, Antwerp Belgium.

[4] Allergy and Immunology Research Group, Department of Microbiology, Immunology and Transplantation, KU Leuven, Leuven, Belgium

[5] Department of Bio-Medical Sciences, HOWEST University of Applied Sciences (Hogeschool West-Vlaanderen), Bruges, Belgium.

[6] Department of Biochemistry and Microbiology, Ghent University, 9052 Ghent, Belgium

Abstract

Members of the gasdermin (GSDM) protein family are involved in several forms of regulated cell death such as pyroptosis and apoptosis-driven secondary necrosis. Recently, their contribution to cell death has been attributed to their capacity to form pores in the plasma membrane. Based on its cryo-electron microscopy (cryo-EM) structure, the N-terminus of murine gasdermin A3 (N-GSDMA3) and by extension all other N-GSDM proteins have been proposed to perforate the plasma membrane *via* the barrel-stave pore-forming mechanism. However, this pore-forming mechanism is only very recently shown for N-GSDMD but not for other GSDMs such as N-GSDME. In this chapter we used a homology based strategy to model the structures of full length GSDME and the pore-forming forms of N-GSDMD and N-GSDME using the published structures of full length GSDMA3 and N-GSDMA3 as templates. Comparison of our model of full length GSDME with published structures of full length GSDMA3 and GSDMD revealed that previously identified mechanisms of auto-inhibition by C-GSDM apply to other GSDM proteins as well. Although the composition of the structures of N-GSDMA3, N-GSDMD and N-GSDME in their full length conformation are largely the same, we observed differences in the membrane-inserting regions between N-GSDMA3, N-GSDMD and N-GSDME in their open conformations, suggesting that the barrel-stave pore-forming mechanism might not be shared by all GSDM proteins. The more amphipathic character of N-GSDME's trans-membrane region might suggest that GSDME permeabilizes the plasma membrane *via* a carpet-like or toroidal pore-formation mechanism.

4.1 INTRODUCTION

For decades, the GSDM gene family was considered a gene family with unknown physiological functions, though some members were associated with several diseases such as alopecia [1,2], asthma [3] and hearing loss [4,5]. Recently, several GSDM proteins came into the spotlights as they were shown to be mediators of regulated cell death [6–10]. GSDM proteins consist of a globular, cytotoxic N-GSDM domain and an inhibitory globular C-terminal domain (C-GSDM) separated by a hinge region. To elicit their cytotoxic function, GSDMs require proteolytic cleavage within the hinge region and the liberation of C-GSDM. The best studied member of the GSDM protein family, GSDMD, is shown to be a substrate of the inflammatory caspases -1 and -4/5 that are activated during pyroptosis by canonical and non-canonical inflammasomes [6,7,11–13]. In contrast, GSDME is proteolytically activated by caspase-3, leading to apoptosis-driven secondary necrosis [8] or direct caspase-3 mediated pyroptosis [14–17]. As N-GSDM proteins are shown to bind membrane phospholipids and to localize at the plasma membrane [12,15,18–20], their cytotoxic function has been attributed to a membrane permeabilization capacity.

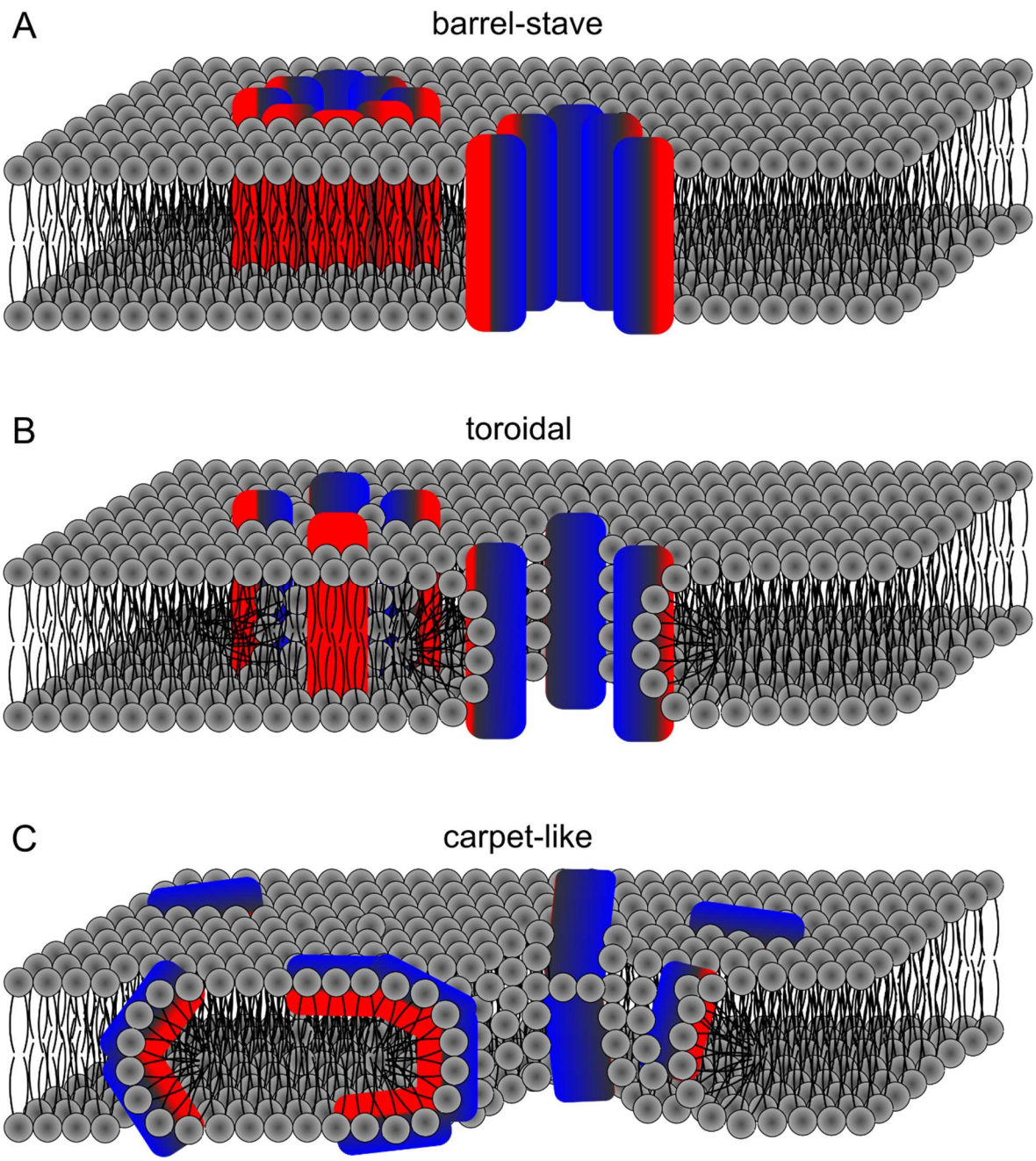

Figure 1. Different mechanisms of pore-formation leading to plasma membrane permeabilization. Schematic overview of different models for pore-formation by peptides and proteins. Hydrophobic sides of pore-forming peptides and proteins are shown in red, hydrophilic sides are shown in blue. **A.** In the barrel-stave pore model, peptides or proteins interact laterally with each other and the membrane lipids to form a channel structure. **B.** In the toroidal pore model, peptide-peptide or protein-protein interactions are absent. Instead, peptides and proteins insert in the membrane while they remain associated with the lipid headgroups, affecting the local curvature of the plasma membrane. **C.** In the carpet-like model, peptides or proteins interact parallel with the plasma membrane, forming a carpet-like structure on the lipid bilayer that destabilizes the plasma membrane.

Membrane permeabilization *via* pore-formation can happen by different mechanisms (Figure 1) [21]. The best known is the barrel-stave pore model in which different subunits interact laterally with each other, oligomerize, and insert in the plasma membrane thereby forming a channel structure (Figure 1A) [21,22]. However, proteins and peptides can also permeabilize membranes in absence of specific peptide-peptide or protein-protein interactions. In the toroidal pore model, peptides still insert perpendicularly in the membrane but remain associated with the lipid head groups, forcing a toroid or high curvature of the plasma membrane (Figure 1B) [21,23]. Lastly, in the carpet-like model, large amounts of peptides interact parallel with the plasma membrane, until the accumulation results in membrane disruption (Figure 1C) [21,24].

Although the protease that activates gasdermin A (GSDMA) as well as the cell death modality that is induced after GSDMA activation are currently unknown, the structure of murine GSDMA3 pores have recently been revealed, showing that GSDMA3 forms pores *via* the barrel-stave pore-forming mechanism [25]. In the full length (FL) conformation, N-GSDMA3 contains both α-helices and β-strands with alternating long loops of undefined structure, while C-GSDMA3 consist predominantly of long α-helices. Upon cleavage and insertion in the membrane, N-GSDMA3 undergoes an extensive conformational change [25]. The short α-helices and β-strands at the carboxyl end of N-GSDMA3 stretch out to form two aligning long antiparallel β-hairpins resulting in a β-sheet that can traverse a lipid bilayer (Figure 2). The N-terminus of N-GSDMA3 preserves its conformation and acts like a globular domain that caps the membrane after insertion of the β-sheet into the membrane. Finally, both the globular domain on top of the membrane and the membrane-inserting β-sheet are proposed to oligomerize with neighbouring subunits to form pores with a 27-fold symmetry and an inner diameter of around 180 Å [25].

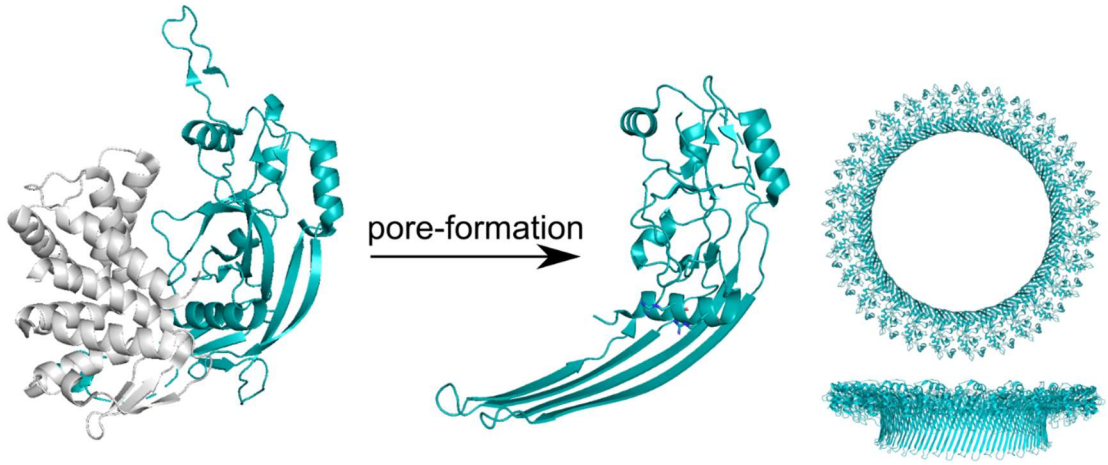

Figure 2. Conformational changes in GSDMA3 upon release from C-GSDMA3 result in an open N-GSDMA3 conformation characterized by a large 4-stranded β-sheet. C-GSDMA3 is colored in grey, N-GSDMA3 is colored in blue. In the closed full length GSDMA3 conformation, N-GSDMA3 is more compact and strongly interacts with C-GSDMA3, resulting in auto-inhibition of its cytotoxic activity. Upon release from C-GSDMA3, N-GSDMA3 undergoes a conformational change forming an open structure characterized by a globular domain and an elongated 4-stranded β-sheet. N-GSDMA3 subunits oligomerize with neighbouring subunits to form pores with a 27-fold symmetry.

Given the functional and sequence similarity between gasdermin proteins, it has been proposed that all GSDM family members exhibit comparable pore-forming activities and share common characteristics of pore formation [18]. However, information about the structures of the membrane inserted forms of other gasdermins as well as their pore-forming mechanisms are currently lacking. As the methods used to determine structures generally involve measurements on vast numbers of identical molecules at the same time, further structural studies on N-GSDM proteins and pores have been complicated by the potent death induction by GSDM proteins and the fact that pores of other GSDMs such as GSDMD vary in size and shape [12,25,26]. In this study, we used a homology-based strategy to model the structures of FL GSDME and the membrane-inserting forms of N-GSDMD and N-GSDME using the published structures of FL GSDMA3 [18] and N-GSDMA3 [25] as templates. Comparison of our model of FL GSDME with FL GSDMA3 and FL GSDMD revealed a strong resemblance of the overall structure including the composition and position of key residues involved in phospholipid binding and autoinhibition. In contrast, comparison of our modeled structures of N-GSDMD and N-GSDME with N-GSDMA3 showed that these GSDMs are indeed closely related proteins with similar properties, but also revealed significant differences in the β-strands that form the membrane-inserting β-sheet of N-GSDME, suggesting that the mechanism of GSDME pore-formation might differ from that of GSDMD and GSDMA3.

4.2 MATERIALS AND METHODS

4.2.1 Crystal structures

The protein structures of full length murine GSDMA3 (PDB ID: 5B5R), N-GSDMA3 (PDB ID: 6CB8) and full length human GSDMD (PDB ID: 6N9N) were obtained from the Protein Data Bank (www.rcsb.org) [27]. Additional information regarding the amino acid sequence, cleavage sites and other protein-specific features were derived from the UniProt Consortium (www.uniprot.org).

4.2.2 Model building and structural analysis

A homology-based model of FL-GSDME was generated using the MODELLER software (www.salilab.org/modeller) [28] using full length GSDMA3 (PDB ID: 5B5R) as template. An homology-based model of GSDMD-N and GSDME-N was generated *via* the SWISS-MODEL server (swissmodel.expasy.org) [29], using the N-GSDMA3 (PDB ID: 6CB8) as template. All ribbon diagrams, protein superimpositions and other structural analyses were visualized and carried out using the PyMOL Molecular Graphics System, Version 2.3.5 (Schrödinger, LLC). Pairwise sequence alignments were performed using the EMBOSS Needle server (www.ebi.ac.uk/Tools/psa/emboss_needle) [30].

4.3 RESULTS

4.3.1 Full length human GSDME shows a strong structural homology with murine GSDMA3 and human GSDMD

To gain insights in the working mechanism of GSDME and evaluate possible similarities between GSDM proteins, we modeled the crystal structure of human GSDME using the MODELLER software [28,31] with the crystal structure of murine GSDMA3 (PDB 5B5R) as template. As expected, subsequent structural comparison of the modeled structure of GSDME with the structure of murine GSDMA3 (PDB 5B5R) [18] using PyMol showed a strong structural homology between both proteins (Figure 3A). However, the GSDME structure was also very similar to the published structure of human GSDMD (PDB 6N9O) [32] (Figure 3B), suggesting a strong structural homology between GSDM family members. Overall, especially the organization and positioning of α-helices and β-strands of the N-terminal domain shows a strong resemblance between GSDMA3, GSDMD and GSDME. In contrast, the C-terminal domain that only consists of α-helices shows slightly more variability, with the loss of an α-helix in C-GSDME as the most notable difference when compared to C-GSDMA3 (Figure 3C) and C-GSDMD (Figure 3E). At last, the hinge regions connecting the GSDM N-terminal and C-terminal domain appeared highly variable and disordered, which can be expected for protease-sensitive interdomain regions (Figure 3D-F).

As it is presumed that the cytotoxic N-GSDM domain is kept in check by the inhibitory C-GSDM domain, we investigated the N-GSDME/C-GSDME interface in more detail. Similarly to what has been reported for GSDMA3 [18], the α1-helix and β1-2 hairpin seemed to form the primary binding surface between N-GSDME and C-GSDME in our model (Figure 4A-B). Arginine residues in the α1-helix have been shown to play an important role in the membranolytic activity of N-GSDMA3 and N-GSDMD [25]. In our full length (FL) GSDME model, the α1-helix contained arginine residues as well and was completely enclosed within the protein core (Figure 4C-D), suggesting a similar important role of the α1-helix that needs to be shielded by C-GSDME. The shielding mechanism by C-GSDM itself has been proposed to be facilitated by the deep insertion of a hydrophobic residue on the β1-2 hairpin of N-GSDM into a hydrophobic groove in C-GSDM [18]. According to Ding *et al.* this role is fulfilled by I313, F388 and A392 as the main residues providing the hydrophobic groove in C-GSDME [18]. Visualization of this region in our GSDME model (Figure 4E-F) revealed indeed that these residues in our C-GSDME model form an hydrophobic region that could provide strong interactions with the hydrophobic W46 residue on the β1-2 hairpin, suggesting that this mechanism of auto-inhibition is similar among GSDM proteins.

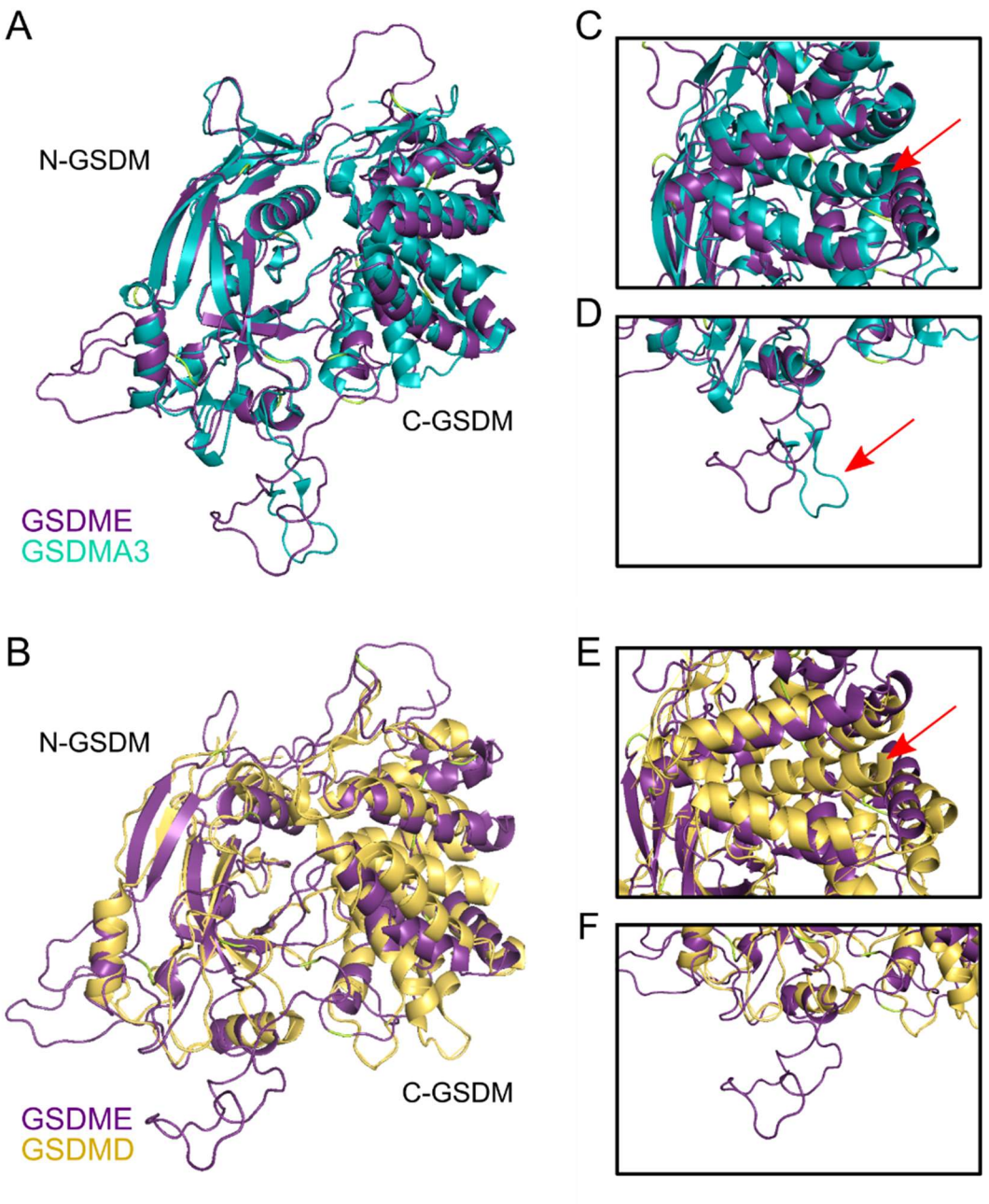

Figure 3. Structural alignment of our model of full length GSDME with full length GSDMA3 and GSDMD shows high overall structural similarity. Full length GSDMA3 (PDB 5B5R) is colored blue, full length GSDME purple and full length GSDMD (PDB 6N9O) yellow. **(A, C, D)** Superposition of full length GSDMA3 and our GSDME model. Comparison of both structures reveals the absence of a C-terminal helix in GSDME (B, red arrow) and variable hinge regions that connect the N- and C-terminal domain (C, red arrow). **(B, E, F)** Superposition of full length GSDMD and our GSDME model. Comparison of both structures reveals again the absence of a C-terminal helix in GSDME (E, red arrow). In contrast to GSDMA3 and GSDME, the hinge region of GSDMD is positioned more closely to the protein core (F).

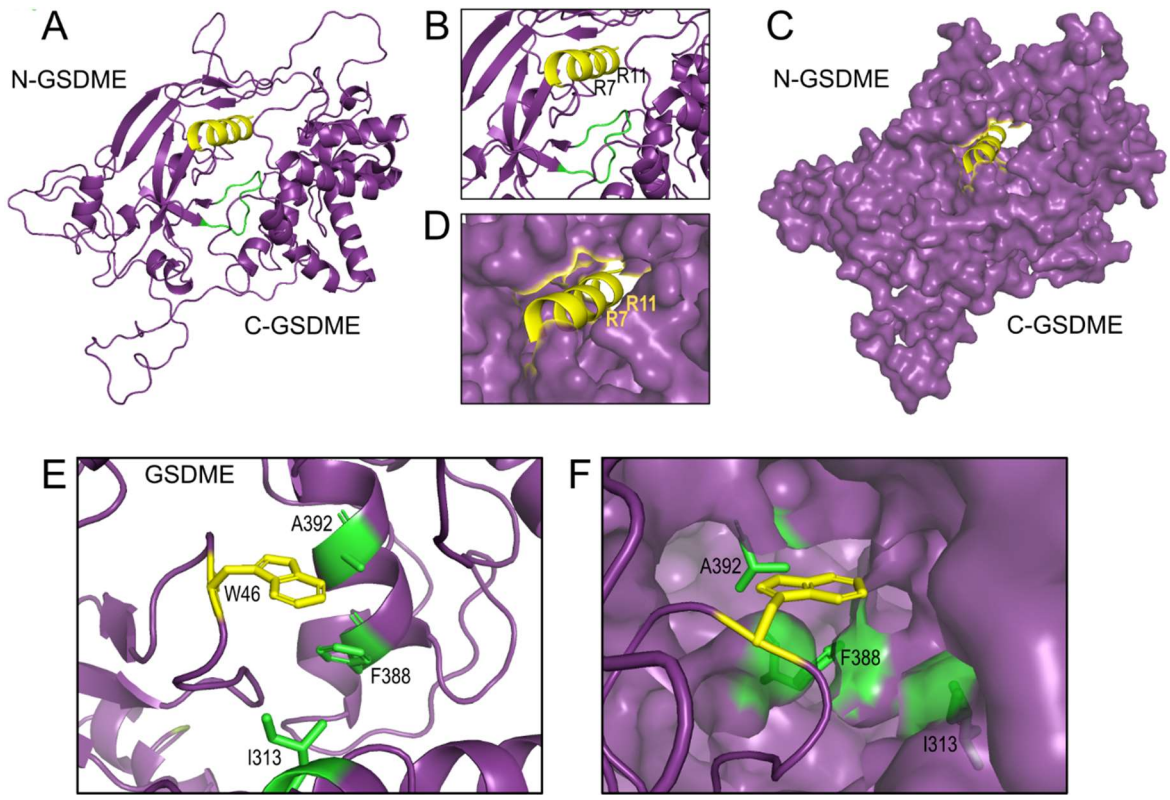

Figure 4. The primary binding surface between N-GSDME and C-GSDME is formed by the α1-helix and β1-2 hairpin of N-GSDME. (A-B) Positioning of the α1-helix (yellow) and β1-2 hairpin (green) in our model of full length GSDME represented in cartoon view. **(C-D)** Positioning of the α1-helix (yellow) in our model of full length GSDME with surface representation. **(E-F)** Interaction site of W46 (yellow) on the β1-2 hairpin in N-GSDME and I313, F388 and A392 (green) in C-GSDME both in cartoon **(E)** and surface **(F)** view.

4.3.2 Homology modelling of N-GSDMD and N-GSDME reveals differences in the transmembrane region

Recently, it has been demonstrated that N-GSDMA3 undergoes a drastic conformational change when released from its inhibitory C-GSDMA3 domain, allowing the binding to and insertion in the plasma membrane [25]. More specifically, the secondary structures in N-GSDMA3 transform resulting in a more open, elongated structure consisting of a globular domain on top of a large 4-stranded β-sheet that serves as a membrane inserting domain. Because at the time we started this analysis the open structure of N-GSDMD and N-GSDME were not available, we generated a homology-based model of both N-GSDMD and N-GSDME using the SWISS-MODEL server [29] and the published N-GSDMA3 (PDB 6CB8) [25] as template. Superimposition of our models of N-GSDMD and N-GSDME with the template structure of N-GSDMA3 shows that the overall structure of the open conformation of N-GSDMs might be highly analogous (Figure 5). Next, we analyzed the α1-helix and the large β-sheet in more detail as they are believed to be the critical regions for binding to and insertion in the plasma membrane. First, the α1-helix was identically positioned in N-GSDMA3, N-GSDMD and N-GSDME (Figure 5, 6A-B). Moreover, it contributes to the formation of a large positively charged patch in both N-GSDMD and N-

GSDME on top of the mainly hydrophobic membrane-inserting region (Figure 6A-B), which might provide an interaction face for binding to negatively charged membrane phospholipids such as cardiolipin, as reported before for N-GSDMA3 [25]. A more detailed analysis of the α1-helix showed the similar positioning of 2 accessible and protruding arginine residues (R9, R13 in GSDMA3; R7, R11 in GSDMD; R7, R11 in GSDME) (Figure 6C). Interestingly, in case of GSDMA3 and GSDMD mutation of these arginine residues was shown to compromise their membranolyitic activity [25], suggesting a similar function for the arginine residues in GSDME. Altogether, these results support our previous finding that this secondary structure is very similar among GSDM proteins and fulfills indeed an important role in the recognition and binding of membrane phospholipids.

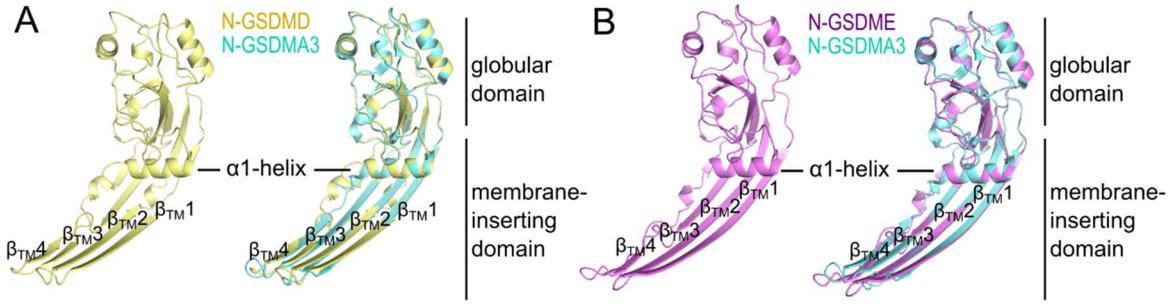

Figure 5. Homology-based models of the N-GSDMD and N-GSDME open conformation show structural similarity with N-GSDMA3. N-GSDM consist of a globular domain and a 4-stranded β-sheet, named βTM1-4 from N- to C-terminus. **(A)** N-GSDMD (yellow) alone and superimposed with N-GSDMA3 (blue). **(B)** N-GSDME (purple) alone and superimposed with N-GSDMA3.

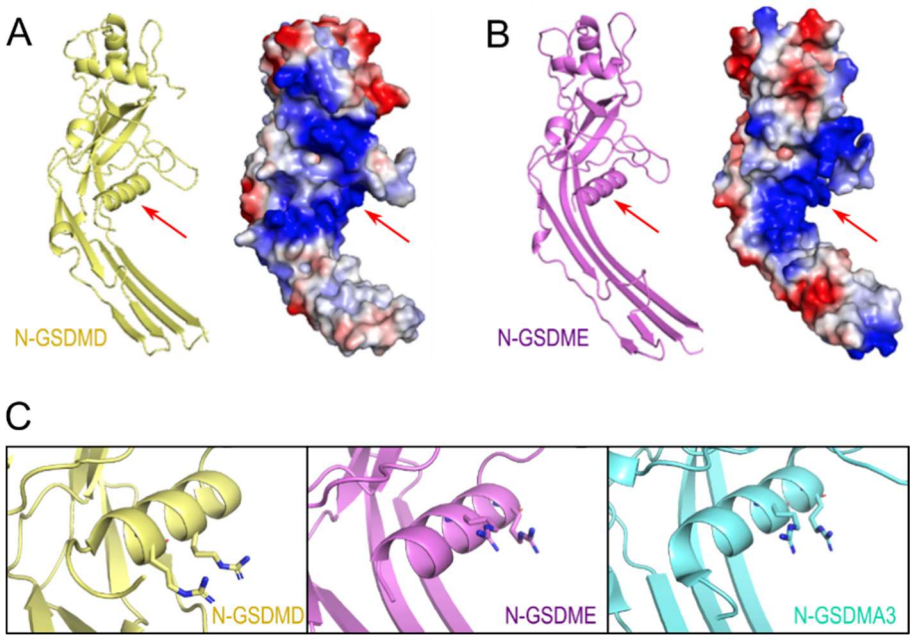

Figure 6. The α1-helix of N-GSDMD and N-GSDME provides an accessible positively charged patch. (A-B) Structural and surface potential representation of N-GSDMD **(A)** and N-GSDME **(B)**. The position of the α1-helix is indicated with a red arrow. Positive charged surfaces are colored blue, negative charged patches are colored red and non-charged hydrophobic regions are shown in white. **(C)** Detail of the α1-helix in N-GSDM with the position of two accessible arginine residues (R7, R11 in GSDMD; R7, R11 in GSDME; R9, R13 in GSDMA3).

To thoroughly analyze the membrane-inserting region, we generated a schematic overview of the position of the secondary structures (Figure 7A-C). Although our models of N-GSDMD and N-GSDME demonstrated that both the globular domain and the elongated 4-stranded β-sheet are very similar, the exact organization of the secondary elements seemed to differ between N-GSDMA3, N-GSDMD and N-GSDME. The C-terminus of N-GSDMD (Figure 7B) and especially N-GSDME (Figure 7C) show much more variation as compared to N-GSDMA3 (Figure 7A), suggesting that they allow more structural flexibility. The aberrant appearance of N-GSDME was supported by a sequence-based comparison of the four β-strands ($\beta_{TM}1$, $\beta_{TM}2$, $\beta_{TM}3$, $\beta_{TM}4$) that form the membrane inserting β-sheet of the N-GSDM proteins (Figure 7D-E), where we specifically looked for short, β-branched (T, I, V) and large, hydrophobic (F, W, Y) amino acids that are known to promote β-sheet formation [33]. Pairwise sequence alignment between GSDMA3 and GSDMD showed that all four β-strands are composed of mainly identical residues (|) and residues with strongly similar properties (:) (Figure 7D), suggesting that functional features are shared. Moreover, an alternating pattern of hydrophilic and hydrophobic residues was seen in all four β-strands of both GSDMA3 and GSDMD, suggesting the formation of a hydrophobic and hydrophilic side of the β-sheet in N-GSDMD that can serve as a lipid-binding surface analogue to what is reported for N-GSDMA3 [25]. On the other hand, pairwise alignment between GSDMA3 and GSDME (Figure 7E) revealed that their similarities in the $\beta_{TM}1$- and $\beta_{TM}2$-strands are more limited and mainly exist of residues with weakly (.) or strongly (:) similar properties next to some identical residues. Nevertheless, both $\beta_{TM}1$- and $\beta_{TM}2$-strands of N-GSDME contain predominantly β-sheet promoting residues and an alternating pattern of hydrophobic and hydrophilic residues, suggesting similar functional properties as the $\beta_{TM}1$- and $\beta_{TM}2$-strands of N-GSDMD and N-GSDMA3. In contrast, the $\beta_{TM}3$- and $\beta_{TM}4$-strands of N-GSDME and N-GSDMA3 appeared to be very different between N-GSDME and N-GSDMA3 with almost no similar amino acids, as illustrated by the presence of large gaps as well. In addition, the $\beta_{TM}3$- and $\beta_{TM}4$-strands of N-GSDME contain multiple adjacent charged residues (E, D, K), which are not preferred for β-sheet formation and could interrupt the formation of an hydrophobic surface at a particular side of the sheet to bind lipids. Altogether this observation suggest that the trans-membrane region of N-GSDME is less rigid when compared to that of N-GSDMD and N-GSDMA3.

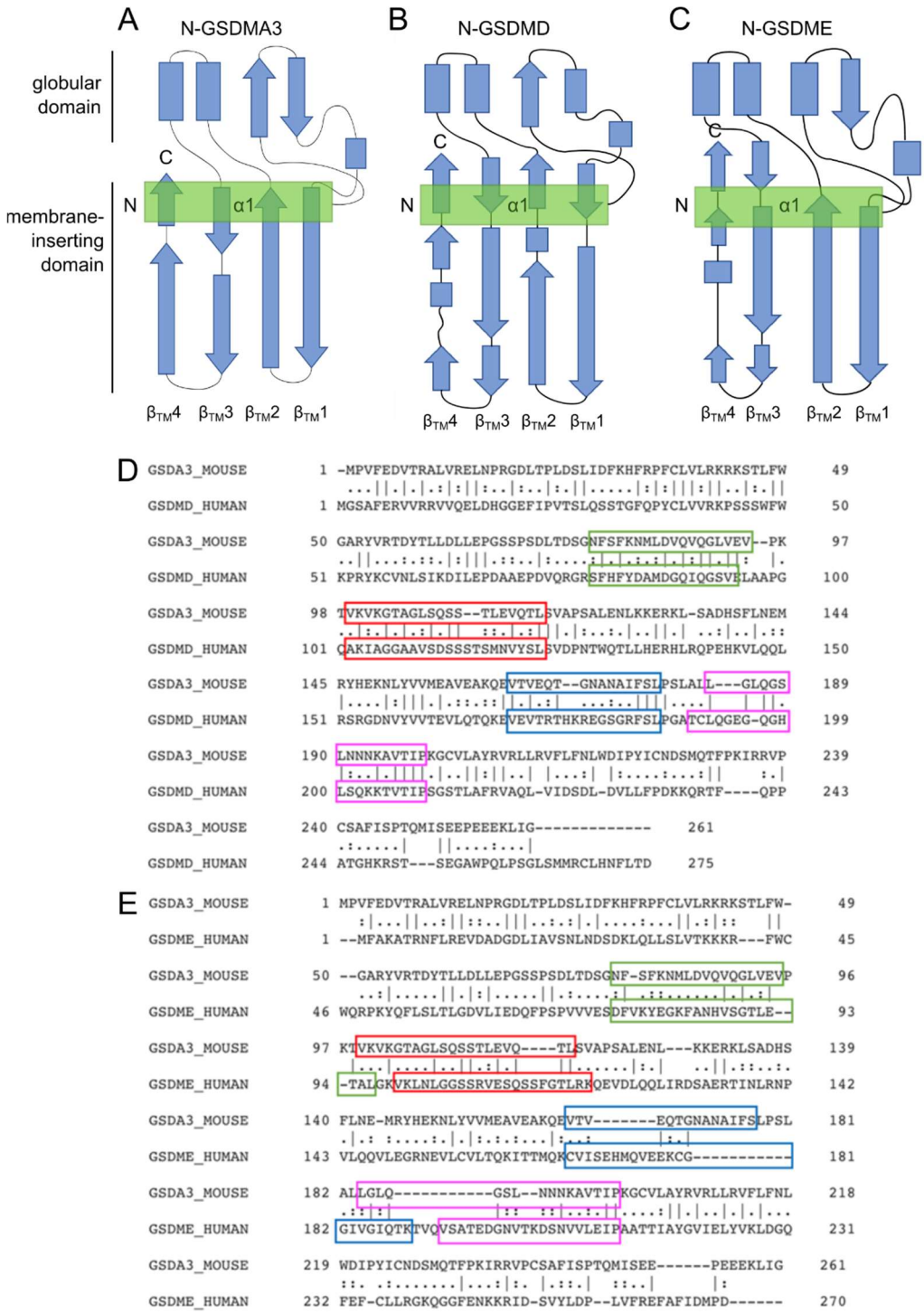

Figure 7. The C-terminus of N-GSDMD and N-GSDME show more structural flexibility when compared to N-GSDMA3. (A-C) Schematic diagram of the position of the secondary structures of N-GSDMA3 **(A)**, N-GSDMD **(B)** and N-GSDME **(C)**. α-helices are presented by rectangles, β-strands are represented by arrows. The position of the α1-helix is represented by a green rectangle. N and C represent the N- and C-terminal end of the protein chain, respectively. The four strands forming the β-sheet are named β_{TM}1-4 from N- to C-terminus. **(D-E)** Pairwise sequence alignment between N-GSDMA3 and N-GSDMD **(D)** and between N-GSDMA3 and N-GSDME **(E)**. The β_{TM}1-strand is colored green, β_{TM}2 red, β_{TM}3 blue and β_{TM}4 pink. "|": identical residues; ".": residues with weakly similar properties; ":": residues with strongly similar residues.

4.3.3 The aberrant trans-membrane region identified in N-GSDME might have implications for interunit oligomerization

Our model suggest that the transmembrane region formed by the 4-stranded β-sheet of N-GSDME is less rigid than the one in N-GSDMA3 and N-GSDMD. As the β_{TM}4-strand has been proposed to be crucial for interunit oligomerization in the GSDMA3 pore [25], the structural flexibility seen in N-GSDME might have implications for its pore-forming mechanism. To make predictions about this aspect, we analyzed the surface potentials of N-GSDMD and N-GSDME in our open conformation models and compared them with N-GSDMA3. As previously reported for GSDMA3 [25], only one side of the membrane-inserting β-sheet of N-GSDMD and N-GSDME is predominantly composed of non-charged or hydrophobic residues (Figure 8A) and is therefore hypothesized to be the side that makes contact with the lipid tails of membrane phospholipids. However, in N-GSDME some charged patches were observed as well on the hydrophobic surface that is proposed to make contact with the plasma membrane. Visualization of the amino acid residues on this surface (Figure 8B) revealed that the hydrophobic character of the β_{TM}4-strand of N-GSDME is disrupted by E197 and K203, which are both charged amino acids that cannot participate in lipid binding. In addition, polar, non-charged residues were observed in β_{TM}1 (T94), β_{TM}2 (S107) and β_{TM}3 (T188), suggesting a more amphipathic character of N-GSDME. In contrast to the hydrophobic side, the other side of the β-sheet of N-GSDMA3, N-GSDMD and N-GSDME consist mainly of hydrophilic, charged residues (Figure 8C), suggesting that this surface is in contact with the aqueous cellular milieu. Remarkably, we observed that the globular domain of N-GSDME is slightly less charged and contains a higher level of hydrophobic residues as compared to N-GSDMA3 and especially N-GSDMD, what is not expected from a surface that is in contact with the aqueous cytoplasm. Lastly, we investigated the side views of the N-GSDM monomers that are proposed to interact with other monomers to establish N-GSDM oligomerization (Figure 8D). In case of GSDMA3, three interfaces for contact between neighboring subunits were reported [25] comprising the globular region (interface I), both ends of the α1-helix (interface II), and the outer β-strands of the elongated β-sheet (interface III). While interface I and II consist of charged residues and interact with the interfaces of the other subunits *via* electrostatic interactions, interface III is predominantly hydrophobic. In our model of N-GSDMD, we were able to identify similar interfaces (Figure 8D), suggesting a similar way of oligomerization as proposed for N-GSDMA3. In contrast, subunit interaction interfaces were much less pronounced in our model of N-GSDME (Figure 8D). Nevertheless, we propose three, though weak, interfaces that might interact between N-GSDME monomers. Altogether, our observations suggest that N-GSDME pore-formation might happen by other mechanisms than the ones proposed for N-GSDMD and N-GSDMA3.

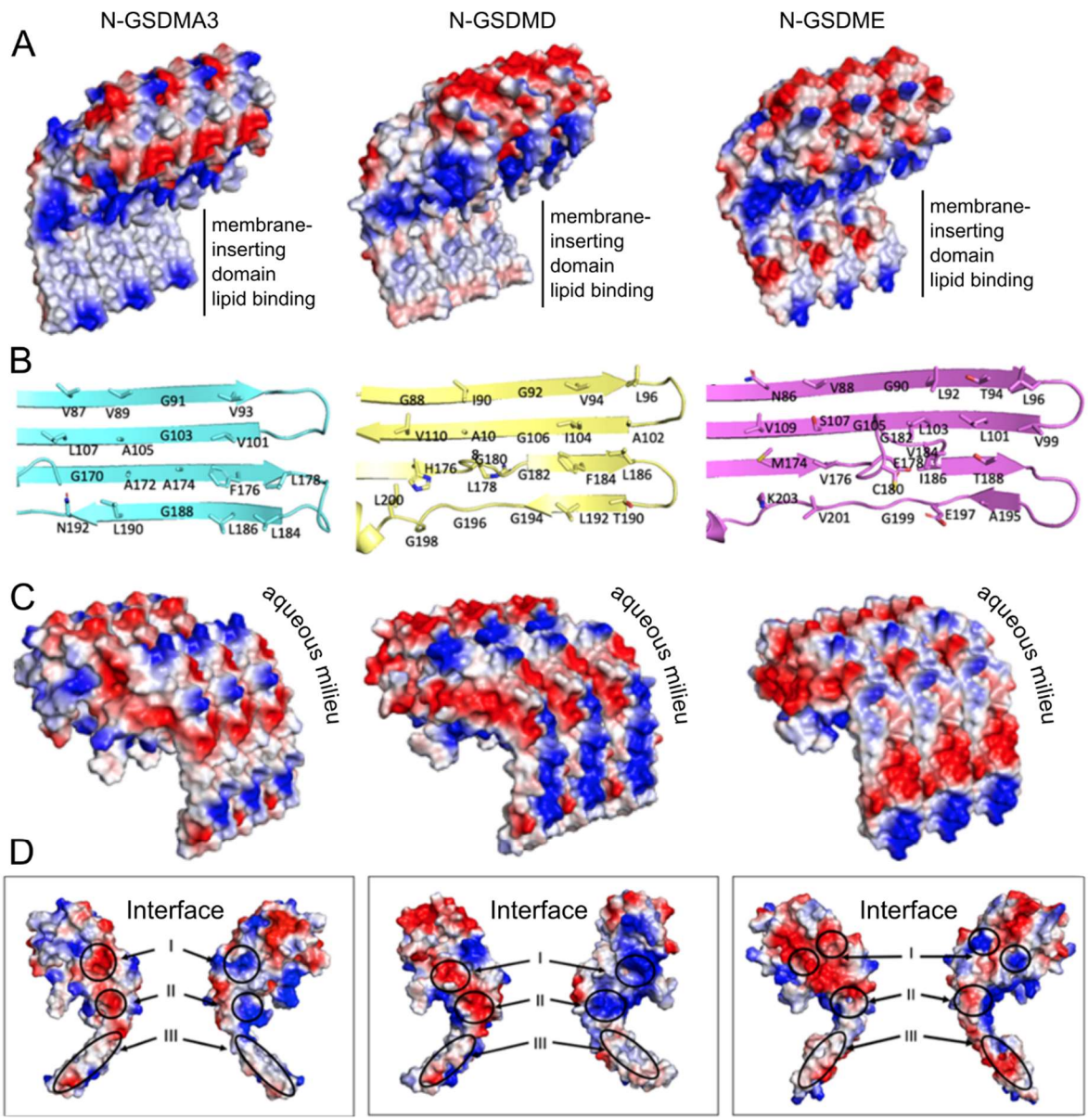

Figure 8. Comparison of the surface electrostatics and β-sheet composition of N-GSDMD and N-GSDME with N-GSDMA3 suggest interunit oligomerization for N-GSDMD but not for N-GSDME. (A) Surface potentials of N-GSDMA3 (left), N-GSDMD (middle) and N-GSDME (right) trimer visualizing the outer side of the pore-forming subunits proposed to interact with membrane phospholipids. **(B)** Side chains of the amino acid residues on the phospholipid-binding site of the β-sheet of N-GSDMA3 (left), N-GSDMD (middle) and N-GSDME (right). **(C)** Surface potentials of N-GSDMA3 (left), N-GSDMD (middle) and N-GSDME (right) trimer visualizing the inner side of the pore-forming subunits proposed to be in contact with the aqueous milieu. **(D)** Side views of N-GSDM monomers. The arrows indicate three interfaces that are possibly involved in interunit oligomerization. In the surface potential view, dark blue represents positive charges, red represents negative charges and white represents hydrophobic and non-charged regions.

4.4 DISCUSSION

Recently, members of the GSDM protein family were shown to be unlocked by inflammatory caspases, apoptotic caspases, elastase or granzymes, thereby instigating lytic cell death modes including pyroptosis and apoptosis-driven secondary necrosis. Based on observations pointing towards membrane recruitment [12,18–20,34–36] and membrane phospholipid binding [15,18,20], it was proposed that N-GSDMs have a plasma membrane permeabilizing capacity. Recently, the cryo-EM structure of N-GSDMA3 has been revealed providing a mechanism how N-GSDMA3 subunits oligomerize and form membrane pores [25]. However, although the crystal structures of both FL GSDMD [32] and FL GSDMA3 [18] are very similar and both GSDMD and GSDMA3 pores could be visualized in vitro, GSDMD pores were highly variable in size and shape [12,25,26], making the latter less suitable to infer a possible crystal structure of N-GSDMD as a pore-subunit. Only very recently, Xia *et al.* succeeded to reveal the cryo-EM structure of the GSDMD pore (PDB 6VFE) [37]. Nevertheless, structural information is currently still lacking for both FL GSDME and N-GSDME. More structural studies of GSDMs in their full length and membrane inserted forms could give insights in their biochemical properties, thereby providing information about the conservation of regulation and pore-forming mechanisms between GSDM proteins. In this study, we used a homology-based modeling strategy to model the structures of FL GSDME and the membrane inserted forms of N-GSDMD and N-GSDME. Comparison of our model of FL GSDME with the published structures of FL GSDMD and FL GSDMA3 revealed a high level of structural similarity between the GSDM family members, including the regions that are reported to be important for auto-inhibition (β1-2 loop) and membrane-targeting (α1-helix). However, comparison of the modeled structures of N-GSDMD and N-GSDME with the published one of N-GSDMA3 indicate that these GSDMs are indeed related proteins with similar properties, but that GSDME exhibits significant differences regarding the composition and structural organization of the membrane inserting subunits, suggesting another pore-forming mechanism as proposed for GSDMA3 and GSDMD. Although our model of N-GSDME showed a clear positive patch formed by arginine residues in the α1-helix that is proposed to interact with phospholipids, we did not observe a clear hydrophobic transmembrane surface, nor clear oligomerization interfaces as was observed in N-GSDMA3 and N-GSDMD. More specifically, β_{TM}3-4 strands appeared to be more disordered and contained more charged and polar residues, resulting in an amphipathic surface that is not likely to allow stable lipid interactions nor to simply insert in the plasma membrane without disturbing the organization of the plasma membrane. It is remarkable how the charged residue E197, that is strongly conserved in GSDME between species, disrupts the hydrophobic character of β_{TM}4, thereby disturbing the hydrophobic surfaces necessary for both interunit oligomerization and interaction with lipid chains of membrane phospholipids. In addition, the interruption of the β-sheet might allow more degrees of freedom in their interaction with membrane proteins and lipids.

Altogether, this observation for GSDME questions whether N-GSDME monomers oligomerize at all and form a classic barrel stave pore, as proposed for GSDMA3. The more amphipathic character of N-GSDME's trans-membrane region might suggest that GSDME permeabilizes the plasma membrane *via* a more carpet-like or toroidal pore-formation mechanism. Knowledge on the real FL and N-GSDME structure could give more insigths in the pore-forming mechanism of GSDME. In addition, it could give clues on why certain residues are highly conserved among species and what their function is. For example, the conserved T6 residue of GSDME was recently proposed to be a phosphorylation site based on the output of predictive software [38]. By *in silico* mutagenesis of T6 in the GSDME structure, the effect of phosphorylation of this residue could be assessed and subsequently be tested by *in vitro* mutagenenis. In order to be able to experimentally assess GSDME auto-inhibition, membrane-targeting and cell death execution, we generated fluorescently labeled GSDME-constructs in chapter 7 that can be used for *in vitro* mutagenesis.

Although we reported a slightly more disordered β_{TM}4-strand in N-GSDMD, we still observed a clear hydrophobic transmembrane surface for lipid binding and several strong oligomerization interfaces similar to the ones observed in GSDMA3 [25], suggesting that this loss of rigidity does not directly affect N-GSDMD subunit oligomerization and the mechanism of pore formation. Indeed, very recently the cryo-EM structure of GSDMD has been revealed showing a barrel-stave pore mechanism similar to the GSDMA3 pore [37]. Although GSDMD pores were previously reported to be heterogeneous in size and shape [12,25,26], Xia *et al.* propose GSDMD assemblies with 31-fold to 34-fold symmetry [37] in contrast to GSDMA3 pores that predominantly have a 27-fold symmetry arrangement [25]. If this heterogeneity would be the consequence of the slightly disordered β_{TM}4-strand in N-GSDMD, this would strengthen our hypothesis that it is very unlikely that the differences we observed in N-GSDME would result in homogenous pore-formation.

In conclusion, although we modeled the structures of FL GSDME, N-GSDMD and N-GSDME using already published structures of FL GSDMA3 and N-GSDMA3, we observed significant differences regarding their composition and structural organization that might suggest differences in their mechanisms of pore-formation.

References

1. Runkel, F. *et al.* (2004) The dominant alopecia phenotypes Bareskin, Rex-denuded, and Reduced Coat 2 are caused by mutations in gasdermin 3. *Genomics* 84, 824–835
2. Lunny, D.P. *et al.* (2005) Mutations in Gasdermin 3 Cause Aberrant Differentiation of the Hair Follicle and Sebaceous Gland. *J. Invest. Dermatol.* 124, 615–621
3. Yu, J. *et al.* (2011) Polymorphisms in GSDMA and GSDMB are associated with asthma susceptibility, atopy and BHR. *Pediatr. Pulmonol.* 46, 701–708
4. Delmaghani, S. *et al.* (2006) Mutations in the gene encoding pejvakin, a newly identified protein of the afferent auditory pathway, cause DFNB59 auditory neuropathy. *Nat. Genet.* 38, 770–8
5. Van Laer, L. *et al.* (1998) Nonsyndromic hearing impairment is associated with a mutation in DFNA5. *Nat. Genet.* 20, 194–197
6. Kayagaki, N. *et al.* (2015) Caspase-11 cleaves gasdermin D for non-canonical inflammasome signalling. *Nature* 526, 666–671
7. Shi, J. *et al.* (2015) Cleavage of GSDMD by inflammatory caspases determines pyroptotic cell death. *Nature* 526, 660–665
8. Rogers, C. *et al.* (2017) Cleavage of DFNA5 by caspase-3 during apoptosis mediates progression to secondary necrotic/pyroptotic cell death. *Nat. Commun.* 8, 14128
9. Sollberger, G. *et al.* (2018) Gasdermin D plays a vital role in the generation of neutrophil extracellular traps. *Sci. Immunol.* 3, 1–12
10. Chen, K.W. *et al.* (2018) Noncanonical inflammasome signaling elicits gasdermin D-dependent neutrophil extracellular traps. *Sci. Immunol.* 3, eaar6676
11. Kang, R. *et al.* (2018) Lipid Peroxidation Drives Gasdermin D-Mediated Pyroptosis in Lethal Polymicrobial Sepsis. *Cell Host Microbe* 24, 97–108
12. Sborgi, L. *et al.* (2016) GSDMD membrane pore formation constitutes the mechanism of pyroptotic cell death. *EMBO J.* 35, 1766–78
13. Xia, X. *et al.* (2018) Atypical Gasdermin D and Mixed Lineage Kinase Domain-like Protein Leakage Aggravates Tetrachlorobenzoquinone-Induced Nod-like Receptor Protein 3 Inflammasome Activation. *Chem. Res. Toxicol.* 13, 1418–1425
14. Wang, Y. *et al.* (2018) GSDME mediates caspase-3-dependent pyroptosis in gastric cancer. *Biochem. Biophys. Res. Commun.* 495, 1418–1425
15. Wang, Y. *et al.* (2017) Chemotherapy drugs induce pyroptosis through caspase-3 cleavage of a gasdermin. *Nature* 547, 99–103
16. Yu, J. *et al.* (2019) Cleavage of GSDME by caspase-3 determines lobaplatin-induced pyroptosis in colon cancer cells. *Cell Death Dis.* 10, 1–20
17. Lu, H. *et al.* (2018) Molecular targeted therapies elicit concurrent apoptotic and GSDME-dependent pyroptotic tumor cell death. *Clin. Cancer Res.* 24, 6066–6077
18. Ding, J. *et al.* (2016) Pore-forming activity and structural autoinhibition of the gasdermin family. *Nature* 535, 111–116
19. Aglietti, R.A. *et al.* (2016) GsdmD p30 elicited by caspase-11 during pyroptosis forms pores in membranes. *Proc. Natl. Acad. Sci.* 113, 7858–7863
20. Liu, X. *et al.* (2016) Inflammasome-activated gasdermin D causes pyroptosis by forming membrane pores. *Nature* 535, 153–8
21. Matsuzaki, K. (2019) Membrane permeabilization mechanisms. In *Advances in Experimental Medicine and Biology* 1117pp. 9–16, Springer New York LLC
22. Qian, S. *et al.* (2008) Structure of the alamethicin pore reconstructed by x-ray diffraction analysis. *Biophys. J.* 94, 3512–3522

23. Yang, L. *et al.* (2001) Barrel-stave model or toroidal model? A case study on melittin pores. *Biophys. J.* 81, 1475–1485
24. Järvå, M. *et al.* (2018) X-ray structure of a carpet-like antimicrobial defensin-phospholipid membrane disruption complex. *Nat. Commun.* 9, 1–10
25. Ruan, J. *et al.* (2018) Cryo-EM structure of the gasdermin A3 membrane pore. *Nature* 557, 62–67
26. Mulvihill, E. *et al.* (2018) Mechanism of membrane pore formation by human gasdermin-D. *EMBO J.* DOI: 10.15252/embj.201798321
27. Berman, H.M. *et al.* The Protein Data Bank. , *Nucleic Acids Research*, 28. 01-Jan-(2000) , Oxford University Press, 235–242
28. Webb, B. and Sali, A. (2017) Protein structure modeling with MODELLER. In *Methods in Molecular Biology* 1654pp. 39–54, Humana Press Inc.
29. Waterhouse, A. *et al.* (2018) SWISS-MODEL: Homology modelling of protein structures and complexes. *Nucleic Acids Res.* 46, W296–W303
30. Madeira, F. *et al.* (2019) The EMBL-EBI search and sequence analysis tools APIs in 2019. *Nucleic Acids Res.* 47, W636–W641
31. Webb, B. and Sali, A. (2016) Comparative protein structure modeling using MODELLER. *Curr. Protoc. Protein Sci.* 2016, 2.9.1-2.9.37
32. Liu, Z. *et al.* (2019) Crystal Structures of the Full-Length Murine and Human Gasdermin D Reveal Mechanisms of Autoinhibition, Lipid Binding, and Oligomerization. *Immunity* DOI: 10.1016/J.IMMUNI.2019.04.017
33. Minor, D.L. and Kim, P.S. (1994) Measurement of the β-sheet-forming propensities of amino acids. *Nature* 367, 660–663
34. Op de Beeck, K. *et al.* (2011) The DFNA5 gene, responsible for hearing loss and involved in cancer, encodes a novel apoptosis-inducing protein. *Eur. J. Hum. Genet.* 19, 965–973
35. Rogers, C. and Alnemri, E.S. (2019) Gasdermins: novel mitochondrial pore-forming proteins. *Mol. Cell. Oncol.* 6, e1621501
36. Chen, X. *et al.* (2016) Pyroptosis is driven by non-selective gasdermin-D pore and its morphology is different from MLKL channel-mediated necroptosis. *Cell Res.* 26, 1007–20
37. Xia, S. *et al.* (2021) Gasdermin D pore structure reveals preferential release of mature interleukin-1. *Nature* DOI: 10.1038/s41586-021-03478-3
38. Rogers, C. *et al.* (2019) Gasdermin pores permeabilize mitochondria to augment caspase-3 activation during apoptosis and inflammasome activation. *Nat. Commun.* 10, 1689

Part 2:
In vitro analysis of GSDME

Chapter 5

Assessing the contribution of GSDME to apoptosis-driven secondary necrosis: many ways to dye

RESEARCH ARTICLE

Published in 'Cell Death Discovery', 2021, 7(1):183

Elke De Schutter[1,2,3], Sofie De Ren, Bartosz Wiernicki[1,2], Benjamine Cappe[1,2], Peter Vandenabeele[1,2] and Franck B. Riquet[1,2,4]

[1] VIB Center for Inflammation Research, 9052 Ghent, Belgium

[2] Department of Biomedical Molecular Biology, Ghent University, 9052 Ghent, Belgium

[3] Center of Medical Genetics, University of Antwerp and Antwerp University Hospital, Prins Boudewijnlaan 43/6, BE-2650 Edegem, Antwerp Belgium.

[4] Université de Lille, Lille, France

Adapted with permission

Abstract

Apoptosis-driven secondary necrosis has long been considered to be an unregulated event as a result of osmotic pressure when phagocytic capacity is absent or insufficient. Recently, apoptosis-driven secondary necrosis was shown to be actually a regulated subroutine driven by the membrane permeabilizer gasdermin E (GSDME) after cleavage by caspase-3. However, despite its cleavage by caspase-3, GSDME has been reported to be dispensable for apoptosis-driven secondary necrosis in some cell types. Interestingly, these conflicting results were based on the uptake of different nuclear dyes with aberrant plasma membrane passing characteristics. In this chapter, we investigated the contribution of GSDME to apoptosis-driven secondary necrosis in L929sAhFas cells by measuring the uptake of the regularly used cell impermeant nuclear dyes 7-aminoactinomycin D (7-AAD), SYTOX Blue (SB) and SYTOX Green (SG) in presence and absence of GSDME expression. Surprisingly, we observed that the uptake of SYTOX dyes was delayed in the absence of GSDME expression in L929sAhFas cells compared to 7-AAD staining while this differential uptake disappeared in the presence of GSDME expression. Based on these results, we question the use of cell impermeant dyes to study plasma membrane permeabilization. In addition, our results suggest that multiple membrane permeabilizing mechanisms take place during apoptosis-driven secondary necrosis in L929sAhFas, allowing the selective uptake of dissimilar nuclear dyes.

5.1 INTRODUCTION

In essence, apoptosis is a containment and recycling program preparing the cell corpse for engulfment by efferocytosis. When the phagocytic capacity is absent or overwhelmed, apoptotic cells undergo cell disintegration accompanied with release of cellular content, also called apoptosis-driven secondary necrosis. As secondary necrotic cells can elicit an inflammatory response [1], insights in the underlying mechanisms or molecules driving secondary necrosis is of major importance to investigate the latter as therapeutic targets. Secondary necrosis has long been considered to be a spontaneous event as a result of osmotic pressure instead of a regulated subroutine of apoptosis. Moreover, the apoptotic caspase-3 was shown to actively prevent pyroptotic lysis by GSDMD through proteolytic cleavage within its N-terminal domain (N-GSDME) [2], thereby disrupting its cytotoxic function. Nevertheless, Rogers *et al.* have reported that secondary necrosis is driven by GSDME [3], which is, unlike GSDMD, activated by the apoptotic caspase-3. The authors provided convincing evidence by showing a decrease in plasma membrane permeabilization measured by propidium iodide (PI) uptake in GSDME knockout (KO) macrophages upon etoposide treatment [3]. However, other reports showed that the loss of GSDME did not result in differential kinetics in plasma membrane permeabilization measured by TO-PRO-3 fluorescent DNA dye in UV irradiated THP-1 and Jurkat T cells [4]. Similarly, the absence of GSDME did not affect membrane permeabilization measured by

YOYO-1 fluorescent DNA dye in macrophages upon anti-Fas treatment [5]. Remarkably, YOYO-1 and TO-PRO-3 belong to the same family of cell membrane impermeant cyanine nucleic acid stains. In theory, cell impermeant DNA-binding dyes seem ideal for assessing the membrane permeabilizing function of GSDME. These dyes enter and bind to nuclear DNA as dying cells lose membrane integrity. Several of them demonstrate little to no solution fluorescence and greatly increased quantum yield when bound to DNA [6–8]. However, most of these dyes were originally designed to stain DNA before they were repurposed to stain cells with compromised membranes. Therefore, little is known about their binding and membrane passing characteristics, though all these cell impermeant nuclear dyes are used to measure plasma membrane permeabilization. For example, some small cationic nuclear dyes were shown to enter the cells through ion channel openings during apoptosis, such as pannexin channels (YO-PRO-1, TO-PRO-3) [9,10] and P2X7 mediated channels (YO-PRO-1, TO-TO-1) [11,12], allowing the labeling of early apoptotic cells. Therefore, they rather detect membrane channel activity than plasma membrane disintegration and should be used in combination with PI or 7-AAD, which cannot enter cells *via* pannexin mediated channels and are used to detect late apoptotic cells [13,14]. In that respect, the contradicting results concerning the role of GSDME during apoptosis-driven secondary necrosis might be attributed to the choice of nucleic acid stain to measure plasma membrane permeabilization rather than to differences in cellular context or GSDME expression levels.

As conflicting findings were reported on the contribution of GSDME to apoptosis-driven secondary necrosis [3–5], we decided to investigate GSDME function in the murine fibrosarcoma cell line L929sAhFas stably expressing the human Fas receptor [15]. L929sAhFas are frequently used in our lab, as it allows to study tumor necrosis factor (TNF)-mediated necroptosis and anti-Fas-mediated secondary necrosis in the same cellular context [16]. Treatment of L929sAhFas cells with anti-Fas antibody results in clustering of Fas and specifically induces apoptosis and caspase-3 activation *via* the caspase-8-dependent proteolytic pathway [15]. The advantage of studying GSDME in this cellular system is that L929sAhFas cells clearly progress towards an apoptotic morphology upon anti-Fas treatment, allowing to draw conclusions about apoptosis-driven secondary necrosis without interference from other cell death modalities. This is of major importance, as caspase-3-mediated activation of GSDME is reported to mediate pyroptosis as well in some conditions such as upon treating cancer cell lines with cytotoxic drugs [17–20]. In contrast to apoptosis-driven secondary necrosis, pyroptosis is a form of primary necrosis characterized by cell swelling and large membrane bulbs without induction of apoptotic features such as blebbing.

Next to 7-AAD, SYTOX dyes are commonly used as dead-cell markers as they provide some advantages with respect to other dyes such as a good signal-to-noise ratio at low concentrations and a low photobleaching rate [7,21]. However, SYTOX dyes are considered

to be small cyanine nuclear dyes (<0.6 kDa) and their exact molecular structure is currently proprietary information of Molecular Probes. As far as we know, SYTOX dyes have never been associated with labeling of early apoptotic cells nor with early entry *via* ion channels. In this study we show that SB marks dying L929sAhFas cells simultaneously to 7-AAD, making it a marker for late apoptotic cells. Surprisingly, SB (0.4 kDa) and SG (0.6 kDa) but not 7-AAD (1.27 kDa) uptake was delayed in absence of GSDME expression in L929sAhFas during apoptosis-driven secondary necrosis, indicating that multiple membrane permeabilization mechanisms might take place during this cell death modality allowing the uptake of specific nuclear dyes.

5.2 MATERIALS AND METHODS

5.2.1 Cell lines and culture conditions

L929sAhFas cells and derivatives were cultured in Dulbecco's Modified Eagle Medium supplemented with 10% of Fetal Bovine Serum (v/v), L-glutamine (2 mM) and sodium pyruvate (400 mM). Cells were cultured in 37 °C in a humidified atmosphere containing 5% CO_2 and were regularly tested against mycoplasma contamination.

5.2.2 Generation of GSDME-deficient L929sAhFas cells

Single guide RNAs (sgRNA) targeting exon 4 of *Gsdme* were selected using the the Wellcome Trust Sanger Institute Genome Editing database (WGE) [22] and were manufactured by Thermo Fischer Scientific. The sgRNA sequences are listed in Supplementary Table S1. The sgRNA oligo sequence was cloned in BpiI-digested pSpCas9(BB)-2A-GFP carrying *Streptococcus pyogenes* WT Cas9 (Addgene, plasmid no. 48138). The sgRNA Cas9 plasmid was transfected into L929sAhFas cells *via* jetPRIME transfection reagent (Polyplus-transfection). 4 µg plasmid was added per 25 000 cells. The medium was replaced after 4 hours, cells were harvested 4 days after transection and GFP-positive cells were sorted (FACSAria III, BD Biosciences). Effective genomic deletion was confirmed with PCR and Sanger sequencing. Allele editing was analyzed using TIDE [23]. The PCR and sequencing primers used are listed in Supplementary Table S1.

5.2.3 Generation of stable GSDME inducible L929sAhFas cells line

The L929sAhFas iGSDME cell line was obtained by transduction of L929sAhFas *Gsdme* KOcl2 cells with a pDG2-m*Gsdme*-blast plasmid. This is a tetracycline-inducible derivative of pLenti6 (Life Technologies) containing a blasticidin selection marker [24], in which the coding sequence of murine *Gsdme* was cloned. Upon lentiviral transduction, the stably transduced cells were selected with 5-10 µg/ml blasticidin.

5.2.4 Cell permeabilization analysis by flow cytometry

L929sAhFas cells were seeded in 24-well suspension plates (100 000 cells/well) in the presence or absence of doxycycline (Sigma-Aldrich, 1 µg/ml unless otherwise stated) and stimulated the next day with 125 ng/ml anti-Fas (clone CH11, Upstate). One hour before each time point, fluorescent probes were added to proper wells: 1.25 µM of SYTOX Blue nucleic acid stain and 1.25 µM of 7-AAD (Molecular Probes). Samples were run on BD Fortessa or BD LSR and data was analysed using FlowJo 10.7.1.

5.2.5 Live cell imaging

Cells were seeded on 8-well dishes ibiTreat (Ibidi) to reach 60-80% confluence at time of imaging and pretreated with doxycycline (Sigma-Aldrich, 1 µg/ml) when necessary. 1 hour before imaging and treatment with anti-Fas (125 ng/ml, clone CH11, Upstate), nuclear dyes were added to the cells: 1.25 µM of 7-AAD and 2.5 µM of SYTOX Blue or 1.25 µM SYTOX Green (Molecular Probes). When 7-AAD was combined with SYTOX Green, Hoechst 33342 (500 nM) was added in order to track the cells. Cells were incubated in a chamber with a 5% CO_2 atmosphere at 37 °C throughout each experiment. Confocal images were captured with an observer Z.1 spinning disk microscope (Zeiss) equipped with a Yokogawa disk CSU-X1 and with a 20X/0.8 M27 Plan-Apochromat objective. Widefield images were captured with a Nikon TiE inverted microscope with a Plan Apo 10X objective.

5.2.6 Western Blotting

After treatment with 500 ng/ml anti-Fas (clone CH11, Upstate), L929sAhFas cells were harvested at specified time intervals and washed twice in ice-cold PBS. Cells were lysed using ice-cold RIPA lysis buffer (50 mM Tris-HCl, pH 7.5; 150 mM NaCl; 1 mM EDTA; 0.5% sodium deoxycholate; 1% Triton X-100 and 0.1% SDS) freshly supplemented with EDTA-free Complete protease inhibitor cocktail tablets and phosphatase inhibitor cocktail tablets (Roche Diagnostics Belgium N.V.). Extracted proteins were separated on 12% SDS polyacrylamide gels and transferred onto nitrocellulose membranes (Amersham Bioscience). Membranes were blocked using TBS with 0.05% Tween20 (TBS-T) containing 5% non-fat dry milk (Biorad) followed by anti-GSDME (ab215191, abcam), anti-GSDMD (Genentech) or anti-actin (69100, MP Biomedicals) incubation. After incubation with the HRP-linked donkey anti-rabbit IgG or HRP-linked sheep anti-mouse (Amersham Biosciences), blots were revealed using Western Lightning Plus-ECL (PerkinElmer).

5.2.7 Statistical analysis

Results are presented as means ± SD. Statistical analyses were performed using PRISM 8 software (GraphPad). Statistical analysis of 7-AAD+/SB- cells was performed using an one-way ANOVA test followed by Dunnett's multiple comparisons test. Statistical analysis of SB+ cells was performed using a two-way ANOVA with the Geisser-Greenhouse correction (matched values were stacked into a subcolumn). Alpha was set at 0.05.

Significance between samples is indicated as follows: *p <0.05; **p <0.01; ***p <0.001, ****p <0.0001.

5.3 RESULTS

5.3.1 GSDME but not GSDMD is activated in L929sAhFas cells upon anti-Fas treatment

First, we verified the presence and proteolytic activation of GSDME in L929sAhFas cells during apoptosis-driven secondary necrosis as previously reported [3,17]. Expression of GSDME was detected in L929sAhFas cells and anti-Fas treatment resulted in the generation of a GSDME fragment at ~35 kDa (Figure 1A), corresponding to the size of the active N-GSDME domain. This fragment was not observed when L929sAhFas was pre-treated with the pan-caspase inhibitor zVAD-fmk (zVAD) (Figure 1B), suggesting proteolytic cleavage of GSDME by caspase-3. In addition, we checked for GSDMD expression and proteolytic cleavage in L929sAhFas cells upon anti-Fas treatment in absence and presence of zVAD. In contrast to GSDME, anti-Fas treatment promoted the generation of a GSDMD fragment at ~43 kDa in absence of zVAD, indicating proteolytic inactivation through cleavage by caspase-3 (Figure 1C). As we want to address the contribution of GSDME to apoptosis-driven secondary necrosis, we first monitored the uptake of SB together with that of 7-AAD in L929sAhFas upon anti-Fas treatment by flow cytometry. SB and 7-AAD stained L929sAhFas cells with the same kinetics upon anti-Fas treatment, indicating that SB is a marker of late apoptotic cells such as 7-AAD (Figure 1D).

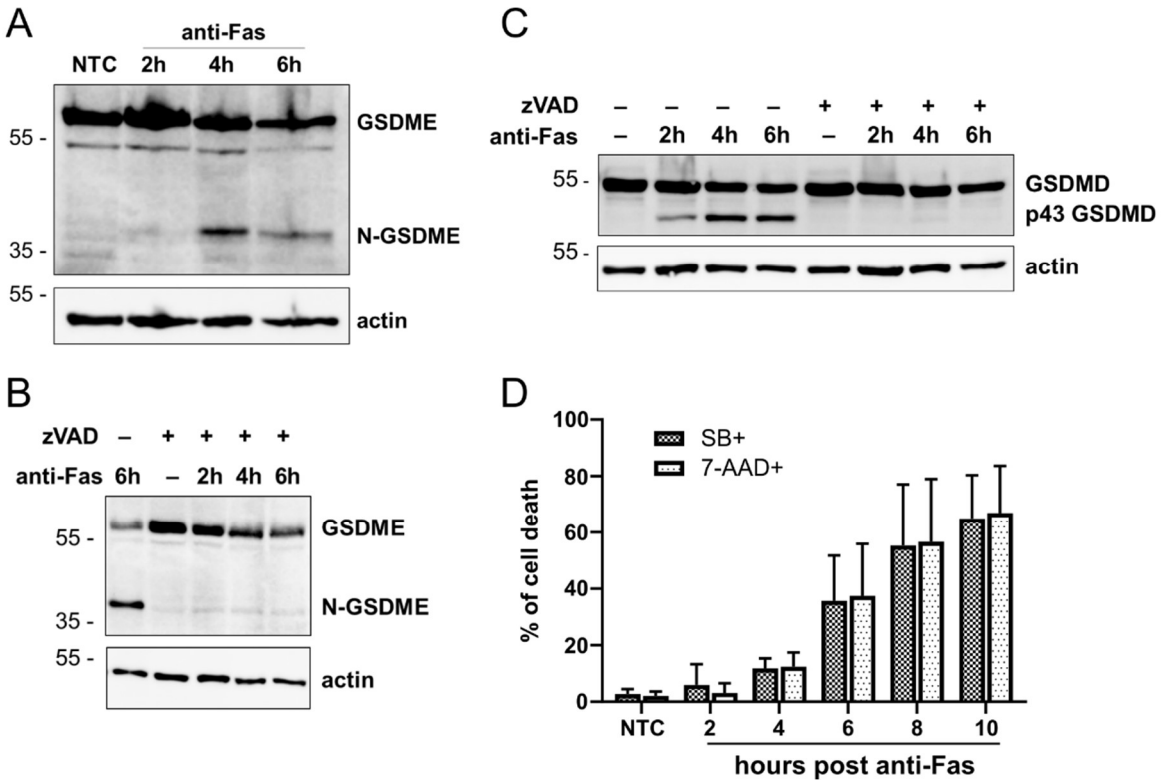

Figure 1. Cleavage of GSDME and cell death kinetics measured by SB and 7-AAD uptake in L929sAhFas upon anti-Fas treatment. (A) Expression of GSDME and proteolytic cleavage of GSDME in L929sAhFas upon anti-Fas treatment. **(B)** Impact of zVAD pre-treatment on the expression and cleavage of GSDME in L929sAhFas upon anti-Gas treatment. **(C)** Expression of GSDMD and proteolytic cleavage of GSDMD in L929sAhFas upon anti-Fas treatment with our without zVAD pre-treatment. **(D)** Levels of SB or 7-AAD staining of L929sAhFas cells upon anti-Fas treatment measured by flow cytometry. NTC, non-treatment control; SB, SYTOX Blue.

5.3.2 Loss of GSDME expression results in distinct uptake patterns of cell death markers

To investigate the role of GSDME in anti-Fas mediated apoptosis-driven secondary necrosis, we successfully generated L929sAhFas *Gsdme* KO clones by CRISPR/Cas9 gene editing (Figure 2A, S1). As gasdermin proteins are considered to be pore-forming molecules, we determined whether cell membrane permeabilization upon anti-Fas treatment is affected in L929sAhFas G*sdme* KO clones by measuring the uptake of both SB and 7-AAD combined. As expected, the L929sAhFas parental cells and wildtype (WT) clones proceeded immediately from a double negative population towards a double positive population (Figure 2C), confirming the simultaneous uptake of both 7-AAD and SB in apoptotic cells. In contrast, L929sAhFas G*sdme* KO clones show a clear 7-AAD single positive stage (7-AAD+/SB-) (Figure 2B) and a decrease in SB uptake (SB+) (Figure 2D) compared to its GSDME WT counterparts upon anti-Fas treatment, suggesting that different plasma membrane permeabilization mechanisms take place.

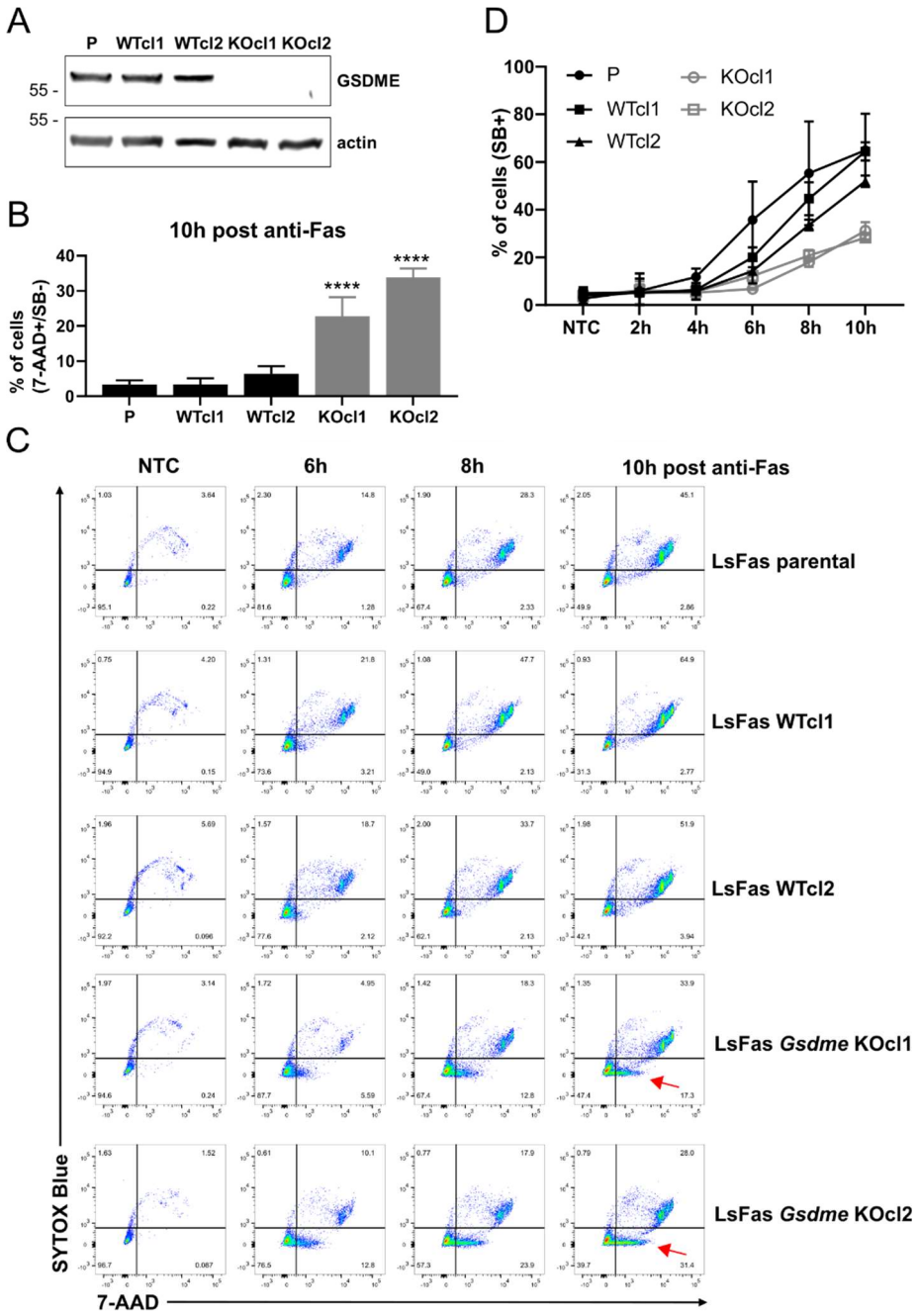

Figure 2. Impact of loss of GSDME expression on SB and 7-AAD uptake in L929sAhFas upon anti-Fas treatment. (A) Presence and loss of GSDME protein expression in L929sAhFas clones modified with CRISPR-Cas9 gene editing. **(B-D)** Flow cytometry analysis of the uptake of SB and 7-AAD in L929sAhFas WT and GSDME KO clones upon anti-Fas treatment. **(B)** Levels of 7-AAD single positive cells given as percentage of total cell population 10 hours post anti-Fas treatment. **(C)** Representative flow cytometric plots with red arrows pointing to 7-AAD single positive (7-AAD+/SB-) cells. **(D)** levels of SB positive cells given as percentage of total cell population upon anti-Fas treatment. LsFas, L929sAhFas; NTC, non-treatment control; P, parental; SB, SYTOX Blue.

In order to determine whether these distinct uptake patterns were due to the presence and absence of GSDME expression instead of clonal effects, L929sAhFas G*sdme* KOcl2 was reconstituted with a doxycycline-inducible m*Gsdme* construct using viral transduction, creating the GSDME inducible cell line 'L929sAhFas iGSDME'. Treatment of this cell line

with doxycycline resulted in a concentration dependent expression of GSDME (Figure 3A) and increased SB uptake upon anti-Fas treatment compared to the cells without doxycycline induced GSDME expression (Figure 2B-C). In addition, no more 7-AAD single positive population (7-AAD+/SB-) was seen in GSDME expressing cells upon doxycycline treatment (Figure 2B,D), showing that reconstituted GSDME expression rescued the differential uptake of SB and 7-AAD in L929sAhFas *Gsdme* KO cells. Altogether, as SB and 7-AAD can only enter cells with compromised plasma membranes, these results shows that GSDME expression provokes a membrane permeabilization mechanism allowing the simultaneous uptake of SB and 7-AAD while loss of GSDME restricts SB uptake in L929sAhFas upon anti-Fas treatment.

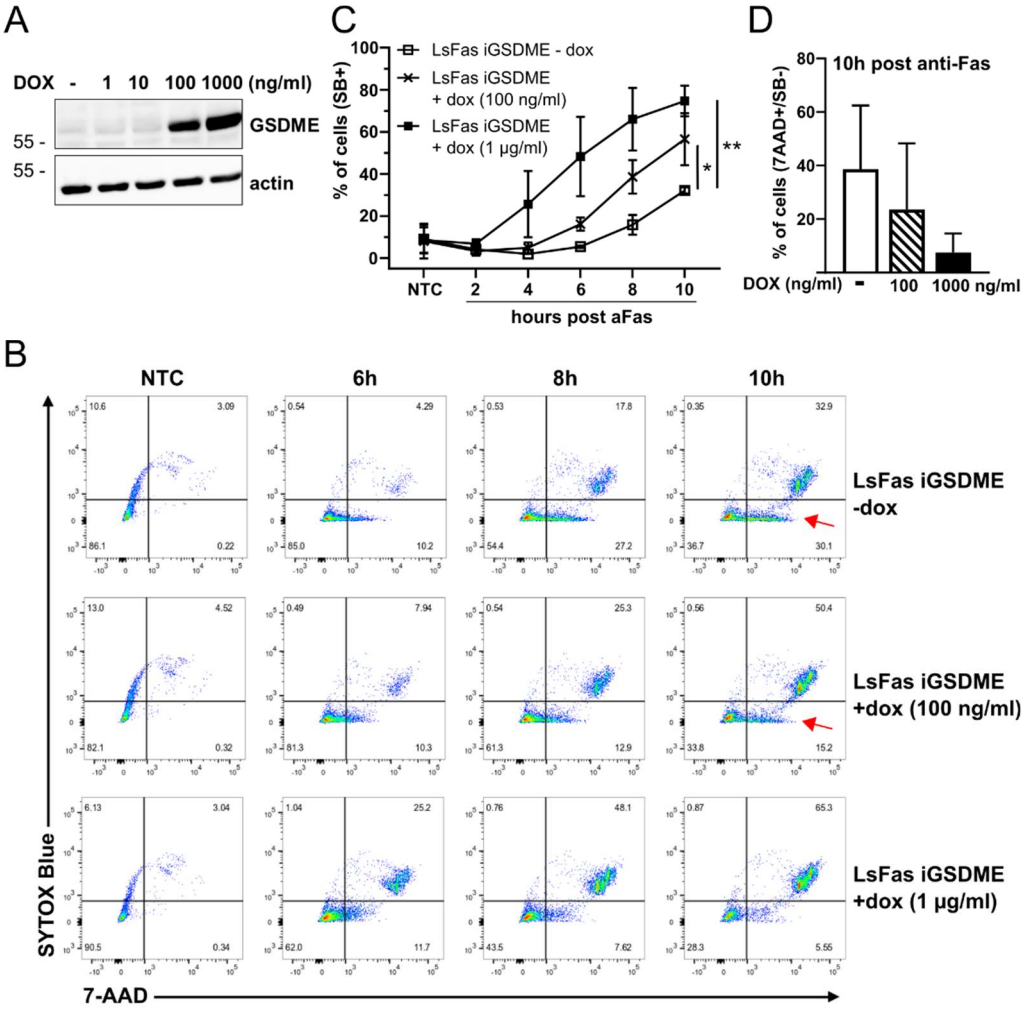

Figure 3. Impact of reconstitution of GSDME expression in L929sAhFas iGSDME on SB and 7-AAD uptake upon anti-Fas treatment. (A) Doxycyline-dependent expression of GSDME in L929sAhFas iGSDME cells. **(B-D)** Flow cytometry analysis of the uptake of SB and 7-AAD in L929sAhFas with (100 ng/ml, 1 µg/ml) our without (-) doxycycline pretreatment upon apoptosis induction by anti-Fas. **(B)** Representative flow cytometry plots with red arrows pointing to 7-AAD single positive (7-AAD+/SB-) population. **(C)** Effect of GSDME expression due to treatment with different concentrations of doxycycline on the uptake of SB in L929sAhFas iGSDME cells upon anti-Fas treatment. **(D)** Effect of GSDME expression due to treatment with different concentrations of doxycycline on the level of 7-AAD single positive (7AAD+/SB-) L929sAhFas iGSDME cells upon 10 hours of anti-Fas treatment. LsFas, L929sAhFas; NTC, non-treatment control; SB, SYTOX Blue.

5.3.3 Loss of GSDME delays the uptake of SYTOX dyes during apoptosis-driven secondary necrosis in L929sAhFas

The observation of a 7-AAD single positive population in L929sAhFas cells lacking GSDME expression upon anti-Fas treatment in our flow cytometry analysis raised the question whether SB uptake in these cells is delayed or completely prevented. Live cell imaging confirmed a delay in SB uptake compared to 7-AAD in cells lacking GSDME (Figure 4). The same was observed when combining 7-AAD with SG (Figure 5). Analysis of live cell imaging data indicated a mean delay of 3 hours. Interestingly, GSDME expression or not had no effect on the uptake of 7-AAD in our analysis, suggesting that other, GSDME independent, cell membrane permeabilization mechanisms could operate in L929sAhFas allowing 7-AAD uptake upon anti-Fas treatment and excluding SB uptake. As reconstitution of GSDME expression results in the simultaneous uptake of 7-AAD and SB/SG upon anti-Fas treatment, our results suggest that GSDME favors cell membrane permeabilization mechanisms allowing the uptake of SYTOX dyes, while 7-AAD is entering the cell by another mechanism.

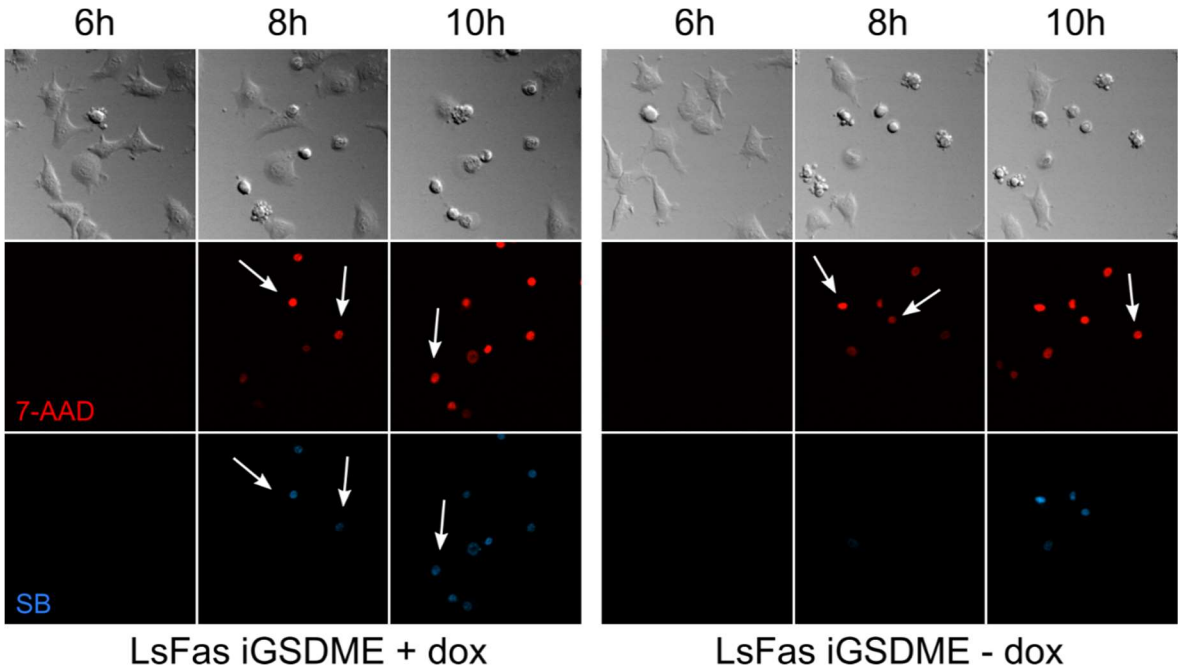

Figure 4. Uptake of 7-AAD and SB in individual L929sAhFas iGSDME cells *via* live cell imaging. Confocal images of L929sAhFas iGSDME cells upon anti-Fas treatment with or without doxycycline pre-treatment. Cells which show a simultaneous uptake of SB (blue) an 7-AAD (red) upon anti-Fas treatment are depicted with a white arrow for L929sAhFas iGSDME pretreated with doxycycline (1 µg/ml). In case of L929sAhFas iGSDME without doxycycline pre-treatment, white arrows point out cells that present a delayed SB uptake compared to 7-AAD.

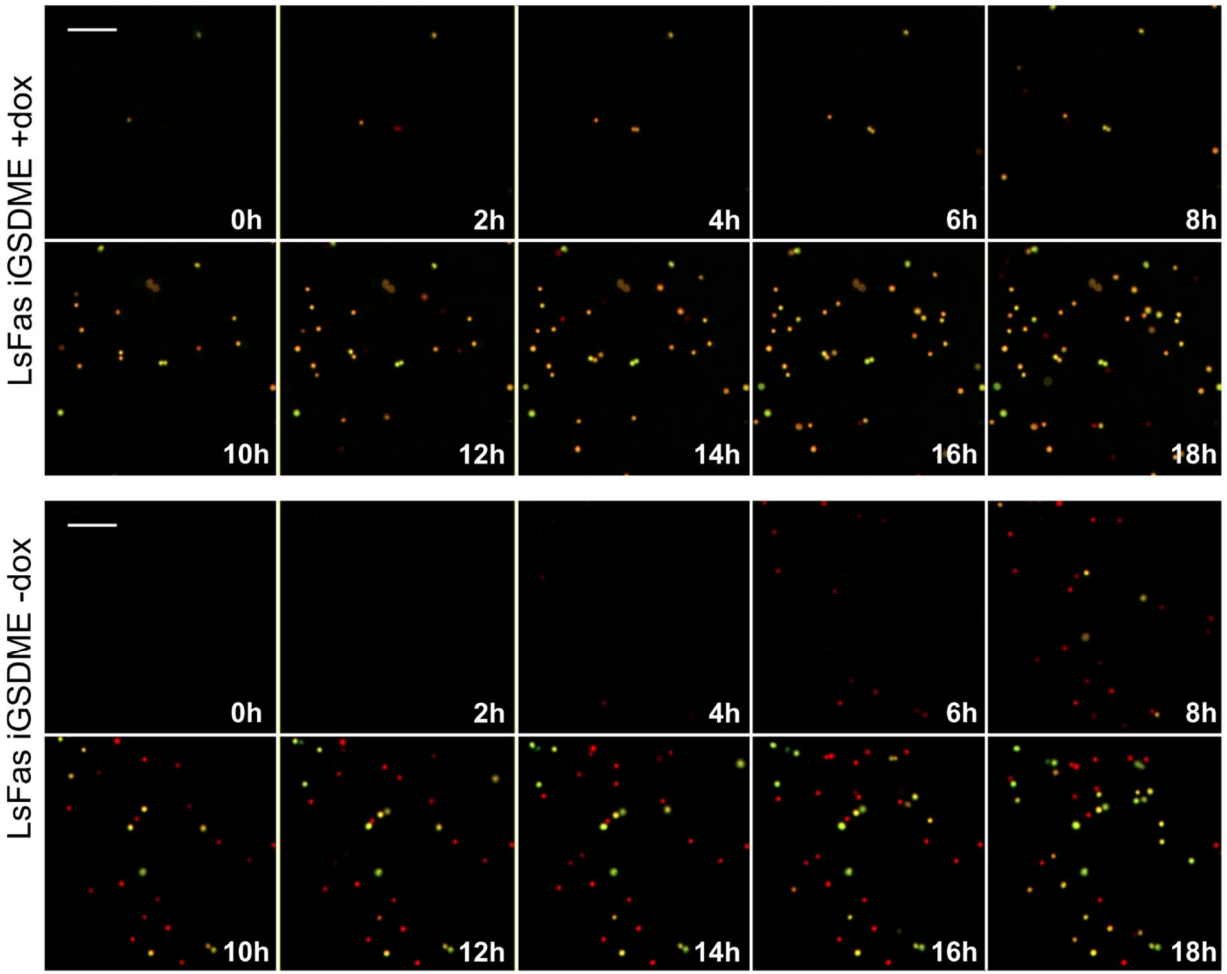

Figure 5. Uptake of 7-AAD and SG in individual L929sAhFas iGSDME cells *via* live cell imaging. Overlay wide-field images of L929sAhFas iGSDME with or without doxycycline pretreatment upon anti-Fas treatment. Staining of cells by 7-AAD (red) and SG (green) is followed in time. Overlay images show double positive cells in yellow. Scale bar represents 100 µm.

5.4 DISCUSSION

The study of plasma membrane permeabilization mechanisms during cell death is of major importance as it is associated with the release of intracellular content such as cytokines, chemokines, metabolites and DAMPs eliciting immune responses and inflammation [1,25–28]. Although apoptosis is well defined since the early nineties by subroutines such as membrane blebbing, phosphatidylserine (PS) exposure, caspase-3 activation and DNA fragmentation, the actual mechanism leading to plasma membrane permeabilization, also called secondary necrosis, is largely unknown. As a substrate of caspase-3 and as a member of the pore forming gasdermin protein family, GSDME is obviously a good candidate to fill this last subroutine. However, with the use of both markers of early apoptotic cells such as YO-YO-1 and TO-PRO-1 [4,5] as well as markers of late-apoptotic cells such as PI [3], the contribution of GSDME to apoptosis-driven secondary necrosis is currently under debate. Moreover, secondary necrosis is always considered to be a spontaneous process following impaired cell clearance. Ours and former published results [2] showing that direct cell lysis by GSDMD is prevented *via* the inactivating caspase-3 mediated cleavage of N-GSDMD, question the need for active lysis *via* GSDME. Additional studies using markers of late apoptotic cells could clarify the current contradicting findings and assess the importance of the choice of marker to investigate cell membrane permeabilization mechanisms. Our results showing the simultaneous labeling of L929sAhFas cells upon anti-Fas treatment by 7-AAD and SB, provide evidence that SB is a marker of late apoptotic cells in contrast to other small cationic dyes entering early apoptotic cells *via* pannexin mediated channels such as YO-PRO-1 and TO-PRO-3 [9–12]. Next, we used both 7-AAD and SB to evaluate the role of GSDME in apoptosis-driven secondary necrosis in L929sAhFas cells. Rather unexpectedly, only SB and not 7-AAD uptake was delayed in L929sAhFas cells lacking GSDME expression upon anti-Fas treatment. Thus, our results based on SB uptake are consistent with the findings of Rogers *et al.* reporting that GSDME is responsible for membrane permeabilization during apoptosis-driven secondary necrosis [3]. On the other hand, our results based on 7-AAD uptake support the findings of Tixeira *et al.* and Lee *et al.* stating that GSDME does not affect cell membrane permeabilization during apoptosis-driven secondary necrosis [4,5]. Therefore, caution is needed when drawing conclusions from different studies using various cell death markers. Altogether, it seems that, next to early channels associated with apoptosis, different GSDME dependent and independent subroutines leading to membrane permeabilization take place during apoptosis-driven secondary necrosis, allowing the selective uptake of dissimilar nuclear dyes.

Our conflicting results when studying plasma membrane permeabilization using cell impermeant dyes question the suitability of cell impermeant dyes without thorough knowledge about their membrane passing mechanism for this purpose. In our experimental settings the big cationic 7-AAD (1.27 kDa) molecules can enter *Gsdme* KO apoptotic cells

3 hours before the smaller SB (0.4 kDa) or SG (0.6 kDa), indicating that this differential uptake cannot simply be attributed to a size dependent effect. An important and as far as we know unexplored aspect is that next to the plasma membrane, nuclear dyes need to pass another barrier to be able to bind DNA, namely the nuclear envelope. It might be that GSDME targets the nuclear membrane as was shown for its family member GSDMD [29], allowing the entrance of SYTOX dyes in the nucleus. Nevertheless, this scenario is less likely as small molecules can pass the nuclear envelope freely. Overall, complementary approaches next to the use of cell impermeant dyes are needed to draw conclusions regarding regulation of apoptosis and secondary necrotic processes.

Although the use of cell impermeant dyes might not be suitable to study membrane permeabilization processes itself, the double staining with SB/SG and 7-AAD may allow functionality studies of GSDME and maybe other GSDMs. This is especially useful when performing mutational analysis to determine critical residues for GSDME functionality or testing the functionality of GSDME fusion proteins. Further research in other cellular systems is necessary to assess the general applicability of this dye combination.

References

1. Sachet, M. *et al.* (2017) The immune response to secondary necrotic cells. *Apoptosis* 22, 1189–1204
2. Taabazuing, C.Y. *et al.* (2017) Pyroptosis and Apoptosis Pathways Engage in Bidirectional Crosstalk in Monocytes and Macrophages. *Cell Chem. Biol.* 24, 507–514
3. Rogers, C. *et al.* (2017) Cleavage of DFNA5 by caspase-3 during apoptosis mediates progression to secondary necrotic/pyroptotic cell death. *Nat. Commun.* 8, 14128
4. Tixeira, R. *et al.* (2018) Gasdermin E Does Not Limit Apoptotic Cell Disassembly by Promoting Early Onset of Secondary Necrosis in Jurkat T Cells and THP-1 Monocytes. *Front. Immunol.* 9, 2842
5. Lee, B.L. *et al.* (2018) ASC- and caspase-8-dependent apoptotic pathway diverges from the NLRC4 inflammasome in macrophages. *Sci. Rep.* 8, 3788
6. Gill, J.E. *et al.* (1975) 7 Amino actinomycin D as a cytochemical probe. I. Spectral properties. *J. Histochem. Cytochem.* 23, 793–799
7. Thakur, S. *et al.* (2015) The fluorescence properties and binding mechanism of SYTOX green, a bright, low photo-damage DNA intercalating agent. *Eur. Biophys. J.* 44, 337–348
8. Fürstenberg, A. *et al.* (2007) Structure–Fluorescence Contrast Relationship in Cyanine DNA Intercalators: Toward Rational Dye Design. *Chem. - A Eur. J.* 13, 8600–8609
9. Chekeni, F.B. *et al.* (2010) Pannexin 1 channels mediate “find-me” signal release and membrane permeability during apoptosis. *Nature* 467, 863–867
10. Qu, Y. *et al.* (2011) Pannexin-1 Is Required for ATP Release during Apoptosis but Not for Inflammasome Activation. *J. Immunol.* 186, 6553–6561

11. Cankurtaran-Sayar, S. *et al.* (2009) P2X7 receptor activates multiple selective dye-permeation pathways in RAW 264.7 and human embryonic kidney 293 cells. *Mol. Pharmacol. Fast Forw.* 76, 1323–1332
12. Holme, A.L. *et al.* (2007) Automated laser scanning cytometry: A powerful tool for multi-parameter analysis of drug-induced apoptosis. *Cytom. Part A* 71A, 80–86
13. Glisic-Milosavljevic, S. *et al.* (2005) Comparison of apoptosis and mortality measurements in peripheral blood mononuclear cells (PBMCs) using multiple methods. *Cell Prolif.* 38, 301–311
14. Jiang, L. *et al.* (2016) Monitoring the progression of cell death and the disassembly of dying cells by flow cytometry. *Nat. Protoc.* 11, 655–663
15. Vercammen, D. *et al.* (1998) Inhibition of caspases increases the sensitivity of L929 cells to necrosis mediated by tumor necrosis factor. *J. Exp. Med.* 187, 1477–85
16. Vanden Berghe, T. Vanden *et al.* (2010) Necroptosis, necrosis and secondary necrosis converge on similar cellular disintegration features. *Cell Death Differ.* 17, 922–930
17. Wang, Y. *et al.* (2017) Chemotherapy drugs induce pyroptosis through caspase-3 cleavage of a gasdermin. *Nature* 547, 99–103
18. Yu, J. *et al.* (2019) Cleavage of GSDME by caspase-3 determines lobaplatin-induced pyroptosis in colon cancer cells. *Cell Death Dis.* 10, 1–20
19. Lu, H. *et al.* (2018) Molecular targeted therapies elicit concurrent apoptotic and GSDME-dependent pyroptotic tumor cell death. *Clin. Cancer Res.* 24, 6066–6077
20. Wang, Y. *et al.* (2018) GSDME mediates caspase-3-dependent pyroptosis in gastric cancer. *Biochem. Biophys. Res. Commun.* 495, 1418–1425
21. Chiaraviglio, L. and Kirby, J.E. (2014) Evaluation of impermeant, DNA-binding dye fluorescence as a real-time readout of eukaryotic cell toxicity in a high throughput screening format. *Assay Drug Dev. Technol.* 12, 219–228
22. Hodgkins, A. *et al.* (2015) WGE: a CRISPR database for genome engineering. *Bioinformatics* 31, 3078–3080
23. Brinkman, E.K. *et al.* (2014) Easy quantitative assessment of genome editing by sequence trace decomposition. *Nucleic Acids Res.* 42, e168–e168
24. De Groote, P. *et al.* (2016) Generation of a new Gateway-compatible inducible lentiviral vector platform allowing easy derivation of co-transduced cells. *Biotechniques* 60, 252–259
25. Feltham, R. *et al.* (2017) Caspase-8: not so silently deadly. *Clin. Transl. Immunol.* 6, e124
26. Galluzzi, L. *et al.* (2014) Molecular mechanisms of regulated necrosis. *Semin. Cell Dev. Biol.* 35, 24–32
27. Medina, C.B. *et al.* (2020) Metabolites released from apoptotic cells act as tissue messengers. *Nature* 580, 130–135
28. Green, D.R. *et al.* (2016) The clearance of dying cells: table for two. *Cell Death Differ.* 23, 915–926
29. Chen, K.W. *et al.* (2018) Noncanonical inflammasome signaling elicits gasdermin D-dependent neutrophil extracellular traps. *Sci. Immunol.* 3, eaar6676

Supplementary Information

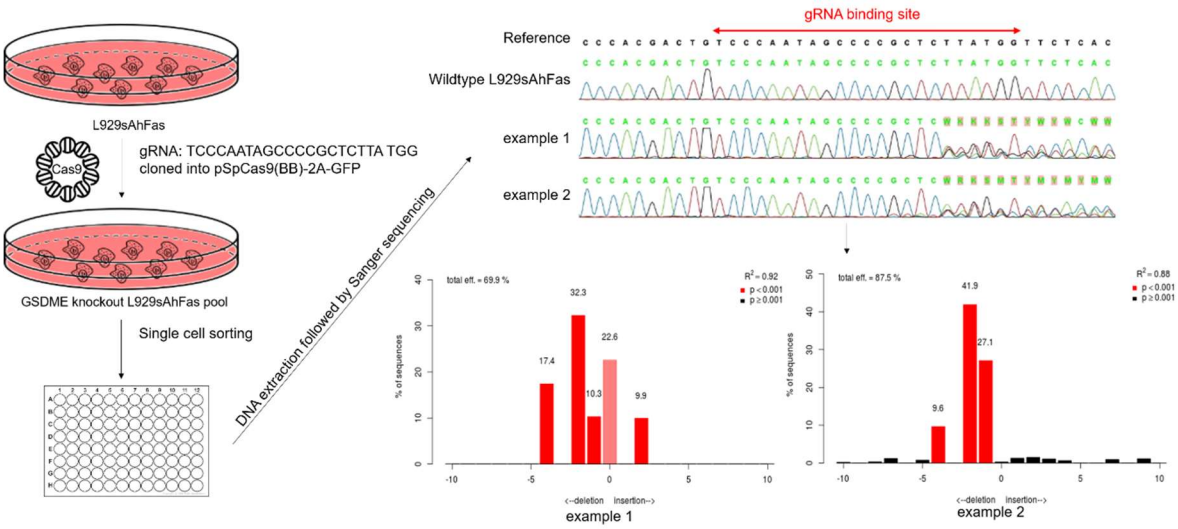

Figure S1. Generation and selection of *Gsdme* KO clones. The sgRNA Cas9 plasmid was transfected into L929sAhFas cells followed by single cell sorting. Next, DNA of single cell clones was extracted and sequenced by Sanger sequencing. The DNA sequence of two example clones are shown after genome editing with Crispr-Cas9 around the gRNA binding site and are visualized by CLC DNA Workbench 3. The editing efficacy and identification of the predominant types of insertions and deletions (indels) in the DNA were quantified using TIDE software [23].

Table S1. sgRNA sequences, PCR and sequencing primers used for *Gsdme* CRISPR-Cas9 gene editing

Sequence	Forward Sequence (5'→3')	Reverse complement (5'→3')
Guide sequence	TCCCAATAGCCCCGCTCTTA	TAAGAGCGGGGCTATTGGGA
Primers	GCATTCAATACATGGTTTTTGG	TAATCACCCCTAGGCTCTGG

Chapter 6

GSDME-dependent and -independent subroutines regulate the passage of dextrans during apoptosis-driven secondary necrosis

RESEARCH ARTICLE

Submitted to 'Cellular and Molecular Life Sciences'

Elke De Schutter[1,2,3,†], Jana Ramon[4,†], Benjamin Pfeuty[5], Caroline De Tender[6,7], Stephan Stremersch[4], Koen Raemdonck[4], Ken Op de Beeck[3,8], Wim Declercq[1,2], Franck B. Riquet[1,2,9,§] and Kevin Braeckmans[4,§] and Peter Vandenabeele[1,2,§,*]

[†] These authors contributed equally to this work

[§] shared senior authorship

[1] VIB Center for Inflammation Research, Ghent, Belgium

[2] Department of Biomedical Molecular Biology, Ghent University, Ghent, Belgium

[3] Center of Medical Genetics, University of Antwerp and Antwerp University Hospital, Antwerp Belgium.

[4] Laboratory of General Biochemistry and Physical Pharmacy, Faculty of Pharmaceutical Sciences, Ghent University, Ghent, Belgium

[5] Université de Lille, CNRS, UMR 8523 - PhLAM - Physique des Lasers Atomes et Molécules, Lille, France

[6] Department of Applied Mathematics, Computer Science and Statistics, Ghent University, Ghent, Belgium

[7] Plant Sciences Unit, Flanders Research Institute for Agriculture, Fisheries and Food, Merelbeke, Belgium

[8] Center for Oncological Research, University of Antwerp and Antwerp University Hospital, Antwerp, Belgium

[9] Université de Lille, Lille, France

Adapted with permission

Abstract

Secondary necrosis has long been perceived as an uncontrolled process resulting in total lysis of the apoptotic cell. Recently, it was shown that progression of apoptosis to secondary necrosis is regulated by Gasdermin E (GSDME), which requires activation by caspase-3. Although the contribution of GSDME in this context has been attributed to its pore-forming capacity, little is known about the kinetics and size characteristics of this. Here we report on the membrane permeabilizing features of GSDME by monitoring the influx and efflux of dextrans of different sizes into/from anti-Fas stimulated L929sAhFas cells undergoing apoptosis-driven secondary necrosis. We found that GSDME accelerates cell lysis measured by SYTOX Blue staining but does not affect the exposure of phosphatidylserine on the plasma membrane. Furthermore, loss of GSDME expression clearly hampered the influx of fluorescently labeled dextrans while the efflux happened independent of the presence or absence of GSDME expression. Importantly, both in- and efflux of dextrans was dependent on their molecular weight. Altogether, our results demonstrate that GSDME regulates the passage of compounds together with other plasma membrane destabilizing subroutines.

6.1 INTRODUCTION

Apoptosis, the best-known form of regulated cell death, is essentially a containment and recycling program that prepares the cell corpse for efficient phagocytosis [1]. However, when phagocytes are absent or the phagocytic capacity is insufficient, apoptotic cells progress to necrotic plasma membrane permeabilization called apoptosis-driven secondary necrosis, which results in a more inflammatory environment [2–5]. The gasdermin (GSDM) protein family gained a lot of interest as plasma membrane permeabilizers during regulated cell death [6–13]. Gasdermin D (GSDMD) is proteolytically activated by caspase-1 and -4 leading to inflammasome-mediated pyroptosis [7,14] and the GSDMD-dependent release of pro-inflammatory cytokines such as interleukin-1β [15]. Similarly, apoptosis-driven secondary necrosis is driven by the activation of gasdermin E (GSDME) [9,10]. To entail its effect, caspase-3-mediated cleavage induces the release of GSDME's cytotoxic N-terminal p30 fragment from the auto-inhibiting C-terminal domain, which is followed by plasma membrane recruitment and plasma membrane permeabilization [6,9,16]. Nevertheless, GSDME may not be the only mechanism responsible for secondary necrosis. GSDME expression is dispensable for secondary necrosis following NLRC4-mediated apoptosis in macrophages [17] or UV irradiation-induced apoptosis in human T cells and monocytes [18].

The structure of GSDMD and the murine gasdermin A3 (GSDMA3) revealed a mechanism how the N-terminal domain is able to form pores [6,19,20]. Using cryo-electron microscopy, it was discovered that the N-terminal domains of GSDMA3 form a large, 27-fold β-barrel-shaped pore with an inner diameter of 18 nm [20]. In addition, 26- and 28-fold

oligomerization structures were reported with similar dimensions as the dominant 27-subunit GSDMA3 pore [20]. In contrast, GSDMD oligomerization is reported to be more heterogeneous [6,21,22]. The N-terminal domain of GSDMD assembles into dynamic arc- and slit-shaped oligomers that finally transform to stable ring-shaped oligomers with varying diameters ranging from 13.5 till 33.5 nm [21,22].

Unlike GSDMA3 and GSDMD, the characteristics of GSDME pore-formation are currently unknown. Therefore, to gain insight in the membrane permeabilizing behavior of GSDME and its role in apoptosis-driven secondary necrosis, we applied two *in vitro* approaches. With the assumption that GSDME forms pores in the plasma membrane, influx or efflux of macromolecules, such as fluorescently labeled dextrans, is expected to happen when cells are exposed to apoptotic stimuli. Monitoring the uptake of fluorescently labeled dextrans in apoptotic cells is quite straightforward, only requiring the addition of the dextrans to the culture medium after apoptosis induction. However, monitoring efflux is less obvious as the cells should be pre-loaded with the dextrans in a manner that does not interfere with cellular processes such as proliferation or without inducing apoptosis by itself. Therefore, we selected nanoparticle-sensitized photoporation, which is an emerging intracellular delivery technique that enables direct cytosolic delivery of membrane-impermeable macromolecules in virtually every cell type with minimal impact on the cellular homeostasis [23–29]. This technique makes use of photothermal nanoparticles, like gold nanoparticles (AuNPs), which are incubated with cells and bind to the plasma membrane. Upon irradiation by a short, yet intense laser pulse, the AuNPs become heated, resulting in the evaporation of the surrounding water and the formation of quickly expanding water vapor nanobubbles (VNBs) around the AuNPs. The mechanical forces resulting from the expansion and collapse of those VNBs lead to the generation of localized pores in the plasma membrane [27,30]. Through those transient plasma membrane pores, which are repaired within seconds to minutes, exchange of molecules between the intra- and extracellular compartment can happen [25,26,28,29]. Importantly, under controlled conditions, complete cellular recovery is reported within 24h upon laser treatment with minimal effect on the cellular homeostasis [23,24,26].

Here, we studied the membrane permeabilizing behavior of GSDME during apoptosis-driven secondary necrosis and attempted to elucidate whether this process is characterized by discrete pore sizes and/or whether GSDME pores grow over time. To this end, we developed GSDME-deficient L929sAhFas cells carrying a doxycycline-inducible system for GSDME expression allowing the exploration of secondary necrosis in the absence or presence of GSDME in the same cellular context. We reveal that absence of GSDME delays nuclear staining by SYTOX Blue (SB), as cells remain longer in the sublytic phase, while phosphatidylserine (PS) exposure was not affected. Next, we investigated the involvement of GSDME in the influx and efflux of fluorescently labeled dextrans of different sizes during apoptosis-driven secondary necrosis induced by anti-Fas. We provide evidence that pore-

formation during apoptosis-driven secondary necrosis is a gradual process that already supports a GSDME-dependent influx of fluorescently labeled dextrans before nuclear DNA of dying cells is stained by SB. Furthermore, the influx method allowed us to make an estimation of molecular sizes able to pass the GSDME pore. In contrast, efflux of fluorescently labeled dextrans seemed to occur independent of GSDME combined with the fact that only significant dextran loss was observed when cells were already stained by SB.

6.2 MATERIALS AND METHODS

6.2.1 Cell Culture

L929sAhFas cells and derivates were cultured in Dulbecco's Modified Eagle Medium supplemented with 10 % of Fetal Bovine Serum (v/v), L-glutamine (2 mM) and sodium pyruvate (400 mM). Cells were cultured in 37 °C in a humidified atmosphere containing 5 % CO_2 and were regularly tested against mycoplasma contamination.

6.2.2 Generation of GSDME-deficient L929sAhFas cells

Single guide RNAs (sgRNA) targeting the exon 4 of *Gsdme* were selected using the the Wellcome Trust Sanger Institute Genome Editing database (WGE) [31] and were manufactured by Thermo Fischer Scientific. The sgRNA sequences are listed in Supplementary Table S1. The sgRNA oligo sequence was cloned in BpiI-digested pSpCas9(BB)-2A-GFP carrying *Streptococcus pyogenes* WT Cas9 (Addgene, plasmid no. 48138). The sgRNA Cas9 plasmid was transfected into L929sAhFas cells via jetPRIME transfection reagent (Polyplus-transfection). 4 µg plasmid was added per 25 000 cells and incubated for 4h at 37 °C, 5 % CO_2. After which the culture medium was replaced and cells were further incubated for 4 days at 37 °C, 5% CO_2. Next, cells were harvested and GFP-positive cells were sorted using a FACSAria III (BD Biosciences). Effective genomic interruption of *Gsdme* was confirmed with PCR and Sanger sequencing. Allele editing was analyzed using TIDE [32]. The PCR and sequencing primers used are listed in Supplementary Table S1.

6.2.3 Generation of stable GSDME-inducible L929sAhFas cells line

The L929sAhFas iGSDME cell line was obtained by transduction of *Gsdme* KOcl2 L929sAhFas cells with a pDG2-mGSDME-blast plasmid. This is a tetracycline-inducible derivative of pLenti6 (Life Technologies) containing a blasticidin selection marker [33], in which the coding sequence of murine GSDME was cloned. Upon lentiviral transduction, the stably transduced cells were selected with 5-10 µg/ml blasticidin.

6.2.4 Analysis of phosphatidylserine exposure and cell death kinetics

L929sAhFas iGSDME cells were seeded in 24-well suspension plates (100 x 10^3 cells/well) in the presence or absence of doxycycline (Sigma-Aldrich, 1 µg/ml) and

stimulated the next day with 125 ng/ml anti-Fas (clone CH11, Upstate). Cell death parameters were analyzed after incubation between 0h and 10h of anti-Fas treatment. 1h before measurement, fluorescent probes were added to the culture medium: 1.25 µM of SYTOX Blue nucleic acid stain and 7.5 nM of annexin V Alexa Fluor 488 conjugate (Molecular Probes). Subsequently, samples were measured by flow cytometry using a four-laser BD Fortessa or three-laser BD LSR II (BD Biosciences) and data was analyzed using FlowJo 10.7.1.

6.2.5 Western Blotting

L929sAhFas iGSDME cells were pretreated with 1 µg/ml doxycycline (Sigma-Aldrich) to allow GSDME expression. L929sAhFas and L929sAhFas iGSDME cells were incubated for 8h with 250 ng/ml anti-Fas (clone CH11, Upstate) at 37 °C, 5 % CO_2. (clone CH11, Upstate), after which they were harvested and washed twice in ice-cold phosphate-buffered saline (PBS). Next, cells were lysed using ice-cold RIPA lysis buffer (50 mM Tris-HCl; pH 7.5; 150 mM NaCl; 1 mM EDTA; 0.5% sodium deoxycholate; 1 % Triton X-100 and 0.1 % SDS) freshly supplemented with EDTA-free complete protease inhibitor cocktail tablets and phosphatase inhibitor cocktail tablets (Roche Diagnostics Belgium N.V.). Extracted proteins were separated on 12 % sodiumdodecylsulfate (SDS) polyacrylamide gels and transferred onto nitrocellulose membranes (Amersham Bioscience). Membranes were blocked using tris-buffered saline containing 0.05 % Tween® 20 (TBS-T) and 5 % non-fat dry milk (Biorad) followed by incubation with anti-GSDME (ab215191, abcam) or anti-actin (69100, MP Biomedicals). After incubation with the horseradish peroxidase (HRP)-linked donkey anti-rabbit IgG or HRP-linked sheep anti-mouse (Amersham Biosciences), blots were revealed using a Western Lightning Plus-ECL (PerkinElmer).

6.2.6 Intracellular delivery of FITC-labeled dextrans by nanoparticle-sensitized photoporation

AuNPs with a core size of 60 nm were in-house synthetized using the Turkevich method and coated with the cationic polymer poly(diallyl dimethyl ammonium chloride) (PDDAC) as reported before [23].

To determine the AuNP concentration that provides optimal photoporation results, L929sAhFas (130 x 10^3) were seeded in 24-well plates and allowed to attach overnight at 37 °C, 5 % CO_2. Next, cells were incubated for 30 min (37 °C, 5 % CO_2) with different concentrations of AuNPs (2, 4, 6, 8 and 16 x 10^7 AuNPs/mL), washed with PBS to remove unbound AuNPs, and replenished with fresh culture medium containing 5 mg/ml FITC-labeled dextran (Sigma-Aldrich) of 10 kDa (FD10). Subsequently, cells were photoporated using an in-house built laser irradiation set-up equipped with a nanosecond pulsed laser (5 ns pulse duration, λ = 532 nm, Tor, Cobolt) and a galvano scanner (Thorlabs, THORLABS-GVS002.SLDPRT) for rapid beam scanning across the samples. A fixed laser pulse fluence (optical energy per unit area) of 1.6 J/cm² was applied. After laser treatment, FD10-diluted

medium was removed and cells were washed twice with culture medium and once with PBS followed by cell detachment using 0.25% trypsin-EDTA. At last, cells were measured for their FD10 content by flow cytometry using a three-laser BD LSR II (BD biosciences) and data was analyzed using FlowJo 10.7.1.

For loading with FITC-labeled dextrans in function of efflux experiments, L929sAhFas iGSDME cells (650 x 10^3 cells/well) were seeded in a 6-well plate and allowed to attach overnight at 37 °C, 5 % CO_2. The same protocol as described before was used. In this case, cells were incubated with the optimal AuNP concentration (6 x 10^7 AuNPs/mL) for 30 min. After washing away of unbound AuNPs, culture medium was added containing FITC-labeled dextrans (Sigma-Aldrich) of 4 kDa (FD4), 10 kDa (FD10), 40 kDa (FD40), 70 kDa (FD70), 150 kDa (FD150), 250 kDa (FD250), 500 kDa (FD500) or 2000 kDa (FD2000). For all sizes a concentration of 5 mg/ml was used, except for 2000 kDa for which the concentration was increased to 10 mg/ml. Cells were subsequently photoporated using a fixed laser pulse fluence of 1.6 J/cm² after which the dextran-containing medium was removed and cells were washed twice with culture medium. After 2h of incubation (37 °C and 5 % CO_2), the same procedure was repeated a second time to further increase the percentage of fluorescently labeled cells. Finally, cells were detached using trypsin-EDTA and re-seeded at 100 x 10^3 cells/well in 24-well suspension plates in the presence or absence of doxycycline (Sigma-Aldrich, 1 µg/ml) and allowed to grow overnight (37 °C, 5 % CO_2).

6.2.7 Influx and efflux of labeled dextrans and cell death analysis

For influx experiments, L929sAhFas iGSDME cells were seeded in 24-well suspension plates (100 x 10^3 cells/well) in the presence or absence of doxycycline (Sigma-Aldrich, 1 µg/ml) and treated the next day with 250 ng/ml anti-Fas (clone CH11, Upstate) for 10h every 2h. Afterwards, cells were harvested by gently pipetting up and down and were immediately centrifuged at 400 g for 5 min at 4 °C. After removing the supernatant, the cells were resuspended in culture medium containing 0.5 mg/ml Texas Red-labeled dextran (Thermofisher Scientific and Nanocs) of 10 kDa (TR10), 40 kDa (TR40), 70 kDa (TR70) of 2000 kDa (TR2000) and incubated for 5 min at room temperature. Next, cells were centrifuged again for 5 min at 400 g and 4 °C, washed and resuspended in culture medium containing 2.5 µM SYTOX Blue (Molecular Probes) for nuclear staining. Samples were subsequently measured by flow cytometry using a four-laser BD Fortessa (BD Biosciences) and data was analyzed using FlowJo 10.7.1.

For efflux experiments, L929sAhFas iGSDME cells were preloaded with FITC-labeled dextrans (Sigma-Aldrich) using nanoparticle-sensitized photoporation and re-seeded in 24-well suspension plates in the presence or absence of doxycycline (Sigma-Aldrich, 1 µg/ml). One day after photoporation, re-seeded L929sAhFas iGSDME were treated with 250 ng/ml anti-Fas (clone CH11, Upstate) for 10h every 2h. Subsequently, cells were stained with

SYTOX blue (Molecular probes) at a concentration of 2.5 µM after which they were collected by gently pipetting up and down and measured by flow cytometry using a three-laser BD LSR II (BD Biosciences). Data was analyzed using FlowJo 10.7.1.

6.2.8 CellTiter-Glo® cell viability assay

In view of determining the optimal AuNP concentration, cell viability was assessed 2h post laser treatment using the CellTiter-Glo® luminescent cell viability assay (Promega) following the manufacturer's protocol. Briefly, culture medium was replaced by equal amounts of fresh culture medium and CellTiter-Glo® reagents and cells were mixed for 30 min using an orbital shaker at 120 rpm. After allowing stabilization of the luminescent signal for 15 min, equal volumes of each well were transferred to an opaque well plate and luminescence was recorded by a Glomax Luminometer (Promega).

6.2.9 Statistical analysis

Results are presented as means ± SD. Statistical analysis of PS exposure and SB staining in function of time were performed using PRISM 8 software (GraphPad) using a two-way ANOVA with the Geisser-Greenhouse correction (matched values were stacked into a subcolumn). For the influx and efflux dataset, homogeneity of variances and data normality were checked graphically (boxplots, QQPlots respectively). Analysis of the influx of Texas Red-labeled dextrans was done making use of a generalized linear model (GLM), poisson family. To study the effect of dextran size on either the SB-negative (SB-) and SB-positive (SB+) cells, the factor variables doxycycline addition and measured point in time (0, 2, 4, 6, 8 and 10h of anti-Fas treatment) and the discrete variable dextran size were included in the model. To study the effect of doxycycline on the influx of Texas Red-labeled dextrans, doxycycline addition, the measured point in time (0, 2, 4, 6, 8 and 10h of anti-Fas treatment) and dextran size were all set as factor variables in the GLM. Multiple comparisons were made making use of the package "multcomp" [34].

To analyze the efflux of FITC-labeled dextrans, the dataset was split in three populations (SB-, SB low+, SB high+). For both datasets, a GLM (Gaussian family) was fitted to study the effect of dextran size and doxycycline on the efflux of detrans. The factor variables doxycycline, measured point in time (0, 2, 4, 6, 8 and 10h of anti-Fas treatment) and the discrete variable dextran size were included in the model. Again, multiple comparisons were made using the package "multcomp". All analysis were done in R, version 4.3 on three biological replicates of each data-set [35].

Differences with a p-value < 0.05 were considered significant and indicated as followed: ns = nonsignificant; * $p < 0.05$; ** $p < 0.01$; *** $p < 0.001$.

6.3 RESULTS

6.3.1 GSDME accelerates plasma membrane permeabilization during apoptosis-driven secondary necrosis as measured by SYTOX Blue-mediated nuclear staining.

As conflicting findings were reported on the contribution of GSDME to apoptosis-driven secondary necrosis [9,10,17,18], we decided to investigate the GSDME function in the murine fibrosarcoma cell line L929 stably expressing the human Fas receptor (L929sAhFas). Treatment of L929sAhFas cells with agonistic anti-Fas antibody induces apoptosis and caspase-3 activation via the caspase-8-dependent proteolytic pathway [36]. As expected, treating L929sAhFas with anti-Fas resulted in the generation of a GSDME fragment of ~35 kDa (Figure 1A), indicating proteolytic activation of GSDME by caspase-3 as previously reported [9,37]. To investigate the role of GSDME in anti-Fas-mediated apoptosis, we generated *Gsdme* knockout (KO) L929sAhFas clones by CRISPR/Cas9 gene editing (Figure 1B). Next, we investigated whether the loss of GSDME expression in *Gsdme* KO L929sAhFas clones (KOcl1 and KOcl2) affected the kinetics of the uptake of the cell-impermeable DNA-binding fluorescent dye SB during apoptosis-driven secondary necrosis (Figure 1C). Upon anti-Fas treatment, *Gsdme* KO L929sAhFas clones (KOcl1 and KOcl2) showed a delay in the uptake of SB compared to the parental cells and *Gsdme* wild-type (WT) clones in which CRISPR/Cas9 gene editing failed to interrupt *Gsdme* (WTcl1 and WTcl2, Figure 1C), indicating delayed plasma membrane permeabilization in absence of GSDME expression, as concluded from the SB staining. To confirm that this delay was GSDME-dependent and did not result from a clonal effect, *Gsdme* KOcl2 L929sAhFas was reconstituted with a doxycycline-inducible mGSDME construct using viral transduction, hereafter referred to as L929sAhFas iGSDME cells. Treatment of these cells with doxycycline resulted in the expression of GSDME that was cleaved to its active form upon treatment with anti-Fas (Figure 1D). To compare the progression of apoptosis between GSDME-expressing (L929sAhFas iGSDME+) and GSDME-deficient (L929sAhFas iGSDME-) cells in more detail, we measured nuclear staining by SB and membrane surface PS exposure with Annexin V (AnnV) (Figure 1E). Reconstitution of GSDME expression in L929sAhFas iGSDME cells by doxycycline treatment accelerated SB-positivity upon anti-Fas treatment compared to GSDME-deficient cells (Figure 1E-F), suggesting that the plasma membrane permeabilization kinetics are slower in cells lacking GSDME. Interestingly, upon anti-Fas treatment, both L929sAhFas iGSDME+ and iGSDME- cells displayed a similar increase in membrane surface PS exposure as measured by AnnV staining (AnnV+ cells, Figure 1G). Given this similar kinetics of AnnV-positivity, the slower SB-positivity in L929sAhFas iGSDME- cells correlates with a prolonged PS single-positive stage (AnnV+/SB-, Figure 1H). The number of AnnV+/SB- cells starts to decline in L929sAhFas iGSDME+ conditions, 4h after anti-Fas treatment, while in cells lacking GSDME a prolonged PS single-positive stage (AnnV+/SB-) can be observed (Figure 1H).

These data suggest that the initial progression of apoptotic signaling, leading to PS exposure, is not affected by GSDME expression, but GSDME is required to speed up plasma membrane permeabilization as measured by SB staining. Moreover, our results indicate that the loss of GSDME expression delays but not prevents plasma membrane permeabilization thereby suggesting that other, GSDME-independent, plasma membrane permeabilization mechanisms exist during apoptosis-driven secondary necrosis in L929sAhFas cells.

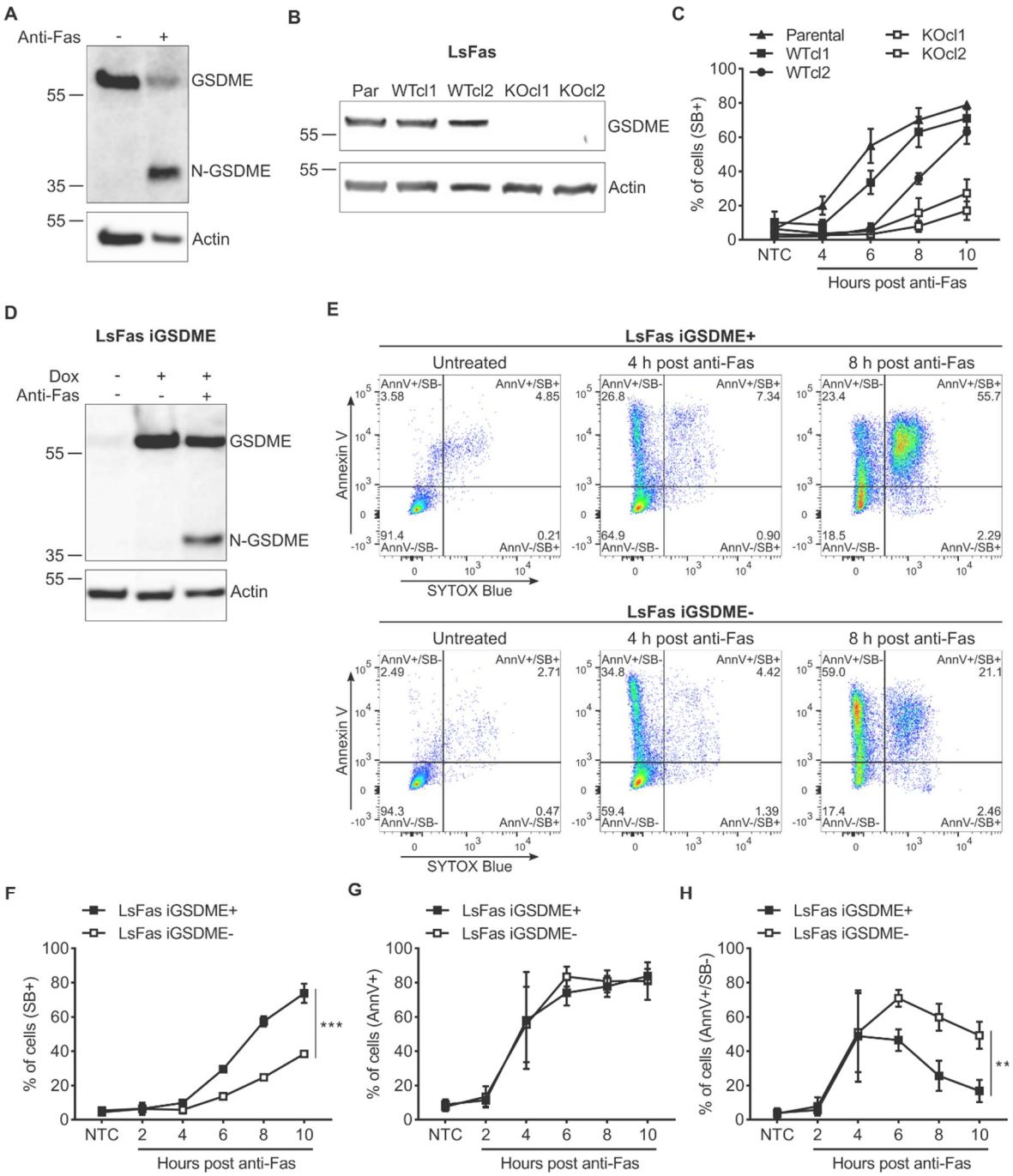

Figure 1. Impact of GSDME expression on apoptosis-driven secondary necrosis in L929sAhFas cells. (A) Expression and proteolytic cleavage of GSDME in L929sAhFas upon anti-Fas treatment. **(B)** Expression of GSDME in different L929sAhFas clones upon CRISPR/Cas 9 gene editing. **(C)** Cell death kinetics of parental, *Gsdme* WT and KO L929sAhFas clones measured by SB staining via flow cytometry. **(D)** Expression of GSDME in L929sAhFas iGSDME cells upon doxycycline treatment. Subsequent treatment with agonistic anti-Fas antibodies promotes the generation of the active 35 kDa N-terminal fragment (N-GSDME). **(E-H)** Flow cytometry analysis of L929sAhFas iGSDME cells with (L929sAhFas iGSDME+) or without (L929sAhFas iGSDME-) doxycycline-induced GSDME expression during apoptosis-driven secondary necrosis. **(E)** Representative flow cytometry dot plots after 4h or 8h treatment with anti-Fas. **(F)** Levels of secondary necrotic (SB+) cells, **(G)** cells exposing PS (AnnV+) and **(H)** PS single-positive (AnnV+/SB-) cells in L929sAhFas iGSDME cells stimulated with anti-Fas. AnnV, Annexin V; Dox, doxycycline; GSDME, gasdermin E; KO, knockout; LsFas, L929sAhFas; NTC, non-treatment control; Par, parental; SB, SYTOX Blue; WT, wild-type.

6.3.2 GSDME pore-formation supports influx of 10 kDa dextrans independent of plasma membrane permeabilization kinetics

Having confirmed that GSDME expression accelerates nuclear DNA staining by SB (Figure 1F), we next evaluated whether GSDME-dependent membrane permeabilization supports the influx of large, membrane-impermeable macromolecules as well. Texas Red-labeled dextrans with a size of 10 kDa (TR10) were used to this end, allowing convenient quantification of influx by flow cytometry (Figure 2A). Texas Red signal was assessed in SB- and SB+ cells separately, according to the zones indicated in Figure 2B. Remarkably, treatment of L929sAhFas iGSDME cells with anti-Fas followed by incubation with TR10 and SB resulted in a TR10 single-positive population (Figure 2B, TR10+/SB-, black arrow) and a double-positive population (Figure 2B, TR10+/SB+), suggesting that TR10 can already enter the cells before SB stains the nuclear DNA (Figure 2B). Unlike Fas-induced PS exposure, which happened independently of GSDME expression (Figure 1G), TR10 tends to accumulate in twice as much SB- L929sAhFas iGSDME+ cells compared to SB- cells lacking GSDME expression (Figure 2C). This observation suggests that the influx of TR10 is enhanced by GSDME-dependent plasma membrane permeabilization in the sublytic phase, before staining by SB. Consistent with this, the TR10+/SB+ population was higher in GSDME-expressing cells (Figure. 2D), which is expected as we showed that, upon anti-Fas treatment, staining by SB was accelerated in L929sAhFas iGSDME+ cells (Figure 1F).

Next, we investigated whether the GSDME-related difference observed in TR10 influx is simply the result of delayed cell death kinetics, measured by SB staining, in L929sAhFas iGSDME- or a direct consequence of the absence of the GSDME pore itself. To neutralize the difference in cell death kinetics in our results, as pointed out in the previous section (Figure 1F), we assessed TR10 uptake in the SB- and SB+ population by normalizing the number of TR10- and TR10+ cells against the total number of cells in the respective populations (Figure 2E-F). Apparently, the fraction of TR10+ cells upon anti-Fas treatment in SB- L929sAhFas iGSDME- cells was limited and significantly less compared to when GSDME was present (Figure 2E). This suggests that GSDME pore-formation itself allows the influx of TR10 before SB-mediated nuclear staining. In SB+ cells, TR10 entered L929sAhFas iGSDME- cells much more easily, pointing to other permeabilization mechanisms taking place as well during apoptosis-driven secondary necrosis (Figure 2F). Still, TR10 entered L929sAhFas iGSDME+ cells significantly more, indicating that plasma membrane permeabilization by GSDME enhances TR10 influx. Interestingly, both in SB- (Figure 2E) and SB+ cells (Figure 2F), the fraction of TR10+ cells increased over time. This suggests that the longer a cell remains SB- upon anti-Fas treatment, the more cells are porated, possibly with bigger pores, thereby promoting the entrance of TR10 while cells are in the sublytic phase and are not yet stained by SB. Altogether, our results indicate that GSDME promotes faster and increased influx of TR10 in both SB- as SB+ cells during apoptosis-driven secondary necrosis.

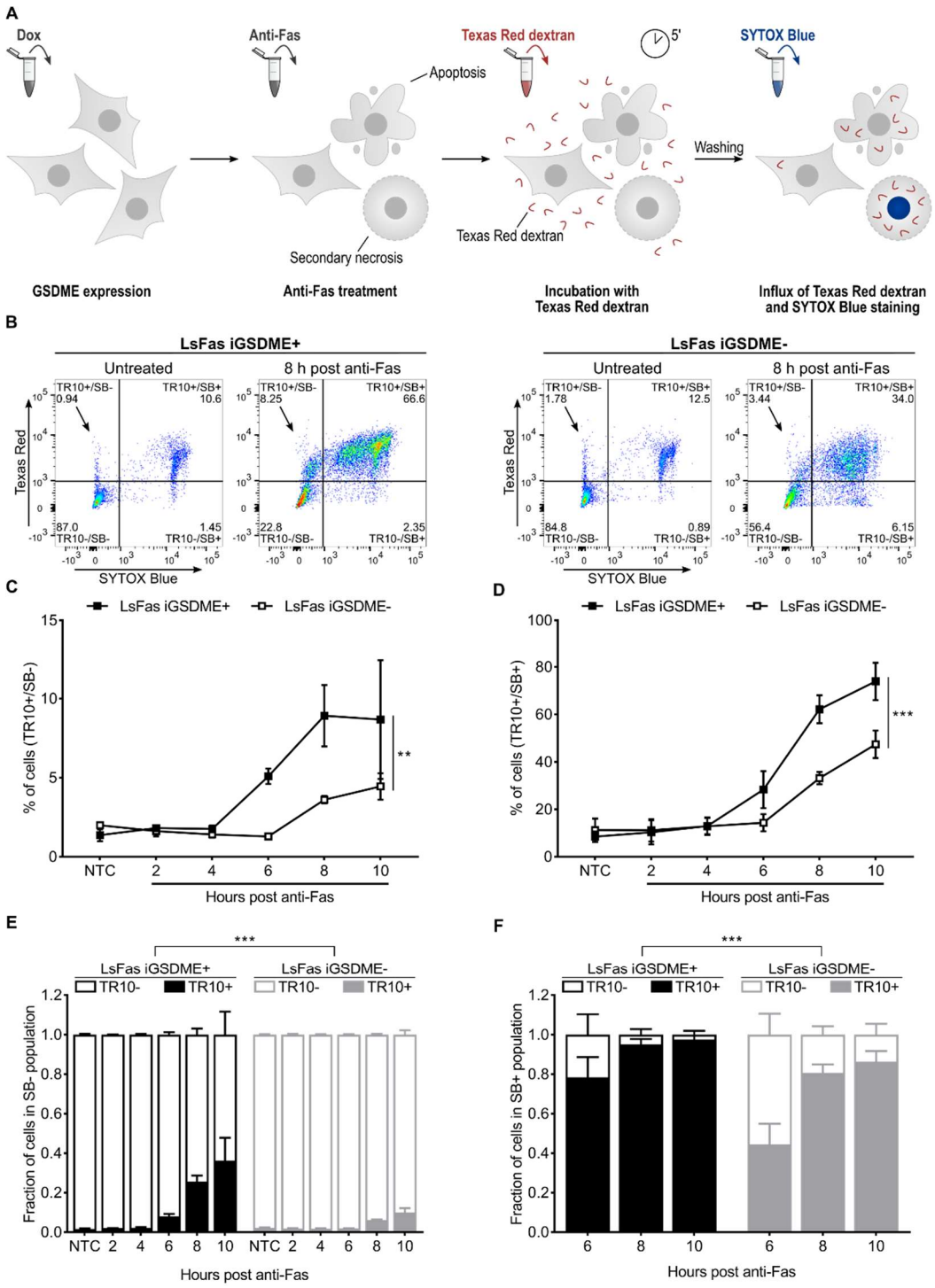

Figure 2. Monitoring of Texas Red-labeled dextran 10 kDa (TR10) influx in L929sAhFas iGSDME cells during apoptosis-driven secondary necrosis. (A) Principle of Texas Red-labeled dextran staining of L929sAhFas iGSDME cells. **(B-F)** Flow cytometry analysis of L929sAhFas iGSDME cells with (L929sAhFas iGSDME+) and without (L929sAhFas iGSDME-) doxycycline-induced GSDME expression during apoptosis-driven secondary necrosis. **(B)** Representative plots of L929sAhFas iGSDME cells untreated and after treatment with anti-Fas for 8h. **(C)** Levels of Texas Red single-positive cells (TR10+/SB-) in L929sAhFas iGSDME cells upon anti-Fas treatment. **(D)** Levels of Texas Red and SB double-positive (TR10+/SB+) cells in L929sAhFas iGSDME cells upon anti-Fas treatment. **(E)** Fraction of Texas Red positive (TR10+) and Texas Red negative (TR10-) cells in the SB- population. **(F)** Fraction of Texas Red positive (TR10+) and Texas Red negative (TR10-) cells in SB+ population. Dox, doxycycline; GSDME, gasdermin E; LsFas, L929sAhFas; SB, SYTOX Blue; NTC, non-treatment control; TR, Texas Red.

6.3.3 GSDME pore-formation facilitates the influx of large dextrans in a size-dependent manner

As TR10 is able to enter L929sAhFas iGSDME cells even when GSDME is absent, we wondered whether there is a molecular weight above which dextrans can no longer enter GSDME-deficient cells. Therefore, we examined the influx of Texas Red-labeled dextrans of 40 kDa (TR40), 70 kDa (TR70) and of 2000 kDa (TR2000) and how this is affected by GSDME expression in L929sAhFas iGSDME cells upon anti-Fas treatment. Influx of Texas Red-labeled dextrans was again assessed in both SB- and SB+ cells separately. Overall, upon 8h (Figure 3A) and 10h (Figure 3B) of treatment with anti-Fas, absence of GSDME expression significantly reduced the influx of all dextran sizes in SB- L929sAhFas iGSDME cells, while influx clearly did happen when GSDME was present, except for TR2000. Although prolonged anti-Fas treatment promoted influx of Texas Red-labeled dextrans up to 70 kDa in both L929sAhFas iGSDME+ and iGSDME- cells, this was still significantly lower in absence of GSDME (Figure 3B). Moreover, the uptake of Texas Red-labeled dextrans in SB- cells decreased with increasing dextran size, both in the absence (10 h, $p < 0.01$) and presence (8 h, $p < 0.05$; 10 h, $p < 0.01$) of GSDME expression (Figure 3A-B). These observations point toward pore-formation during apoptosis-driven secondary necrosis with a rather variable instead of a fixed size. These results suggest that GSDME pores formed in SB- L929sAhFas iGSDME cells allow the passage of dextrans up to at least 70 kDa while they exclude the entrance of Texas Red-labeled dextrans equal or larger than 2000 kDa. Importantly, note that the GSDME-dependent influx of Texas Red-labeled dextrans happened prior to SB staining, suggesting that GSDME membrane permeabilization during apoptosis-driven secondary necrosis does not occur concurrently with nuclear DNA staining by small SB molecules (0.4 kDa) and already happens prior to secondary necrosis.

The GSDME dependency for the influx in SB+ L929sAhFas iGSDME cells was less pronounced for TR10 after treatment with anti-Fas for 8h (Figure 3C), whereas after 10h influx of sizes 10 to 70 kDa revealed to be non-significant between L929sAhFas iGSDME+ and iGSDME- cells (Figure 3D). Nevertheless, GSDME expression clearly promoted the entrance of TR2000 in SB+ L929sAhFas iGSDME+ cells after treatment with anti-Fas for 10h (Figure 3D). Although this suggests that GSDME pores in SB+ cells might even favor the entrance of molecules up to 2000 kDa, most of the cells (~70 %) were still negative for TR2000. Furthermore, similar to the influx in SB- cells, influx of Texas Red-labeled dextrans significantly decreased with increasing dextran size. On average, dextran size had an overall statistical significant effect on the influx 8h after anti-Fas treatment in L929sAhFas iGSDME- cells (Figure 3C, $p < 0.001$) and 10h after anti-Fas treatment in L929sAhFas iGSDME+ (Figure 3D, $p < 0.05$) and iGSDME- (Figure 3D, $p < 0.001$) cells. Linear fit of the data points for TR10, TR40 and TR70 upon 8h (Figure 3E) and 10h (Figure 3F) of anti-Fas treatment, allowed us to estimate the size of molecules that can enter 50 % of the cells (Figure 3E-F). According to our calculations, GSDME expression would allow the uptake of

molecules between 115 (8 h) and 125 kDa (10 h) in 50 % of the SB+ L929sAhFas iGSDME+ cells, while absence of GSDME limits the molecular size to 53 (8 h) and 87 kDa (10 h).

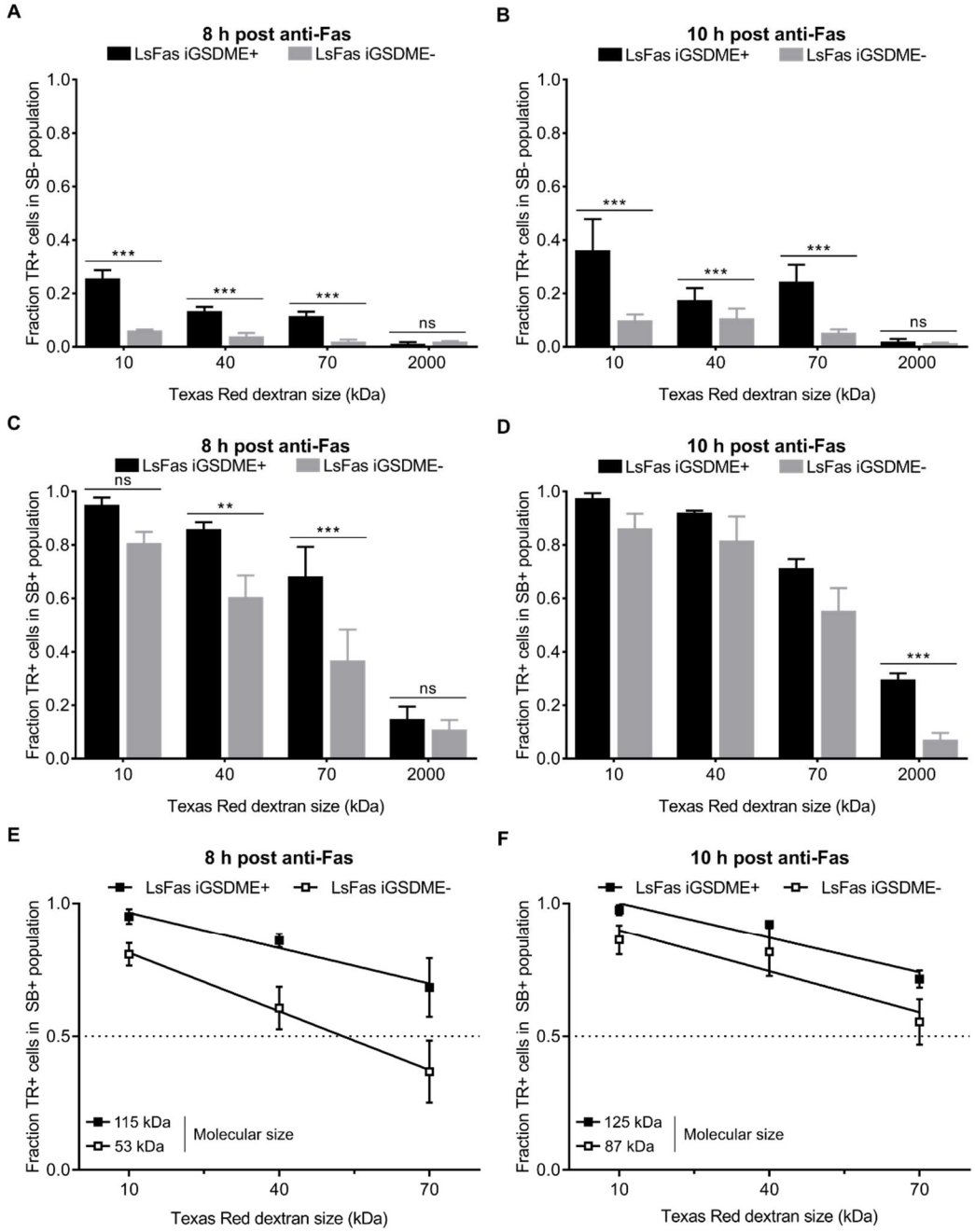

Figure 3. Influx of Texas Red-labeled dextrans of 10 kDa (TR10), 40 kDa (TR40), 70 kDa (TR70) and 2000 kDa (TR2000) in L929sAhFas iGSDME during apoptosis-driven secondary necrosis. (A-F) Flow cytometry analysis of Texas Red-labeled dextran uptake in L929sAhFas iGSDME cells with (L929sAhFas iGSDME+) and without (L929sAhFas iGSDME-) doxycycline-induced GSDME expression after 8h and 10h treatment with anti-Fas. **(A-B)** Fraction of the SB- population that is positive for various sizes of Texas Red-labeled dextrans. **(C-D)** Fraction of the SB+ population that is positive for various sizes of Texas Red-labeled dextrans. **(E-F)** Linear fit of data points for the fractions of the SB+ population positive for TR10, TR40 and TR70. Intersection of this line with the dotted line provides a rough estimation of molecular sizes that can enter 50 % of the SB+ population. LsFas, L929sAhFas; SB, SYTOX Blue; TR, Texas Red.

6.3.4 Nanoparticle-sensitized photoporation constitutes a suitable method for introducing dextrans into cells without influencing apoptosis kinetics

Although monitoring the influx of Texas Red-labeled dextrans provided insight in the molecular weight of molecules that can enter during apoptosis-driven secondary necrosis, we aimed to evaluate whether the same conclusions are reached when monitoring the efflux of macromolecules. Monitoring efflux should better reflect the physiological situation where intracellular content like Damage Associated Molecular Patterns (DAMPs) or even cell organelles are released from dying cells. Instead of Texas Red-labeled dextrans, of which we observed that they tend to interact with intracellular constituents, we used FITC-labeled dextrans, which are inert in cells [38]. For delivery of FITC-labeled dextrans in the cytosol of L929sAhFas cells, we used nanoparticle-sensitized photoporation as an emerging intracellular delivery technique that minimally perturbs the cellular homeostasis (Figure 4A) [23,24,27]. L929sAhFas cells were first incubated with cationic AuNPs, which attach to the plasma membrane. After washing away unbound AuNPs, cells were irradiated with a 5 nanosecond laser pulse (λ = 532 nm, 1.6 J/cm²), resulting in the formation of transient pores in the plasma membrane through which the fluorescently labeled dextrans can diffuse into the cytosol.

First, we optimized the AuNP concentration as function of delivery efficiency and cell metabolic activity. To maximize cell loading and minimize potential cell cytotoxicity by photoporation, different AuNP concentrations (2, 4, 6, 8 and 16 x 10^7 AuNPs/mL) were screened using a fixed laser pulse fluence of 1.6 J/cm². We observed an increase in the percentage of cells positive for FITC-labeled dextran of 10 kDa (FD10) (Figure S1A), as measured by flow cytometry, and a decrease in metabolic activity, as measured with the CellTiter-Glo® assay (Figure S1B), for increasing AuNP concentrations. Allowing a 30 % reduction in metabolic activity, determined by the ATP content of live cells, the optimal AuNP concentration was set at 6 x 10^7 AuNPs/mL for all further experiments, in which case near 100 % of the cells are FD10 positive. In addition, we tested whether photoporation of FD10 influenced cell death kinetics of L929sAhFas cells when treated with anti-Fas. *Gsdme* WT and KOcl2 L929sAhFas cells were photoporated in the presence of FD10 and cell death kinetics, as determined by SB staining, was compared with untreated control cells. Cell death kinetic measurements of photoporated cells remained unchanged compared to the untreated control cells (Figure S2). Based on these results, we concluded that photoporation can efficiently deliver FITC-labeled dextrans in L929sAhFas cells without influencing anti-Fas-mediated apoptosis-driven secondary necrosis.

6.3.5 Efflux of dextrans of 10 kDa occurs independently of GSDME expression and cell death kinetics during apoptosis-driven secondary necrosis

Having optimized the cytosolic delivery of FD10 with nanoparticle-sensitized photoporation, we investigated the efflux of the dextrans from L929sAhFas iGSDME cells upon anti-Fas treatment, as a function of the SB signal of the cells (Figure 4A). Following this strategy, we gated the whole cell population undergoing anti-Fas treatment into: no SB signal (SB-), a low SB signal (SB low+) and a high SB signal (SB high+) (Figure 4B). Flow cytometry data revealed that both in presence and absence of GSDME, FD10 was released from the cells when they became positive for the SB-mediated nuclear staining (Figure 4B-C). Interestingly, a bimodal distribution in the FITC signal was observed in cells with a low SB signal (Figure 4C, middle panel), which was not observed in the influx experiments. This observation indicates that in the initial stage, when the nucleus of cells gets stained by SB, a part of those cells had already lost FD10 content while the other part was still clearly FD10 positive. In contrast, only a very few SB- cells were negative for FD10 (Figure 4C, left panel), while cells with a high SB+ signal had practically all lost their dextran content (Figure 4C, right panel). Of note, these results were observed independent of GSDME expression.

This strong heterogeneity of dextran release between SB- and SB high+ cells is confirmed when plotting the mean fluorescent intensity of FD10 relative to the untreated SB- cells (rMFI) for the SB-, SB low+ and SB high+ population, respectively (Figure 4D-F). Note that we chose to use the rMFI to present the loss of FITC-labeled dextrans, as photoporation delivery efficiency (i.e. the percentage of FD10 positive cells) decreases with increasing dextran size [24,39]. Only a minimal amount of FD10 content was released from SB- cells (Figure 4D). Surprisingly, the rMFI decreased slightly but significantly more in the absence of GSDME than in GSDME-reconstituted cells, suggesting that there would be more content release over time in SB- cells when GSDME is lost. This is a counterintuitive result, which is in contrast with our influx data that pointed toward facilitated uptake of dextrans when GSDME pores are formed in SB- cells. However, referring to the prolonged stage of PS-positivity in SB- cells without GSDME expression (Figure 1H), we hypothesize that the larger drop in rMFI in those cells can be attributed to the prolonged release of FD10-loaded apoptotic membrane blebs in cells lacking GSDME. Taken together, based on these data, we could not claim that GSDME expression facilitates the efflux of small dextrans in SB- L929SAhFas iGSDME cells upon anti-Fas treatment.

In strong contrast to the SB- population, SB high+ cells have lost almost all of their FD10 content irrespective of GSDME expression (Figure 4F). While the SB low+ population had an intermediate rMFI level, there was no difference between GSDME-expressing and non-expressing cells (Figure 4E). Interestingly, treating cells for longer time periods with anti-Fas resulted in a decreased rMFI of FD10 in the SB low+ population, indicating a different content release behavior of slower-dying cells. More specifically, based on these

observations, it seems that cells in which SB-staining is initiated later upon anti-Fas treatment, are more likely to lose their content earlier in the dying process, while the opposite holds true for faster-dying cells.

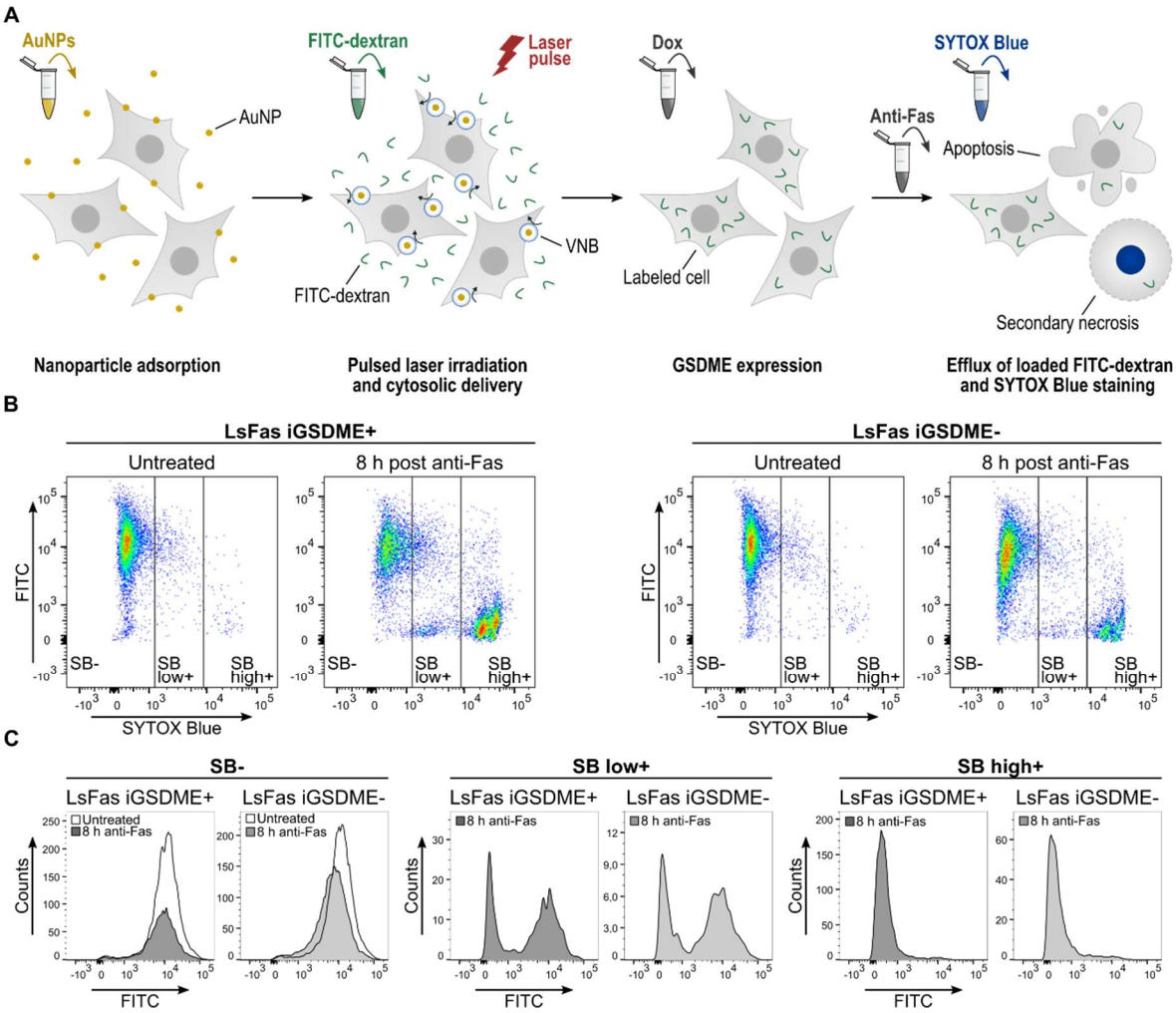

Figure 4. Efflux of FITC-labeled dextrans 10kDa (FD10) from L929sAhFas iGSDME cells during apoptosis-driven secondary necrosis. (A) Principle of monitoring efflux of FITC-labeled dextrans after photoporation-based dextran loading. **(B-F)** Flow cytometry analysis of FD10 release in L929sAhFas iGSDME with (L929sAhFas iGSDME+) and without (L929sAhFas iGSDME-) doxycycline-induced GSDME expression when stimulated with anti-Fas. **(B)** Scatter plots of L929sAhFas iGSDME in presence (left) and absence (right) of GSDME expression untreated and after 8h treatment with anti-Fas. **(C)** Histogram plots representing the distribution of the FD10 signal in the three zones of SB staining: SB- (left), SB low+ (middle) and SB high+ (right).

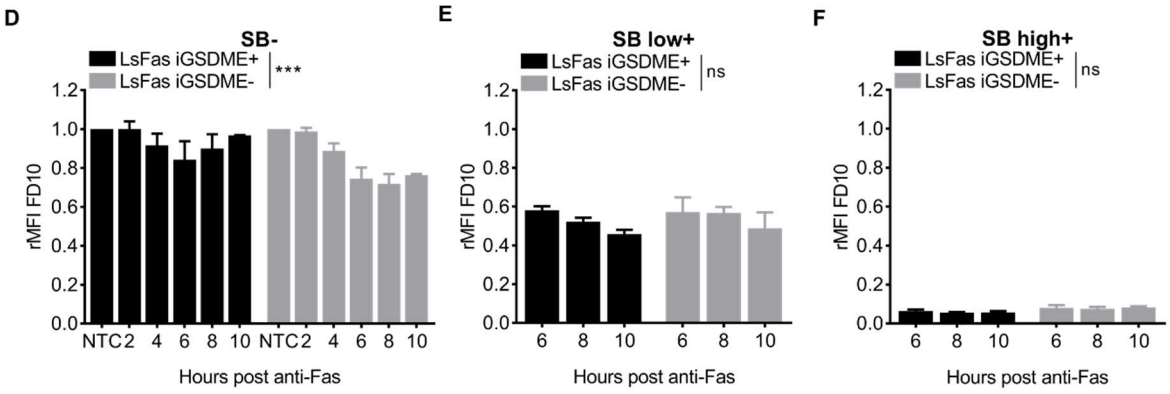

Figure 4 (continued) (D) Graph representing the mean fluorescent intensity of FD10 in the SB- population relative to the untreated SB- cells (rMFI) as a function of anti-Fas treatment. **(E)** Graph representing the mean fluorescent intensity of FD10 in the SB low+ population relative to the untreated SB- cells (rMFI) in function of anti-Fas treatment. **(F)** Graph representing the mean fluorescent intensity of the SB high+ population relative to the untreated SB- cells (rMFI) as a function of anti-Fas treatment. AuNP, gold nanoparticle; Dox, doxycycline; FD, FITC-dextran; GSDME, gasdermin E; LsFas, L929sAhFas; NTC, non-treatment control; SB, SYTOX Blue; VNB, vapor nanobubble.

6.3.6 Efflux of dextrans is size-dependent but GSDME-independent during apoptosis-driven secondary necrosis

To evaluate whether the release of dextrans from anti-Fas-treated L929sAhFas iGSDME cells is size-dependent, we monitored the efflux of FITC-labeled dextrans of increasing molecular weights: 4 kDa (FD4), 40 kDa (FD40), 70 kDa (FD70), 150 kDa (FD150), 250 kDa (FD250), 500 kDa (FD500) and 2000 kDa (FD2000). Efflux in SB- cells was size independent, albeit that L929sAhFas iGSDME- cells had lost more FITC-labeled dextrans compared to L929sAhFas iGSDME+ cells (Figure 5A). This supports our previous hypothesis that dextran loss is dominated by blebbing in SB- cells, especially in the absence of GSDME. In contrast, SB high+ cells have lost almost all FITC-labeled dextran content of all sizes independent of GSDME expression (Figure 5C). Nevertheless, a slight size-dependent trend was seen, indicating less dextran release with increasing molecular weight, which was significant in the absence of GSDME expression (Figure 5C). This size-dependent trend was more obvious in SB low+ (Figure 5B), although again only significant for GSDME-deficient cells. Together these data point towards a size-dependent but GSDME-independent release of dextrans as soon as cells start to become positive for SB. Although no clear size cut-off of the GSDME pore could be determined *via* this strategy, release of FITC-labeled dextrans in general is size-dependent during apoptosis-driven secondary necrosis. This can be concluded from the stronger release of smaller-sized dextrans in SB low+ cells compared to larger-sized dextrans, which tend to be released rather at the end of permeabilization (Figure 5A-B, Figure S3A-B).The fact that larger-sized dextrans are less easily released as compared to smaller-sized dextrans may indicate the presence of another, GSDME-independent, plasma membrane permeabilization subroutine in SB+ cells that allows the release of FITC-labeled dextrans in a size-dependent way. Of note, as limited efflux was observed in SB- cells, the subroutine promoting efflux of FITC-labeled dextrans coincided with SB staining in our cells. Importantly, as concluded from

previous sections, cell death kinetics measured by SB-mediated nuclear staining is delayed in L929sAhFas iGSDME cells in the absence of GSDME expression (Figure 1F). Therefore, one can expect that a delayed efflux of FITC-labeled dextrans is similar to the delay of influx (not corrected for cell death kinetics) in L929sAhFas iGSDME cells in absence of GSDME expression (Figure 2C-D). Indeed, when evaluating the rMFI (relative to all untreated cells) of the complete cell population (without gating for SB signal), overall a slower efflux of FITC-labeled dextrans was observed in L929sAhFas iGSDME- cells in function of anti-Fas treatment (Figure 5D). Although efflux of FITC-labeled dextrans through the GSDME pore seems unlikely, this observation highlights the importance of GSDME in the overall cellular release of FITC-labeled dextrans. Altogether, our results suggest that GSDME contributes to a larger set of mechanisms steering membrane permeabilization during apoptosis-driven secondary necrosis and by consequence content release.

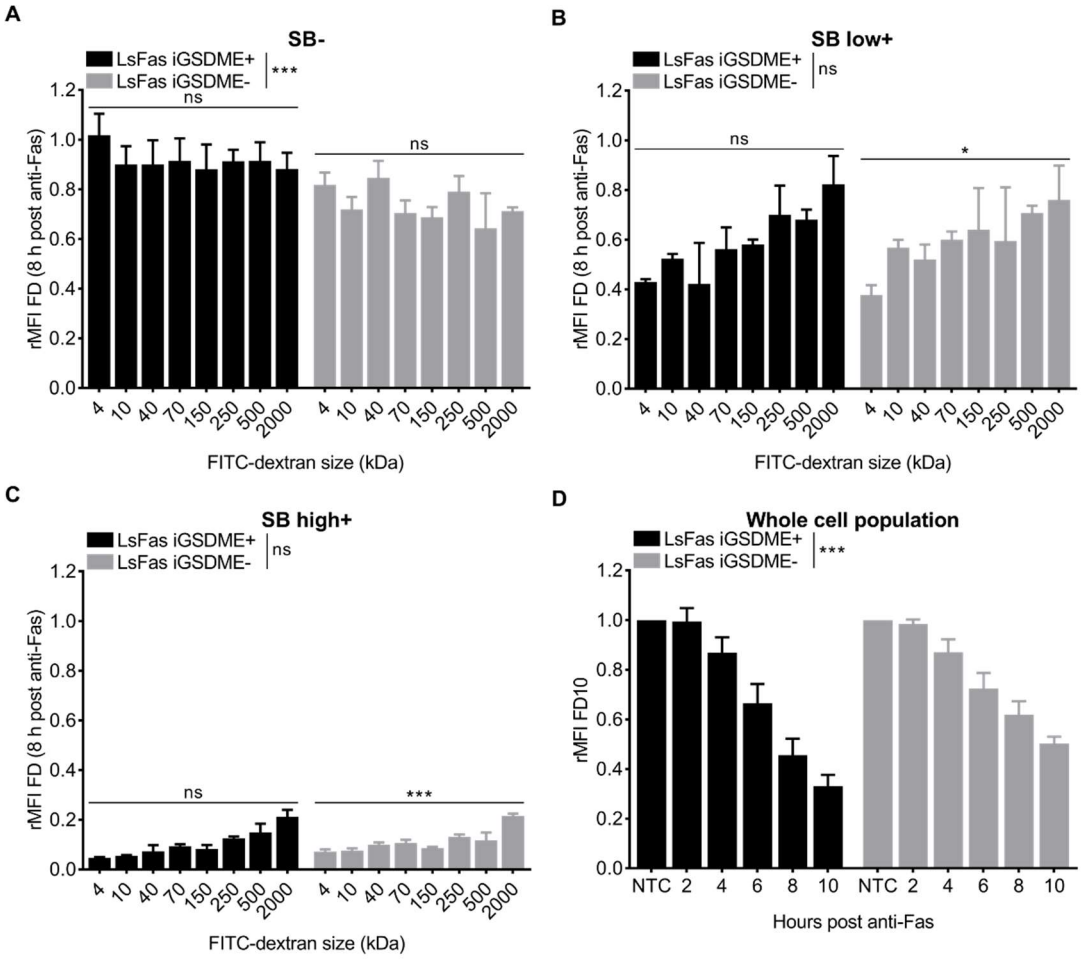

Figure 5. Efflux of FITC-labeled dextrans of different sizes from L929sAhFas iGSDME cells during apoptosis-driven secondary necrosis. (A-D) Flow cytometry analysis of FITC-labeled dextran release in L929sAhFas iGSDME cells with (L929sAhFas iGSDME+) and without (L929sAhFas iGSDME-) doxycycline-induced GSDME expression upon treatment with anti-Fas. **(A-C)** Graphs representing the mean fluorescent intensity relative to the untreated SB- cells (rMFI) for increasing sizes of FITC-labeled dextrans **(A)** in the SB- population, **(B)** in the SB low+ population and **(C)** in the SB high+ population after 8h treatment with anti-Fas. **(D)** Graph representing the mean fluorescent intensity relative to the untreated cells (rMFI) for the whole cell population in function of anti-Fas exposure time. FD, FITC-labeled dextran, LsFas, L929sAhFas, NTC, non-treatment control.

6.4 DISCUSSION

Plasma membrane permeabilization following apoptosis-driven secondary necrosis has always been perceived as a non-regulated process of apoptotic cells in the absence of sufficient phagocytic cell capacity [2,40]. Recently, it was shown that this plasma membrane permeabilization is a regulated process driven by caspase-3-mediated activation of GSDME [9]. This finding indicates that the cell can accelerate the process of permeabilization by engaging GSDME-mediated release of intracellular content, which affects the inflammatory response [41]. Although pore-formation by GSDMA3 and GSDMD has already been extensively studied [20–22], the kinetics and size characteristics of GSDME pore-formation during apoptosis-driven secondary necrosis are currently unknown. Determining the degree of membrane permeabilization and identifying molecular sizes able to pass the plasma membrane upon GSDME expression may give insights in the membrane destabilizing behavior of GSDME and its role in progressing apoptotic cells toward secondary necrosis.

In the first part of this study, we showed that GSDME expression contributes to apoptosis-driven secondary necrosis in L929sAhFas cells by accelerating cell death kinetics measured by SB staining. This is consistent with the findings of Rogers *et al*. stating that GSDME is necessary for the quick progression of apoptotic cells toward secondary necrosis [9]. Additionally, we demonstrated that GSDME expression is dispensable for Fas-induced PS exposure in L929sAhFas, which is an early subroutine of apoptosis. As GSDME expression does accelerate plasma membrane permeabilization, dying cells remain longer in the PS single-positive stage in the absence of GSDME expression. The physiological consequences of these observations are currently unknown. It is tempting to speculate that prolonged exposure of eat-me signals facilitates efficient clearance of these cells. Yet, GSDME expression was shown to increase phagocytosis of tumor cells by macrophages as well as the number and cytolytic activity of tumor-infiltrating natural-killer and CD8+ T lymphocytes, thereby suppressing tumor growth [41].

In the second part of this study, we monitored the influx and efflux of dextran molecules of various sizes in L929sAhFas iGSDME cells with and without GSDME expression. Our results based on the influx of Texas Red-labeled dextrans suggest that GSDME-dependent pore-formation in the sublytic phase, before SB-mediated nuclear staining, allows the passage of molecules with sizes up to 70 kDa, while influx is reduced and delayed in the absence of GSDME expression. This is consistent with earlier reports presenting that GSDMD and GSDME pores in sublytic cells upon pyroptotic stimuli are crucial for the release of cytokines such as active IL-1β (18 kDa) [42–44]. Additionally, our influx-based results imply that GSDME also facilitates the uptake of larger dextrans in SB+ cells, which possibly elucidates the contribution of GSDME to final cell lysis. From our influx experiments we could estimate that GSDME-driven plasma membrane permeabilization favors the passage of molecules up until ~125 kDa. This is consistent with Evavold *et al.* reporting that macromolecules such as lactate dehydrogenase (144 kDa) were unable to pass GSDMD

pores and were only released after complete cell lysis [42]. Although our results based on the influx of dextrans allowed us to conclude that GSDME favors the entrance of macromolecules, a clear cut-off size for molecules able to pass GSDME pores was not observed since we report a decrease in the uptake of Texas Red-labeled dextrans with increasing sizes. These observations might suggest that at any moment during cell death, permeabilization of plasma membranes may involve pores of different sizes that are simultaneously present in the cell population referring to the presence of alternative pore-forming molecules or less controlled pore-formation by GSDME. However, the formation of GSDME membrane pores of different sizes only seems plausible in case of a plasma membrane-destabilizing mechanism such as the carpet-like model or the formation of toroid-like pores since oligomerization and formation of discrete β-barrel-shaped pores are dependent on thermodynamic stability. Nevertheless, the presence of different pore sizes could indicate that intermediate pores are formed that undergo a growing process until they reach their final stable form as shown for GSDMD pores [21,22].

While influx experiments provided us with valuable insights regarding membrane permeabilization during apoptosis-driven secondary necrosis, we were keen to investigate the effect of this process on the efflux FITC-labeled dextrans. Monitoring efflux should better reflect the physiological situation where intracellular content is released from dying cells. Interestingly, more intermediate dextran sizes are available with the FITC fluorophore, which could aid in drawing more precise conclusions about GSDME. We used nanoparticle-sensitized photoporation as an efficient intracellular delivery technique, of which we could show that it does not interfere with apoptosis kinetics. However, upon triggering of apoptosis-driven secondary necrosis, we did not find a contribution of GSDME to the efflux of FITC-labeled dextrans from L929sAhFas cells. In addition, SB high+ cells released almost all FITC-labeled dextrans while in our influx experiments, TR2000 failed to enter in most of the SB+ cells. These observations suggest that other, GSDME-independent, subroutines exist that allow the release of FITC-labeled dextrans. The existence of different subroutines supporting membrane permeabilization during cell death has recently been shown by Kayagaki *et al*. They report that the cell-surface protein nerve injury-induced protein 1 (NINJ1) contributes to plasma membrane permeabilization during apoptosis-driven secondary necrosis, pyroptosis and necroptosis next to GSDME, GSDMD and mixed lineage kinase domain-like (MLKL) [45]. Which subroutine is responsible for the efflux of FITC-labeled dextrans in our system remains elusive, but similar to the influx of Texas Red-labeled dextrans, efflux of FITC-labeled dextrans occurs in a size-dependent manner. As to why GSDME pores seem to exclude FITC-labeled dextrans, we cannot rule out an electrostatic effect. FITC-labeled dextrans are anionic while Texas Red-labeled dextrans are more neutral. Recently, the GSDMD pore was shown to be predominantly negatively charged preventing the passage of negatively charged cargos [46].

6.5 CONCLUSIONS

We developed two strategies to elucidate the influence of GSDME in apoptosis-driven secondary necrosis and gained insights in the pore-forming and membrane permeabilizing behavior during this process. While a size dependency was observed for both influx and efflux of fluorescently labeled dextrans, we could only attribute an altered influx pattern to GSDME presence. Altogether, our results point to the existence of different subroutines that simultaneously regulate the passage of compounds during the cellular permeabilization process during apoptosis-driven secondary necrosis.

Acknowledgements

Research in the Vandenabeele group is supported by Flemish grants (EOS MODEL-IDI, FWO Grant 30826052), the Research Foundation Flanders (FWO) research grants (G.0E04.16N, G.0C76.18N, G.0B71.18N, G.0B96.20N), Methusalem (BOF16/MET_V/007), iBOF20/IBF/039 ATLANTIS, Foundation against Cancer (FAF-F/2016/865, F/2020/1505, F/2020/1434), the Cancer Research Institute Ghent (CRIG) and the Ghent Gut Inflammation Group (GIGG) consortia, and the Flanders Institute for Biotechnology (VIB). E.D.S. acknowledges funding by Excellence of Science EOS MODEL-IDI (FWO Grant 30826052), Foundation against cancer (FAF-F/2016/865) and Methusalem (BOF16/MET_V/007). K.B. gratefully acknowledges the funding by the European Research Council (ERC) under the European Union's Horizon 2020 research and innovation program (grant number 648124). J.R. and C.D.T. acknowledge funding of the Research Foundation Flanders (FWO, grant numbers 1110721N and 12S9418N respectively).

Competing interest

The authors declare that there are no competing interests.

References

1. Green, D.R. *et al.* (2016) The clearance of dying cells: table for two. *Cell Death Differ.* 23, 915–926
2. Vanden Berghe, T. Vanden *et al.* (2010) Necroptosis, necrosis and secondary necrosis converge on similar cellular disintegration features. *Cell Death Differ.* 17, 922–930
3. Boeltz, S. *et al.* Towards a pro-resolving concept in systemic lupus erythematosus. , *Seminars in Immunopathology*, 41. 01-Nov-(2019) , Springer, 681–697
4. Nagata, S. (2018) Apoptosis and Clearance of Apoptotic Cells. *Annu. Rev. Immunol.* 36, 489–517

5. Sachet, M. *et al.* (2017) The immune response to secondary necrotic cells. *Apoptosis* 22, 1189–1204
6. Ding, J. *et al.* (2016) Pore-forming activity and structural autoinhibition of the gasdermin family. *Nature* 535, 111–116
7. Kayagaki, N. *et al.* (2015) Caspase-11 cleaves gasdermin D for non-canonical inflammasome signalling. *Nature* 526, 666–671
8. Shi, P. *et al.* (2015) Loss of conserved Gsdma3 self-regulation causes autophagy and cell death. *Biochem. J.* 468, 325–336
9. Rogers, C. *et al.* (2017) Cleavage of DFNA5 by caspase-3 during apoptosis mediates progression to secondary necrotic/pyroptotic cell death. *Nat. Commun.* 8, 14128
10. Rogers, C. *et al.* (2019) Gasdermin pores permeabilize mitochondria to augment caspase-3 activation during apoptosis and inflammasome activation. *Nat. Commun.* 10, 1689
11. Hou, J. *et al.* (2020) PD-L1-mediated gasdermin C expression switches apoptosis to pyroptosis in cancer cells and facilitates tumour necrosis. *Nat. Cell Biol.* 22, 1264–1275
12. Sollberger, G. *et al.* (2018) Gasdermin D plays a vital role in the generation of neutrophil extracellular traps. *Sci. Immunol.* 3, 1–12
13. Chen, K.W. *et al.* (2018) Noncanonical inflammasome signaling elicits gasdermin D-dependent neutrophil extracellular traps. *Sci. Immunol.* 3, eaar6676
14. Shi, J. *et al.* (2015) Cleavage of GSDMD by inflammatory caspases determines pyroptotic cell death. *Nature* 526, 660–665
15. He, W. *et al.* (2015) Gasdermin D is an executor of pyroptosis and required for interleukin-1β secretion. *Cell Res.* 25, 1285–1298
16. Op de Beeck, K. *et al.* (2011) The DFNA5 gene, responsible for hearing loss and involved in cancer, encodes a novel apoptosis-inducing protein. *Eur. J. Hum. Genet.* 19, 965–973
17. Lee, B.L. *et al.* (2018) ASC- and caspase-8-dependent apoptotic pathway diverges from the NLRC4 inflammasome in macrophages. *Sci. Rep.* 8, 3788
18. Tixeira, R. *et al.* (2018) Gasdermin E Does Not Limit Apoptotic Cell Disassembly by Promoting Early Onset of Secondary Necrosis in Jurkat T Cells and THP-1 Monocytes. *Front. Immunol.* 9, 2842
19. Liu, Z. *et al.* (2019) Crystal Structures of the Full-Length Murine and Human Gasdermin D Reveal Mechanisms of Autoinhibition, Lipid Binding, and Oligomerization. *Immunity* DOI: 10.1016/J.IMMUNI.2019.04.017
20. Ruan, J. *et al.* (2018) Cryo-EM structure of the gasdermin A3 membrane pore. *Nature* 557, 62–67
21. Sborgi, L. *et al.* (2016) GSDMD membrane pore formation constitutes the mechanism of pyroptotic cell death. *EMBO J.* 35, 1766–78
22. Mulvihill, E. *et al.* (2018) Mechanism of membrane pore formation by human gasdermin-D. *EMBO J.* DOI: 10.15252/embj.201798321
23. Fraire, J.C. *et al.* (2020) Vapor nanobubble is the more reliable photothermal mechanism for inducing endosomal escape of siRNA without disturbing cell homeostasis. *J. Control. Release* 319, 262–275
24. Xiong, R. *et al.* (2016) Cytosolic Delivery of Nanolabels Prevents Their Asymmetric Inheritance and Enables Extended Quantitative in Vivo Cell Imaging. *Nano Lett.* 16, 5975–5986
25. Xiong, R. *et al.* (2014) Comparison of gold nanoparticle mediated photoporation: Vapor nanobubbles outperform direct heating for delivering macromolecules in live cells. *ACS Nano* 8, 6288–6296

26. Raes, L. *et al.* (2020) Intracellular Delivery of mRNA in Adherent and Suspension Cells by Vapor Nanobubble Photoporation. *Nano-Micro Lett.* 12, 1–17
27. Ramon, J. *et al.* (2021) Vapor Nanobubble-Mediated Photoporation Constitutes a Versatile Intracellular Delivery Technology. *Curr. Opin. Colloid Interface Sci.* 54, 101453
28. Liu, J. *et al.* (2018) Repeated photoporation with graphene quantum dots enables homogeneous labeling of live cells with extrinsic markers for fluorescence microscopy. *Light Sci. Appl.* 7, 2047–7538
29. Wayteck, L. *et al.* (2017) Comparing photoporation and nucleofection for delivery of small interfering RNA to cytotoxic T cells. *J. Control. Release* 267, 154–162
30. Lukianova-Hleb, E. *et al.* (2010) Plasmonic nanobubbles as transient vapor nanobubbles generated around plasmonic nanoparticles. *ACS Nano* 4, 2109–2123
31. Hodgkins, A. *et al.* (2015) WGE: a CRISPR database for genome engineering. *Bioinformatics* 31, 3078–3080
32. Brinkman, E.K. *et al.* (2014) Easy quantitative assessment of genome editing by sequence trace decomposition. *Nucleic Acids Res.* 42, e168–e168
33. De Groote, P. *et al.* (2016) Generation of a new Gateway-compatible inducible lentiviral vector platform allowing easy derivation of co-transduced cells. *Biotechniques* 60, 252–259
34. Hothorn, T. *et al.* Simultaneous inference in general parametric models. , *Biometrical Journal*, 50. Jun-(2008) , Biom J, 346–363
35. R Core Team (2020) , R: A language and environment for statistical computing. , *R Foundation for Statistical Computing*. [Online]. Available: https://www.r-project.org/. [Accessed: 10-Apr-2021]
36. Vercammen, D. *et al.* (1998) Inhibition of caspases increases the sensitivity of L929 cells to necrosis mediated by tumor necrosis factor. *J. Exp. Med.* 187, 1477–85
37. Wang, Y. *et al.* (2017) Chemotherapy drugs induce pyroptosis through caspase-3 cleavage of a gasdermin. *Nature* 547, 99–103
38. Lénárt, P. and Ellenberg, J. (2006) Monitoring the permeability of the nuclear envelope during the cell cycle. *Methods* 38, 17–24
39. Raes, L. *et al.* (2019) Gold Nanoparticle-Mediated Photoporation Enables Delivery of Macromolecules over a Wide Range of Molecular Weights in Human CD4+ T Cells. *Crystals* 9, 411
40. Galluzzi, L. and Kroemer, G. (2017) Secondary Necrosis: Accidental No More. *Trends in Cancer* 3, 1–2
41. Zhang, Z. *et al.* (2020) Gasdermin E suppresses tumour growth by activating anti-tumour immunity. *Nature* 579, 1–6
42. Evavold, C.L. *et al.* (2018) The Pore-Forming Protein Gasdermin D Regulates Interleukin-1 Secretion from Living Macrophages. *Immunity* 48, 35-44.e6
43. Heilig, R. *et al.* (2018) The Gasdermin-D pore acts as a conduit for IL-1β secretion in mice. *Eur. J. Immunol.* 48, 584–592
44. Zhou, B. and Abbott, D.W. (2021) Gasdermin E permits interleukin-1 beta release in distinct sublytic and pyroptotic phases. *Cell Rep.* 35, 108998
45. Kayagaki, N. *et al.* (2021) NINJ1 mediates plasma membrane rupture during lytic cell death. *Nature* DOI: 10.1038/s41586-021-03218-7
46. Xia, S. *et al.* (2021) Gasdermin D pore structure reveals preferential release of mature interleukin-1. *Nature* DOI: 10.1038/s41586-021-03478-3

Supplementary information supporting

Table S1. sgRNA sequences, PCR and sequencing primers used for *Gsdme* CRISPR-Cas9 gene editing.

Sequence	Forward Sequence (5'→3')	Reverse complement (5'→3')
Guide sequence	TCCCAATAGCCCCGCTCTTA	TAAGAGCGGGGCTATTGGGA
Primers	GCATTCAATACATGGTTTTTGG	TAATCACCCCTAGGCTCTGG

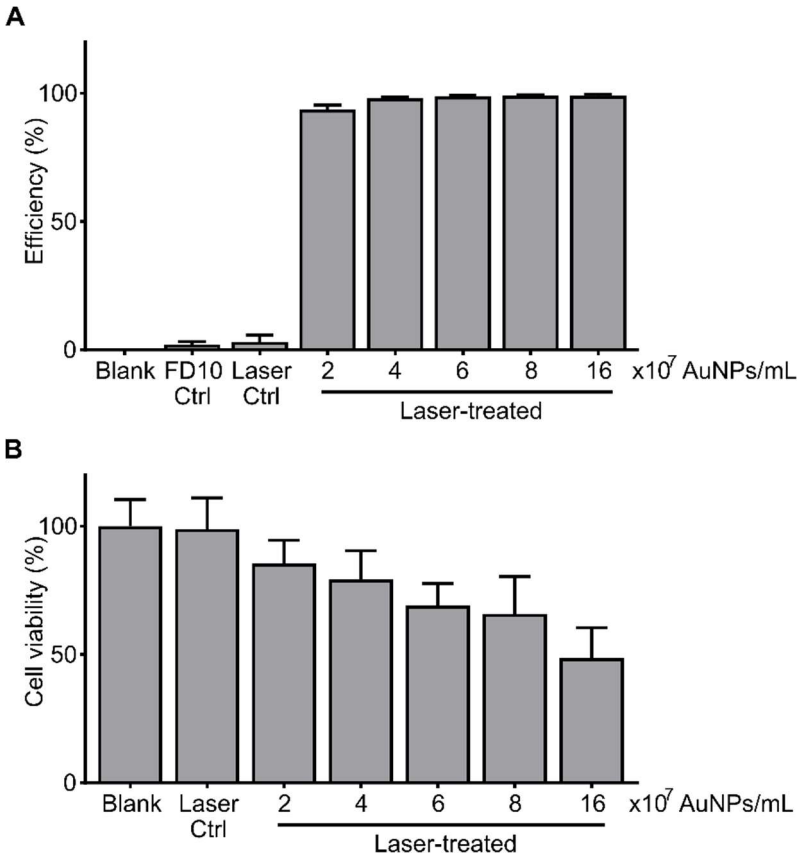

Figure S1. Optimalization of AuNP concentrations using a fixed laser pulse fluence of 1.6 J/cm² in L929sAhFas cells. (A) Delivery efficiency of FITC-labeled dextran 10 kDa (FD10) in function of increasing AuNP concentrations. (B) Cell viability in function of increasing AuNP concentrations.

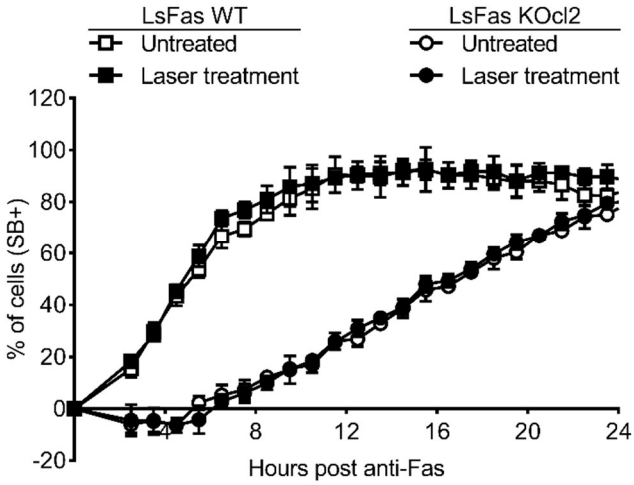

Figure S2. Cell death kinetics, as determined by the SYTOX Blue (SB) staining, in untreated and laser-treated cells, both in L929sAh wildtype (WT) as L929 GSDME knockout (KOcl2) cells.

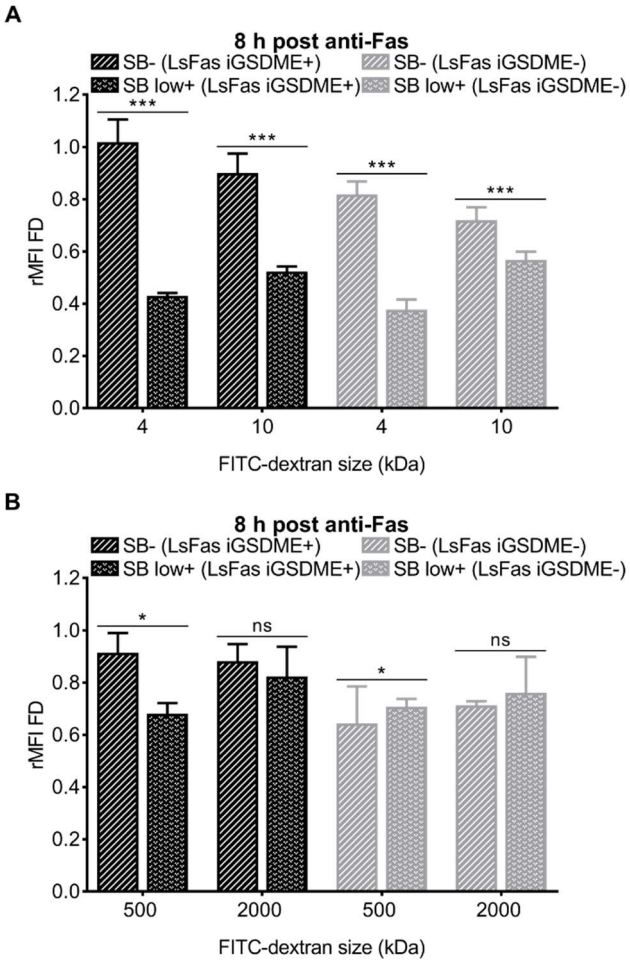

Figure S3. Comparison of the mean fluorescent intensity relative to the untreated SB- population (rMFI) between the SB- and SB low+ population upon 8h of anti-Fas treatment. (A) FITC-labeled dextran 4 kDa (FD4) and 10 kDa (FD10). (B) FITC-labeled dextran 500 kDa (FD500) and 2000 kDa (FD2000).

Chapter 7

Live cell visualization of GSDME during apoptosis-driven secondary necrosis

RESEARCH ARTICLE

Work in progress

Elke De Schutter[1,2,3], Inge Bruggeman[1,2], Eef Parthoens[2,4], Savvas Savvides[1,5], Franck B. Riquet[1,2,6] and Peter Vandenabeele[1,2]

[1] VIB Center for Inflammation Research, 9052 Ghent, Belgium

[2] Department of Biomedical Molecular Biology, Ghent University, 9052 Ghent, Belgium

[3] Center of Medical Genetics, University of Antwerp and Antwerp University Hospital, Prins Boudewijnlaan 43/6, BE-2650 Edegem, Antwerp Belgium.

[4] VIB Bioimaging Core, VIB, 9052 Ghent, Belgium

[5] Department of Biochemistry and Microbiology, Ghent University, 9052 Ghent, Belgium

[6] Université de Lille, Lille, France

Abstract

The N-terminus of gasdermin E (N-GSDME) has recently been shown to drive apoptosis-driven secondary necrosis and caspase-3/granzyme B-mediated pyroptosis. Given the functional and sequence similarity between the members of the gasdermin (GSDM) protein family, they are all proposed to induce cell death *via* the formation of membrane permeability pores, although this is only intensively studied for murine GSDMA3 and GSDMD. Currently, the study of GSDME pore formation has been complicated by both the rapid induction of cell death by N-GSDME and the impossibility to tag GSDME N-terminally. In this chapter, we strategically placed fluorescent protein tags within GSDME to generate a new tool to study GSDME and to facilitate live cell imaging of N-GSDME and C-GSDME before, during and after cleavage by caspase-3 or granzyme B. We validated the functionality of the GSDME fusion proteins by using our own functional assay based on SYTOX blue and 7-aminoactinomycin D staining. Visualization of GSDME internally tagged with mNeonGreen during apoptosis-driven secondary necrosis confirmed plasma membrane targeting and mitochondrial targeting of N-GSDME.

7.1 INTRODUCTION

Recently, several members of the gasdermin (GSDM) protein family came to the attention as mediators of different forms of regulated necrosis [1–5]. GSDM proteins are produced as precursor proteins consisting of a cytotoxic N-terminal domain (N-GSDM) and an inhibitory C-terminal globular domain (C-GSDM), separated by a variable hinge region [6–8]. Similar as described for bacterial pore forming toxins [9,10], GSDMs require proteolytic activation within the hinge region to release the cytotoxic p30 fragment. GSDMD, the best studied GSDM protein, is shown to be a substrate of the inflammatory caspases -1 and -4/5 that are activated during pyroptosis by canonical and non-canonical inflammasomes [2,3,7,11,12]. In contrast, GSDME is proteolytically activated by caspase-3 and granzyme B, resulting in apoptosis-driven secondary necrosis [1] or direct caspase-3/granzyme B mediated pyroptosis [5,13–15]. The cytotoxic function of GSDM proteins has recently been attributed to their capacity to form pores resulting in plasma membrane permeabilization. The course of structural change of N-GSDM domains following cleavage, lipid membrane binding, oligomerization and eventually pore-formation has already been intensively studied for GSDMA3 and –D [7,8,16–18] but still needs to be elucidated for GSDME. However, the rapid induction of cell death by N-GSDME and the impossibility to tag GSDME N-terminally, complicates the study of GSDME pore formation [1,19]. Although the same hurdles are true for GSDMD, these limitations have recently been overcome by adding a fluorescent tag internally in the GSDMD protein [20]. In this study we applied a similar strategy to fluorescently tag GSDME right before its caspase-3 cleavage site and validated the functionality of the tagged GSDME molecules using our own functional assay based on SB and 7-AAD staining (chapter 5). Additionally, we successfully added a

fluorescent protein tag after the caspase-3 cleavage site. Visualization of GSDME-mNeonGreen-mScarlet (GSDME-mNe-mSc) and GSDME-mNeonGreen (GSDME-mNe) during secondary necrosis allowed the direct monitoring of both N-GSDME and C-GSDME during apoptosis driven secondary necrosis before, during, and after cleavage. By doing so using live cell imaging, we were able to confirm plasma membrane targeting and mitochondrial targeting of N-GSDME during apoptosis-driven secondary necrosis. Altogether, our internally tagged versions of GSDME provide a new potent tool to investigate GSDME and GSDME-mediated cell death.

7.2 MATERIALS AND METHODS

7.2.1 Cell Culture

L929sAhFas cells and derivatives were cultured in Dulbecco's Modified Eagle Medium supplemented with 10% of Fetal Bovine Serum (v/v), L-glutamine (2 mM) and sodium pyruvate (400 mM). Cells were cultured in 37 °C in a humidified atmosphere containing 5% CO_2 and were regularly tested against mycoplasma contamination.

7.2.2 Flow cytometry measurements

L929sAhFas derivatives were seeded in 24-well suspension plates (100 000 cells/well) in the presence or absence of doxycycline (Sigma-Aldrich, 1 µg/ml) and stimulated the next day with 125 ng/ml anti-Fas (clone CH11, Upstate). One hour before each time point, fluorescent probes were added to proper wells: 1.25 µM of SYTOX Blue nucleic acid stain and 1.25 µM of 7-AAD (Molecular Probes). Samples were run on BD Fortessa or BD LSR and data was analysed using FlowJo 10.7.1.

7.2.3 Generation of stable GSDME inducible L929sAhFas cells lines

The L929sAhFas iGSDME, iGSDME[FLAG], iGSDME[mNe] and iGSDME[mNe-mSc] cell lines were obtained by transduction of L929sAhFas *Gsdme* knockout cells with a pDG2-mGSDME-blast plasmid. This is a tetracycline-inducible derivative of pLenti6 (Life Technologies) containing a blasticidin selection marker, in which the coding sequence of murine GSDME, GSDME-FLAG, GSDME-mNeonGreen or GSDME-mNeonGreen-mScarlet was cloned. Upon lentiviral transduction, the stably transduced cells were selected with 5-10 µg/ml blasticidin.

7.2.4 Live cell imaging

Cells were seeded on 8-well dishes ibiTreat (Ibidi) to reach 60-80% confluence at the time of imaging and pretreated with doxycycline (Sigma-Aldrich, 1 µg/ml) when necessary. Cells were incubated in a chamber with a 5% CO_2 at 37 °C throughout each experiment. Confocal images to confirm the expression of GSDME fusion proteins were captured with an observer Z.1 spinning disk microscope (Zeiss) equipped with a Yokogawa disk CSU-X1

making use of a 20X/0.8 M27 Plan-Apochromat objective. High resolution images were captured with a LSM880 airyscan confocal laser scanning microscope (Zeiss) using a 40X/1.3 Oil DIC UV-IR M27 Plan-Apochromat objective. Cell were treated for 4 or 6 hours with anti-Fas (125 ng/ml, clone CH11, Upstate). 1 hour before imaging, dyes were added to the cells: 2.5 µM of SYTOX Blue, 100 nM MitoTracker Red CM-H2Xros or 50 nM Lysotracker Red DND-99 (Molecular Probes). 25 nM Lipilight EX 640 nm/FI 681 (idylle) was added to the cells 10 minutes before imaging.

7.2.5 Western Blotting

After treatment with 500 ng/ml or 250 ng/ml anti-Fas ((clone CH11, Upstate) and/or 1 µg/ml doxycycline (Sigma Aldrich), L929sAhFas cells and derivatives were harvested at specified time intervals and washed twice in ice-cold PBS. Cells were lysed using ice-cold RIPA lysis buffer (50 mM Tris-HCl, pH 7.5; 150 mM NaCl; 1 mM EDTA; 0.5% sodium deoxycholate; 1% Triton X-100 and 0.1% SDS) freshly supplemented with EDTA-free Complete protease inhibitor cocktail tablets and phosphatase inhibitor cocktail tablets (Roche Diagnostics Belgium N.V.). Extracted proteins were separated on 12% SDS polyacrylamide gels and transferred onto nitrocellulose membranes (Amersham Bioscience). Membranes were blocked using TBS with 0.05% Tween20 (TBS-T) containing 5% non-fat dry milk (Biorad) followed by anti-GSDME (ab215191, abcam) or anti-actin (69100, MP Biomedicals) incubation. After incubation with the HRP-linked donkey anti-rabbit IgG or HRP-linked sheep anti-mouse (Amersham Biosciences), blots were revealed using Western Lightning Plus-ECL (PerkinElmer).

7.2.6 Statistical analysis

Results are presented as means ± SD. Statistical analyses were performed using PRISM 8 software (GraphPad). Statistical analysis of 7-AAD/SB- cells was performed using an one-way ANOVA test followed by a Šidák's multiple comparisons test. Statistical analysis of SB+ cells was performed using a two-way ANOVA with the Geisser-Greenhouse correction (matched values were stacked into a subcolumn). Alpha was set at 0.05. Significance between samples is indicated as follows: *p <0.05; **p <0.01; ***p <0.001, ****p <0.0001.

7.3 RESULTS

7.3.1 Design and validation of GSDME with an internal small FLAG tag

To study GSDME during apoptosis-driven secondary necrosis, we previously generated *Gsdme* knockout (KO) L929sAhFas cells and a GSDME inducible L929sAhFas cell line (L929sAhFas iGSDME) (chapter 5). In the latter, murine GSDME expression is reconstituted upon doxycycline treatment and apoptosis and caspase-3 activation is induced upon anti-Fas treatment. Based on the analysis of progressive C-terminal deletion mutants, Rogers *et al.* identified residues 1-234 as the minimal sequence of GSDME necessary to induce necrosis. As GSDME is cleaved by caspase-3 at D270 [1,5], residues 235-270 provide the best chance to insert a tag without disrupting the cytotoxic function of the GSDME N-terminal domain. The possibility to generate a functional gasdermin protein with an internal fluorescent tag has been previously reported for murine GSDMD [20]. In this case a mNeonGreen tag was inserted in the flexible linker region after residue 248, before the caspase-1, -11 cleavage site D276, and this insertion did not disrupt the pyroptosis inducing function of GSDMD. Given the structural similarities between GSDM proteins, we decided to insert a FLAG tag after residue 246 of murine GSDME, corresponding to the insertion site used before for GSDMD [20]. Similar as reported in chapter 5, we stably reconstituted L929sAhFas *Gsdme* KO cells with a GSDME-FLAG construct under a doxycycline dependent promoter (Figure 1A), resulting in the inducible cell line L929sAhFas iGSDME[FLAG]. Same as for L929sAhFas iGSDME, expression of GSDME-FLAG is reconstituted upon doxycycline treatment (Figure 1B). Subsequent treatment of these cells with anti-Fas promoted the generation of a ~35 kDa fragment, suggesting that insertion of the FLAG tag did not prevent proteolytic cleavage by caspase-3 (Figure 1C). To assess whether GSDME-FLAG could recapitulate wildtype (WT) GSDME behavior, we monitored the uptake of 7-aminoactinomycin D (7-AAD) and SYTOX blue (SB) in L929sAhFas iGSDME and L929sAhFas iGSDME[FLAG] upon anti-Fas treatment as previously shown in chapter 5 (Figure 1D). Figure 1E shows that doxycycline treatment resulting in the expression of WT GSDME or GSDME-FLAG accelerated the uptake of SB to the same extent in L929sAhFas upon anti-Fas treatment. Similarly, both the expression of WT GSDME or GSDME-FLAG limited the accumulation of 7-AAD single positive cells compared to their non-induced counterparts, suggesting that GSDME-FLAG is as functional as WT GSDME (Figure 1E). Altogether, these results suggest that insertion of a tag after residue 246 in murine GSDME minimally disrupts GSDME-function.

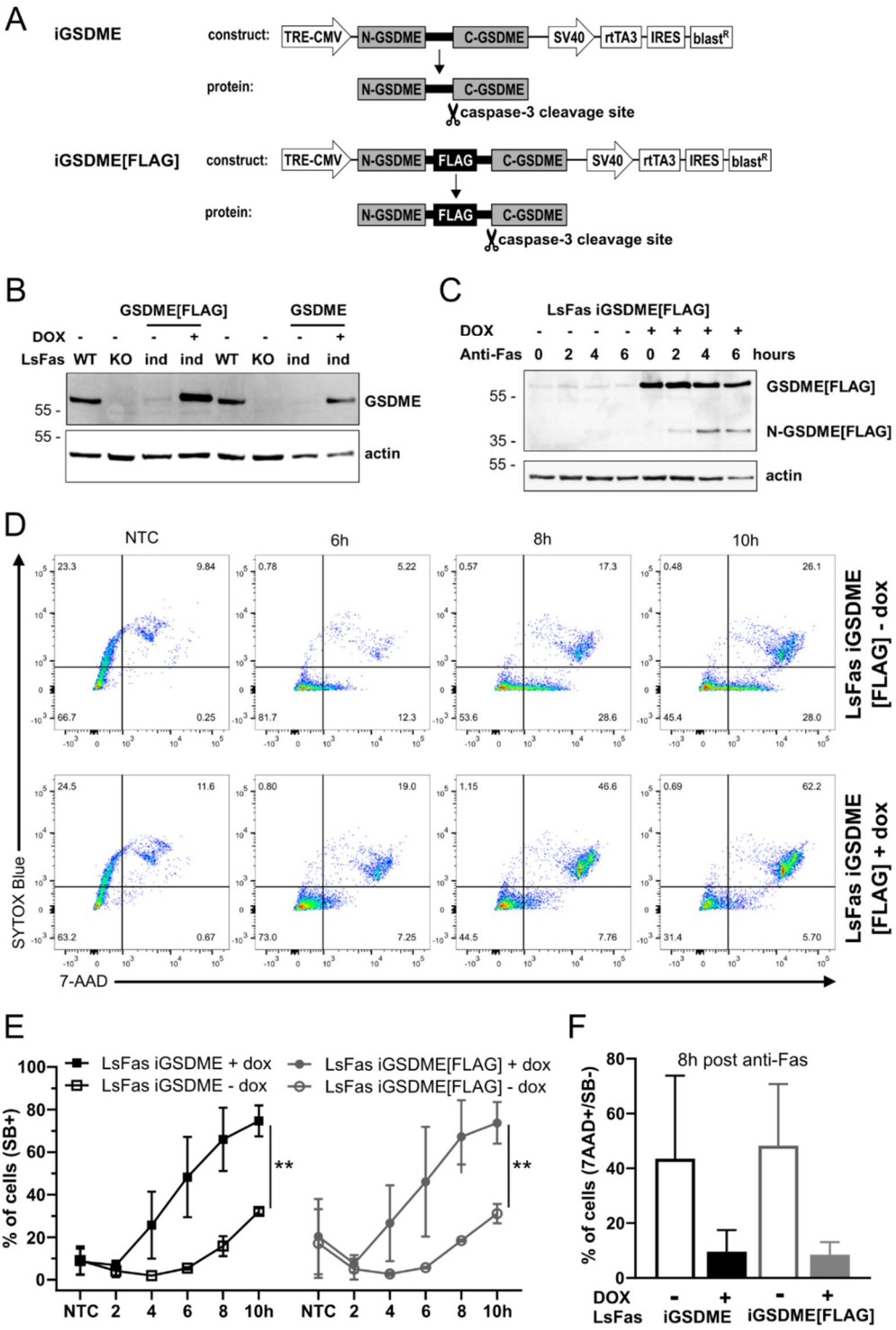

Figure 1. Design and validation of L929sAhFas iGSDME[FLAG]. (A) Design of the WT and GSDME-FLAG lentiviral constructs used to generate the L929sAhFas iGSDME and L929sAhFas iGSDME[FLAG] cell lines, respectively. **(B)** Induction of GSDME(-FLAG) expression upon doxycycline treatment of L929sAhFas iGSDME and L929sAhFas iGSDME[FLAG]. **(C)** Cleavage of GSDME-FLAG in L929sAhFas iGSDME[FLAG] upon apopotis induction by anti-Fas treatment. **(D-F)** Flow cytometry analysis monitoring the uptake of 7-AAD and SB. **(D)** Representative Flow cytometry plots showing the uptake of SB and 7-AAD in L929sAhFas iGSDME and L929sAhFas iGSDME[FLAG] upon anti-Fas treatment, with or without doxycycline pretreatment. **(E)** Impact of GSDME(-FLAG) expression on cell death kinetics measured by SB uptake in L929sAhFas inducible cell lines upon anti-Fas treatment. **(F)** Impact of GSDME(-FLAG) expression on the amount of 7-AAD single positive (7-AAD+/SB-) cells. Dox, doxycycline; LsFas, L929sAhFas.

7.3.2 Design and validation of GSDME with internal fluorescent protein tags

Given that insertion of a FLAG tag internally in GSDME does not affect the functionality of GSDME, we next attempted to insert a much larger mNeonGreen fluorescent tag at the same insertion site, allowing the visualization of the N-terminal domain of GSDME before, during, and after caspase-3 cleavage (Figure 2A). In order to be able to simultaneously visualize C-GSDME, we also attempted to insert a mScarlet fluorescent tag after residue 272 (Figure 2B). Before and after each sequence coding for the fluorescent tags, we provided sequences coding for 6 glycine residues when designing the lentiviral constructs to allow more flexibility of the fluorescent tags in the fusion proteins. Finally, we used these constructs to generate the doxycycline inducible cell lines L929sAhFas iGSDME[mNe] and L929sAhFas iGSDME[mNe-mSc]. Treating these cell lines with doxycycline induced the expression of the fusion proteins GSDME-mNe and GSDME-mNe-mSc and subsequent treatment with anti-Fas resulted in the generation of a ~55 kDa fragment (Figure 2B), corresponding to the size of N-GSDME with an internal mNeonGreen tag after caspase-3 cleavage. The latter suggest that insertion of fluorescent tags around the caspase-3 cleavage site did not prevent proteolytic activation. Expression and functionality of the fluorescent tags in our cell lines was confirmed by flow cytometry (Figure 2C) and live cell imaging (Figure 2D). To assess the functionality of the GSDME protein tagged with fluorescent proteins, we monitored the uptake of SB during apoptosis induction by anti-Fas in both L929sAhFas iGSDME[mNe] and L929sAhFas iGSDME[mNe-mSc]. Both doxycycline induced expression of GSDME-mNe and GSDME-mNe-mSc accelerated the uptake of SB upon anti-Fas treatment compared to counterparts not treated with doxycycline. Altogether these results show that the fluorescent protein tags are functional and that their insertion in GSDME does not disrupt the cytotoxic function of N-GSDME.

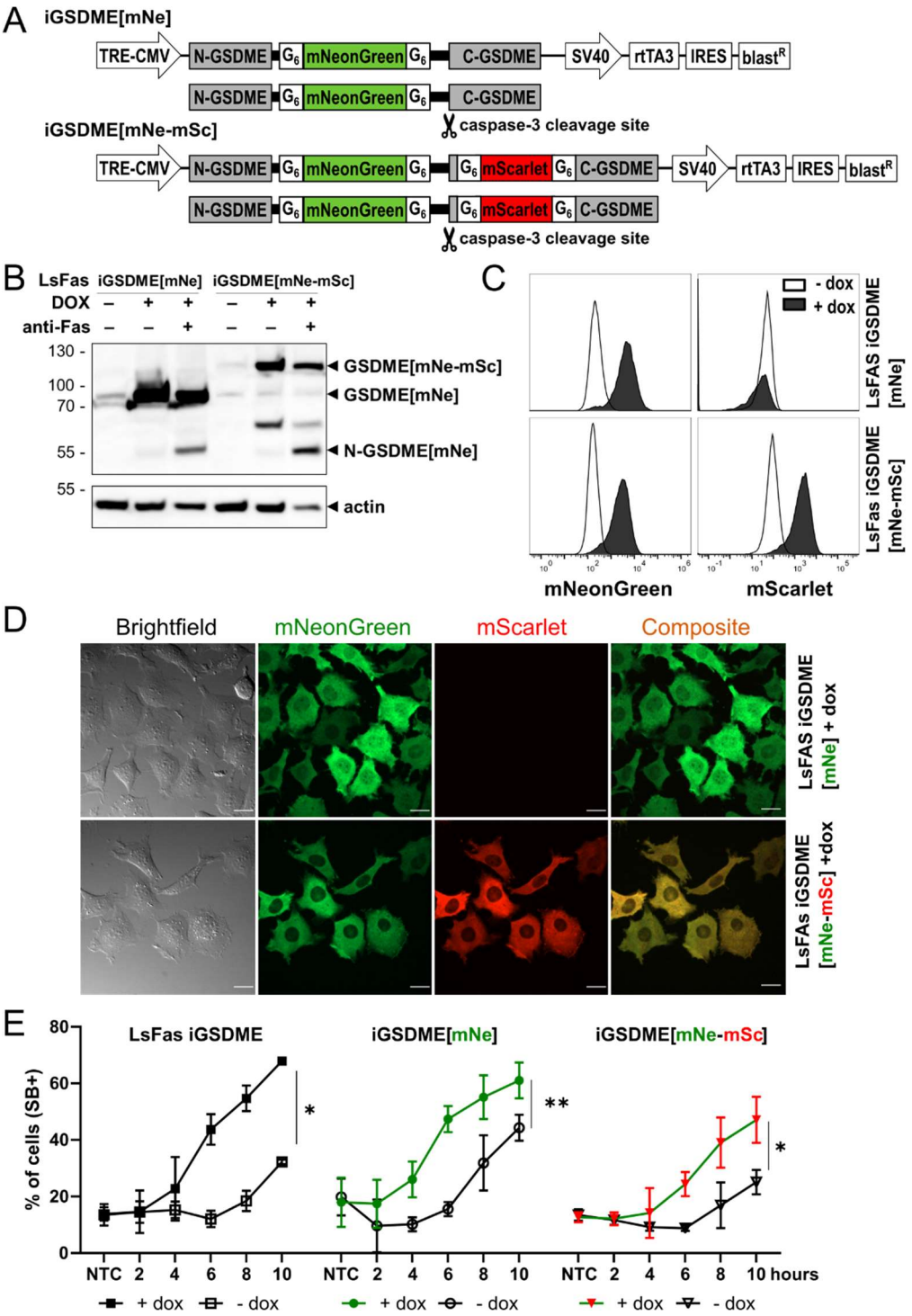

Figure 2. Design and validation of L929sAhFas iGSDME[mNe] and L929sAhFas iGSDME[mNe-mSc] (A) Design of lentiviral constructs used to generate the L929sAhFas iGSDME[mNe] and L929sAhFas iGSDME[mNe-mSc] cell lines, respectively. **(B)** Induction of GSDME-mNe and GSDME-mNe-mSc expression upon doxycycline treatment of L929sAhFas iGSDME[mNe] and L929sAhFas iGSDME[mNe-mSc]. Subsequent anti-Fas treatment results in cleavage of GSDME-mNe and GSDME-mNe-mSc to the N-GSDME-mNe fragment. **(C)** Flow cytometry analysis measuring mNeonGreen and mScarlet fluorescence in L929sAhFas iGSDME[mNe] and L929sAhFas iGSDME[mNe-mSc] upon doxycycline treatment. **(D)** Live cell confocal images of L929sAhFas iGSDME[mNe] and L929sAhFas iGSDME[mNe-mSc] upon doxycycline treatment. Scale bar = 20 µm. **(E)** Impact of GSDME-mNe(-mSc) expression on cell death kinetics measured by SB uptake using flow cytometry in L929sahFas inducible cell lines upon anti-Fas treatment. Dox, doxycycline; LsFas, L929sAhFas; mNe, mNeonGreen; mSc, mScarlet.

7.3.3 Visualizing GSDME during apoptosis-driven secondary necrosis

Our L929sAhFas cellular systems with internal fluorescent tags provide new tools to visualize GSDME activity during apoptosis-driven secondary necrosis induced by anti-Fas treatment. As apoptotic and secondary necrotic cells are easily washed away, we decided to visualize GSDME *via* live cell imaging. We imaged L929sAhFas reconstituted with GSDME-mNe-mSc expression after staining with SB as cell death marker and Lipilight, a Membright probe designed to stain cell plasma membranes since GSDME is a pore forming protein. As expected, untreated cells show colocalization of mNeonGreen and mScarlet diffusely spread in the cytosol (Figure 3A), indicating that the GSDME fusion protein was present in its full, inactive and auto-inhibitory form. In contrast, mNeonGreen and mScarlet signals were visible as separate dots in apoptotic (no SB staining) (Figure 3B) and secondary necrotic L929sAhFas cells (SB staining) (Figure 3B-D), suggesting proteolytic cleavage of GSDME after caspase-3 activation by anti-Fas treatment. Interestingly, next to small mNeonGreen punctae (~ Ø 0.6 µm) present at the plasma membrane upon anti-Fas treatment (Figure 3C-D), big mNeonGreen dots (~ Ø 1 µm) were present in the cytosol that are reminiscent of membrane-bound organelles (Figure 3B-D). These dots were already present in non-permeabilized apoptotic cells (Figure 3B), suggesting that N-GSDME might target cellular organelles prior to the plasma membrane. Similarly, in apoptotic and secondary necrotic cells mScarlet was visible as distinct dots, suggesting that C-GSDME might target cellular organelles as well. However, these dots were less uniform as compared with the mNeonGreen signal.

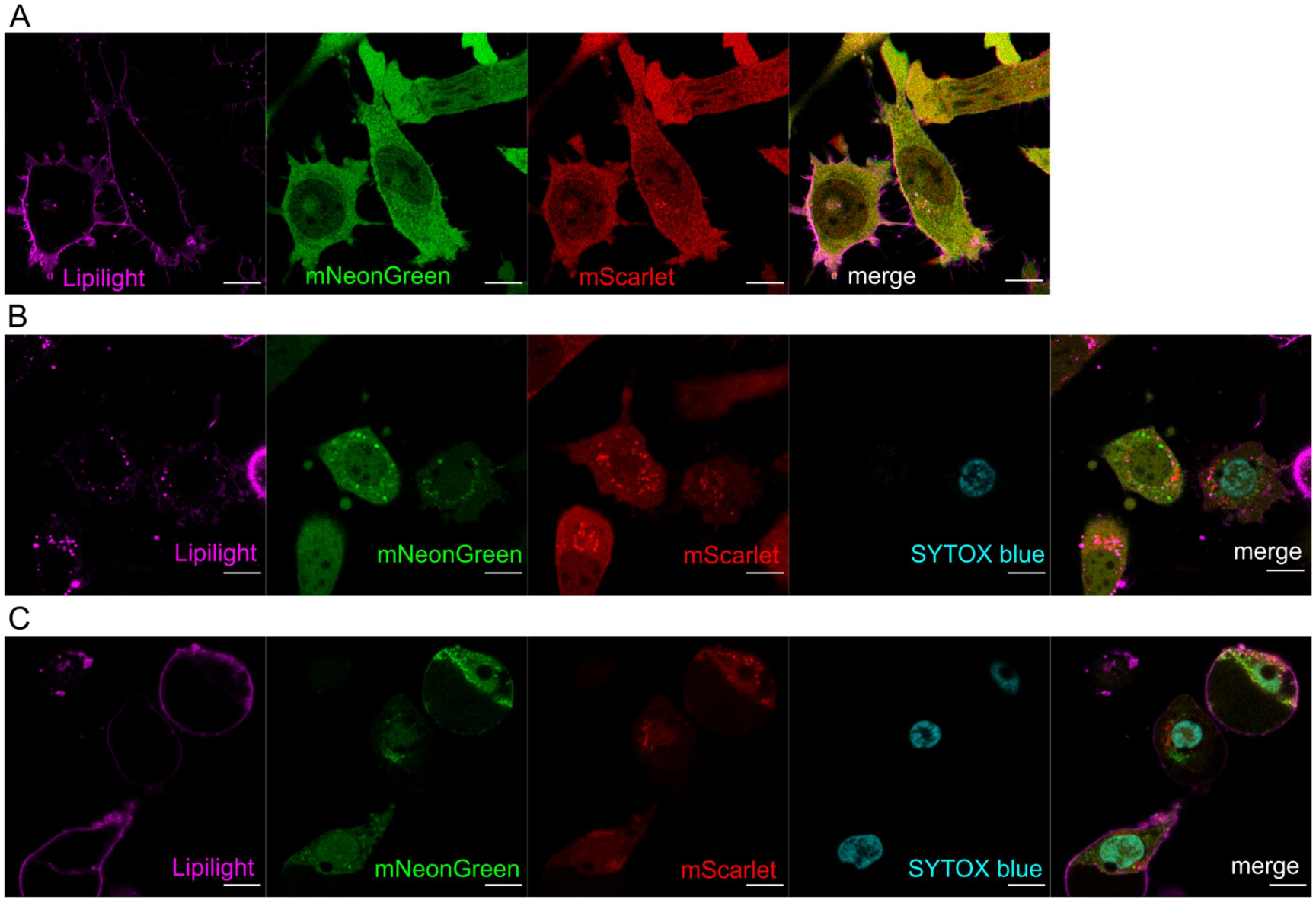
A
Lipilight
mNeonGreen
mScarlet
merge
B
Lipilight
mNeonGreen
mScarlet
SYTOX blue
merge
C
Lipilight
mNeonGreen
mScarlet
SYTOX blue
merge

D

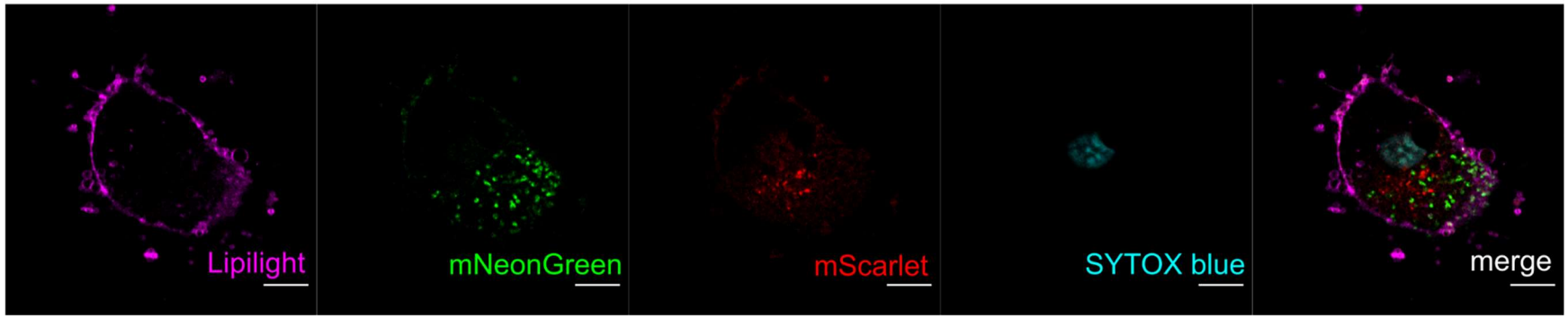

Figure 3. Visualization of doxycycline-induced GSDME-mNe-mSc expression in L929sAhFas iGSDME[mNe-mSc] cells *via* live cell imaging. Plasma membrane staining using Lipilight is shown in pink. mNeonGreen signal is shown in green, mScarlet in red. The nuclei of dead cells were stained with the cell impermeant nuclear dye SYTOX blue and are shown in blue. **(A)** High resolution confocal images of L929sAhFas iGSDME[mNe-mSc] after doxycycline pre-treatment. **(B-D)** High resolution confocal images of L929 iGSDME[mNe-mSc] cells pre-treated with doxycycline during apoptosis-driven secondary necrosis induced by 4-6h of anti-Fas treatment. Scale bar = 10 µm.

7.3.4 GSDME targets mitochondria

Our observations suggesting colocalization of N-GSDME with cellular organelles are not surprising as N-GSDMA3, -D and -E were recently shown to target mitochondria [23,24]. To assess whether GSDME colocalizes with mitochondria in our cellular system, we imaged L929sAhFas reconstituted with GSDME-mNe expression after staining with Lipilight and Mitotracker Red probes. The latter specifically stains active mitochondria. Like GSDME-mNe-mSc, GSDME-mNe was diffusely spread in the cytosol prior to apoptosis induction (Figure 4A). In addition, mitochondria were arranged as tubular shapes as is shown by Mitotracker Red staining (Figure 4A), indicating healthy cells [25–27]. In contrast, upon anti-Fas treatment, cells demonstrated numerous dots stained by Mitotracker (Figure B-D), suggesting disintegration of the mitochondrial network. Interestingly, mitochondrial fragmentation was already visible prior to mNeonGreen dot formation in apoptotic cells (Figure 4B). Although Mitotracker signal decreased in L929sAhFas iGSDME[mNe] upon anti-Fas treatment, mNeonGreen dots exhibited similar shapes and partially overlapped with Mitotracker signal (Figure 4C-D), indicating colocalisation of N-GSDME with mitochondria.

Next to mitochondria, also lysosomes are degraded during apoptosis [28–30]. Therefore, we wanted to assess whether N-GSDME-mNe might colocalize with Lysotracker Red as well during apoptosis-driven secondary necrosis. In normal conditions, lysosomes are present as numerous small dots in the cell as shown by Lysotracker Red (Figure 5A). However, Lysotracker Red signal decreased rapidly upon anti-Fas treatment, making it difficult to assess colocalization (Figure 5B-E). Although clearly less numerous, lysosomes were still visible in apoptotic cells (Figure 5B-C) and necrotic (Figure 5D-E) L929 iGSDME[mNe] cells. However, no clear colocalization could be observed.

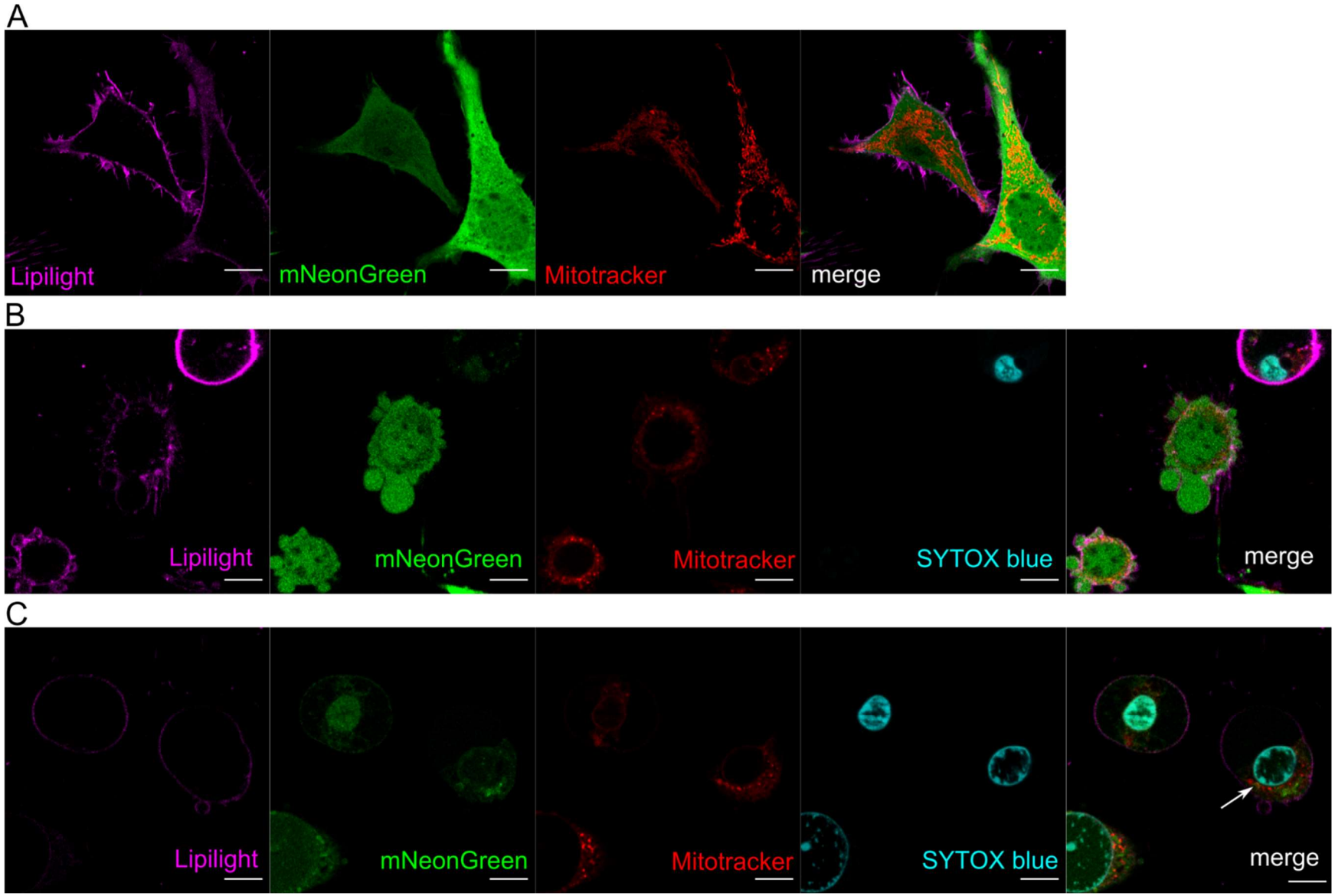
A
Lipilight
mNeonGreen
Mitotracker
merge
B
Lipilight
mNeonGreen
Mitotracker
SYTOX blue
merge
C
Lipilight
mNeonGreen
Mitotracker
SYTOX blue
merge

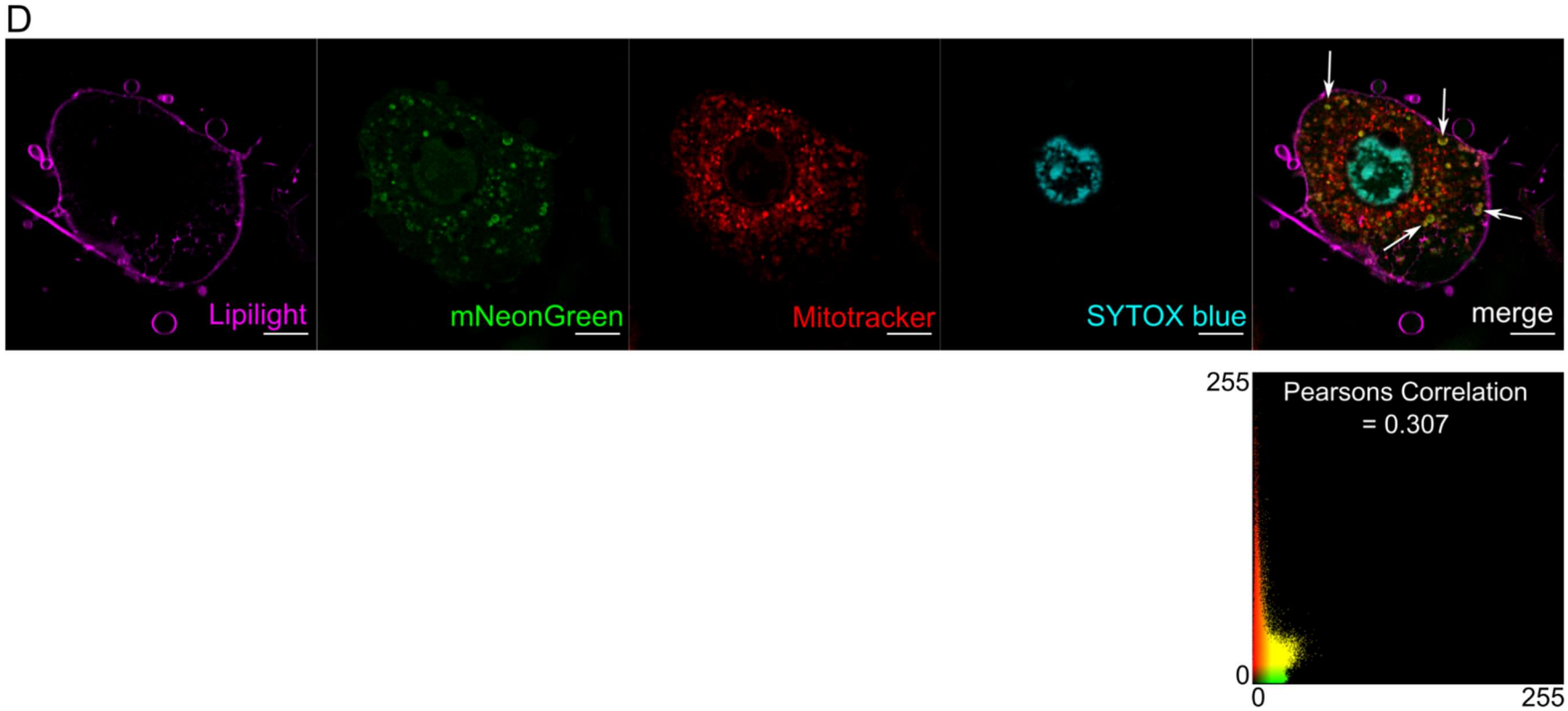

Figure 4. Visualization of doxycycline-induced GSDME-mNe expression and mitochondria in L929sAhFas iGSDME[mNe] cells *via* live cell imaging. Plasma membrane staining using Lipilight is shown in pink. mNeonGreen signal is shown in green. Mitochondria are stained with Mitotracker Red and are shown in red. The nuclei of dead cells were stained with the cell impermeant nuclear dye SYTOX blue and are shown in blue. **(A)** High resolution confocal images of L929sAhFas iGSDME[mNe] after doxycycline pre-treatment. **(B-D)** High resolution confocal images of L929 iGSDME[mNe-mSc] cells pre-treated with doxycycline during apoptosis-driven secondary necrosis induced by 4h of anti-Fas treatment. Colocalization between mNeonGreen and Mitotracker Red is indicated by white arrows **(C, D)** and a cytofluorogram showing the distribution of green and red pixels from the cell shown in **(D)**. Scale bar = 10 µm.

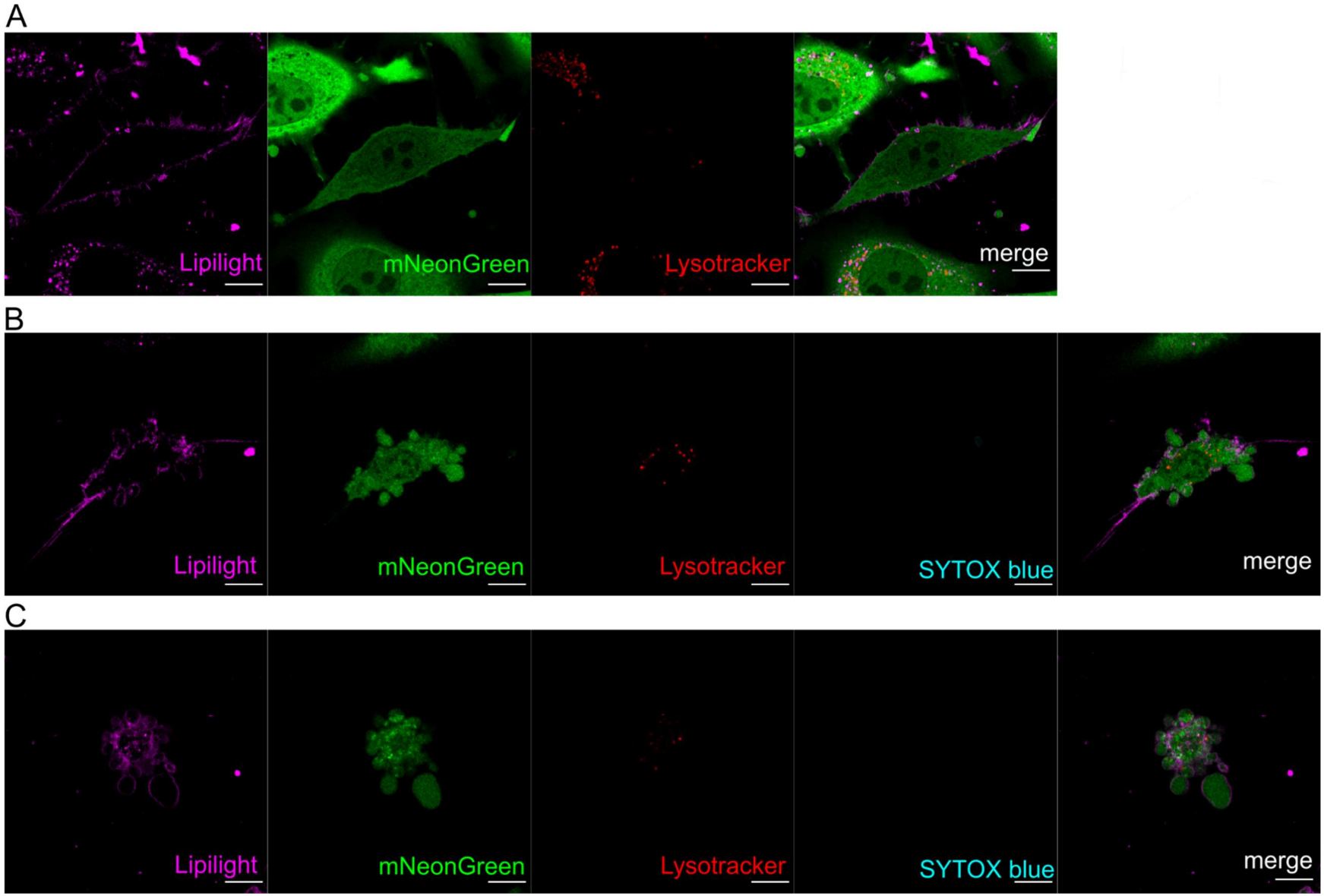
A
Lipilight
mNeonGreen
Lysotracker
merge
B
Lipilight
mNeonGreen
Lysotracker
SYTOX blue
merge
C
Lipilight
mNeonGreen
Lysotracker
SYTOX blue
merge

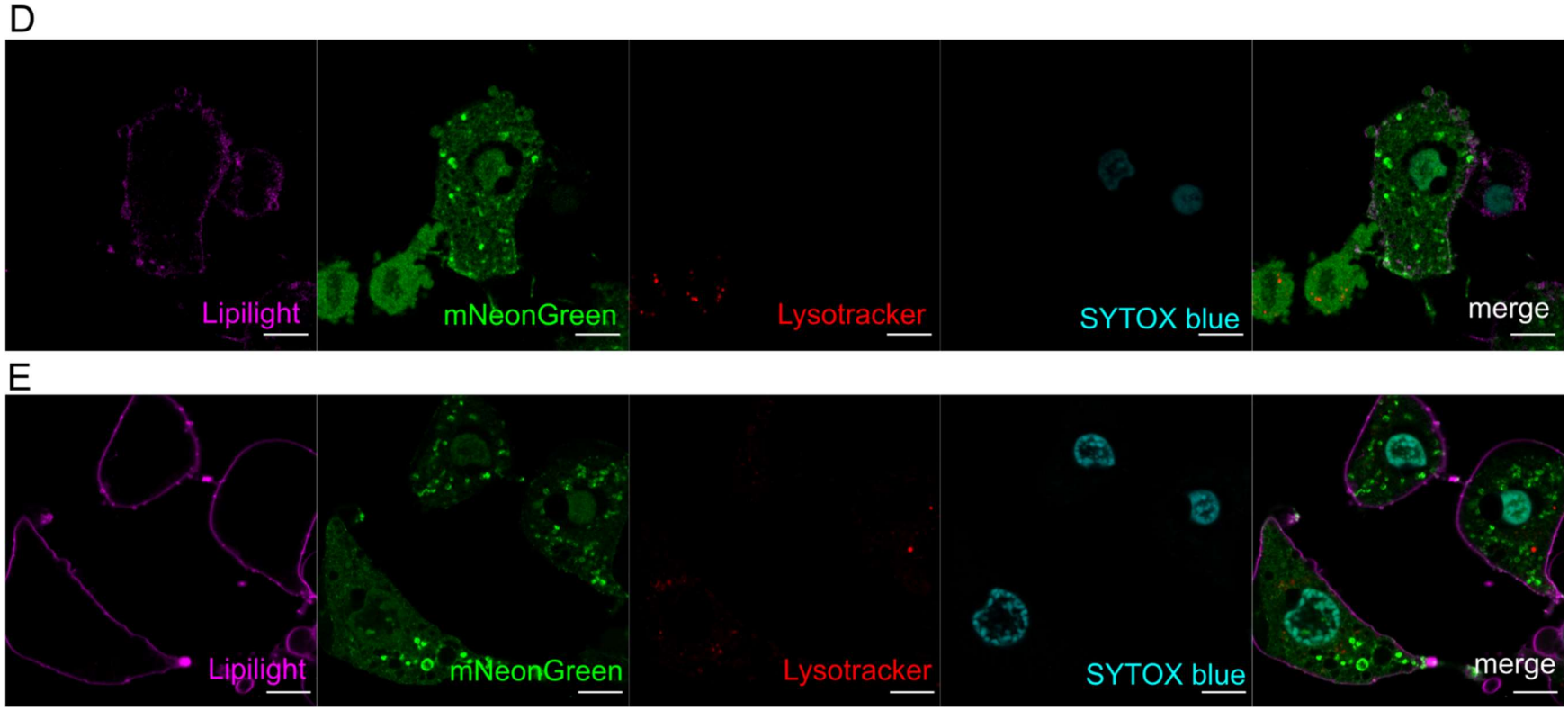

Figure 5. Visualization of doxycycline-induced GSDME-mNe expression and lysosomes in L929sAhFas iGSDME[mNe] cells *via* live cell imaging. Plasma membrane staining using Lipilight is shown in pink. mNeonGreen signal is shown in green. Lysosomes are stained with Lysotracker Red and are shown in red. The nuclei of dead cells were stained with the cell impermeant nuclear dye SYTOX blue and are shown in blue. **(A)** Confocal images of L929sAhFas iGSDME[mNe] after doxycycline pre-treatment. **(B-E)** Confocal images of L929 iGSDME[mNe-mSc] cells pre-treated with doxycycline during apoptosis-driven secondary necrosis induced by 4-6h of anti-Fas treatment. Scale bar = 10 µm.

7.4 DISCUSSION

Several members of the GSDM protein family were recently shown to be implicated in different forms of regulated necrosis after proteolytic cleavage by caspases and granzymes [1–5,31]. Visualization of GSDM proteins after caspase or granzyme activation in relevant cell types would facilitate the investigation of their molecular function. However, the potent killing activity of N-GSDM proteins hampers visualization and clear assessment of its subcellular localization [1,20,32]. An extra hurdle in the study of GSDMs has been the disruption of N-GSDM's cytotoxic activity when it is N-terminally tagged [19,33], limiting GSDM visualization to irrelevant cell types after transient transfection of C-terminally tagged N-GSDM constructs. Recently, these problems have been overcome in the case of GSDMD. Rathkey *et al.* successfully placed a fluorescent tag internally in the GSDMD protein without disrupting the cytotoxic function of N-GSDMD [20]. In this study we fluorescently tagged GSDME with a mNeonGreen tag right before its caspase-3/granzyme B cleavage site and additionally added a mScarlet protein tag after the caspase-3/granzyme B cleavage site. Using our own functional assay based on SB and 7-AAD staining (chapter 5) we confirmed the functionality of the tagged GSDME molecules. Visualization of GSDME-mNe-mSc and GSDME-mNe during secondary necrosis allowed the direct monitoring of both N-GSDME and C-GSDME after caspase-3 activation. In secondary necrotic L929sAhFas cells, N-GSDME was present at the plasma membrane which is expected from a pore forming protein and which is consistent with the localization of transiently transfected N-GSDME in HeLa and 293T cells [1,23]. In addition, we observed both N-GSDME and C-GSDME as separate dots in the cytosol both in apoptotic and secondary necrotic L929sAhFas cells. As these dots were considerably larger than N-GSDME punctae at the plasma membrane, it is not likely that these represent pre-pores that are already oligomerized but still need to insert in the plasma membrane. Instead, they resembled cell organelle structures. Recently it was shown that N-GSDME targets mitochondria facilitating cyt c release and creating a positive feedback loop that expedites apoptosis [23]. Mitochondrial network disintegration has always been perceived as an early apoptotic event. We observed an overlap between N-GSDME and mitochondria in secondary necrotic but remarkable not in apoptotic L929sAhFas cells. Moreover, mitochondrial network already disintegrated in L929sAhFas cells upon anti-Fas treatment before N-GSDME dots were visible, questioning the driving force of N-GSDME in mitochondrial permeabilization. However, although MitoTracker probes are membrane potential-insensitive dyes, mitochondrial disintegration in L929sAhFas cells was accompanied by a reduced Mitotracker Red signal, complicating correct analysis.

Next to mitochondria (GSDMA,-D,-E), GSDM proteins were shown to target nuclear envelope membranes (GSDMD), azurophylic granules (GSDMD) or peroxisomes (PJVK) [34,35], suggesting that GSDMs can target both plasma membranes and cellular organelle membranes. Similar to mitochondria, lysosomes are permeabilized during apoptosis

thereby releasing lysosomal proteases in the cytosol expediting apoptosis [28,30]. Moreover, lysosomes and mitochondria share similar permeabilization mechanisms such as the involvement of ANT-like proteins and Bax [29]. Therefore, we wanted to assess whether GSDME would target lysosomes as well during apoptosis-driven secondary necrosis. However, the amount of lysosomes was limited in apoptotic and secondary necrotic L929sAhFas cells and we observed no clear colocalization with N-GSDME.

In contrast to N-GSDME, knowledge about a physiological role of C-GSDM once it is released from the cytotoxic N-GSDM domain is lacking. Surprisingly we observed C-GSDME clusters in addition to N-GSDME dots upon apoptosis induction, suggesting that C-GSDME could perform a function after proteolytic cleavage as well. However, these C-GSDME dots were smaller and unequal in size compared to N-GSDME dots and we are currently not able to assess whether C-GSDME is functional when an internal tag is added. Nevertheless, investigating co-localization with other cell structures could give a first clue.

Next to investigating the function of GSDME during apoptosis-driven secondary necrosis, GSDME-mNe(-mSc) provides a tool for various other applications. On the level of research on GSDME, it would be interesting to assess whether GSDME exhibits the same behavior during caspase-3-mediated pyroptosis as during apoptosis-driven secondary necrosis. In addition, mutational analyses in GSDME-mNe-mSc would allow to assess the role of different residues on GSDME function and localization. Similarly, it could be used to screen for activating and inactivating drugs while simultaneously get a clue about the interference mechanism of the drug. On the level of apoptotic and caspase-3-mediated pyroptotic cells death, monitoring GSDME-mNe-mSc might allow to investigate different gradations of cell death by visualizing GSDME activation relative to other subroutines such as PS exposure, mitochondrial degradation, etc… In that respect, GSDME-mNe-mSc could be used as a biosensor for caspase-3 activity as well, as mNeonGreen and mScarlet can serve as a fluorescence resonance energy transfer (FRET) pair. Altogether, tagging GSDME internally opens doors in the wide field of cell death research.

References

1. Rogers, C. *et al.* (2017) Cleavage of DFNA5 by caspase-3 during apoptosis mediates progression to secondary necrotic/pyroptotic cell death. *Nat. Commun.* 8, 14128
2. Kayagaki, N. *et al.* (2015) Caspase-11 cleaves gasdermin D for non-canonical inflammasome signalling. *Nature* 526, 666–671
3. Shi, J. *et al.* (2015) Cleavage of GSDMD by inflammatory caspases determines pyroptotic cell death. *Nature* 526, 660–665
4. Hou, J. *et al.* (2020) PD-L1-mediated gasdermin C expression switches apoptosis to pyroptosis in cancer cells and facilitates tumour necrosis. *Nat. Cell Biol.* 22, 1264–1275
5. Wang, Y. *et al.* (2017) Chemotherapy drugs induce pyroptosis through caspase-3 cleavage of a gasdermin. *Nature* 547, 99–103
6. Op de Beeck, K. *et al.* (2011) The DFNA5 gene, responsible for hearing loss and involved in cancer, encodes a novel apoptosis-inducing protein. *Eur. J. Hum. Genet.* 19, 965–973
7. Sborgi, L. *et al.* (2016) GSDMD membrane pore formation constitutes the mechanism of pyroptotic cell death. *EMBO J.* 35, 1766–78
8. Ding, J. *et al.* (2016) Pore-forming activity and structural autoinhibition of the gasdermin family. *Nature* 535, 111–116
9. Walker, B. *et al.* (1992) Assembly of the oligomeric membrane pore formed by Staphylococcal alpha-hemolysin examined by truncation mutagenesis. *J. Biol. Chem.* 267, 21782–6
10. Howard, S.P. and Buckley, J.T. (1985) Activation of the hole-forming toxin aerolysin by extracellular processing. *J. Bacteriol.* 163, 336–40
11. Kang, R. *et al.* (2018) Lipid Peroxidation Drives Gasdermin D-Mediated Pyroptosis in Lethal Polymicrobial Sepsis. *Cell Host Microbe* 24, 97–108
12. Xia, X. *et al.* (2018) Atypical Gasdermin D and Mixed Lineage Kinase Domain-like Protein Leakage Aggravates Tetrachlorobenzoquinone-Induced Nod-like Receptor Protein 3 Inflammasome Activation. *Chem. Res. Toxicol.* 13, 1418–1425
13. Wang, Y. *et al.* (2018) GSDME mediates caspase-3-dependent pyroptosis in gastric cancer. *Biochem. Biophys. Res. Commun.* 495, 1418–1425
14. Yu, J. *et al.* (2019) Cleavage of GSDME by caspase-3 determines lobaplatin-induced pyroptosis in colon cancer cells. *Cell Death Dis.* 10, 1–20
15. Lu, H. *et al.* (2018) Molecular targeted therapies elicit concurrent apoptotic and GSDME-dependent pyroptotic tumor cell death. *Clin. Cancer Res.* 24, 6066–6077
16. Mulvihill, E. *et al.* (2018) Mechanism of membrane pore formation by human gasdermin-D. *EMBO J.* DOI: 10.15252/embj.201798321
17. Ruan, J. *et al.* (2018) Cryo-EM structure of the gasdermin A3 membrane pore. *Nature* 557, 62–67
18. Aglietti, R.A. *et al.* (2016) GsdmD p30 elicited by caspase-11 during pyroptosis forms pores in membranes. *Proc. Natl. Acad. Sci.* 113, 7858–7863
19. Op De Beeck, K. (2011) , Elucidation of the role of the DFNA5 gene in the pathophysiology of hearing impairment and cancer. , Universiteit Antwerpen (Belgium)
20. Rathkey, J.K. *et al.* (2017) Live-cell visualization of gasdermin D-driven pyroptotic cell death. *J. Biol. Chem.* 292, 14649–14658
21. Hodgkins, A. *et al.* (2015) WGE: a CRISPR database for genome engineering. *Bioinformatics* 31, 3078–3080

22. Brinkman, E.K. *et al.* (2014) Easy quantitative assessment of genome editing by sequence trace decomposition. *Nucleic Acids Res.* 42, e168–e168
23. Rogers, C. *et al.* (2019) Gasdermin pores permeabilize mitochondria to augment caspase-3 activation during apoptosis and inflammasome activation. *Nat. Commun.* 10, 1689
24. Platnich, J.M. *et al.* (2018) Shiga Toxin/Lipopolysaccharide Activates Caspase-4 and Gasdermin D to Trigger Mitochondrial Reactive Oxygen Species Upstream of the NLRP3 Inflammasome. *Cell Rep.* 25, 1525-1536.e7
25. Wasilewski, M. and Scorrano, L. The changing shape of mitochondrial apoptosis. , *Trends in Endocrinology and Metabolism*, 20. Aug-(2009) , Trends Endocrinol Metab, 287–294
26. Karbowski, M. and Youle, R.J. Dynamics of mitochondrial morphology in healthy cells and during apoptosis. , *Cell Death and Differentiation*, 10. 01-Aug-(2003) , Nature Publishing Group, 870–880
27. Suen, D.F. *et al.* Mitochondrial dynamics and apoptosis. , *Genes and Development*, 22. 15-Jun-(2008) , Cold Spring Harbor Laboratory Press, 1577–1590
28. Wattiaux, R. *et al.* (2007) Lysosomes and Fas-mediated liver cell death. *Biochem. J.* 403, 89–95
29. Kågedal, K. *et al.* (2005) Lysosomal membrane permeabilization during apoptosis - Involvement of Bax? *Int. J. Exp. Pathol.* 86, 309–321
30. Guicciardi, M.E. *et al.* Lysosomes in cell death. , *Oncogene*, 23. 12-Apr-(2004) , Nature Publishing Group, 2881–2890
31. Zhang, Z. *et al.* (2020) Gasdermin E suppresses tumour growth by activating anti-tumour immunity. *Nature* 579, 1–6
32. Aglietti, R.A. and Dueber, E.C. Recent Insights into the Molecular Mechanisms Underlying Pyroptosis and Gasdermin Family Functions. , *Trends in Immunology*, 38. 01-Apr-(2017) , Elsevier Ltd, 261–271
33. He, W. *et al.* (2015) Gasdermin D is an executor of pyroptosis and required for interleukin-1β secretion. *Cell Res.* 25, 1285–1298
34. Delmaghani, S. *et al.* (2015) Hypervulnerability to Sound Exposure through Impaired Adaptive Proliferation of Peroxisomes. *Cell* 163, 894–906
35. Defourny, J. *et al.* (2019) Pejvakin-mediated pexophagy protects auditory hair cells against noise-induced damage. *Proc. Natl. Acad. Sci. U. S. A.* 116, 8010–8017

Chapter 8

General Discussion and Future Perspectives

8.1 Overview of the results obtained in this thesis

Chapter 4	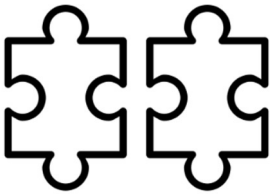	A homology based-model of N-GSDME does not show clear oligomerization interfaces in N-GSDME nor a clear hydrophobic transmembrane surface. Instead, N-GSDME monomers demonstrate an amphipathic character.
Chapter 5	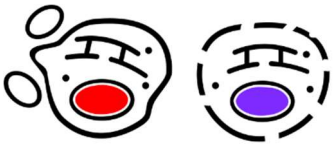	Nuclear staining by SYTOX dyes, but not by 7-AAD, is delayed in L929sAhFas cells in absence of GSDME expression during apoptosis-driven secondary necrosis. Therefore, cell impermeant dyes might not be suitable to study membrane permeabilization processes itself.
Chapter 6	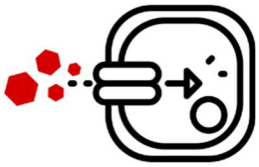	GSDME pore-formation facilitates the influx of Texas Red-labeled dextrans in a size dependent manner during apoptosis-driven secondary necrosis. In contrast, the efflux of FITC-labeled dextrans occurs independent of GSDME expression.
Chapter 7	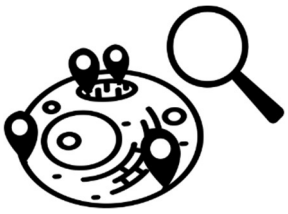	N-GSDME targets the plasma membrane and mitochondria during apoptosis-driven secondary necrosis.

8.2 Studying GSDME in cell death and the need for the right tools

The study of cell death has been complicated by several factors such as the existence of numerous cell death modalities and the potent cell death induction of some of its mediators. In addition, cells within a population often appear to die rather heterogeneous as the result of both distinct and partially overlapping biochemical cascades. Lastly, some intrinsic factors such as detachment of dying cells complicate experimental settings that require washing steps. In this thesis, we chose to investigate GSDME mediated apoptosis-driven secondary necrosis in the murine fibrosarcoma cell line L929sAhFas, which is frequently used in the lab of prof. Peter Vandenabeele because it is a well characterized cellular model. This cell line stably expresses the human Fas receptor which multimerizes upon treatment with anti-Fas antibody, resulting in the specific induction of apoptosis and caspase-3 activation *via* the caspase-8-dependent proteolytic pathway [1]. We successfully

applied CRISPR-Cas9 gene editing to interrupt murine *Gsdme* in L292sAhFas and identified two L929sAhFas *Gsdme* knockout (KO) clones. In a next step, we stably reconstituted one of these *Gsdme* KO clones with several variants of murine *Gsdme* cDNA under a tetracycline dependent promotor, allowing the expression of GSDME upon doxycycline treatment. The use of a stable cellular system prevents that observations which actually result from clonal variation are incorrectly assigned to GSDME. In addition, it eliminates variations due to differences in transfection efficiencies and subsequent protein expression levels. In chapter 5 and 6, we used L929sAhFas *Gsdme* KO cells stably reconstituted with wildtype *Gsdme* to evaluate the role of GSDME-mediated pore-formation during apoptosis driven secondary necrosis. Firstly, we aimed to determine whether cell membrane permeabilization in L929sAhFas cells upon anti-Fas treatment is affected when GSDME expression is lost. Therefore, we chose to measure the uptake of cell impermeant nuclear dyes, which are often used as cell viability stains and are used interchangeably depending on availability and spectral properties. To our own surprise, we observed different results when staining our cells with 7-aminoactinomycin D (7-AAD), which is often used in flow cytometry, compared to SYTOX dyes (SYTOX blue (SB), SYTOX green). Using both dyes combined, we confirmed that they stained the nucleus of L929sAhFas cells at different times in absence of GSDME expression during apoptosis-driven secondary necrosis. More specifically, we showed that nuclear staining by SB but not by 7-AAD was delayed in absence of GSDME expression compared to GSDME expressing L929sAhFas cells. This observation raises a problem in the interchangeable use of cell impermeant dyes to evaluate plasma membrane permeabilization. Indeed, the membrane passing characteristics of most impermeable nuclear dyes are currently unknown. Using microscopy techniques, we observed that SB staining coincided with the cellular explosion of L929sAhFas cells while 7-AAD entered already apoptotic cells with intact membranes. Although these results suggest that cell impermeant dyes might not be suitable to study plasma membrane permeabilization processes itself, the differential staining pattern of 7-AAD and SB in L929sAhFas cells in absence of GSDME expression offers an opportunity to use this dye combination as a functional assay to assess GSDME functionality. In chapter 7, we took advantage of this observation to successfully create and evaluate inducible *Gsdme* constructs with internal mNeonGreen and mScarlet tags. These constructs allow the visualization of N-GSDME and C-GSDME both before and after caspase-3 activation in relevant cell types. Attempts to visualize GSDME-mediated cell death are currently limited to transient transfection of tagged N-GSDME constructs in HEK 293T cells [2–4].

8.2.1 Limitations and future perspectives

Next to apoptosis, also tumor necrosis factor (TNF)-mediated necroptosis and both canonical and non-canonical pyroptosis can be induced in L929sAhFas cells [5,6]. This provides a major advantage as it allows to study the contribution of GSDME to other cell death modalities as well in the same cellular context. Although GSDME has been linked

with apoptosis-driven secondary necrosis and caspase-3 mediated pyroptosis [2,3,7,8], it is possible that it also contributes to other cell death modalities as is shown for GSDMD, another member of the GSDM protein family that is involved in both inflammasome-dependent pyroptosis and NETosis [9–12]. Although the L929sAhFas cell line provides a good tool to study different cell death modalities, it might be appropriate to study GSDME in other cellular contexts as well, e.g. in cancer cell lines as GSDME expression is shown to be downregulated in several breast and colorectal cancer cell lines [7,8,13]. Although it remains to be seen whether the differential staining pattern by SB and 7-AAD in absence of GSDME is also valid in other cell types, the different *Gsdme* constructs generated during this thesis were validated for their functionality and hence, can be used to transduce other cell types in order to investigate GSDME in different cellular contexts. Especially the construct coding for GSDME-mNe-mSc generated in chapter 7 is of interest, as it can serve a dual role in the study of GSDME-mediated cell death. The mNeonGreen and mScarlet tag on either side of the caspase-3 and granzyme B cleavage site constitute a fluorescence resonance energy transfer (FRET) donor/acceptor pair, providing both a biosensor for caspase-3 cleavage and a tool to visualize N-GSDME and C-GSDME in real time.

8.3 GSDME: a pore forming molecule?

Cellular membranes are critical components of cellular systems as they both separate cells from the extracellular milieu and compartmentalize biochemical processes in the cell, allowing cellular homeostasis. Therefore, disruption of cellular membranes is an effective way to eliminate infected or cancerous host cells [14,15]. Quite early after the identification of GSDM proteins as drivers of cell death, the GSDM family has been put forward as a novel class of pore-forming molecules. The cryo-electron microscopy structure of GSDMA3 pores showed that GSDMA3 pore-formation is executed *via* a barrel-stave pore mechanism [16]. In this mechanism, N-GSDMA3 monomers oligomerize forming a channel of which the outer surface is hydrophobic and interacts with the lipid tails of the membrane whereas the inner surface consists of charged residues that come in contact with the aqueous cytoplasm. Given the high degree of functional and sequence similarity between the GSDM family members, the barrel-stave pore mechanism has been proposed to be not only specific for GSDMA3 but to describe a more general mechanism applicable to all members of the GSDM protein family. However, our results elucidated in this thesis question this hypothesis in case of GSDME. First, our model of the open conformation of N-GSDME generated in chapter 4 shows that the hydrophobic surface of the β-sheet that is proposed to insert the membrane might be disrupted by hydrophilic, charged residues suggesting a more amphipathic character of the N-GSDME trans-membrane region. Moreover, no strong interaction surfaces for interunit oligomerization could be identified, questioning the ability of N-GSDME monomers to assemble a stable multimeric structure. Second, although our fluorescently tagged versions of GSDME showed localization at the plasma membrane after

caspase-3 activation in chapter 7, we did not see local increases in fluorescent intensity at the plasma membrane compared to the cytosolic fluorescent intensity in untreated cells, what is expected when N-GSDME-mNe would oligomerize. Finally, when we monitored the influx of Texas Red-labeled dextrans of different sizes in chapter 6, we were not able to determine a discrete pore size for GSDME. Therefore, we propose a toroidal pore-forming or carpet-like mechanism for GSDME pore formation. These models do not require lateral oligomerization of the subunits, are more in line with the amphipathic character seen in our model of N-GSDME and allow more disordered pore formation [17,18]. It is possible that different members of the GSDM protein family execute their cytotoxic function *via* other pore-forming mechanisms. We and Tamura *et al*. reported that GSDME and PJVK are located in a different phylogenetic cluster than GSDMA, -B, -C and -D [19,20]. It is conceivable that the barrel-stave pore mechanism has evolved later in the latter GSDM family members after their divergence from GSDME during evolution. Other pore-forming mechanisms than a barrel-stave model might also not be unusual during cell death, as Bax, a pro-apoptotic protein that permeabilizes mitochondria and allows the release of cytochrome c along with GSDME, is proposed to form heterogeneous assemblies and toroidal pores [21]. Similarly, the membrane permeabilizing mechanism of MLKL, the executioner of necroptosis, is still unsolved [22,23]. The current ongoing model includes a multi-step and partial membrane insertion of monomers mediated by specific side chains to interact with the phospholipids to disrupt membranes [24–26].

8.3.1 Limitations of our study and future perspectives

Although our results in several chapters of this thesis question GSDME pore-formation *via* the barrel-stave pore mechanism, our study only provides indirect evidence for this. Our choice to investigate GSDME pore formation during the process of apoptosis-driven secondary necrosis allowed us to evaluate the contribution of GSDME pore formation to a real physiological situation but complicates the evaluation of the GSDME pore formation itself as concomitant events might blur our results. To further investigate the pore forming mechanism of GSDME, it would be interesting to compare the pore-forming mechanisms of GSDMA3, GSDMD and GSDME with other already intensively studied pore-forming molecules *in vitro* in- and outside of a cellular context. The bacterial toxins α-hemolysin (*Staphylococcus aureus*) and streptolysin O (*Streptococcus pyogenes*) have been reported to form barrel-stave pores *via* membrane-inserting β-sheets [27–29] similar to what is proposed for GSDMA3 [16]. Melittin, the main component of honeybee venom, is an anti-microbial peptide known to perforate plasma membranes *via* the toroidal-pore forming mechanism [17,30,31]. In contrast, another anti-microbial peptide, aurein 1.2, was reported to disturb plasma membranes *via* the 'carpet'-like mechanism [32,33]. *In vitro* study and comparison of all of these different membrane permeabilizers with GSDMs could give more certainty about the plasma membrane mechanisms of the GSDM proteins. Special attention should be given to the visualization of these pores, for example *via* a combination of

fluorescently tagged versions of these membrane permeabilizers and ultrahigh-resolution electron microscopy or atomic force microscopy. Our GSDME constructs with internal mNeonGreen tag generated in chapter 7 could be used for this purpose. In addition, it would be interesting to evaluate further the role of the conserved residue E197 in GSDME. We showed in chapter 4 that this charged residue disrupts the hydrophobic character of the outer β_{TM}4-strand, thereby disturbing the hydrophobic surfaces necessary for both interunit oligomerization and interaction with lipid chains of membrane phospholipids, making a barrel-stave pore mechanism very unlikely. Generation of leucine (analogous to L186 in GSDMA3 and L192 in GSDMD) or alanine mutants of this residue in GSDME followed by functional analyses and the study of the pore-forming mechanism might provide more evidence that GSDMA3 and GSDME act *via* another pore-forming model. Whether the structural differences between pore-forming mechanisms comprise different membrane permeabilizing efficiencies or even result in different outcomes for the cell, remains currently unknown. It is tempting to speculate that barrel-stave pores enable more specificity and therefore primarily aid in cell signaling while uncontrolled membrane permeabilization processes aim at destroying the cell. However, although toroidal pore-formation by melittin was originally proposed to disrupt membranes in a detergent-like manner, melittin peptides are shown to form transient ion conducts at low concentrations, to induce stable pores at micromolar concentrations and to act as a detergent at higher concentrations [34,35]. Moreover, the cellular and physiological consequences of membrane pore-formation also depend on the extent of membrane repair mechanisms such as the ESCRT system which might prevent lytic death and render cells hyperactive to stimulate adaptive immune responses [19,36,37]. Altogether, this illustrates that the way membrane pore-formation affects the cell is a result of the concurrence of spatial, temporal and quantitative events.

8.4 Impact of GSDME expression on cell death

A link between GSDME and apoptosis has been demonstrated several times, even long before the GSDM protein family was identified as a family of cell death executioners. Apoptotic events such as DNA fragmentation and caspase-3 activity were shown to significantly increase in the presence of GSDME expression after etoposide treatment in melanoma cells [38]. In addition, expression of apoptosis-related proteins such as Fas and caspase-8 was increased in hepatocellular carcinoma cells transiently transfected with GSDME [39]. Research in the lab of prof. Van Camp revealed that transient transfection of a mutant form of GSDME that is involved in hearing loss in HEK 293T and yeast cells results in cell death marked by PI staining [4,40]. Interestingly, most GSDME mutations that were identified in hearing loss families each result in skipping of exon 8 at the mRNA level thereby disrupting the inhibitory C-terminal domain at the protein level [41–49]. However, further research in the Van Camp lab also revealed that cell death induction by deafness mutant GSDME happened in absence of yeast caspase (Mca1) activity or apoptotic caspase-3, -8

and -9 activity [40,50]. Therefore, the contribution of GSDME to apoptosis was under debate. The recent identification of GSDME as a substrate of caspase-3 and thus downstream molecule instead of inductor of the apoptotic pathway offered an explanation for this presumed paradox [3,7]. Since then, GSDME activation by caspase-3 cleavage was reported to augment necrotic cell death, either following apoptotic features such as blebbing and therefore called apoptosis-driven secondary necrosis [2,3] or direct necrosis and hence called pyroptosis [7,8,51–54] analogous to GSDMD-mediated pyroptosis. However, in some cell types GSDME was reported to be dispensable for apoptosis-driven secondary necrosis, although the presence of cleaved N-GSDME was observed [55,56]. In chapter 5 we hypothesized that this aberrant result might be due to the use of nuclear dyes inappropriate to measure GSDME dependent membrane permeabilization. The observation of delayed SB but not 7-AAD staining in absence of GSDME expression, suggests that both dyes enter the cell *via* different membrane permeabilization events. The existence of GSDME dependent and GSDME independent membrane permeabilization subroutines in L929sAhFas during apoptosis-driven secondary necrosis was also seen in chapter 6. Here we showed that Texas Red-labeled dextrans entered L929sAhFas cells in a GSDME dependent manner while efflux of FITC-labeled dextrans happened independent of GSDME expression during apoptosis-driven secondary necrosis. Altogether these results show that plasma membrane permeabilization of apoptotic cells is the result of GSDME dependent but also independent subroutines following caspase-3 activation and that GSDME expression boosts final plasma membrane permeabilization.

8.4.1 Limitations of our study and future perspectives

Whether caspase-3 mediated secondary necrosis and pyroptosis are really different cell death modalities, needs further investigation and will depend on the features that are unlocked after caspase-3 activity. It is possible that some cell types proceed very quick to the necrotic phase due to high GSDME expression levels masking the presence of classic apoptotic features such as blebbing. Several publications reporting on GSDME and caspase-3 dependent direct pyroptosis also demonstrated a switch from a pyroptotic morphology towards an apoptotic morphology upon the same stimulus when GSDME expression was lost [7,8,51,52], supporting this hypothesis. In addition, the current redefinition of pyroptosis to “GSDM-mediated cell death” is problematic, as it does not take the particular cellular context into account in which different GSDMs are active: e.g in combination with caspase-3 dependent events [2,3,7,8,51,52], in combination with the release of NETs during NETosis [9,10], or during inflammasome-mediated pyroptosis and IL-1β release [11,12,57]. Assuming that GSDM proteins act solely as membrane permeabilizers, one may wonder whether we should put so much emphasis in the cell death nomenclature on the ‘tunnel digger’ (GSDMs) without regard to all the prisoners (cytokines, damage-associated molecular patterns (DAMPs),…) who can escape. In that respect, the generation of the mature form of the pro-inflammatory cytokine IL-1β is dependent on

cleavage by caspase-1. Although the quick release of IL-1β is directly related to the pore-forming capacity of N-GSDMD during inflammasome-mediated pyroptosis [58,59], GSDMD is not absolutely required for IL-1β secretion as *Gsdmd*$^{-/-}$ dendritic cells do release IL-1β after inflammasome and caspase-1 activation, only significantly delayed compared to their wildtype counterparts [60]. Interestingly, GSDME was recently shown to be responsible for the release of IL-1β in *GSDMD*$^{-/-}$ THP-1 cells after NLRP3 and NLRC4 inflammasome activation [61]. On the other hand, the release of other pro-inflammatory molecules such as high mobility group box 1 (HMGB1) has been reported to happen in a nerve injury-induced protein 1 (NINJ1)-dependent but GSDMD-independent manner during pyroptosis in macrophages [62]. Nevertheless, it is conceivable that a delay in the release of particular pro-inflammatory molecules can have far-reaching consequences with regard to provoking an inflammatory response. Although the role in facilitating necrosis downstream of caspase-3 activation is well documented and we showed that GSDME pores facilitate the passage of large molecules up to at least 70 kDa (chapter 6), there is currently no knowledge about what kind of content would escape the cell upon GSDME-mediated plasma membrane permeabilization during caspase-3 dependent cell death. This creates a major gap in the study on GSDME and complicates the proper assessment of its importance in caspase-3 mediated cell death. Fas-induced apoptosis was shown to be associated with the production and secretion of multiple cytokines and chemokines such as IL-6, IL-8, CXCL1, MCP-1 and GMCSF [63]. Similarly adenosine triphosphate (ATP), acting as a 'find-me' signal for efferocytosis, and the DAMP HMGB1 are released during apoptosis [64–67]. Especially the latter is of interest, as HMGB1 gets oxidized when it is exposed to high levels of ROS, which is the case in apoptotic cells, thereby inactivating the immunostimulatory activity of HMGB1 [67,68]. The quick plasma membrane permeabilization of apoptotic cells mediated by GSDME might prevent extensive oxidation of HMGB1 and conserve its immunostimulatory function. Loss of GSDME in intestinal epithelial cells was shown to decrease the release of HMGB1 in the supernatant after treatment with TNF-α or cycloheximide [69]. Nevertheless, this study did not show whether the decrease was the consequence of a lower amount of cell death or delayed cell death kinetics versus the consequence of the loss of GSDME itself. Overall, future studies should focus on monitoring the release of metabolites, cytokines, chemokines and DAMPs in the supernatant during caspase-3 mediated cell death in the presence and absence of GSDME while taking the degree of cell death into account. In a next step, the effect of a quick release in the presence of GSDME versus the accumulation of these molecules in the cell and blebs due to a prolonged membrane integrity in absence of GSDME, should be evaluated. For example, direct cleavage of GSDME next to apoptosis induction via caspase-3 activation in target cells by granzyme B from natural killer cells [70], might limit the temporal range to produce cytokines. Also the effect on efferocytosis should be evaluated. On one hand, restricted chemokine or ATP release in absence of GSDME expression might prevent proper recruitment of phagocytes to sites of cell death, as these molecules serve as 'find-me' signals that establish a

chemotactic gradient to attract phagocytic cells [71–73]. On the other hand, preserved membrane integrity in absence of GSDME might prolong the temporal window for phagocytes to engulf intact, apoptotic cells before they release pro-inflammatory molecules, allowing a tolerogenic or immunologically 'silent' clearance of dying cells. Indeed, apoptotic cells present 'eat me' signals on their surface to differentiate them from viable cells and to allow recognition by phagocytes [71,72]. In chapter 6 we showed that the exposure of phosphatidylserine (PS), the best known 'eat me' signal, is unaffected during apoptosis of L929sAhFas cells when GSDME expression is absent, thereby prolonging the PS single positive status. Phagocytes that engulf intact apoptotic cells secrete anti-inflammatory cytokines such as TGFβ and IL-10 while simultaneously suppressing pro-inflammatory cytokines such as IL-1 and IL-12 [71,72,74,75]. In contrast, DAMPs release from necrotic cells attracts pro-inflammatory innate immune cells from the blood such as macrophages and neutrophils that clear the cell debris and release pro-inflammatory cytokines such as TNF-α [76–78]. In that respect, GSDME expressing tumor cells were shown to increase macrophage-mediated phagocytosis [70] and to attract more tumor-infiltrating natural-killer and T lymphocytes [70,79]. Moreover, subsequent release of natural-killer granzyme B and its entry in target cells results in direct activation of GSDME and necrotic death of the target cells [70].

8.5 CONCLUSION

Although the GSDMs are currently in the spotlights is the regulated cell death field, most publications focus on the role of GSDMD during inflammasome-mediated pyroptosis. In this thesis, we aimed to unravel the role of GSDME in apoptosis-driven secondary necrosis. Therefore we explored different aspects such as the composition of secondary structures in GSDME and N-GSDME, the GSDME-dependent nuclear staining by DNA dyes and influx of Texas Red-labeled dextrans and the localization of N-GSDME during apoptosis-driven secondary necrosis. Our results show that GSDME facilitates the quick permeabilization of the plasma membrane after activation of caspase-3 favoring the staining by SYTOX dyes and Texas Red-labeled dextrans. However, GSDME is probably not the only executor of membrane permeabilization acting downstream of caspase-3 activation, as the nuclear staining by 7-AAD and efflux of FITC-labeled dextrans happened independent of GSDME expression during apoptosis-driven secondary necrosis. Future research should focus on the consequences of GSDME-mediated plasma membrane permeabilization in terms of release of pro-inflammatory molecules and clearance by phagocytic cells. However, our results also question the universality of the barrel-stave pore model as the pore-forming mechanism of GSDM proteins. Further comparative analysis with other known pore-forming molecules should be done to provide more certainty about the pore-forming mechanism of GSDME.

References

1. Vercammen, D. *et al.* (1998) Inhibition of caspases increases the sensitivity of L929 cells to necrosis mediated by tumor necrosis factor. *J. Exp. Med.* 187, 1477–85
2. Rogers, C. *et al.* (2019) Gasdermin pores permeabilize mitochondria to augment caspase-3 activation during apoptosis and inflammasome activation. *Nat. Commun.* 10, 1689
3. Rogers, C. *et al.* (2017) Cleavage of DFNA5 by caspase-3 during apoptosis mediates progression to secondary necrotic/pyroptotic cell death. *Nat. Commun.* 8, 14128
4. Op de Beeck, K. *et al.* (2011) The DFNA5 gene, responsible for hearing loss and involved in cancer, encodes a novel apoptosis-inducing protein. *Eur. J. Hum. Genet.* 19, 965–973
5. Vanden Berghe, T. Vanden *et al.* (2010) Necroptosis, necrosis and secondary necrosis converge on similar cellular disintegration features. *Cell Death Differ.* 17, 922–930
6. Wiernicki, B. *et al.* (2020) Excessive phospholipid peroxidation distinguishes ferroptosis from other cell death modes including pyroptosis. *Cell Death Dis.* 11,
7. Wang, Y. *et al.* (2017) Chemotherapy drugs induce pyroptosis through caspase-3 cleavage of a gasdermin. *Nature* 547, 99–103
8. Yu, J. *et al.* (2019) Cleavage of GSDME by caspase-3 determines lobaplatin-induced pyroptosis in colon cancer cells. *Cell Death Dis.* 10, 1–20
9. Sollberger, G. *et al.* (2018) Gasdermin D plays a vital role in the generation of neutrophil extracellular traps. *Sci. Immunol.* 3, 1–12
10. Chen, K.W. *et al.* (2018) Noncanonical inflammasome signaling elicits gasdermin D-dependent neutrophil extracellular traps. *Sci. Immunol.* 3, eaar6676
11. Kayagaki, N. *et al.* (2015) Caspase-11 cleaves gasdermin D for non-canonical inflammasome signalling. *Nature* 526, 666–671
12. Shi, J. *et al.* (2015) Cleavage of GSDMD by inflammatory caspases determines pyroptotic cell death. *Nature* 526, 660–665
13. Kim, M.S. *et al.* (2008) Methylation of the DFNA5 increases risk of lymph node metastasis in human breast cancer. *Biochem. Biophys. Res. Commun.* 370, 38–43
14. Mondal, A.K. *et al.* (2018) Structural basis and functional implications of the membrane pore-formation mechanisms of bacterial pore-forming toxins. In *Advances in Experimental Medicine and Biology* 1112pp. 281–291, Springer New York LLC
15. Krawczyk, P.A. *et al.* To Kill But Not Be Killed: Controlling the Activity of Mammalian Pore-Forming Proteins. , *Frontiers in Immunology*, 11. 13-Nov-(2020) , Frontiers Media S.A., 2972
16. Ruan, J. *et al.* (2018) Cryo-EM structure of the gasdermin A3 membrane pore. *Nature* 557, 62–67
17. Sengupta, D. *et al.* (2008) Toroidal pores formed by antimicrobial peptides show significant disorder. *Biochim. Biophys. Acta - Biomembr.* 1778, 2308–2317
18. Matsuzaki, K. (2019) Membrane permeabilization mechanisms. In *Advances in Experimental Medicine and Biology* 1117pp. 9–16, Springer New York LLC
19. De Schutter, E. *et al.* (2021) Punching Holes in Cellular Membranes: Biology and Evolution of Gasdermins. *Trends Cell Biol.* DOI: 10.1016/j.tcb.2021.03.004
20. Tamura, M. *et al.* (2007) Members of a novel gene family, Gsdm, are expressed exclusively in the epithelium of the skin and gastrointestinal tract in a highly tissue-specific manner. *Genomics* 89, 618–629

21. Uren, R.T. *et al.* (2017) Pore formation by dimeric Bak and Bax: an unusual pore? *Philos. Trans. R. Soc. B Biol. Sci.* 372, 20160218
22. Czabotar, P.E. and Murphy, J.M. A tale of two domains - A structural perspective of the pseudokinase, MLKL. , *FEBS Journal*, 282. 01-Nov-(2015) , Blackwell Publishing Ltd, 4268–4278
23. Petrie, E.J. *et al.* (2018) Conformational switching of the pseudokinase domain promotes human MLKL tetramerization and cell death by necroptosis. *Nat. Commun.* 9,
24. Quarato, G. *et al.* (2016) Sequential Engagement of Distinct MLKL Phosphatidylinositol-Binding Sites Executes Necroptosis. *Mol. Cell* 61, 589–601
25. Petrie, E.J. *et al.* Insane in the membrane: A structural perspective of MLKL function in necroptosis. , *Immunology and Cell Biology*, 95. 01-Feb-(2017) , Nature Publishing Group, 152–159
26. Dondelinger, Y. *et al.* (2014) MLKL compromises plasma membrane integrity by binding to phosphatidylinositol phosphates. *Cell Rep.* 7, 971–81
27. Gilbert, R.J.C. *et al.* (2014) Membrane pore formation at protein–lipid interfaces. *Trends Biochem. Sci.* 39, 510–516
28. Peraro, M.D. and van der Goot, F.G. (2016) Pore-forming toxins: ancient, but never really out of fashion. *Nat. Rev. Microbiol.* 14, 77–92
29. Bhakdi, S. *et al.* Staphylococcal alpha-toxin, streptolysin-O, and Escherichia coli hemolysin: Prototypes of pore-forming bacterial cytolysins. , *Archives of Microbiology*, 165. (1996) , Springer, 73–79
30. Yang, L. *et al.* (2001) Barrel-stave model or toroidal model? A case study on melittin pores. *Biophys. J.* 81, 1475–1485
31. Hong, J. *et al.* (2019) How melittin inserts into cell membrane: Conformational changes, inter-peptide cooperation, and disturbance on the membrane. *Molecules* 24,
32. Fernandez, D.I. *et al.* (2012) The antimicrobial peptide aurein 1.2 disrupts model membranes via the carpet mechanism. *Phys. Chem. Chem. Phys.* 14, 15739–15751
33. Mechler, A. *et al.* (2007) Specific and selective peptide-membrane interactions revealed using quartz crystal microbalance. *Biophys. J.* 93, 3907–3916
34. Lee, M.T. *et al.* (2008) Mechanism and kinetics of pore formation in membranes by water-soluble amphipathic peptides. *Proc. Natl. Acad. Sci. U. S. A.* 105, 5087–5092
35. Lee, M.T. *et al.* (2013) Process of inducing pores in membranes by melittin. *Proc. Natl. Acad. Sci. U. S. A.* 110, 14243–14248
36. Rühl, S. *et al.* (2018) ESCRT-dependent membrane repair negatively regulates pyroptosis downstream of GSDMD activation. *Science (80-.).* 362, 956–960
37. Lieberman, J. *et al.* (2019) Gasdermin D activity in inflammation and host defense. *Sci. Immunol.* 4, eaav1447
38. Lage, H. *et al.* (2001) DFNA5 (ICERE-1) contributes to acquired etoposide resistance in melanoma cells. *FEBS Lett.* 494, 54–59
39. Wang, C.J. *et al.* (2013) The expression and regulation of DFNA5 in human hepatocellular carcinoma DFNA5 in hepatocellular carcinoma. *Mol. Biol. Rep.* 40, 6525–6531
40. Van Rossom, S. *et al.* (2012) The splicing mutant of the human tumor suppressor protein DFNA5 induces programmed cell death when expressed in the yeast Saccharomyces cerevisiae. *Front. Oncol.* 2, 1–14
41. Van Laer, L. *et al.* (1998) Nonsyndromic hearing impairment is associated with a mutation in DFNA5. *Nat. Genet.* 20, 194–197

42. Park, H.-J. *et al.* (2010) Evidence for a founder mutation causing DFNA5 hearing loss in East Asians. *J. Hum. Genet.* 55, 59–62
43. Yu, C. *et al.* (2003) A 3-nucleotide deletion in the polypyrimidine tract of intron 7 of the DFNA5 gene causes nonsyndromic hearing impairment in a Chinese family. *Genomics* 82, 575–9
44. Bischoff, A.M.L.C. *et al.* (2004) A novel mutation identified in the DFNA5 gene in a Dutch family: a clinical and genetic evaluation. *Audiol. Neurootol.* 9, 34–46
45. Cheng, J. *et al.* (2007) A novel DFNA5 mutation, IVS8+4 A>G, in the splice donor site of intron 8 causes late-onset non-syndromic hearing loss in a Chinese family. *Clin. Genet.* 72, 471–477
46. Nishio, A. *et al.* (2014) A DFNA5 mutation identified in Japanese families with autosomal dominant hereditary hearing loss. *Ann. Hum. Genet.* 78, 83–91
47. Chai, Y. *et al.* (2014) A novel splice site mutation in DFNA5 causes late-onset progressive non-syndromic hearing loss in a Chinese family. *Int. J. Pediatr. Otorhinolaryngol.* 78, 1265–8
48. Li-Yang, M.-N. *et al.* (2015) IVS8+1 DelG, a Novel Splice Site Mutation Causing DFNA5 Deafness in a Chinese Family. *Chin. Med. J. (Engl).* 128, 2510–5
49. Booth, K.T. *et al.* (2018) Exonic mutations and exon skipping: Lessons learned from DFNA5. *Hum. Mutat.* 39, 433–440
50. Van Rossom, S. (2014) , Elucidation of the DFNA5 protein through the study in yeast and human cell lines. , Universiteit Antwerpen en KU Leuven
51. Wang, Y. *et al.* (2018) GSDME mediates caspase-3-dependent pyroptosis in gastric cancer. *Biochem. Biophys. Res. Commun.* 495, 1418–1425
52. Lu, H. *et al.* (2018) Molecular targeted therapies elicit concurrent apoptotic and GSDME-dependent pyroptotic tumor cell death. *Clin. Cancer Res.* 24, 6066–6077
53. Deng, B.B. *et al.* (2020) BIX-01294 enhanced chemotherapy effect in gastric cancer by inducing GSDME-mediated pyroptosis. *Cell Biol. Int.* DOI: 10.1002/cbin.11395
54. Hu, L. *et al.* Chemotherapy-induced pyroptosis is mediated by BAK/BAX-caspase-3-GSDME pathway and inhibited by 2-bromopalmitate. DOI: 10.1038/s41419-020-2476-2
55. Tixeira, R. *et al.* (2018) Gasdermin E Does Not Limit Apoptotic Cell Disassembly by Promoting Early Onset of Secondary Necrosis in Jurkat T Cells and THP-1 Monocytes. *Front. Immunol.* 9, 2842
56. Lee, B.L. *et al.* (2018) ASC- and caspase-8-dependent apoptotic pathway diverges from the NLRC4 inflammasome in macrophages. *Sci. Rep.* 8, 3788
57. Aglietti, R.A. *et al.* (2016) GsdmD p30 elicited by caspase-11 during pyroptosis forms pores in membranes. *Proc. Natl. Acad. Sci.* 113, 7858–7863
58. Karmakar, M. *et al.* (2020) N-GSDMD trafficking to neutrophil organelles facilitates IL-1β release independently of plasma membrane pores and pyroptosis. *Nat. Commun.* 11, 1–14
59. He, W. *et al.* (2015) Gasdermin D is an executor of pyroptosis and required for interleukin-1β secretion. *Cell Res.* 25, 1285–1298
60. Schneider, K.S. *et al.* (2017) The Inflammasome Drives GSDMD-Independent Secondary Pyroptosis and IL-1 Release in the Absence of Caspase-1 Protease Activity. *Cell Rep.* 21, 3846–3859
61. Zhou, B. and Abbott, D.W. (2021) Gasdermin E permits interleukin-1 beta release in distinct sublytic and pyroptotic phases. *Cell Rep.* 35, 108998
62. Kayagaki, N. *et al.* (2021) NINJ1 mediates plasma membrane rupture during lytic cell death. *Nature* DOI: 10.1038/s41586-021-03218-7

63. Cullen, S.P. *et al.* (2013) Fas/CD95-Induced Chemokines Can Serve as “Find-Me” Signals for Apoptotic Cells. *Mol. Cell* 49, 1034–1048
64. Bell, C.W. *et al.* (2006) The extracellular release of HMGB1 during apoptotic cell death. *Am. J. Physiol. - Cell Physiol.* 291,
65. Qu, Y. *et al.* (2011) Pannexin-1 Is Required for ATP Release during Apoptosis but Not for Inflammasome Activation. *J. Immunol.* 186, 6553–6561
66. Chekeni, F.B. *et al.* (2010) Pannexin 1 channels mediate “find-me” signal release and membrane permeability during apoptosis. *Nature* 467, 863–867
67. Kazama, H. *et al.* (2008) Induction of Immunological Tolerance by Apoptotic Cells Requires Caspase-Dependent Oxidation of High-Mobility Group Box-1 Protein. *Immunity* 29, 21–32
68. Janko, C. *et al.* Redox modulation of HMGB1-related signaling. , *Antioxidants and Redox Signaling*, 20. 01-Mar-(2014) , Mary Ann Liebert, Inc., 1075–1085
69. Tan, G. *et al.* (2020) HMGB1 released from GSDME-mediated pyroptotic epithelial cells participates in the tumorigenesis of colitis-associated colorectal cancer through the ERK1/2 pathway. *J. Hematol. Oncol.* 13,
70. Zhang, Z. *et al.* (2020) Gasdermin E suppresses tumour growth by activating anti-tumour immunity. *Nature* 579, 1–6
71. Green, D.R. *et al.* (2016) The clearance of dying cells: table for two. *Cell Death Differ.* 23, 915–926
72. Hochreiter-Hufford, A. and Ravichandran, K.S. (2013) Clearing the dead: Apoptotic cell sensing, recognition, engulfment, and digestion. *Cold Spring Harb. Perspect. Biol.* 5,
73. Elliott, M.R. and Ravichandran, K.S. The Dynamics of Apoptotic Cell Clearance. , *Developmental Cell*, 38. 25-Jul-(2016) , Cell Press, 147–160
74. Ravichandran, K.S. and Lorenz, U. Engulfment of apoptotic cells: Signals for a good meal. , *Nature Reviews Immunology*, 7. 21-Nov-(2007) , Nat Rev Immunol, 964–974
75. Voss, J.J.L.P. *et al.* (2017) Modulation of macrophage antitumor potential by apoptotic lymphoma cells. *Cell Death Differ.* 24, 971–983
76. Sachet, M. *et al.* (2017) The immune response to secondary necrotic cells. *Apoptosis* 22, 1189–1204
77. Nagata, S. (2018) Apoptosis and Clearance of Apoptotic Cells. *Annu. Rev. Immunol.* 36, 489–517
78. Lövgren, T. *et al.* (2004) Induction of interferon-α production in plasmacytoid dendritic cells by immune complexes containing nucleic acid released by necrotic or late apoptotic cells and lupus IgG. *Arthritis Rheum.* 50, 1861–1872
79. Peng, Z. *et al.* GSDME enhances Cisplatin sensitivity to regress non-small cell lung carcinoma by mediating pyroptosis to trigger antitumor immunocyte infiltration. , *Signal Transduction and Targeted Therapy*, 5. 01-Dec-(2020) , Springer Nature, 1–3

List of Abbreviations

7-AAD	7-aminoactinomycin D
A	alanine
AnnV	Annexin V
ATP	adenosine triphosphate
AUC	area under the curve
AuNPs	gold nanoparticles
C-GSDM	gasdermin C-terminal domain
CHiP	chromatin immunoprecipitation
CIMP	CpG island methylator phenotype
cryo-EM	cryo-electron microscopy
ctDNA	circulating tumor DNA
CXCL1	C-X-C motif ligand 1
cyt c	cytochrome c
D	aspartic acid
DAMP	damage-associated molecular pattern
DFNA5	deafness, autosomal dominant, 5
DFNB59	deafness, autosomal recessive, 59
dox	doxycycline
E	glutamic acid
ER	estrogen receptor
ESCRT	endosomal sorting complexes required for transport
EV71	enterovirus 71
FRET	fluorescence resonance energy transfer
GMCSF	Granulocyte macrophage colony-stimulating factor
GSDM	gasdermin
GSDMA3	gasdermin A3
GSDMB	gasdermin B
GSDMC	gasdermin C
GSDMD	gasdermin D
GSDME	gasdermin E
GSDME-mNe	GSDME-mNeonGreen
GSDME-mNe-mSc	GSDME-mNeonGreen-mScarlet
HEK	human embryonic kidney
HMGB1	high mobility group box 1
HRP	horseradish peroxidase
ICERE	inversely correlated with estrogen receptor
IL-1	interleukin 1
IL-10	interleukin 10
IL-12	interleukin 12
IL-1β	interleukin 1-beta

IL-6	interleukin 6
IL-8	interleukin 8
iTOL	Interactive Tree of Life
K	lysine
KO	knockout
L	leucine
LDH	lactate dehydrogenase
MCP-1	Monocyte chemoattractant protein 1
MLKL	mixed lineage kinase domain-like
mNe	mNeonGreen
MOMP	mitochondrial outer membrane permeabilization
mSc	mScarlet
N-GSDM	gasdermin N-terminal domain
NINJ1	nerve injury-induced protein 1
NTC	non-trreatment control
PAMP	pathogen-associated molecular patterns
PBS	phosphate-buffered saline
PDB	protein data bank
PDDAC	poly(diallyl dimethyl ammonium chloride)
PJVK	pejvakin
Plk1	polo kinase 1
PR	progesteron receptor
pro-IL-1β	pro-interleukin 1-beta
PS	phosphatidylserine
Q	glutamine
R	arginine
rMFI	relative mean fluorescent intensity
SB	SYTOX Blue
SDS	sodiumdodecylsulfate
SG	SYTOX Green
sgRNA	single guide RNA
T	threonine
TBS-T	tris-buffered saline containing 0.05 % Tween® 20
TCGA	the cancer genome atlas
thr	threonine
TNF	tumor necrosis factor
TNM	tumor-node-metastasis
V	valine
VNB	vapor nanobubbles
W	tryptophan
Y	tyrosine

Curriculum Vitae

PERSONAL INFORMATION

Name:	Elke De Schutter
Address:	Tervuursesteenweg 120, 2800 Mechelen
Phone number:	+32 474 61 23 17
E-mail:	deschutter.elke@gmail.com
Date of birth:	14/04/1991
Place of birth:	Borgerhout (Antwerpen)
Nationality:	Belgian

EDUCATION

2015-present **Joint PhD**
PhD in biomedical sciences (University of Antwerp)
PhD in sciences: biochemistry and biotechnology (University of Ghent)
University of Antwerp, Center of Medical Genetics
University of Ghent, VIB-UGhent Center for Inflammation Research
Promotors: Prof. Dr. Guy Van Camp, Prof. Dr. Peter Vandenabeele and Prof. Dr. Franck B. Riquet
Title: *Elucidation of the role of GSDME during apoptosis-driven secondary necrosis*

2014 - 2015 **Specific teacher training programme (SLO)**
KU Leuven
Major: Mathematics - minor: Biology
Graduated *Magna cum laude*

2012 – 2014 **Master in Bioscience engineering**
KU Leuven
Major: Cell and Gene technology - minor: animal production
Graduated *Magna cum laude*
Master's thesis: *"Functional analysis of BRCA2 variants of unknown significance"* – Promotor: Prof. Gert Matthijs

2012 **Laboratory Animal Science**
KU Leuven
- Certificate category B

2009 – 2012 **Bachelor in Bioscience engineering**
KU Leuven
Major: Cell and Gene technology
Graduated *Magna cum laude*

2003 – 2009 **General secondary education: Latin-Mathematics**
Sint-Romboutscollege, Mechelen

PUBLICATIONS

De Schutter E, Cappe B, Wiernicki B, Vandenabeele P, Riquet F. B. Plasma membrane permeabilization following cell death: many ways to dye! (2021) *Cell Death Discov.* 7(1): 183.

De Schutter E, Roelandt R, Riquet FB, Van Camp G, Wullaert A, Vandenabeele P. Punching Holes in Cellular Membranes: Biology and Evolution of Gasdermins. (2021) *Trends Cell Biol.* 31(6): 500–513.

Ibrahim J, **De Schutter E**, Op de Beeck K. GSDME: A Potential Ally in Cancer Detection and Treatment. (2021) *Trends Cancer* 7(5): 392-394.

De Schutter E, Croes L, Ibrahim J, Pauwels P, Op de Beeck K, Vandenabeele P, Van Camp G. GSDME and its role in cancer: From behind the scenes to the front of the stage. (2020) *Int J Cancer* 148(12): 2872-2883.

POSTER PRESENTATIONS

De Schutter E, Riquet F, Vanden Berghe T, Op de Beeck K, Van Camp G, Vandenabeele P.: ‘DFNA5-induced cell death: secondary necrosis or more?’
25th Conference of the European Cell Death Organization (ECDO): ‘Cell Death and Immunity in Disease: from molecules to translational medicine', 2017, Leuven.

STUDENT SUPERVISION

Master’s thesis Biochemistry and Biotechnology, University of Ghent. Emma Ruysseveldt: ‘Structure-based search for regulatory mechanisms controlling the activity of gasdermins (GSDMs)’. 2019-2020.

Master’s thesis Biomedical Sciences, University of Antwerp. Sofie De Ren: ‘The role of gasdermin E in secondary necrosis’. 2018-2019.

Bachelor thesis Biochemistry and Biotechnology, University of Antwerp. Laurens Bosmans: ‘Zoektocht naar ziekteveroorzakende genen voor King-Kopetzky syndroom’. 2016-2017.

Dankwoord

Na mijn studies in Leuven begon ik in 2015 aan een gloednieuw avontuur in Antwerpen. Toen had ik nooit durven denken dat mijn doctoraat, nu 6 jaar later niet alleen een Antwerps, maar ook Gents verhaal zou worden waar vandaag een einde aan komt. Tijdens dit dubbeldoctoraat heb ik de kans gekregen om in verschillende omgevingen te werken en mij te verdiepen in verschillende expertisedomeinen. Maar bovenal zijn het de geweldige mensen die ik heb ontmoet en die me hebben bijgestaan tijdens dit avontuur die me het meest zullen bijblijven. Het is tijd om hen nu te bedanken.

Vooreerst zou ik mijn promotoren Guy, Peter en Franck willen bedanken. Guy, bedankt om me de kans te geven om een doctoraat in de genetica te starten, ook al had ik geen brede achtergrond in de moleculaire genetica. Uw deur stond echter altijd open en u maakte altijd tijd om mijn vragen te beantwoorden. Ook toen mijn oorspronkelijke project niet echt leek op gang te komen, zag u de opportuniteit om het project te heroriënteren naar GSDME, in het lab ook wel beter gekend als DFNA5, en zijn rol in celdood. Vol enthousiasme gingen we dit nieuwe project voorstellen aan Peter Vandenabeele in Gent. Peter, bedankt om mee te stappen in dit verhaal en mij in te wijden in de wereld van de celdood. Ik zal me altijd onze, soms intense maar altijd boeidende, open discussies herinneren die leidden tot nieuwe inzichten en ideeën. Bedankt om me te stimuleren om *out of the box* te denken en nieuwe technieken op te zoeken. Franck, although you only recently became officially my promotor, you guided me throughout this PhD project as soon as I entered the IRC building. Thank you of reminding me about the bigger picture in performing a PhD and putting everything in perspective when I lost motivation. Thank you for listening.

Naast mijn promotoren wil ik ook Wim Declercq en Ken Op de Beeck bedanken voor hun inhoudelijke bijdragen aan deze thesis. Doordat jullie wat verder van het project stonden, was het heel verrijkend om met jullie de resultaten te bediscussiëren en evalueren.

Next, I would like to express my gratitude to the members of my jury, prof. Dr. Vincent Timmerman, prof. Dr. Frank Kooy, prof. Dr. Patrizia Agostinis, Dr. Lieselotte Vande Walle and Dr. Jonathan Maelfait for reviewing my thesis during summer holidays and for their valuable comments.

Graag wil ik ook prof. Dr. Kevin Braeckmans, Dr. Stephan Stermersch en natuurlijk Jana Ramon bedanken voor de fijne samenwerking van de afgelopen twee jaar. Jana, bedankt voor al je inspanningen tijdens de lange experimenten en het continu mee denken over hoe het verder moest. Zonder jou was dit project niet gelukt. Also many thanks to Caroline De Tender and Benjamin Pfeuty for their help to untangle the complex data.

Daarnaast wil ik ook Sofie en Emma, twee studenten die in het kader van hun masterproef hebben meegewerkt aan een aantal experimenten in deze thesis, bedanken voor hun flexibiliteit en doorzettingsvermogen. De omstandigheden waarin we soms moesten werken (laat op de avond, in covid periodes,…) waren zeker niet altijd evident!

Om de resultaten in deze thesis te bekomen was er uiteraard ook een heleboel fancy equipment nodig. Maar vooral ook mensen die met die fancy equipment kunnen werken… . Daarom wil ik graag Amanda, Eef en Evelien van de VIB Bio-Imaging Core bedanken voor hun vele hulp en oneindige geduld tijdens mijn microscopie experimenten. Hoewel de spinning disk er vaak al de brui aan gaf vanaf ik er nog maar naar keek, deden jullie altijd jullie uiterste best om toch nog resultaat uit mijn experimenten te halen. Daarnaast heb ik ook erg genoten van onze leuke gesprekken tijdens de experimenten! Ook een hele dikke merci aan Gert en Julie van de VIB Flow Core voor alle hulp en het onderhoud van de flow cytometers. Zonder jullie geen experimenten en geen onderzoek!

Ook geen PhD zonder fijne collega's om mee samen te werken of gewoon samen te lachen en te lunchen! Hoewel de meeste collega's van de DOOF groep reeds (lang) elders aan de slag zijn, hebben ze toch een belangrijk aandeel gehad in het behalen van mijn PhD. Manou en Hanne, jullie hebben me meteen wegwijs gemaakt in de sensoriële aandoeningen en welkom geheten bij jullie in de bureau. Dankjulliewel om mij niet te serieus te nemen en met mijn flauwe mopjes te lachen, ik heb me altijd enorm geamuseerd met jullie! Hanne, ook bedankt voor je eeuwige enthousiasme, dat doen er niet veel je na! Ook in de bureau naast ons kon ik altijd terecht voor een praatje en een lach! An, de mater familias en rots in de branding van de groep, wat zouden we zonder jou moeten aanvangen! Altijd stond je klaar om me te helpen met raad en daad, ook al was het niet altijd even gemakkelijk werken voor jou in Antwerpen wanneer ik in Gent was. Ik keek er ook altijd enorm naar uit om bij jou binnen te vallen als ik dan toch eens in Antwerpen was om even bij te babbelen. Dankzij jou was ik altijd volledig op de hoogte van het reilen en zeilen op het CMG ;-). Voor een goeie babbel en schaterlach kon ik ook altijd bij Marieke, Lieselot, Nele en Gitta terecht. Lieselot, ik vond het zeer fijn om in de laatste fase van je doctoraat samen te werken aan de review en ons te verdiepen in het grotere plaatje van GSDME. Ook bedankt voor de steeds steengoede adviezen wanneer ik op zoek was naar een lekker restaurantje in Antwerpen! Marieke, schijnbaar de iets stillere van de groep maar zeker een vrouw die weet wat ze wil. Ik heb genoten van onze gesprekken op de fiets en je rechtschapen analyses, iets wat ik ten zeerste apprecieer! Nele, als ik terugdenk aan jouw schaterlach die door de muren heen te horen was, verschijnt er spontaan een lach op mijn eigen gezicht. Ook van je nuchtere kijk op het leven heb ik veel opgestoken, waarvoor dank! Gitta, bedankt voor je luisterend oor wanneer ik even moest ventileren en je realistische kijk op de zaken. Ik wens je veel succes met het afleggen van je doctoraat, het zijn de laatste loodjes! Meisjes, hopelijk zien we elkaar snel weer!

Ook de mannelijke leden van de Doof-groep mag ik niet vergeten. Matthias en Timon, bedankt voor de interessante discussies aan het begin van mijn doctoraat. Special thanks also to Joe for our nice collaboration on the review and the forum article. Good luck with finalizing your PhD dissertation. Daarnaast wil ik ook alle nieuwe leden van de DOOF groep veel succes wensen met hun doctoraat!

Ook mijn oude bureaugenoten en overige collega's verdienen een bedankje. Ilse L., jij was veruit het meeste betrokken bij de laatste loodjes van mijn doctoraat. Bedankt voor je niet aflatende interesse, je luisterend oor en je bemoedigende woorden wanneer ik ze nodig had. Ook een hele dikke merci om me te helpen met de praktische kant van het indienen van de thesis. Ik hoop dat je bouwwerken voorspoedig verlopen en wens je veel interessante onderzoeksresultaten toe. Maar bovenal hoop ik vooral dat we elkaars successen snel nog eens kunnen vieren met een lekker biertje!

Dorien, Gerarda, Ilse VDW, Jean, Ellen E, Ellen S, Sara, Silke, Raphaël, Esther, Maaike, Aline en Arvid, tot ziens en nog veel succes met jullie professionele activiteiten in de toekomst! Eline en Jolien, nog heel veel succes met het afleggen van jullie doctoraat, het was steeds een genoegen om jullie te zien op het CMG en samen met jullie te lachen!

Ook in Gent heb ik heel wat fijne mensen leren kennen. I would like to thank Benjamin and Inge for the nice team meetings we had together with Franck in the Death Dynamics Team. Our weekly 'catching up' hour was both a way to relax and keep track of all ongoing experiments and projects. Also, many thanks to Bartosz for our nice discussions about my project and your help with the design of many of my experiments. You teached me everything I needed to know to perform my experiments and always had good ideas about how to get more out of them. In addition, I always enjoyed your dry sense of humor. It really helped to put our frustrations in perspective. Good luck with your public defense, you really are a very good scientist so I'm convinced that you will deal with it like a pro! Ook een hele dikke merci aan Ria, Barbara, Jolien, Sofie, Teodora, Sandy, Vera en Veronique voor de leuke gesprekken en gezellige lunches! We hebben vaak goed wat afgelachen! Een extra bedankje voor Ria voor haar werk omtrent de fylogenetische analyse van de gasdermines en ook een extra merci aan Veronique voor alle hulp met de administratieve rompslomp die bij een PhD komt kijken. Daarnaast wil ik ook alle andere collega's van de UPVA groep heel veel succes wensen met het afleggen van hun PhD en/of met hun toekomstige professionele activiteiten!

Het harde werk van een PhD dient natuurlijk afgewisseld te worden met deugddoende ontspanning. Daarom wil ik heel graag Annes, Hannelore en Sarah oftewel de Illoe-gang bedanken voor hun jarenlange steun en vriendschap. Hoewel we wel wat diepere watertjes hebben moeten doorzwemmen de afgelopen jaren (waar een doctoraat maar klein bier tegen is), bleven jullie altijd jullie interesse tonen voor mijn PhD en waren jullie altijd bereid te luisteren naar mijn bekommernissen of me gewoon af te leiden na een zware werkdag. Jullie vriendschap is onbetaalbaar!

Ook Elisa, Evelien, Jasper, Lore, Maaike, Marie, Maya, Nele, Rena, Ruth, Sarah en Tine van de Tea-time groep wil ik bedanken voor de vele gezellige avonden waarbij we samen dronken, aten, dansten, spelletjes speelden of gewoon gezellig bijbabbelden! Ook al zien we elkaar niet zo vaak als we zouden willen, ik weet dat ik altijd bij jullie terecht kan. Ook Kaat en Griet wil ik heel hard bedanken voor de leuke babbels en etentjes!

Als het gaat over ontspanning mag ik natuurlijk ook mijn lieve familie niet vergeten. Speciale dank aan Anke, Jeroen, Ruben, mijn allerliefste en kersverse neefje Phil, en natuurlijk ook mijn fijne schoonfamilie Annelies, Guy, Carine, Opa, Simonne, Dominique en Frank. Bedankt voor de vele leuke en ontspannende momenten en vakanties de afgelopen jaren. Jullie konden me mijn doctoraat helemaal doen vergeten.

Lieve mama en papa, hoe kan ik jullie ooit bedanken voor alles wat jullie voor mij, Anke en Ruben gedaan hebben en nog steeds doen. Bedankt dat wij steeds onze eigen keuzes mochten maken en jullie onvoorwaardelijke steun hierin. Bedankt voor de goede raad en ook voor het begrip als we deze niet altijd opvolgden. Bedankt voor alle kansen die jullie ons hebben gegeven om ons te ontwikkelen op professioneel en persoonlijk vlak. Bedankt om ons steeds op het hart te drukken dat ‘als er iets is, dan belt ge maar he’ en steeds voor ons klaar te staan. Zonder jullie hadden we niet gestaan waar we nu staan en kunnen doen wat we graag doen. Bedankt! Bedankt! Bedankt!

Dan last but not least, Wouter, de jongen die nog liever dan ik dit alles achter de rug wil hebben en dus niet vindt dat ik tijd moet steken in hem te bedanken in het dankwoord. Toch kan ik er niet omheen. Wouter, je bent mijn rots in de branding, diegene die me kan kalmeren en me de dingen in perspectief doet zien. Bij jou kom ik thuis, waar dat op dat ogenblik ook is. Ik kan niet wachten om binnenkort aan het grootste avontuur van ons leven te beginnen! Bedankt voor alles!

Elke